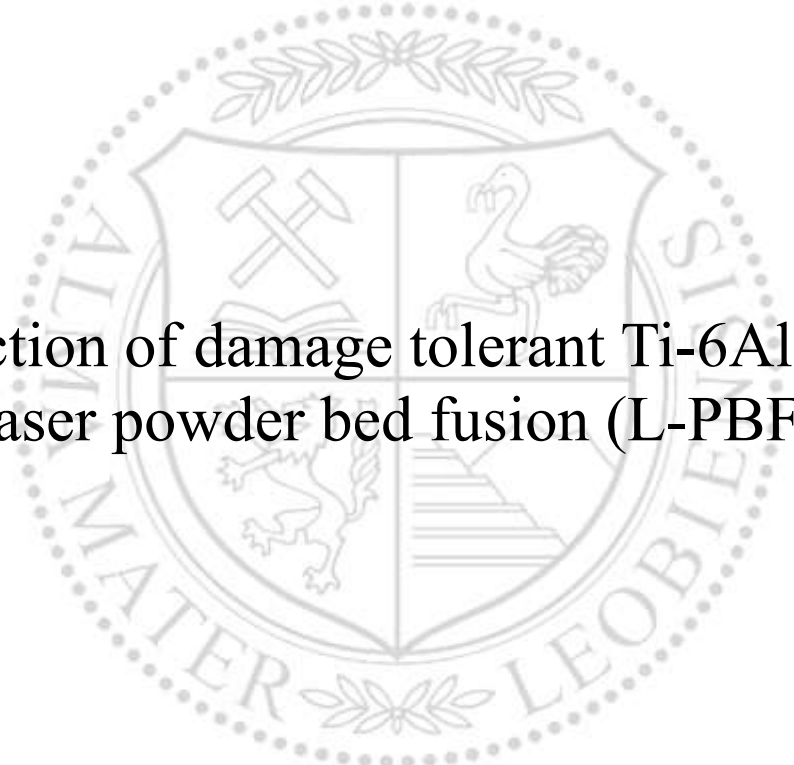Chair of Design of Steels

Master's Thesis

Production of damage tolerant Ti-6Al-4V by laser powder bed fusion (L-PBF)

Joseph Munyika Kapala

December 2023

AFFIDAVIT

I declare on oath that I wrote this thesis independently, did not use other than the specified sources and aids, and did not otherwise use any unauthorized aids.

I declare that I have read, understood, and complied with the guidelines of the senate of the Montanuniversität Leoben for "Good Scientific Practice".

Furthermore, I declare that the electronic and printed version of the submitted thesis are identical, both, formally and with regard to content.

Date 07.12.2023

Signature Author
Joseph Munyika Kapala

Abstract

Laser powder bed fusion (L-PBF) is an additive manufacturing technology that uses laser beam energy to melt layers of material powders in order to create a fully dense part. It uses a computer aided approach to creates a 3D model that is later sliced into distinct layers for printing. The printing process (part production) involves addition of material powders in a layer after layer process which is contrary to the subtractive conventional metal production process. As a technology powder bed fusion encompasses several printing techniques namely Electron beam melting (EBM), Selective heat sintering (SHS), Direct metal laser sintering (DMLS), Selective laser melting (SLM) and Selective laser sintering (SLS).

As a novel technology L-PBF has gained hearts in both industrial (airspace, medical, oil and gas industries) and research field due to its ability to produce part having intricate shape which means flexibility and creativity, also due to little or no waste material produced, and reduction of production time which means short time to market (which important business wise) and also due to possibility to produce fully dense parts having density of up to 99.98%. as such, several materials like polymers, aluminum, copper, iron and titanium alloys like Ti6Al4V are produced using L-PBF.

Even though L-PBF production process offers some exciting technical advantages, Ti6Al4V parts produced by it proves otherwise. It has been reported by several studies and noted during this study that L-PBF produced Ti6Al4V (as-build Ti6Al4V) has higher strength but very low elongation percentage when compared to conventionally produced Ti6Al4V as a result of higher thermal gradient that exist in L-PBF process that leads to the formation of acicular martensite microstructure. This pre-existing fallibility is the Achilles' heel of L-PBF produced Ti6Al4V and renders Ti6Al4V parts produced by L-PBF inadequate for industries in which conventionally produce Ti6Al4V is used. As industries such as biomedical, aviation, oil and gas, automotive, marines, and offshores relies on Ti6Al4V properties.

Studies have shown that it is possible to transform the acicular martensite microstructure observed in as-build Ti6Al4V through heat treatment and by doing so improve its mechanical properties as well. However, a bi-lamellar microstructure has not been achieved from L-PBF Ti6Al4V produced Ti6Al4V.

This thesis aim was to improve mechanical properties of L-PBF produced Ti6Al4V through heat treatment to transform the acicular martensite microstructure found in L-PBF to bi-lamellar microstructure and conducted comparative studies of observed mechanical properties from as-build, lamellar, and bi-lamellar microstructure. Two heat treatment approaches: one stage heat treatment and two-stage heat treatment were used in this thesis.

ABSTRACT

The one stage heat treatment approach in was consisted of heat-treating L-PBF produced Ti6Al4V parts above the β transus to a temperature of 1030°C then slowly furnace cooled while the two-stage heat treatment approach consisted of the first stage in which L-PBF produced Ti6Al4V samples were solution heat treated above the β transus at 1030°C followed by slow furnace cooling (like in one stage heat treatment), and a second stage heat treatment consisting of ageing L-PBF produced Ti6Al4V parts to different ageing temperature vis 800, 880 and 960°C then air cooled.

All the samples (as-build, heat treated) were analyzed using scanning electron microscopy (SEM) then mechanically tested (tensile test, fracture crack growth test).

The obtained results showed that the acicular martensite phase initially observed in as-build parts was transformed to lamellar microstructure following one stage heat treatment approach and to bi-lamellar microstructure after the two-stage heat treatment approach. Mechanical test of all samples showed that as-build samples had higher tensile strength, lower elongation, and no resistance to crack propagation, while heat-treated samples had very good combination of strength, improved elongation and good resistance to crack compared to as-build samples.

Based on the observed results it was concluded there are scientific possibilities to transform the acicular martensite microstructure obtained in as-build Ti6Al4V to lamellar and bi-lamellar microstructure and improve mechanical properties of L-PBF produced Ti6Al4V and it was noted that bi-lamellar microstructure offered the best combination of mechanical strength when compared to as-build and lamellar samples.

Dedication

My father worked in diamond exploration, my childhood memories are made of me travelling with him to diamond buyers' meetings and mostly for private diamonds buyers from Antwerp. My motivation, inspiration for engineering comes from him.

So, I dedicate this work to my parents, Jean Romain Ngoy Kapala, and my mother Marie Therese Kapinga Kapala. To my son who is born here in Europe and away from my home. I hope that my efforts in attempting to fulfill my engineering dream encourages him to achieve whatever he might wish to in his life.

Finally, I dedicate this thesis to 12 million unfortunate Congolese who have lost their lives in the mineral war that is currently going on in the Republic Democratic of Congo. While some of us might have survived and left the war, there are many people that did not.

Acknowledgements

Table of contents

TABLE OF CONTENTS

List of figures

List of tables

List of abbreviations

Abbreviation	Meaning
α	Alpha phase
β	Beta phase
α_{GB}	Grain boundary α
ΔK	Stress intensity factor
σ	Stress
AC	Air Cooling
Al	Aluminum
AM	Additive Manufacturing
ASTM	American society for testing and materials
BCC	Body cantered cube
CAD	Computer aided design
Cu	Copper
da/dN	Cack growth rate and the stress intensity range ΔK as
DLD	Direct laser deposition
SLS	Selective laser sintering
DMLS	Direct metal laser sintering
EBM	Electron beam melting
EQ	Equiaxed microstructure
FC	Furnace Cooling
Fe	Iron
$FeTiO_3$	Ilmenite
FSC	Fatigue stress cracking
FL	Fully lamellar microstructure
H	Hydrogen
HCF	High cyclic failure
HCP	Hexagonal closed pack is cantered cube
HIP	Hot isostatic pressing
ISO	International organization for standardization
L-PBF	Laser powder bed fusion
Mn	Manganese
Mo	Monlybdenum
Nb	Niobium

LIST OF ABBREVIATIONS

Ni	Nickel
PM	Powder Metallurgy
SEM	Scanning Electron microscopy
Si	Silicon
Ta	Tantalum
Ti	Titanium
TiO_2	rutile
TiCl4	Titanium tetrachloride
V	Vanadium
VAM	vacuum arc melting
WQ	Water quenching.

<div align="right">

CHAPTER 1

</div>

1. Introduction

Laser Powder Bed Fusion (L-PBF) is an additive manufacturing (AM) technique that has garnered lot of attention from academia and industry in the last decade, due to its numerous advantages such as manufacturing of complex geometry, capability of on-site manufacturing, low wastage of raw materials. L-PBF processing involves following steps:

1. Preparation of the 3D CAD model for the part to be manufactured.
2. Slicing the 3D model into the desired layer thickness.
3. Applying desired laser parameters such as laser power, laser scan speed, hatch spacing etc.
4. Uploading the sliced STL file to the L-PBF machine server.
5. Preparation of the powder bed according to CAD model.
6. Fusing the powder bed at certain locations, according to the CAD design, with a high-power laser.
7. Repeating steps 5 and 6 to build the part in a layer-by-layer fashion.

Ti-6Al-4V, being an alloy with low density, higher tensile strength and excellent corrosion resistance, is used in aerospace (aircraft engine) and bio-medical industry (hip implants). Due to the high demand of the geometrically complex Ti-6Al-4V for these application, L-PBF processed Ti-6Al-4V has received considerable interest from industry. Numerous investigations have been carried to optimize the L-PBF processing of Ti-6Al-4V. However, there are still some challenges associated with the L-PBF processing of Ti-6Al-4V such as:

1. **Presence of residual stresses**: Due to extremely high cooling rates involved during L-PBF processing, significant residual stresses are generated inside the part which could cause bending or cracking.
2. **Brittle Martensitic microstructure**: Formation of martensitic microstructure is another challenge that is the direct result of extremely high cooling rates.
3. **Heterogeneous microstructure:** Different regions of a complex shaped parts undergo different thermal histories which affects the local microstructure.

Thus, a post heat treatment is always required to address these challenges. But it is difficult to select design a post heat treatment schedule for Ti-6Al-4V, as the final microstructure is heavily influenced

by the temperature, dwell time and, cooling rate etc. of the heat treatment. The links between the heat treatment parameters on the final microstructure have been established for the conventionally produced Ti-6Al-4V. However, due to the difference in the starting microstructure in L-PBF and conventional processing, it is difficult to simply the apply this knowledge to L-PBF processed Ti-6Al-4V. There are mainly three different kinds of microstructures in Ti-6Al-4V viz. lamellar, bimodal and equiaxed. Lamellar microstructure has been shown to have higher resistance against crack propagation whereas bimodal microstructure possesses better combination of tensile strength and elongation. During the operational service, engineering components often undergo cyclic loading conditions. Thus, it is important to have both good quasi-static and dynamic mechanical behavior. Thus, bi-lamellar microstructure has been proposed to achieve best combination of quasi-static mechanical properties and crack propagation. However, such microstructure has never been generated in the L-PBF processed Ti-6Al-4V. **Thus, the aim of the thesis is to:**

1. Design a post heat treatment to obtain bi-lamellar microstructure in L-PBF processed Ti-6Al-4V.

2. Investigate the effect of different heat treatment parameters on the resulting bi-lamellar microstructure.

3. Understand the effect of the bi-lamellar microstructure on the quasi-static and dynamic mechanical properties.

The thesis is divided into 6 different chapters (including Introduction), chapter 2 gives a general overview of the state-of-the regarding Ti-6Al-4V alloy, different heat treatments, effect of these heat treatments on the microstructure and finally the influence of these microstructures on the mechanical properties. Chapter 3 presents the overview of the experimental techniques used during the thesis, Chapter 4 presents the results of the microstructural characterization, quasi-static mechanical testing, and dynamic mechanical testing. Finally, chapter 5 presents main conclusions obtained during this study.

CHAPTER **2**

2. Literature review

This chapter gives detailed descriptions of various relevant literature that were consulted and reviewed to create an understanding of the thesis topic and establish a relationship between existing studies and the selected research topic study. The objective of this chapter is to provide basis for understand this research. This literature presented in this chapter takes into considerations applications of titanium in various industries and highlights the usage of Ti6Al4V in various industries. The literature presented in this chapter also offers a brief description of conventional (subtractive) techniques used in manufacturing Ti6Al4V, gives an overview of alloying elements utilized in titanium alloying with obtained alloys and discuss the microstructures obtained in the conventional Ti6Al4V manufacturing technic. This chapter also considered heat treatment and its effect (effect of temperature, time, aging time) on both microstructure and mechanical. Additionally, this chapter discusses additive manufacturing, it advantages and disadvantages, with special focus on L-PBF, the as-build T6Al4V obtained through L-PBF, post treatment process and it effect on microstructure and mechanical properties (tensile and fatigue properties) of L-PBF produced Ti6Al4. Finally, this chapter reviews chapter mechanics concepts.

2.1. Titanium

Titanium (Ti) is the fourth most abundant structural metal (after aluminum, iron, and magnesium), it concentration in the earth crust is reported to be 0.6% [87]. The following minerals: ilmenite, rutile , titanomagnetite, anatase, and brookite are concentrated mineral source that can be processes to obtain titanium [94]. Ilmenite ($FeTiO_3$) and rutile (TiO_2) are the most important titanium mineral resources [87].

Titanium was discovered in 1971 by William Gregor, a British clergyman interested in mineralogy. During his analysis of black magnetic iron sand in Cornwall (UK), William Gregor suspected the existence of unfamiliar element. He then proceeded by extracted iron substances from this sand, and then he treated the remaining byproduct with hydrochloric acid to obtain oxides (titanium oxide with impurities) [87]. Later on, in 1975 a German scientist M.H. Klaproth conducted analysis on rutile minerals obtained from Hungary. During his analysis Klaproth observed unfamiliar oxides element of the same nature as reported by William Gregor [94],[95]. Klaproth referred to the obtained element

as titanium in honor of the powerful Greek deities who were shut in the underworld by their father as stated in Greek mythology [87], 52- 53].

Traditionally, processes utilized in production of titanium from ore to final product encompasses reduction of titanium ore (ilmenite or rutile) to sponge, melting of sponge and scrap in order to produce ingot, and remelting and casting into finished shape.

2.1.1. Properties

As an advantage titanium has a high strength-to-weight ratio, compared to other metallic material as shown in Table 2. 1 titanium has low density compared to Fe, Ni for the same yield stress level. This allows titanium to be used in industry such as the aerospace where it can be used over other heavier metals such as steels and preferred over light weight frame metal such as aluminum due to its higher strength (In Ti, we find higher strength combined with low density) and high temperature.

Table 2. 1: Comparison of key qualities of titanium and titanium alloy based to structural metallic materials based on Fe, Ni, and Al [87].

	Ti	Fe	Ni	Al
Melting point (°C)	1670	1538	1455	660
Allotropic Transformation (°C)	β --> α (882°C)	ϒ -> α (912 °C)	-	-
Crystal Structure	bcc -> hex	fcc -> bcc	fcc	fcc
Room temperature E (GPa)	115	215	200	72
Yield Stress Level (MPa)	1000	1000	1000	500
Density (g/cm^3)	4.5	7.9	8.9	2.7
Comparative corrosion resistance	Very high	Low	Medium	High

As stated earlier, Ti and its alloys are utilized in military due to it high level of performance even when utilized at elevated temperatures, in aerospace for aircraft parts due to its weight reduction with no loss in strength when compared to steel, hence part such as turbine and turbine blades, airframe titanium is utilized [96]. Alloying elements added to titanium improves fatigue strength, crack propagation resistance, fracture toughness [96]. Titanium shows fantastic resistance to corrosion resistance in oxidizing acid environments by virtue of a passive oxide film that forms when titanium is in contact with air or moisture, hence it utilization in chemical, marine's, and architectural industry [96],[97]. Titanium has good formability properties and can be forged; it may be also wrought or cast. Its usage in architectural industry all over the world is a result of its availability in wide variety of types and forms. Additionally, titanium has biological compatibility, and this explains it utilization in human body as part of medical progress.

2.1.2. Application

Titanium finds it usage in various industrial applications (Aerospace, automotive, marine, and chemical industry) due to its main properties such as low density when compared to other structural metals (iron, nickel), high strength, and excellent corrosion resistance [87]. The combination low density and high strength in titanium makes it appropriate metal for aircraft, while the combination of low density with high strength and creep resistance (up to about 550°C) makes it well suited for aero-engine [87]. Hence the consideration of airframes and aeroengine as the two classical utilizations areas for titanium alloys [87].

2.1.2.1.   Automotive industry

The automotive industry had already made use of titanium in mid-1950s. For instance, General Motors (GM) developed experimental turbine-driven vehicle that had an outer skin made entirely of titanium, this was the titanium firebird II, the firebird II was part of quartet prototype cars set made by GM (Firebird I, II, III, and IV) [95]. **Fehler! Verweisquelle konnte nicht gefunden werden.** bellow shows the titanium firebird II made of titanium.

Figure 2. 1: Titanium Firebird II produced by General Motors Corp., USA [95].

Even though utilization of alternative materials in the production of vehicles could result in efficiency improvement, weight reductions and fuel consumption reduction, the cost associated with titanium is the limiting factor when it comes to it extensive usage in commercial vehicles, and it can only be utilized for specific component. For instance, titanium alloys are utilized to produce a lightweight valves used in German automotive industry due to low density, very good strength at high temperatures, good oxidation resistance, and it excellent creep resistance [87]-[95]. Figure 2. 2 shows potential applications of titanium in automobiles (specific components are made with titanium).
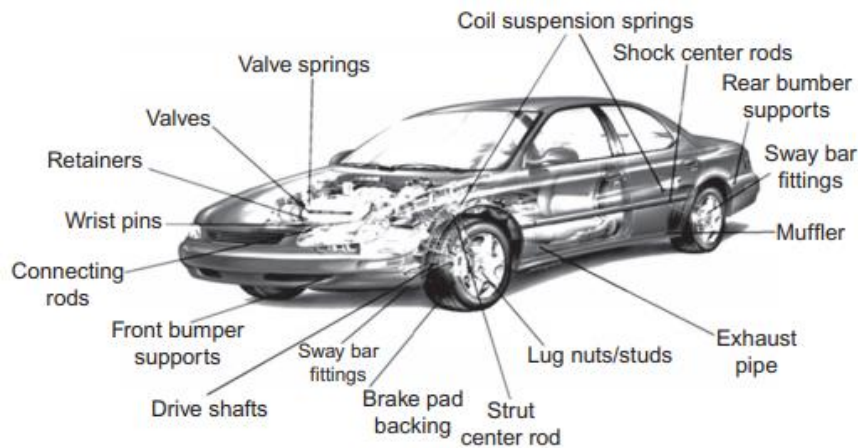
Figure 2. 2: Titanium applications in automotive [98].

Low density (reduced weight), high strength and rigidity found in titanium increases it utilization in race industry, this explains why when it comes to utilization of titanium, and it alloys in automotive and motorcycle the focus is more given to racing applications.

2.1.2.2.   Aerospace industry

Titanium alloys utilization in in both commercial and military aircraft in particular Ti-6Al-4V have increased in recent decades. Figure 2. 3 bellow shows titanium content usage in both commercial and military aircraft [98].
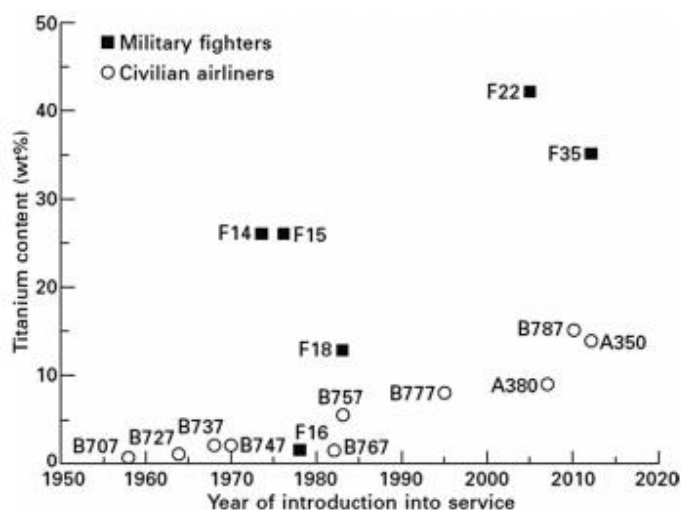
Figure 2. 3: Titanium content used in an aircraft and their years of introduction [98].

The use of titanium alloys for various applications in aircrafts is the result of their properties and superior structural efficiency [87]. In aircraft, titanium alloys are used in airframe and aeroengine [87].
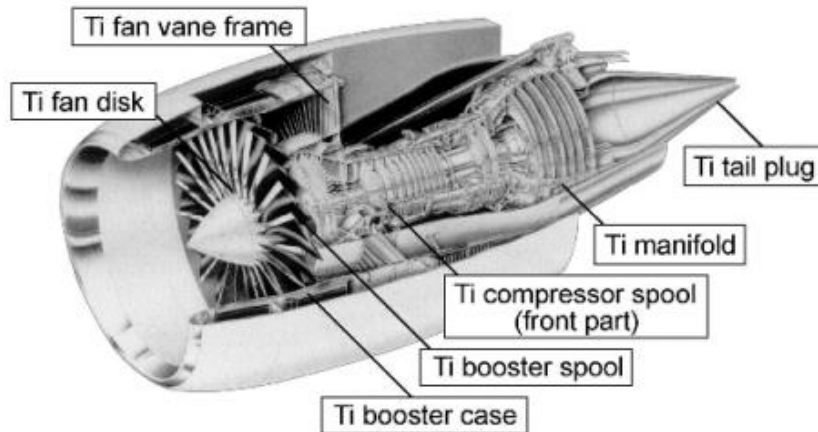
Figure 2. 4: Utilization of titanium in GE-90 aero-engine [87].

Figure 2. 4 shows the usage of titanium alloys in GE-90 aero-engine that is utilized in Boeing 777 aircraft [87].

Ti alloys have been further used to manufacture aircraft part such as [87]:

- ❖ spring used in aircraft as
  - up-lock and down-lock springs in the landing gear,
  - flight control springs,
  - door counter-balance springs,
  - hydraulic return springs
- ❖ Fasteners in
  - airframes,
  - engine,
  - wings,
  - propellers, and some parts of the landing gear system

2.1.2.3. Other industries

Titanium properties among others corrosion resistance makes it very attractive to other industries. Above the fact that titanium has higher strength, good formability, and weldability, it is also extremely corrosion resistant as a result of its higher affinity to oxygen and moisture. When exposed to oxygen or moisture or both, titanium develops a stable, protective, strongly adherent oxide film that makes it corrosion resistance[87]. Furthermore, titanium is very stable in stearic, formic, tartaric, tannic and citric acids, and can be utilized in equipment where mixture of organic solvents, organic acids, and salt take place[87]-[95].

This explains the popularity and usage of titanium industry such as [87] :

- Chemical, Process and Power Generation Industries

- Heat Exchangers and Condensers

- Petrochemical Refineries.

- Flue Gas Desulphurization

- Steam Turbine Blades

- Extractive Metallurgy

- Marine and Offshore Applications

Figure 2. 5 shows shell and tube heat exchanger made of Ti6A4V.

Figure 2. 5: Titanium Shell and tube heat exchangers [99].

2.2. Conventional Manufacturing of Titanium Alloys

As stated earlier, titanium is not found in pure form but in ore form, and the ore have to through several processes in order to obtain the final products. With Ilmenite ($FeTiO_3$) and rutile (TiO_2) being the most important titanium mineral resources [87]. From the initial state (the ore) to the final titanium metal product, the ore have to undergo several process steps[87]:

- The reduction of titanium ore into a porous form of titanium metal, described as sponge,

- Melting and remelting of the produced sponge or sponge and a master alloy to form an ingot,

- Primary fabrication when ingots are converted into general kinds of mill products,

- Secondary fabrication of the mill products into finished shapes.

Figure 2. *6*: shows overview of steps involved in conventional titanium manufacturing.
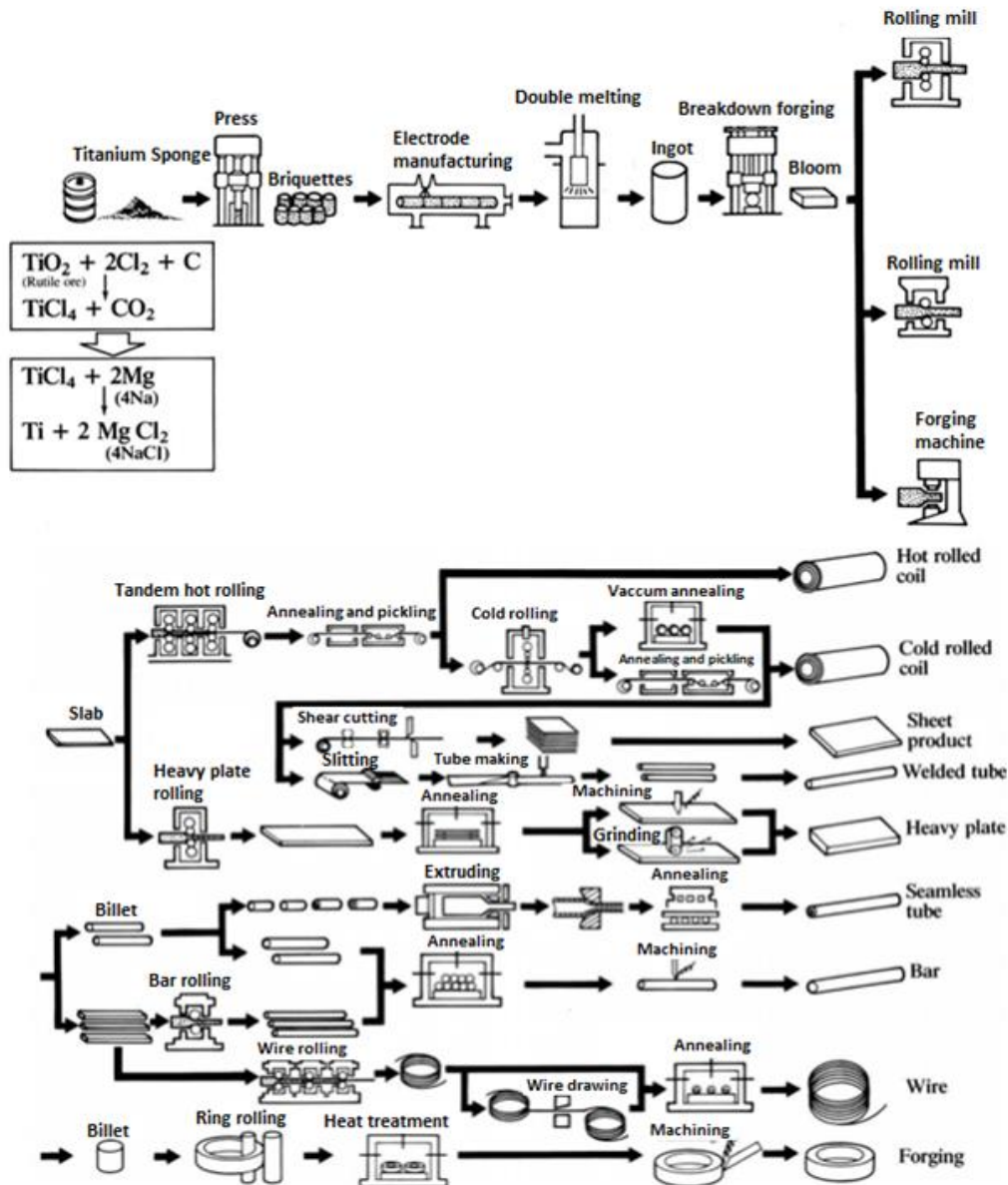
Figure 2. 6: Titanium production flowsheet overview [96].

2.2.1. Primary Manufacturing of Ti Alloys

The primary manufacturing of titanium alloys consists of the sponge production, and purification, melting of the sponge using VAM to form ingot, and production of mill product using ingot.

Sponge is the name given to the metallic titanium obtained from processing the ore. In order to extract the metallic titanium (produce the sponge) the following steps need to be followed[87]:

- Chlorination of the ore to produce TiCl4,
- Distillation of the TiCl4 to purify it,
- Reduction of the TiCl4 to produce metallic titanium (the Kroll process),

- Purification of the metallic titanium (the sponge) to remove by-products of the reduction process,

- Crushing and sizing of the metallic titanium to create a suitable product for subsequent melting of CP titanium and titanium alloys.

The industrial reduction process utilized for the sponge production is commonly known as the Kroll's process. As a process, it (K(roll's process) is a very energy-intensive, and contributes to the high cost associated with the production of Ti alloys [100]. Even though several attempts have been made to find other deduction methods that can replace Kroll's process, it is still the main method utilized in the reduction process [101]. The sponge is than utilized in the production of the ingot.

The composition of the ingot is very dependent on the sponge, hence in order to ensure the control of the ingot composition very strict specifications have to be considered during the sponge production. So, the produced sponge has to be purified, and removal of fragment of brittle, hard, and refractory titanium oxides, titanium nitrides, or other complex titanium oxynitride have to be done in order to avoid crack initiations, in further steps, as the presence of impurities and such fragments may easily lead to crack initiation in further manufacturing steps or in end products [87].

The melting of the sponge to form ingots is made using the vacuum arc melting (VAM) as shown in Figure 2. 7 [87]. VAM is the main methods utilized in the fabrication of titanium alloy ingots. Addition of alloying element can take place during this stage of production.
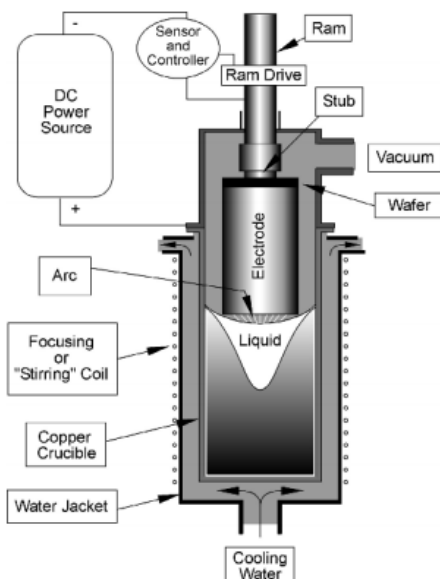
Figure 2. 7: Schematic of VAR furnace and ingot during a second melt [87].

As a process VAM, has been employed in effective making of larger and larger ingots. Utilization of VAM result in lower cost due to the fact that In this process, heat treatment and cooling rate can be utilized to control the chemical state and type of microstructural of the ingots (the conducted heat

treatment is done bellow the β transus temperature) [87]. The process utilized to produce mill products (billets, bars, pallets, wire and powder) from ingots is described as the primary production of Ti alloys [102].

2.2.2. Secondary production process of Ti Alloys

In manufacturing process, secondary production are processes that takes place after the initial stage (separation of ore from impurities, ore processing) so in case of Ti alloys, secondary production process consists of shaping process [103][54]. In shaping we have shaping into components and near net shaping [54]. Shaping for components is done through technic such as forging, ring rolling, and machining or metal removal, while near net shaping is done through forming (laser forming, conventional sheet forming, superplastic forming), casting, and powder metallurgy (it is important to highlight that even though powder metallurgy is used for near net shape, it does not start with ingot, but compacted metal powder, and description of this process will be provided later in this chapter) [87]. In this section forging, casting, and powder metallurgy.

2.2.2.1.   Forging

Studies have shown that forging alone account for approximately 70% of the whole Ti production cost, and it is the primary process utilized in shaping mill products into final titanium components, Generally, to finalize the shape of the component, after forging machining is utilized [87],[104]. Forging utilizes different types of dies in order to produce shapes. The principal approaches utilized in die takes place either bellow β transus temperature or above β transus temperature[105],[106]. Major titanium alloys forging process:

- Free forging,
- Open die forging,
- Closed die forging,
- Isothermal die forging
- Multi direction die forging,
- Partial die forging, and
- Extrusion die forging,

The appellation of these forging process refers to the manner in which the forging process is caried out. For instance, open die forging refers to the process in which the die is heated to the forging temperature of the blank prior to forging, and the die and the blank are maintained at the same temperature during the whole forging process.

Figure 2. 8: Closed-die forging [107].

Figure 2. 8 above shows closed die forging schematics.

As a process, forging permits the control of final microstructure of the produced alloys through heat treatment and consecutive forging stages. Through time, a considerable progress has been made in forging process as compared to it primitive usage in early society where it was used for making hand tool, war weapons, and jewelry. The two main advantages the modern forging are, firstly, the capability of forging as a process to produce or make part with similar shape to what is desired (almost as near net shape) how the desire to have near net shape affect the price, the higher cost of production is a limiting factor if near net shape have to be pursued in forging. Secondly, the possibility to influence the microstructure to obtain desired properties in the produced part, controlling the microstructure implies determining the performance of the produced part[49].

2.2.2.2.   Casting

Utilization of casting for the production of titanium alloy have become very popular in the last 20 years[49]. As stated earlier, obtaining near net shape through forging is very costly, and after forging successive machining steps have to take place in order to obtain the final shape, this also increase the cost [49]. For all conventional machining method, it is has been reported that in comparison to steel or aluminum alloys, titanium and titanium alloys are usually considered as challenging to machine [49]. Hence, casting as manufacturing process for titanium alloys, has attracted more and more attention. Casting has the potential to reduce material waste produced through the machining process that takes place after forging and also, also joining process such as welding, braznig, and solering are reduced by utilisation of casting as alloy production process[49].

Casting can be divided into, mould casting and semi-finished casting as shown in Figure 2. 9.
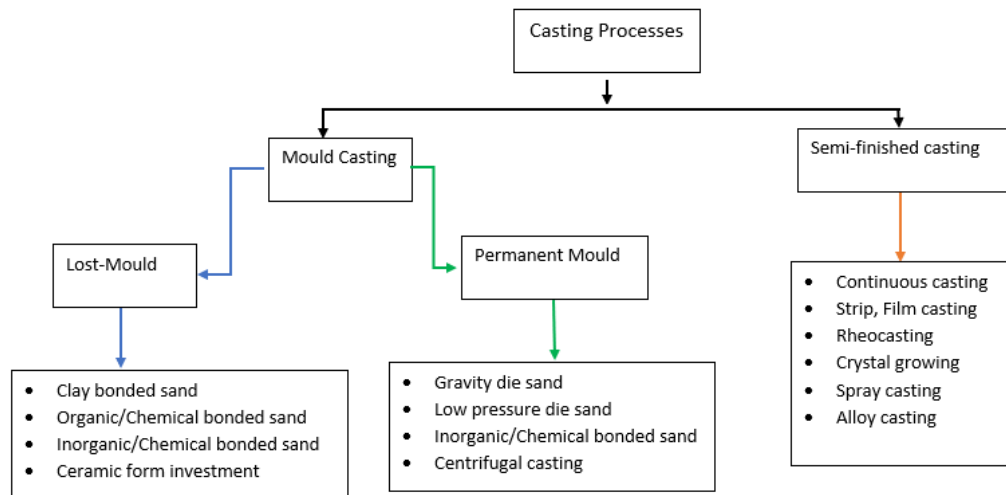
Figure 2. 9: Casting processes [108].

As opposed to forging, casting suffers from some qualities related difficulties sometimes, for instance when utilized for manufacturing complex part, problem such as porosity (which can be a crack initiation site) can be encountered [49]. Studies conducted on high cycle fatigue damage mechanisms in cast aluminum have shown that fatigue crack in casting are always prone to initiate where there is porosity in case where both uniaxial and combined tension-torsion loads are used. To avoid formation of porosity and crack initiation site in casting manufactured product, isostatic pressing (HIP) is utilized [49]. For TI6Al4V alloy, the casting is subjected to elevated temperature and isostatic gas pressure during the HIP process, usually to 900°C and 103 MPa pressure for the duration of 2 h [109]. The HIP process is conducted with as purpose to reduce internal void defects by collapse and diffusion bonding [110].

Product made by other methods are being replaced by casting, due to the following reasons [49]:

1. Casting technology contributes to the progress of near net shape manufacturing,

2. Reduction of internal porosity, crack initiation and improvement of fatigue properties, as a result of utilization of hot isostatic pressing (HIP) makes casting product more and more desired compared to products of other manufacturing processes and

3. There is a less metal-mold reaction during casting.

For titanium alloys, casting is achieved under vacuum in order to prevent oxygen and nitrogen pickup, and to some extent in order to reduce the reaction of the mould to the molten material special mould materials utilized [111]. Lost-mould and permanent mould casting are utilized for the production of titanium. However, investment casting which falls under lost mould, is the most widespread utilized method of casting for titanium [111]. Even though several other casting approaches are utilized in casting of titanium alloys, these techniques are not so much used as often as investment casting [111] Figure 2. 10 shows investment casting steps, the process steps start from left to right.
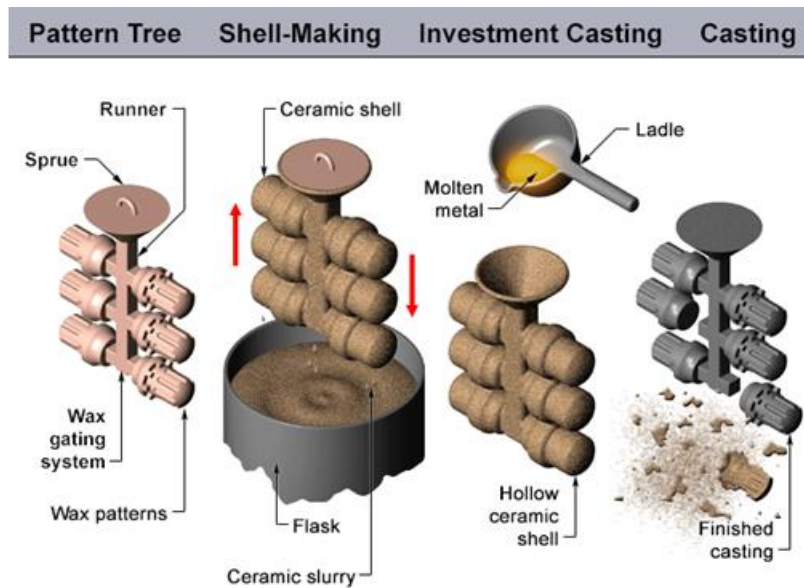
Figure 2. 10: Investment Casting [112].

2.2.3. Powder Metallurgy of Ti Alloys

Powder metallurgy (PM) is metal processing, consolidation and processing technology in which solid metal parts are manufactured by consolidating metallic powders to make a fully dense solid metal [49] [113]. Advantages of PM over other manufacturing methods include mass production of near net shape or net shape, which implies great shape flexibility, PM has or offers a reduction processing steps, and also has efficient utilization of material, 97% of the starting powders are converted to product , hence there is no requirement for machining like it is the case of in forging [49] [113]. Efficient material utilization also implies cost effective.

Even though several methods have been utilized for powder preparation in PM such as water atomization, centrifugal atomization, rotating disk atomization, ultrarapid solidification process, ultrasonic atomization have been developed [114]. Atomization is the utilization of high pressure fluid jets to split up a molten metal stream in extremely fine droplets, the droplets solidifies later into fine particles [114]. Gas atomization is the most dominant process utilized in PM for manufacturing of Fe, Ni, Cu based alloys [115]. While several laboratory experimental research have shown that titanium can be produced using gas atomization, however, on a larger scale direct gas atomization of molten titanium is not achievable when using an atomization process like the one utilized for Ni, Cu and Fe based alloys[49]. When gas atomization is utilized for titanium production, lower volume of powder is produced, with spherical particles that are attached to other smaller particles referred to as satellite as shown in Figure 2. 11 a [49].
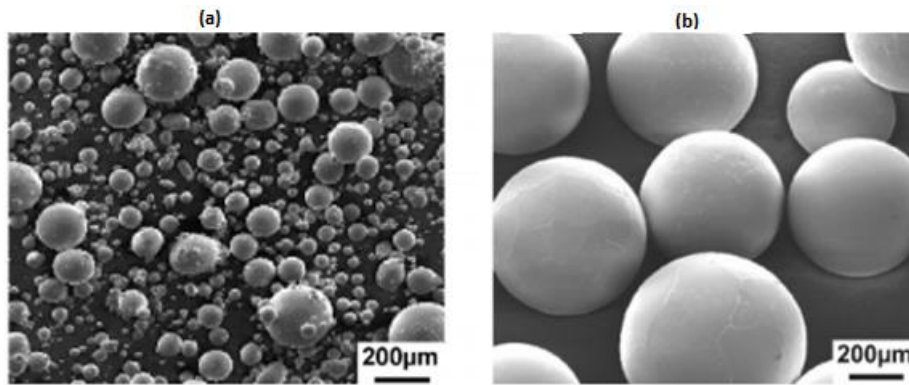
Figure 2. 11: pre-alloyed titanium made powder with spherical form (200µm) [87].

Usually, for the manufacturing of pre-alloyed titanium powder the rotating electrode process (REP) method, also referred to as Plasma Rotating Electrode is utilized[49, [116]. REP is some sort of centrifugal atomization, where the metal or alloy are rendered into consumable, that is rotated (1500-1800rpm), while its end is being heated using either an electric arc or a plasma torch, in an inert gas (argon or helium). If the source of the heat is an electric arc, the resulting powder is referred to as REP powder, while if it is a plasma torch, the produced powder is referred to as PREP powder[49, [116]. A centrifugal force is utilized to separate the molten metal (in our case titanium) from the electrode that is still in rotation. Final obtain powder have a spherical size that varies between 30 0 to 500 µm as shown in Figure 2. 11b[49]. After obtaining the powder further processing steps may be considered such as mixing or blending, compacting, sintering and finial product or even considered secondary metallurgy.

2.3.   Alloying of titanium and utilized stabilizing components

There exist 3 primary groups of titanium alloys namely α, β, and α+ β[117]. Additionally, there exist two more categories that is near α and near β alloys. It is important to highlight that when an alloy is referred to as α alloys it does not imply exclusively α as in some cases there are some quantity of β present in α alloys [118]. What characterizes each alloys class or category (α, β) is the phase that is dominant at ambient temperature. It is also possible to have both phases present in a titanium alloy such alloys are referred to as α+β alloys, alloys such as Ti6Al4V, Ti3Al2.5V, Ti7AI4Mo etc. such alloys are achieved through addition of a certain amount of certain alloying elements that render each phase stable (α and β stabilizers). Element such as B, C, O, Al can be used in order to stabilize α phase in an alloy, these element as referred to as α-stabilizers[117],[118]. So, alloying elements found in titanium are classified based on their capacity to raise or lowers β transus temperature [96],[117],[118]. With that in mind, alloys that lowers the β transus temperature are referred to as α-stabilizer and elements alloys that raises β transus temperature are described or characterized as β-Stabilizers [118].

Furthermore, β stabilizers are classified in to two sub-grouped viz. eutectoid stabilizer and isomorphous stabilizer as shown in Table 2. 2.

Table 2. 2: β Stabilizers classification and used element for each sub-group [117]–[119].

β Stabilizers sub-group	Elements	Effects
Eutectoid β Stabilizers	Fe, Mn, Ni, Cu, Si and H	leads to eutectoid phase transformation
isomorphous stabilizer.	as V, Mo, Nb, and Ta	Leads to formation of isomorphous phase

Furthermore, a neutral phase diagram can be obtained when stabilizers referred to as neutral are utilized. Elements such as Zr, and Sn, are referred to as neutral stabilizers due to the fact that they do not have an effect on the β transus transformation temperature and these element are observed for both theα and β phase [118]–[120]. Figure 2. 12 below shows a binary phase diagram containing principal titanium alloys. It is important to mention that a rise in quantity of β stabilizer as indicated by Figure 2. 12 will cause alloy transformation to lean toward the left side of this phase diagram the change will be for instance from α to produce α+ β or from alloy α to produced β depending on β stabilizers quantity [118],[119].

Figure 2. 12: Binary titanium phase diagram temperature vs alloy and stabilizer [121].

Figure 2. 13 shows different stabilizers elements and their effects of on resultant titanium alloy phase diagram where (a) α-stabilizers, (b) isomorphous β-stabilizers, (c) eutectoid β-stabilizers, (d) neutral

stabilizers.

Figure 2. 13: Titanium stabilizers and the subsequent alloy phases (a) α stabilizer (b) β isomorphous (c) β eutectoid (d) neutral [122].

2.4. Ti6Al4V

Ti6Al4V is the most and frequently used titanium alloy and it is a two phase α + β titanium alloy. Ti6Al4V is widely utilized various industries in energy, automotive, chemicals and biomedical industries [123]. This is due to its properties such as low density compared to iron and nickel while having the same yield strength with iron and nickel, and better yield strength than aluminium. Due to its excellent corrosion resistance, high specific strength, higher fracture toughness, exceptional biocompatibility, and high-thermal and mechanical properties [105],[106].

Ti6Al4V is also utilised in aircraft as it present a very good option to aircraft industry because of its strength to weight ratio contributed to reduction of aircraft weight, energy consumption and wear and corrosion resistance. It is utilised in airframe components, gas turbines and jet engines [124]–[127]. Ti6Al4V finds its applications in numerous other fields like chemical, bio chemical, automobile, marine and energy industries due to its high corrosion resistance to most corrosive acids and alkalis, low density, high strength, and biocompatibility [106],[128],[129],[125]–[127].

Solidification of Ti-6Al-4V takes place between or below 1605-1660°C, and the solidification temperature is partly reliant on the purity of the alloy [130]. When Ti6Al4V is melted only β phase exist at higher temperature, due to the fact that this temperature is above the β transus. As the temperature of the melt drops below 1600°C, formation of β grains starts to take place. The β transus temperature for Ti6Al4V alloy varies between 975 to 995°C, when heat treating above this temperature only the β. There are several factors that affects the β transus temperature [96],[118]:

- Purity of the produced alloy,
- Substitutional elements,

- Interstitial elements,

- Etc.

Being as the alloy is further cooled, once the temperature is below the β transus α phase start to nucleate from the β grain boundary and gradually nucleate to the final stage (nucleation is complete), this process is temperature dependent. Like in other metals, the morphological feature of the microstructure formed in Ti6Al4V is reliant on the cooling rate. Faster cooling rate has been known to lead to thinner α lamellae while slow cooling rate has been known to leads to coarse αlamellae. Figure 2. 14 below shows α phase nucleation process from β grain boundary as a result of cooling rate. This is Widmanstätten microstructure that can be obtained through moderate cooling rate, this microstructure is composed of alternating α and β plates where α laths are parallels to each other's within a colony [117],[118]. Initially, above the β transus there was only β phase and as seen in Figure 2. 14, and progressively as the alloy is cooled below the β transus α phase starts to nucleate[96],[118].

The cooling rate plays a significant role in α nucleation, lamellae size, colony size, retained β thickness etc. [96],[118]. An exceedingly fast cooling rate could lead to formation of martensite.
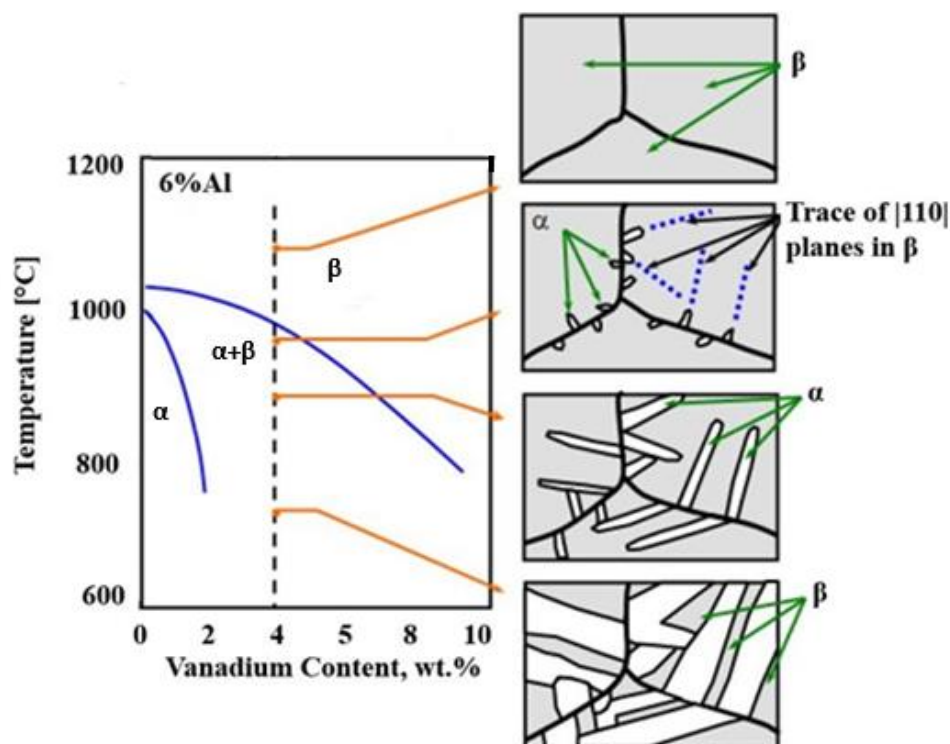
Figure 2. 14: Widmanstätten microstructure development for a titanium alloy [131].

Unlike in the case of Widmanstätten where slow cooling leads to α laths that are parallels to each other and separated by retained β within a colony. When fast cooling (air cooling) is applied from β transus concurrent nucleation of α plates happens withing β grain and at the grain boundary and later on

overlap when nucleation is completed this is referred to as basket-weave microstructure as shown in Figure 2. 15 [117],[118],[133],[134].
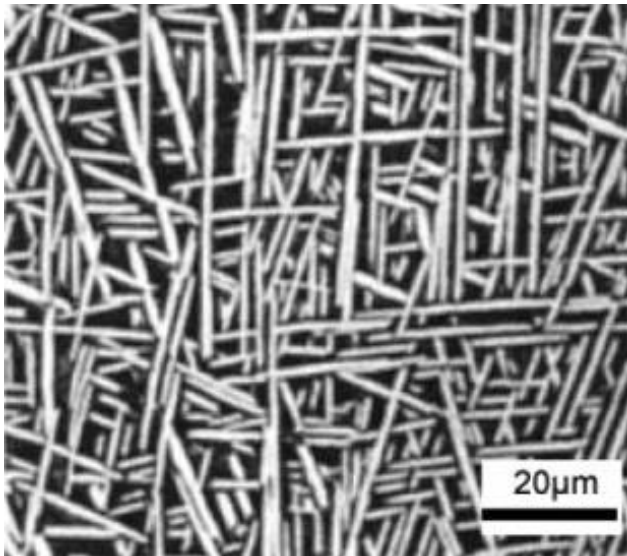
Figure 2. 15: Basket-weave Ti6Al4V microstructure [132].

When the cooling rate is exceedingly higher, a diffusionless transformation takes place leading to acicular martensitic microstructure formation in Ti6Al4V having a distorted hexagonal closed packed (HCP) crystal structure labelled α′ [117]. The acicular martensite is characterized by needle like features in columnar β, inclined to each other at the 30, 60 or 90° in which each laths contains a different variant of Burger relationship [118], [133]. In order to transform the acicular martensite, heat treatment above β transus temperature is required in order to ensure full transform the acicular martensite to β phase and through slow cooling from β transus to obtain an α+β Ti6Al4V such as lamellar microstructure characterized by α lamellae in retained β.

2.4.1. Allotropic transformation in Ti6Al4V

Titanium has two different crystal structures HCP exist low temperature and BCC exists at higher temperature. These crystal structures and atoms positioning in HCP (a) and BCC (b) lattices are shown in Figure 2. 16. It is known that pure titanium go through allotropic transformation when heated above 882°C, in which the α phase HCP (Hexagonal closed pack) is transformed to β phase BCC (Body cantered cube) [134]. The transformation temperature from HCP to BCC is affected by the presence of stabilizers (α or β stabilizers) as discussed earlier. As α stabilizers will increase the transition α-β transition temperature while β stabilizers will lower the α-β transition temperature [134].

It is generally maintained that the β phase possesses better ductility than the α phase, and that the α phase is characterised by better strength compared to the β phase. This due to the fact that the HCP

has lower number of slip system compared to the BCC hence the brittle behaviour observed in HCP [134].
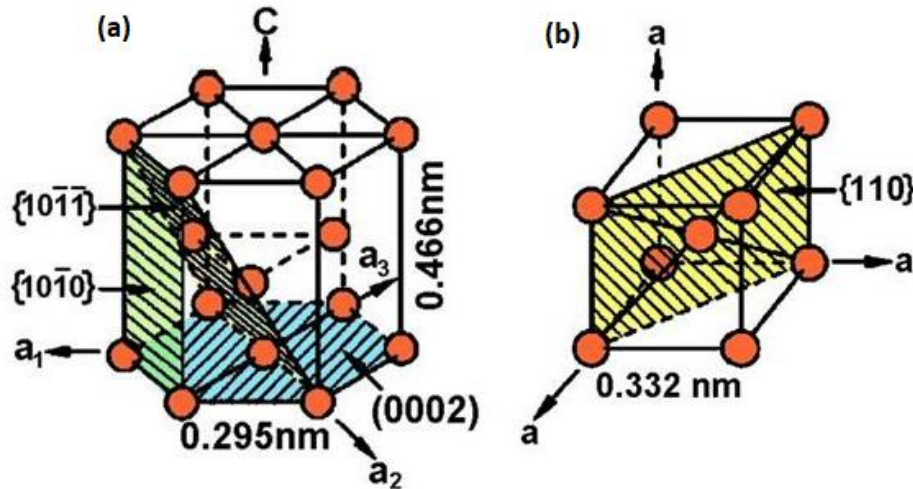
Figure 2. 16: HCP(a) and BCC (b) crystal structure [135],[134].

The HCP crystal structure have the following lattice parameters [134]:

a=0.295 nm
c=0.468 nm
 c/a ratio of 1.587.

The HCP slip system [134]:
- basal
- pyramidal
- Prismatic.

Table 2. 3 below shows titanium thermal properties.

Table 2. 3: Titanium thermal properties [134].

Thermal properties						
Meting point	Max. service temp	Min. service temp	K (W/m.°C)	C (J/kg. °C)	α (µstrain/°C)	L(KJ/Kg)
1.61 E+03-1.6166E+03	350-420°C	-273	7.1-7.3	528-548	8-7-9.1	360-370

2.5. Ti6Al4V obtained microstructure during convention production process

The reason behind the emphasis on distinguishing microstructures and observed mechanical properties of conventionally produced Ti6Al4V and L-PBF produced Ti6Al4V is because in this thesis the studied Ti6Al4V was produced using laser powder bed fusion. Therefore, it is of essence to briefly establish and highlight differences observed in microstructure and mechanical properties between

conventionally produced and L-PBF produced Ti6Al4V. Lütjering maintains that through thermo-mechanical processing utilized in conventional T6Al4V production 4 different microstructures can be attained[54]. These microstructures can be described using the size and arrangement of the α and ß phases present in Ti6Al4V.

Table 2. *4* shows microstructure obtained through thermo-mechanical treatment during conventional Ti6Al4V production namely lamellar, equiaxed, bi-modal, bi-lamellar [49].

In conventional Ti6Al4V production, lamellar microstructure is achieved by heat treating the Ti6Al4V alloy above the β transus, then slowly cooled. Bi-lamellar microstructure is achieved through two-stage heat treatment while bi-modal and equiaxed are achieved by utilizing deformation and recrystallization in combination with higher temperature.

Table 2. 4: Microstructures achieved through thermos-mechanical treatment in conventional Ti6Al4V manufacturing [87], [136].

Microstructure			
Lamellar	**Bi-lamellar**	**Equiaxed**	**Bi-modal**
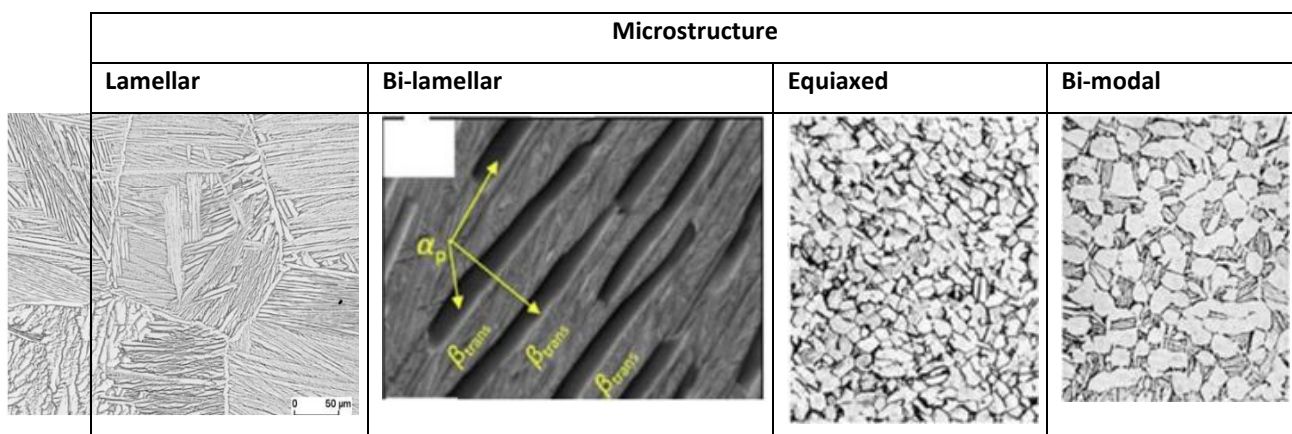
Figure 2. 16 shows two titanium crystal structure, at higher temperature above the β transus titanium has BCC crystal structure (β) while at low temperature it has HCP structure (α) [134][136]. A combination of thermos-mechanical process can lead to titanium to have different microstructure with various volume fraction of α and β.

Figure 2. 17 (a) and (b) shows Ti6Al4V phase diagram and the effect of cooling rate on achieved transformation. It can be observed that in Ti6Al4V when cooling from β transus to the α+β region depicted by the grey area, the α volume fraction is present. Unlike above the β transus where only β exists as soon as the temperature is in the α+β region there is the presence of α phase. Near the β transus temperature there is 10% volume fraction of α and 90% volume fraction of β, while as the temperature is nearing the α phase the β phase volume fraction is reduced to 10% and the α volume fraction increased to 90%. This seems to be inversed, as the temperature increases the β volume

fraction increases, and as the temperature decreases the α volume fraction increases. The selected amount of α and β stabilizers, selected temperature cooling rate contributes to microstructure features and to mechanical properties, so a more detailed approach have to be considered when aiming to achieve a certain microstructural feature and when analysing it as it is understood that several parameters impact the final obtained microstructures and mechanical properties hence these parameters have to be taken into account [118],[137].

Figure 2. 17 (b) shows the effect of the cooling rate on transformation, final phase present and microstructure. After Ti6Al4V have been heat treated above the β transus during the cooling process from the β phase, the cooling rate plays an important role into the achieved microstructures features [118],[137]. Slow cooling rate leads to diffusion-controlled transformation in which there is nucleation of α phase from the β phase. While fast cooling rate leads to diffusionless transformation that leads to formation of martensite microstructure [118],[137].
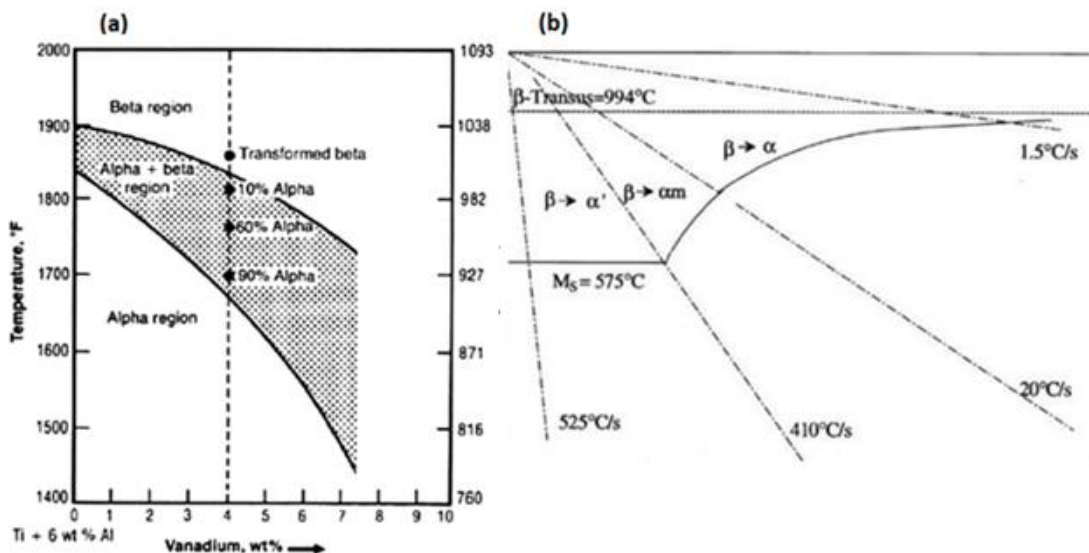
Figure 2. 17: (a) Ti6Al4V phase diagram and (b) impact of cooling rate on transformation [138] [118].

Various cooling method are utilized:

- Furnace,
- Air cool,
- Water quenching or other mediums.

Water leads to a cooling rate faster than air cooling while air cooling leads to a cooling rate faster than furnace cooling. In today's modern furnace a specific cooling rate can be selected from the furnace.

In Figure 2. 17 (b) it can seen that several cooling rates are utilised to cool alloy from β transus and faster the cooling rate leads to diffusionless transformation. For instance when the colling rate is above

410°C/S non-equilibrium martensite (α') phase forms β→α', and when the cooling rate is between 1.5 to 20 °C/s the β phase transforms to α through there is diffusion controlled transformation β→α [136],[139]. This shows the importance of cooling in achieved microstructure.

Figure 2. 18 shows the effect of cooling rate on lamellar microstructure obtained by Lütjering [54]. It can be observed in Figure 2. 18 that as the colling rate increases the lamellae within the microstructures becomes finer and finer. Research conducted by Ahmed and Rack maintained that when Ti6Al4V alloy was cooled at a rate above 410 ◦C/s martensitic microstructure formation took place, and they also noted that a when the alloy was cooled using slow cooling rate of below 20°C/s Widmanstätten microstructure formed through diffusion controlled transformation [140]. The selected cooling rate during cooling plays a vital role in final microstructure features.
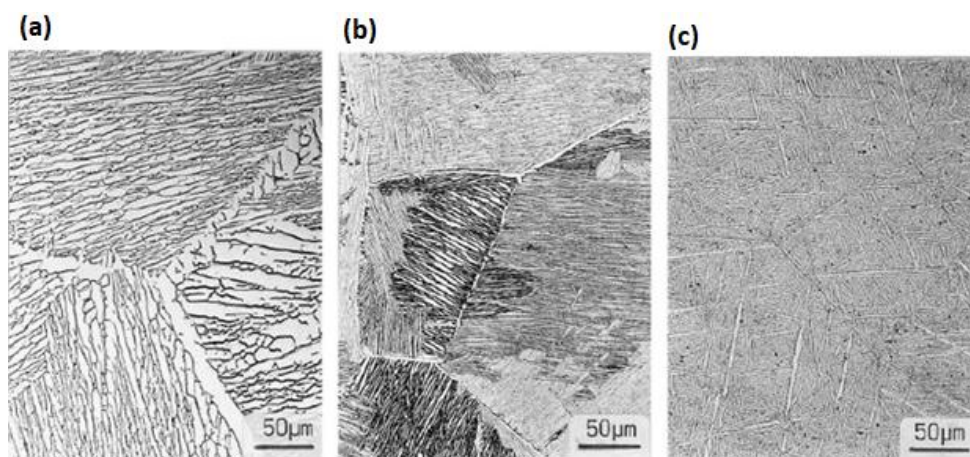
Figure 2. 18: Cooling rate effect on Ti6Al4V microstructure (a) slow,(b) medium, (c) [40].

Figure 2. 18 show the results of studies conducted by Seo *et al*. [141]. This research confirms what has already been pointed out from Lütjering [54] and Ahmed and Rack [140] studies. Figure 2. 19 shows the effect of cooling rate on the thickness of α plates in Ti6Al4V, it can be seen that as the cooling rate increases the α plates thickness decreases, this experiment was conducted for both aged and none aged Ti6Al4V samples [141].

A good contrast of microstructures features such as α lamellae thickness, retained β thickness, colony size, β contributes to mechanical properties are controlled through heat treatment and the selected cooling rate. Controlling the cooling rate leads to the desired microstructural features and desired mechanical properties.
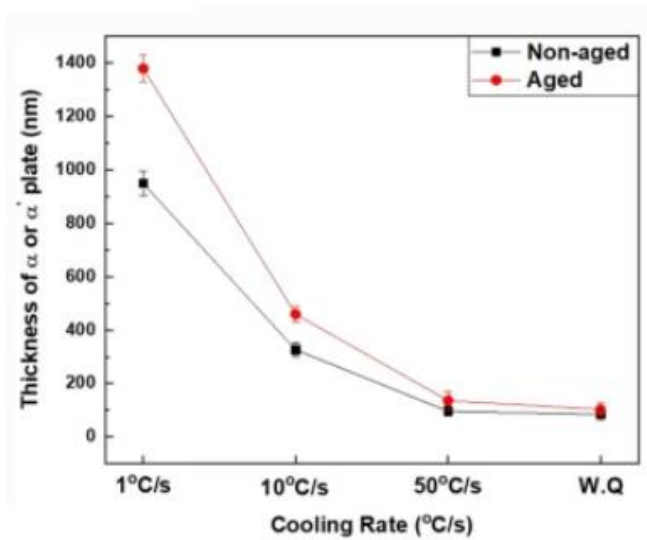
Figure 2. 19: Effect of cooling rate on α plate thickness [141].

So, parameter such as cooling rate, heat treatment and chemistry of the alloy plays an important role, for Ti6Al4V there seem to be a direct effect of these parameters on achieved microstructures features. affect the volume fraction and nature of α and β phase. So, it is possible to change phase composition and microstructure features by controlling these parameters [136],[139].

2.5.1. Lamellar microstructures achieved in conventional Ti6Al4V manufacturing

In conventional Ti6Al4V production, lamellar microstructure is achieved by following the process route shown in Figure 2. 20.
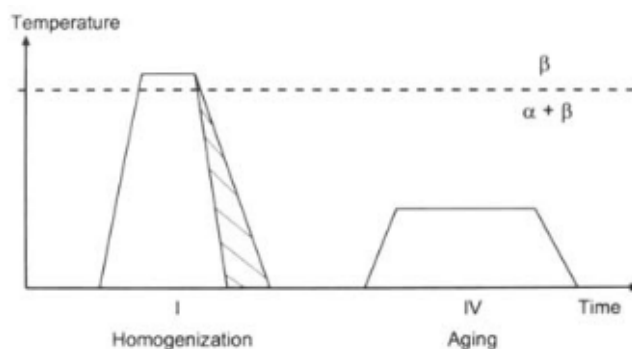
Figure 2. 20: process route for obtaining a fully lamellar microstructure[40].

According to Figure 2. 20, in order to achieve lamellar microstructure Ti6Al4V alloy has to undergo both homogenization and aging. Homogenization is to ensure that the entire alloy phase is β as it is heat treated above the β transus, then followed by slow cooling to achieve lamellar microstructure. The ageing process is to obtain further desired microstructure features. Normally, after the homogenization process and slow cooling lamellar microstructure is already achieved [93]. While slow

cooling rate (furnace cooling) leads to fully lamellar microstructure with coarse lamellar and large colony size, it is understood that coarse lamellar microstructure and large colony size affect negatively some mechanical properties such as elongation, and strength[96],[118],[142] [143]. In order to overcome this an additional ageing step is utilized, ageing process with the temperature range from 700 to 800°C is proposed control β grain size [118],[142].

The lamellar microstructure is characterized by alternating α lamellae and retained β phase between the α lamellae in a colony. Figure 2. 21 shows lamellar microstructure [144],[145].

Common recommended practice for heat treating Ti6Al4V above the β transus is to select a temperature 30 to 50°C above the β transus temperature this is because when heat treatment is conducted using a temperature more than 50°C above the β transus lead to growth of larger coarse β prior grain size [118],[143],[146].
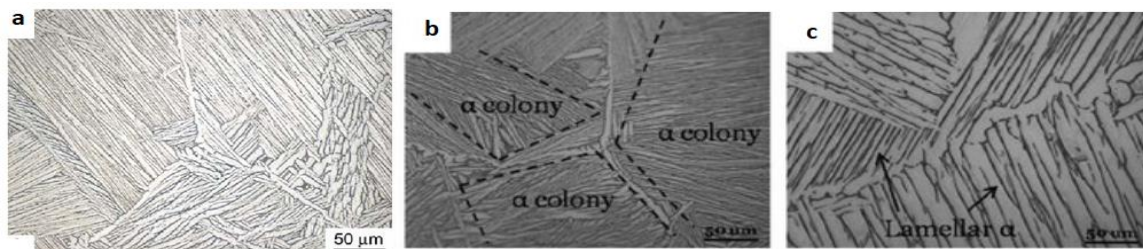
Figure 2. 21: Lamellar microstructure [144],[145].

Figure 2. 22 shows the effect of cooling rate on lamellar thickness and highlights one more time the importance of Cooling rate on microstructure features
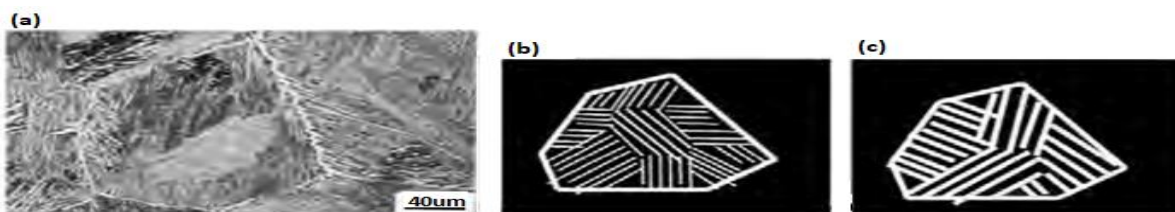
Figure 2. 22: cooling rate impact on thickness of lamellar (b) faster cooling rate, (C) slow cooling rate [147].

Figure 2. 22 (b) and (c) confirms that rapid cooling rate leads to thinner and shorted lamellar while slow cooling rate leads to thicker and elongated lamellar.

A very fast cooling rate above 410°C/s could lead to formation of martensitic microstructure. Through diffusion-controlled nucleation α phase nucleates from the β grain boundary till nucleation is complete. α plates nucleation from β phase follows the Burger's orientation relation that exist between β BCC and α HCP. This Burgers orientation relationship between α and β phases is shown in in the equation below [148]:

$$\{0001\}_\alpha \| \{110\}_\beta \;\; and \;\; \langle 11\overline{2}0 \rangle_\alpha \| \langle 111 \rangle_\beta \tag{2.1}$$

Figure 2. 23 shed light on the effect α colony size (slip length) on the mechanical properties. Lamellar size, retained β size, and other microstructural features are depending on cooling rate and effect of cooling rate on lamellar thickness is shown in Figure 2. 22 (b) and (c), it can be observed that in Figure 2. 22 (b), as a result of faster cooling both lamellar thickness and colony size are smaller ore less compared to lamellar thickness and colony size in colony size in in Figure 2. 22 (c) where slow cooling is applied. So, Figure 2. 23 not only present the effect of colony size (slip length) to several mechanical properties in lamellar microstructure but also can be correlated to cooling rate as faster cooling rate leads to less coarse lamellar and smaller colony size while slow cooling rate leads to coarse lamellar and large colony size.
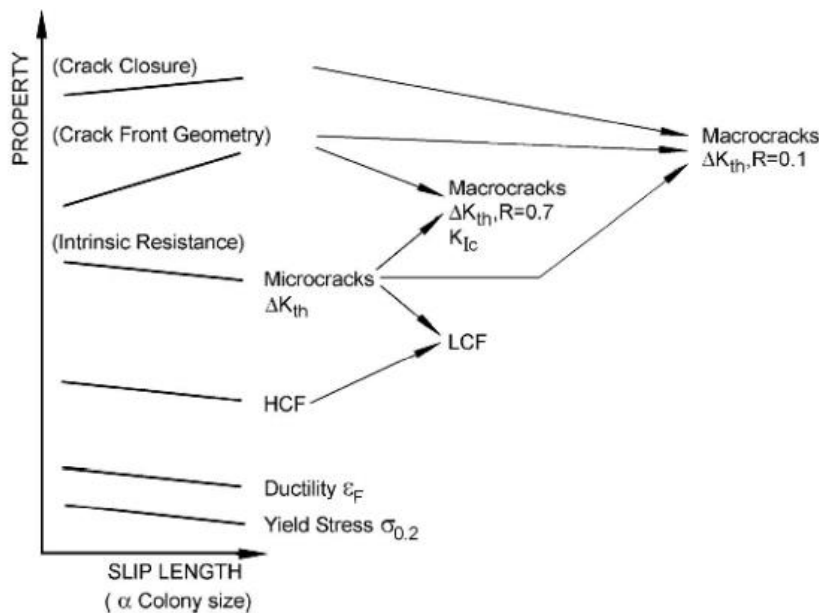
Figure 2. 23 : Dependency Ti6Al4V alloy mechanical property on the α colony size [87].

To achieve best possible microstructural features combination and ameliorate mechanical properties shown in Figure 2. 23 the best possible cooling rat sequence has to be selected [87], [96].

2.5.2. Bi-Modal microstructures obtained in conventional Ti6Al4V production

During convention Ti6Al4V production bi-modal or duplex microstructure is achieved by following the process flow shown in Figure 2. 24.
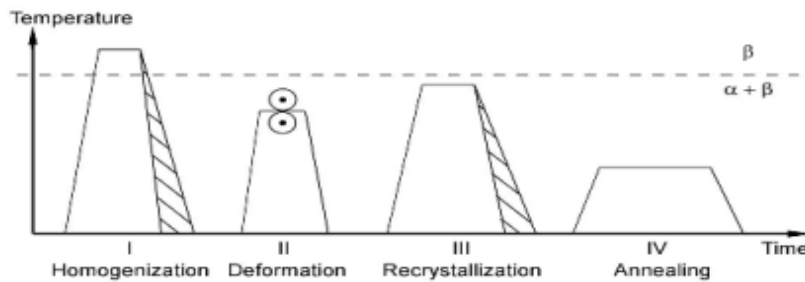
Figure 2. 24: Thermo-mechanical process for achieving bi-modal microstructure in Ti6Al4V [40].

Unlike in lamellar microstructure that was consist of alternating α plats with retained β, Bi-modal microstructure comprises primary $α_P$ phase grains in transformed β matrix (β trans) as shown in Figure 2. 25 [149].
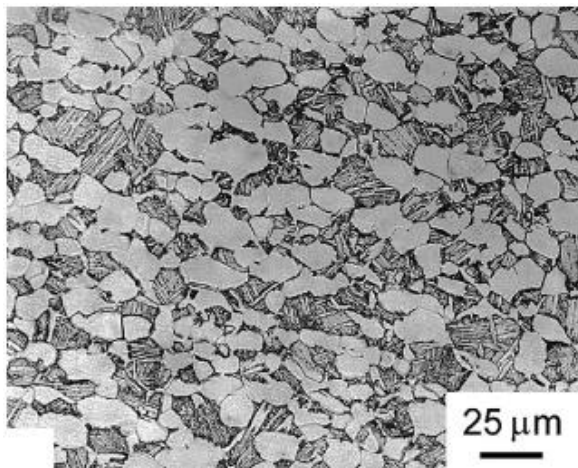
Figure 2. 25: Bi-modal microstructure Ti6Al4V [149].

Steps involved in production of bi-modal microstructure shown in Figure 2. 24. Are:

- Homogenization,
- Deformation,
- Recrystallization, and
- Annealing.

Homogenization stage is characterised by heat treating the alloy above the β transus temperature then cooled. As in the case of lamellar microstructure the cooling rate plays a very important role as well in in bi-modal as it is the controlling factor in determining the width (size) of α lamellar [40],[87],[118].

Deformation stage is carried out utilizing temperature below β transus in the α+β zone. During the deformation stage crystallographic texture is formed. It is reported that parameters that plays important role in deformation are deformation temperature, the level of deformation and type of deformation.

Like deformation recrystallisation stage is as well conducted using a temperature (recrystallization temperature) below the β transus in the α+β zone, the recrystallization temperature plays important role. during this stage the recrystallization temperature referred to as solution heat treatment is used, this temperature plays an important role the primary α_P volume fraction in bi-modal microstructure [40],[87]. Studies have shown that primary α_p volume fraction improves crack nucleation (HCF strength) resistance in bi-modal samples [142],[149].   The final stage in achieving bi-modal microstructure in conventional Ti6Al4V production according to Figure 2. 24 is annealing or ageing stage. During heat treatment annealing stage contribute to improvement of microstructures features and therefore improves mechanical properties [142],[149].

Higher strength and ductility compared to lamellar and equiaxed microstructure have been reported in bi-modal microstructure [118].
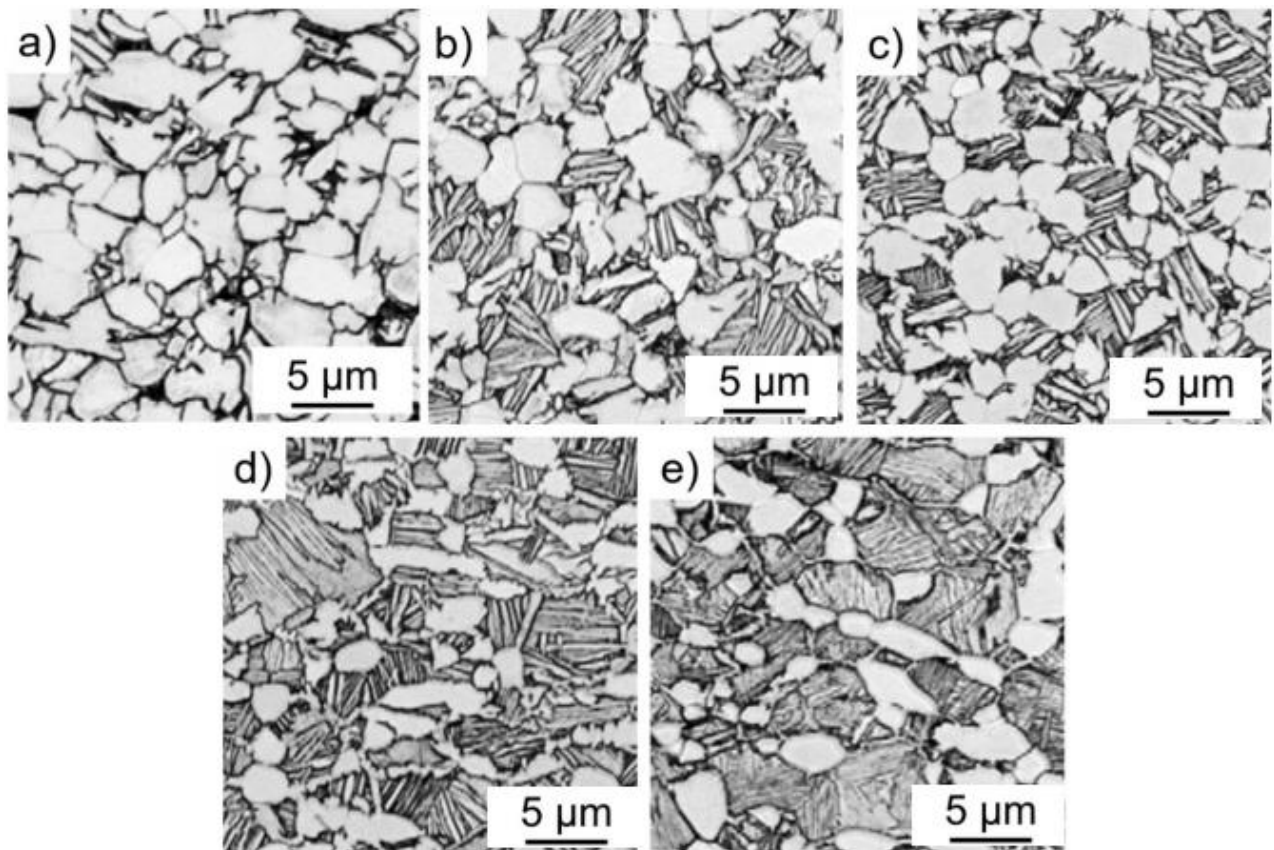
Figure 2. 26: Effect of cooling rate on bimodal microstructure a) 10°C/min; b)30°C/min; c) 40°C/min; d) 100°C/min; e) 300°C/min [150].

Figure 2. 26 shows the effect of cooling rate on bi-modal microstructure with different cooling rate selected where a) 10°C/min; b) 30°C/min; c) 40°C/min; d) 100°C/min; e) 300°C/min. It can be seen that at 10°C/min the phase present seems to look like equiaxed microstructure due to the fact that there is higher thickness and volume fraction of primary α_P, however when the cooling rate starts to increase

30, 40, 100 and 300°C/min the primary α_P volume fraction and thickness is decreasing there is more pronounced retained β as well. This is similar to the observed phenomenon in lamellar microstructure where the cooling rate also plays avital role.

Table 2. 5 shows process steps that affect finial microstructure and mechanical properties in Ti6Al4V. This table is not an exhaustive list of parameters because there are many other aspects that affect microstructures and mechanical.

Table 2. 5: Processing steps impacting microstructure and mechanical properties [49].

Processing steps affecting finial microstructure feature and mechanical properties
Cooling rate
Deformation temperature
Deformation mode
Deformation degree
Recrystallization temperature
Ageing temperature
Ageing time

Table 2. 6 shows different microstructure (lamellar, bi-lamellar, bi-modal, and equiaxed) steps (When these steps are modified) followed in alloy processing to achieve these microstructures during Ti6Al4V manufacturing, important processing parameters that impacts these microstructures and the mechanical properties affected by these processes [49]. These process parameters affect the microstructures which in return affect mechanical properties. For instance, when slow cooling rate leads to coarse lamellar microstructure while faster cooling rate leads thinner lamellar microstructure. As it was already pointed out in Figure 2. 23 increase α colonies size decreases some of the mechanical properties. So, key factors shown in Table 2. 6 affect several mechanical properties through microstructure. Studies have shown α lamellae thickness, the width of α layers, α colony size and the β grain boundaries are affected by cooling in Ti6Al4V production [118]. So, the cooling rate, ageing time, and may other key parameters have shown in Table 2. 6 contributes to final mechanical properties observed in Ti6Al4V alloy.

Table 2. 6: Microstructure and steps utilised to achieve them important parameter microstructures features and affected mechanical properties [49].

Microstructure	Stage	Key factors	Microstructural features	Mechanical properties
Lamellar	I	Cooling rate	Large β grain size α Lamellae size colony size GB α-layer	Yield stress Fracture strain High cyclic fatigue microcracks macrocracks Fracture toughness Creep
	IV	Aging Temp	Ti$_3$Al in α Secondary α in β	
Bi-modal	**Step**	**Important parameters**	**Microstructural features**	**Mechanical properties**
	I	Cooling rate	GB α-layer Width of α Lamellae ($\rightarrow$ αp Size)	N. A
	II	Temperature Deformation Deformation mode Deformation degree	Texture type -Texture Intensity - Dislocation Density Texture Symmetry	N. A
	III	Recyst temperature Recyst time Cooling rate	- αp Vol% -($\rightarrow$ β Grain Size) -Alloy Element Partitioning -α lamellae size -colony size -Width of α Lamellae -GB α-layer	HCF Creep Creep strength 0.2% Fracture strain High cyclic fatigue Da/dan microcracks Fracture toughness Creep
		Recyst time Cooling rate	-α lamellae size -colony size -Width of α Lamellae -GB α-layer	Yield strength Fracture strain High cyclic fatigue Da/dan microcracks Fracture toughness Creep
	IV	Aging (Annealing) temperature	Ti3Al in α Secondary α in β	N. A

2.5.3. Equiaxed microstructures

Equiaxed microstructure is shown in Figure 2. 27. As a microstructure, it contains entirely α phase having roughly the same size in equiaxed grains forms with β phase at the grain boundary described as "triple points" as shown in in Figure 2. 27.
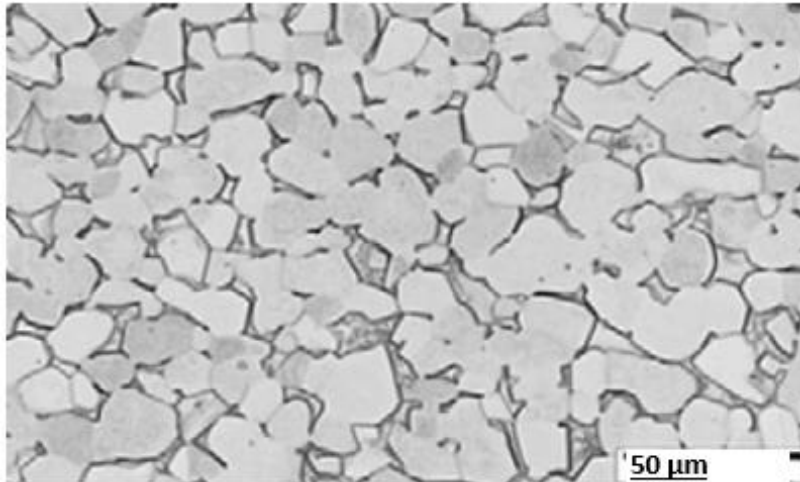
Figure 2. 27: Fully equiaxed microstructure [151].

One of the routes used to produced equiaxed microstructure is to start with a sample or components having lamellar microstructure, then this sample undergoes annealing step in which recrystallization takes place by heat treating to a temperature below β transus. In fact, this is a very important step as it affects volume fraction primary α [118]. Equiaxed microstructure is α dominant with retained β and the α grain size largely determines its mechanical properties because the slip length is determined by the α grain size, as such the mechanical properties of equiaxed microstructures are also affected by the slip length as well as it was for the case of lamellar microstructure and shown in Figure 2. 27. Equiaxed microstructure has been linked with good ductility and higher strength but also low fracture toughness [118].

2.5.4. Achieving bi-Lamellar microstructures in conventional Ti6Al4V process

Bi-lamellar microstructure is developed as a response to overcome some of mechanical shortcomings of lamellar microstructure. This is because lamellar microstructure in Ti-6Al-4V have rather low fatigue strength which can be explained by the fact that mechanical properties of lamellar microstructures in general are dependent on affect the slip length which depend on α colony size as shown in Figure 2. 23 it can be seen that numerous mechanical properties are positively and negatively affected by the slip length. As the slip length increases the crack resistance, fatigue strength decreases. To surmount mechanical properties problems associated with slip length in lamellar microstructure, the slip length has to be reduced. Production of bi-lamellar microstructure through series of heat treatment is one of the solutions use in order to overcome the mechanical shortcomings of lamellar microstructure [49].

Bi-lamellar microstructure in conventional Ti6Al4V manufacturing can be achieved by following the process flow shown in Figure 2. 28.
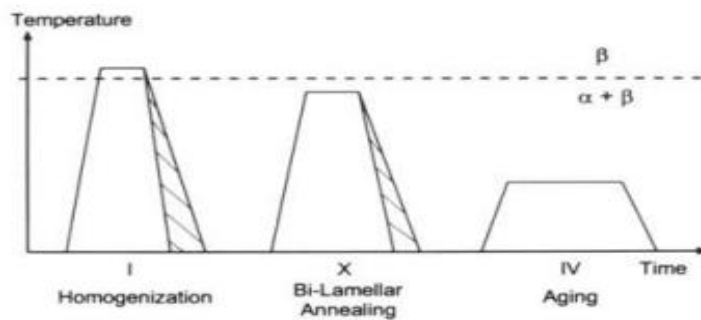
Figure 2. 28: Process flow achieving bi-lamellar microstructure [40].

So, in the first stage the samples are heat treated above the β transus then slowly cooled (preferably furnace cooled), at this point the obtained microstructure is coarse lamellar. Then in the second stage the samples are heat treated below β followed by slow cooling rate as well, literatures have suggested cooling rate not lower than 17°C/min [49].   This is because when the alloy us cooled below 17°C/min there will be lamellar microstructures formed instead of bi-lamellar.
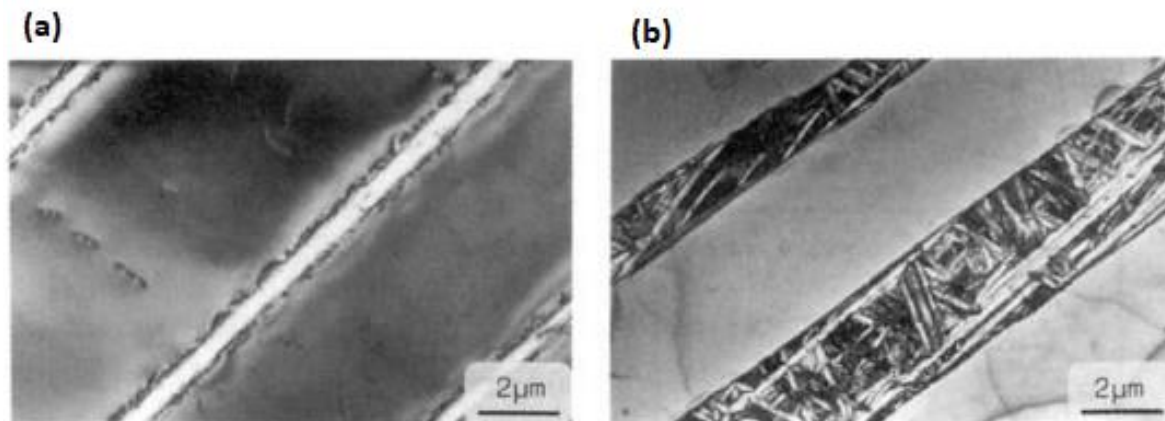
Figure 2. 29: Lamellar (a) and bi-lamellar microstructure (b)[49].

When looking at Figure 2. 29 shows (a) lamellar microstructure (b) bi-lamellar microstructure. Lamellar microstructure visually is characterized with α lamellar surrounded by retained β, while bi-lamellar microstructure is characterized by is characterized by primary α_P, transformed β and secondary α_S. The primary α_P are not as coarse as the α phase in lamellar microstructure this is because during the second stage heat treatment as the samples is heat treated and as the temperature increase the α phase decrease while β phase increases and as the cooling commence the β phase is then again reduced and the secondary α_S nucleates. Formed secondary α_S serves as a barrier due to the fact that they have random orientation. Compared to lamellar microstructure where there is only retained β.

When looking at Figure 2. 30 compared the effect of cooling rate on a) yield strength, b9) HCF, c) ΔK. It can be seen that as the cooling rate increases bi-lamellar microstructure yield strength increases, HCF increases as well, and ΔK increases as well while the elongation in a) decreases [49]. This due to the fact that the hardened β "lamellae" in the bi-lamellar structure act as valuable barriers to slip transfer, additionally the strength and the volume of hardened β "lamellae" increases with fast cooling rate [49].
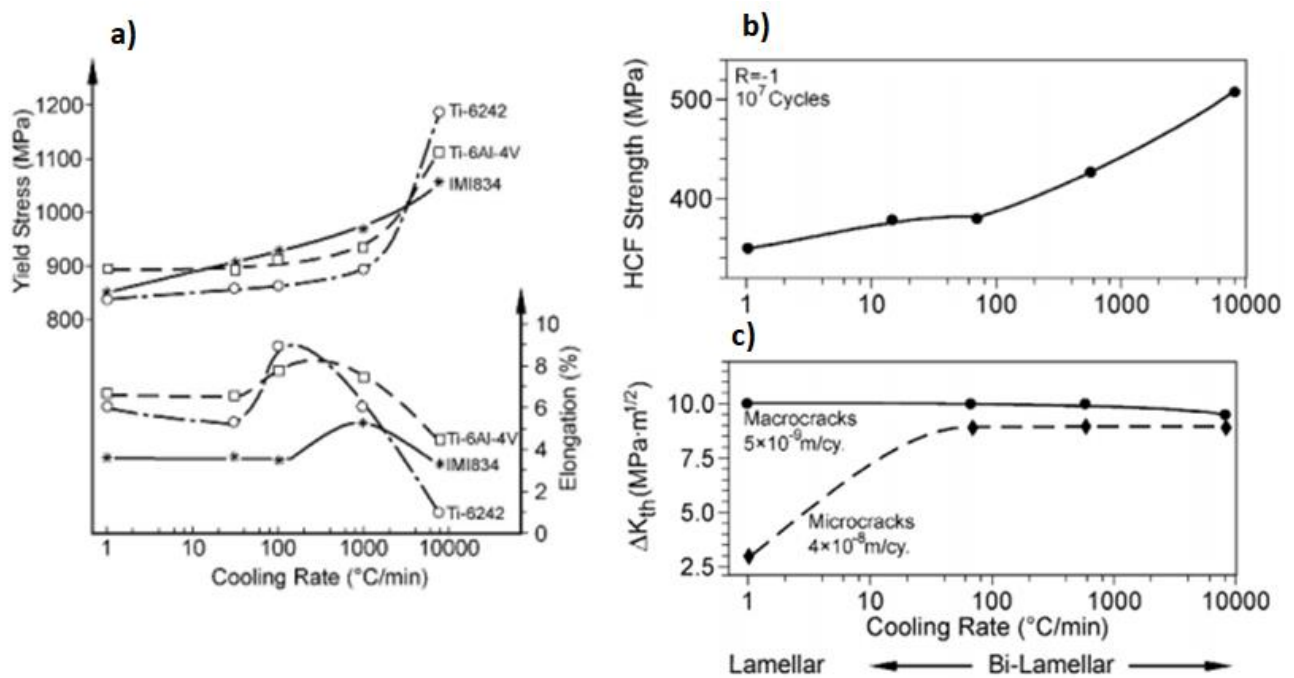
Figure 2. 30: Effect of cooling rate on a) yield strength, b) HCF strength, c) ΔK.

Figure 2. 30 above compares the effect of cooling rate on yield strength and elongation of Ti6Al4V, Ti6242, and IMI84 titanium alloys. It can be seen that when the cooling rate increases the yield strength increases while the elongation decreases. It is important to highlight that the increase in elongation seen in figure30 is the result of decreased in slip length [49].

2.6. Heat treatment of Ti6Al4V in conventionally production.

heat treatment is the heating up of a material (metal) to a specific selected temperature below its melting point then cooling it. The process is done to alter metal microstructure, to improve it physical and mechanical properties. Current technological advancement allows heat treatment of metal to be done in various types of furnaces in different atmosphere using various inert gases.

Applications of heat treatment in metal industries varies from phase transformation to improvement of several mechanical properties. Some of usages of heat treatment in metal industry is shown in Figure 2. 31 [152]–[154].

Figure 2. 31:Use of heat treatment in metal industry [152]–[154].

Heat treatment can be done in thermally using sets temperature in furnace or thermos-mechanically in a process where simultaneous combination of heat and mechanical force such as in the case of hot isostatic pressure machine, hot-forging quenching machines and many other equipment utilized in thermos-mechanical metal treatment process. Either way (thermal, thermo-mechanical) after being heated the material have to be cooled.

Several cooling technics are utilized after material heat treatment, required properties governs the cooling process as the cooling medium and technic plays an important role on microstructures features and mechanical properties. Materials can be:

- Furnace cooled,
- Air cooled,
- Water quenched and
- in some extent oil is utilized as cooling medium.

In this literature section the influence of heat treatment, cooling rate and cooling mode on Ti6Al4V microstructure and mechanical properties will be covered.

2.6.1. The effect of heat treatment on Ti6Al4V microstructure

Several studies have been conducted on the effect of heat treatment (effect of temperature, residence time, cooling rate) on microstructure and mechanical properties (hardness, tensile, toughness, fatigue, etc.). This is because Ti6Al4V microstructure is of great importance to the mechanical properties observed this alloy. Hence, the numerous amount of researches conducted on   establishing the relationship between heat treatment, microstructure and mechanical properties [136],[139] [140].

greatly affected by heat treatment and colling rate. Several research have been conducted to address the effect of heat treatment on microstructure [136],[139] [140].

Heat treatment parameters such as temperature, cooling rate and selected ageing time plays important role in the final microstructure composition and mechanical properties. The residence time from time to time referred to as ageing time is the time spent by samples in the furnace during heat treatment, it has an impact on microstructure and eventually also affect the mechanical properties.

Gil *et al* [155] conducted research on effect of cooling rate on microstructure and mechanical properties of Ti6Al4V. The result of impact of temperature and ageing time on grain size obtained Gil *et al* [155] shown in Figure 2. 32 where residence time is plotted (x-axis) vs the grain size (y-axis). The obtained result of grain size was group by ageing temperature 1050, 1100, 1150, and 1200°C respectively.
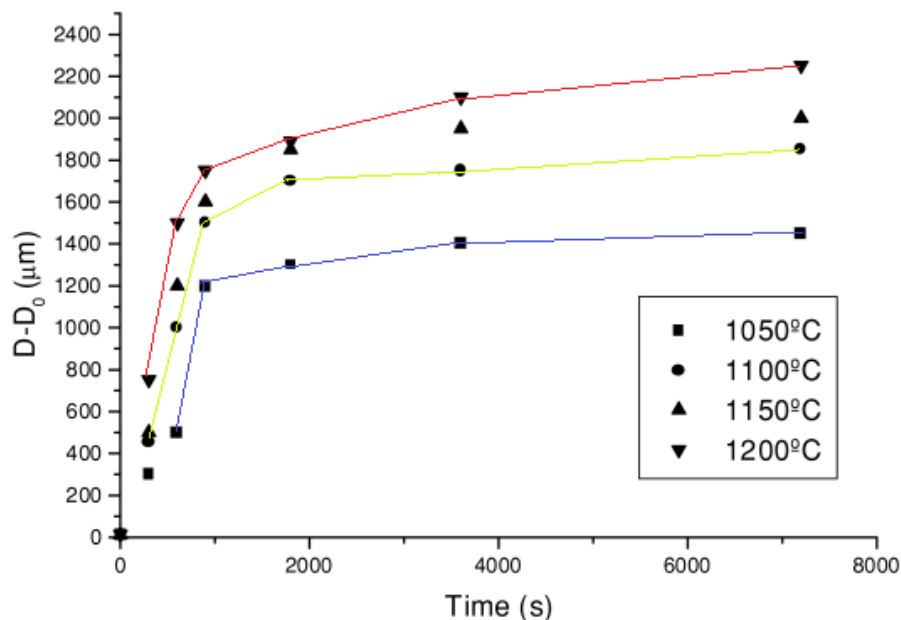
Figure 2. 32: Impact of heat treatment selected temperature and residence time on grain size [155].

It was observed that [155]:

- For samples heat treated at the same temperature, as the ageing time increases there is an increase in grain size. At start there is a very higher increase in grain size, and then the grain size growth is very slow very slow this is observed for all the temperature groups. The slow grain growth observed was attributed to the decrease in grain boundary area per volume ratio that is cause by grain size increase. This implied that there was a decrease in grain boundary interfacial energy per unit volume hence the slow observed or decrease in grain growth.

- When the same ageing time 4000s is considered for samples heat treated at different temperature, it can be seen that for different temperature there is different grain size, so as the temperature increases the grainsize also increase.

Finer grain size contributes to increase strength, ductility decreases, coarse grain size has been reported to have good creep properties. Heat treatment temperature, cooling rate and ageing time selection pays major role in final microstructure and mechanical properties.

Seo *et al* [156] conducted a study on the effects of mill annealing temperature on the microstructure and Hardness of Ti-6Al-4V Alloys. The result of this study showed that average grain size α, α and β increased with temperature as shown in Figure 2. 33. This is in a way similar to the finding obtained by Gil *et al* [155].
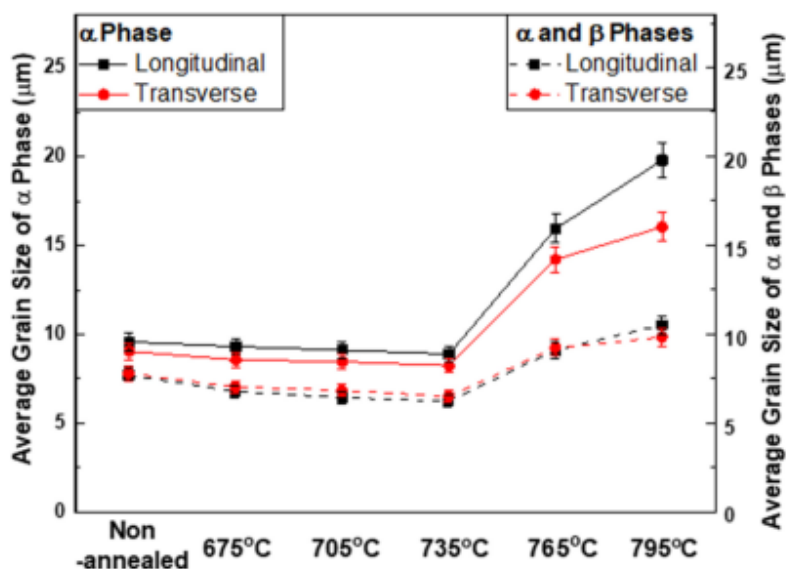
Figure 2. 33: Average grain size of α and α + β phases as a result of mill-annealing temperatures [156].

Shaikh *et al* [157] conducted research on effect of temperature and cooling rate on Ti6Al4v morphology where 3 different types of heat treatment temperature were selected and in each heat treatment approach samples were water quenched (WQ), air cooled(AC) and Furnace cooled (FC) as shown in Figure 2. 34 .
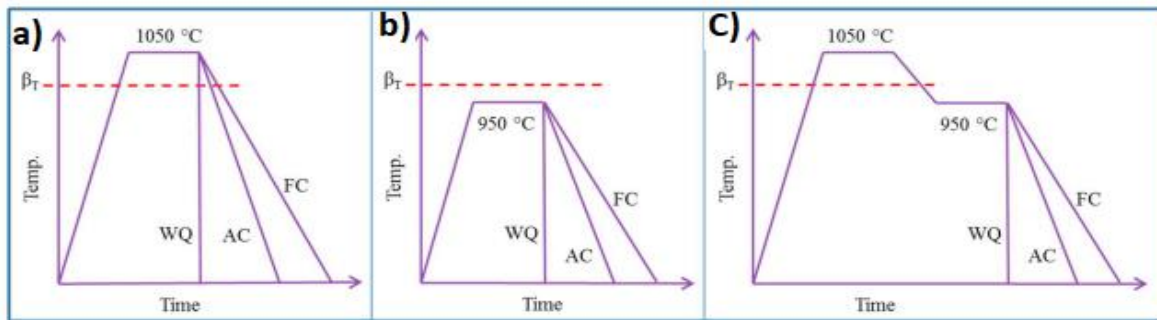
Figure 2. 34: Heat treatment strategy a), b), c) [157].

The first heat treatment approach in Figure 2. 34 .a). is conducted using a temperature of 1050°C, which is above the β transus. The obtained microstructure as a result of the effect of heat treating above the β transus, and utilizing 3 different cooling rates viz. WQ, AC, FC are shown in Figure 2. 35. Even though these samples were heat treated above the β transus, the cooling rate resulting from the cooling technique leads to microstructural difference. So, after heat treating above the β transus then followed by water quenching, there was formation of martensitic microstructure consisting of α' and transformed β shown in Figure 2. 35. (a-b) are martensite consisting of α' in transformed β, while the observed microstructure after air cooling shown in Figure 2. 35. (c-d) are fine lamellar microstructure consisting of fine α, and transformed β, and the observed microstructure after furnace cooking shown in Figure 2. 35 (e-f) are coarse microstructure due to slow furnace cooling [157].

The second heat treatment method was done using the temperature of 950°C below the β transus following the approach shown in Figure 2. 34 .b) [157]. It was noted that after-water quenching microstructure consisted of a mixture α', α lamellae and transformed β as shown in Figure 2. 36. (a-b), the microstructure obtained after air cooling included a duplex like microstructures containing α_P, lamellae α and transformed β as shown in Figure 2. 36. (c-d), and the microstructure obtained through furnace cooling was composed of primary equiaxed α, thin lamellae, and intergranular β [157].

The third heat treatment method was conducted at 1050°C then furnace cooled until 950°C then heat treated again at 950° C then samples were cooled following the same cooling technic WQ, AC, FC.

The obtained microstructures are shown in shown in Figure 2. 37. The WQ result shown in Figure 2. 37. (a-b) is composed of by α' and short or disconnected α lamellae. In the case of air cooling shown in Figure 2. 37. (c-d) the microstructure was characterized by thin α retained β. After furnace cooling, the obtained microstructure shown in Figure 2. 37.(e-f) were characterized by coarse lamellar microstructure.
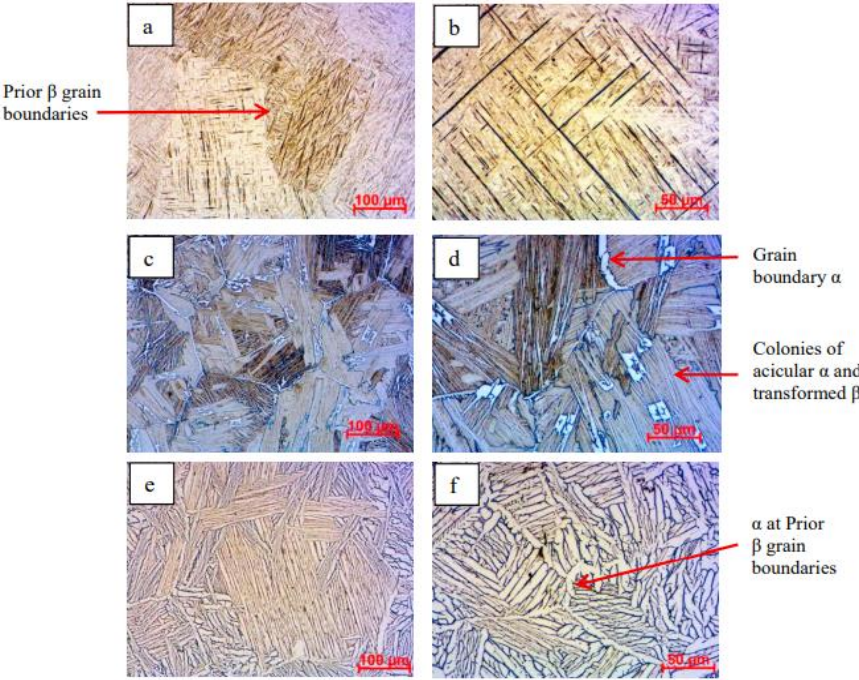
Figure 2. 35: First heat treatment approach, effect of heat treatment and different cooling rate (a- b) WQ, (c-d) AC, (e-f) FC [157].
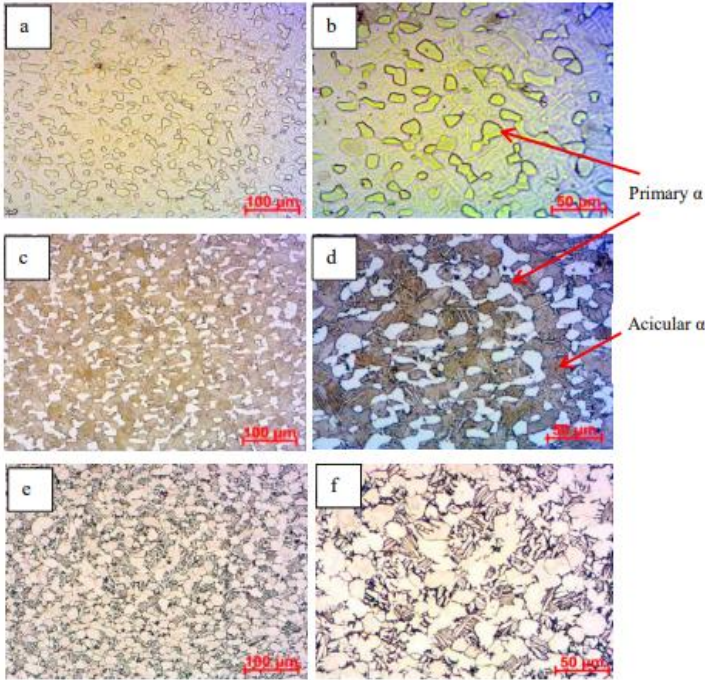
Figure 2. 36: Second heat treatment approach, impact of heat treatment and different cooling rate (a- b) WQ, (c-d) AC, (e-f) FC [157].
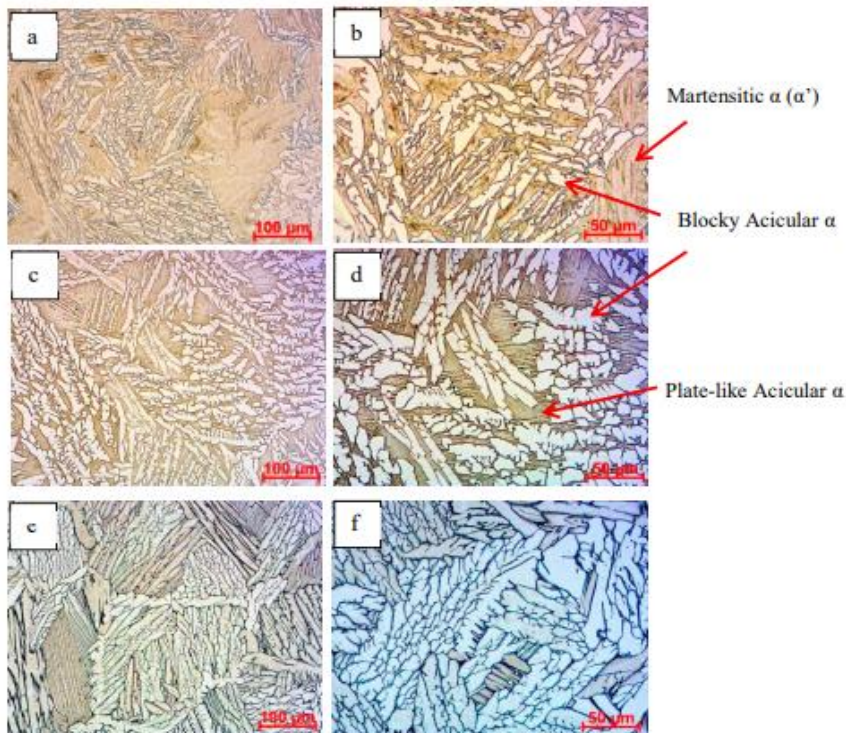
Figure 2. 37: Second heat treatment approach, impact of heat treatment and different cooling rate (a- b) WQ, (c-d) AC, (e-f) FC [157].

Studies conducted by Shaikh *et al.* [157] and results shown in Figure 2. 35, Figure 2. *36*Figure 2. 37 shows clearly the effect of selected heat treatment temperature (heat treating above, below, β transus), cooling rate (water quenching, air cooling and furnace cooling) on the resulting microstructure. In all the heat treatment process whether it was conducted above or below the β transus in a one or two stage heat treatment once the samples were subjected to water quenching as cooling rate, the resultant microstructure was composed of martensitic needle surrounded by prior β [157]. When air cooling was utilized in all the heat treatment lamellar microstructure was achieved. The obtained lamellar microstructures were different due to the different heat treatment temperature utilized. Samples that were furnace cooled were characterized by coarse grains.

Similar studies were conducted by Müller *et al.* [158] on the effects of Supra and Subtransus heat treatment (using temperature above and below β transus for heat treatment) on fatigue performance of hot rolled Ti6Al4V. In this study, hot rolled through Ti6Al4V plates were heat treated following 3 different heat treatment approach as shown in Figure 2. 38 with as purpose to achieve fully lamellar (FL), equiaxed (EQ), and duplex microstructures. These different selected heat treatment temperature for these studies are shown in Figure 2. 38.

In all the 3-heat treatment approach, two different cooling methods were utilised, air cooling, and water quenching.

In the first heat treatment approach selected for achieving fully lamellar microstructure (FL) two stage heat treatment were utilised, the first stage heat treatment was conducted at the temperature above the β transus of 1050°C for 1 hour then cooled, after cooling, samples were subjected to the second stage heat treatment samples were heat treated at 800°C then cooled. In the second heat treatment approach utilised to attain equiaxed microstructure (EQ), samples were also subjected to two stage heat treatment. The first stage was conducted using a temperature below β transus of 950°C for 1 hour, followed by slow furnace cooling at 2.5°C/min to 800°C, then heat treated at 800°C for 1 hours then cooled. In the third and last heat treatment approach utilised to get duplex microstructure (D) samples were as well subjected to two stage heat treatment. The first heat treatment was conducted below β transus at a temperature of 950°C for 1 hours then cooled, after that these samples were heat treated at 800°C then cooled. For all of these treatment approaches samples were air cooled, and water quenched [158] as shown in Figure 2. 38.
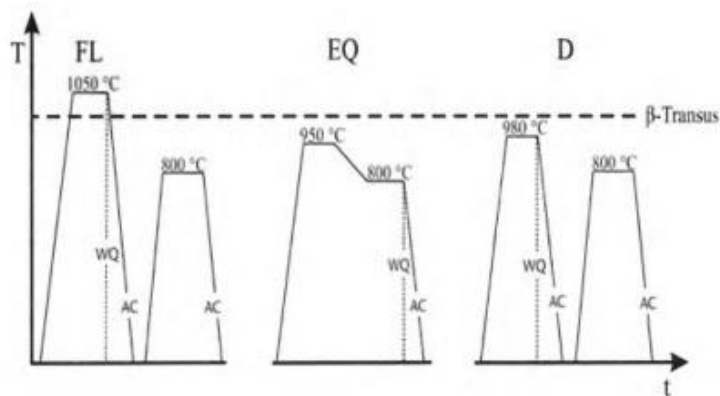
Figure 2. 38: Heat treatment approach for achieving virous microstructure[158].

The observed results of the study conducted by Müller *et al.* [158] are shown in Figure 2. 39, these results showed that in all the heat treatment approaches first fully lamellar (FL), and third duplex (D) when water quenching was utilized the there is an observed difference in microstructure features. Water quenched samples had thinner while air cooled samples from first fully lamellar (FL), and third duplex (D) approach where characterized by coarser microstructure as shown in [158].

However, there was not visual observed or measured difference of phase thickness in samples having equiaxed microstructure for water quenched and air-cooled samples achieved during second heat treatment approach (EQ). Studies conducted by Müller *et al.* [158] highlight the importance of selected heat treatment temperature and cooling rate on achieved microstructure features.
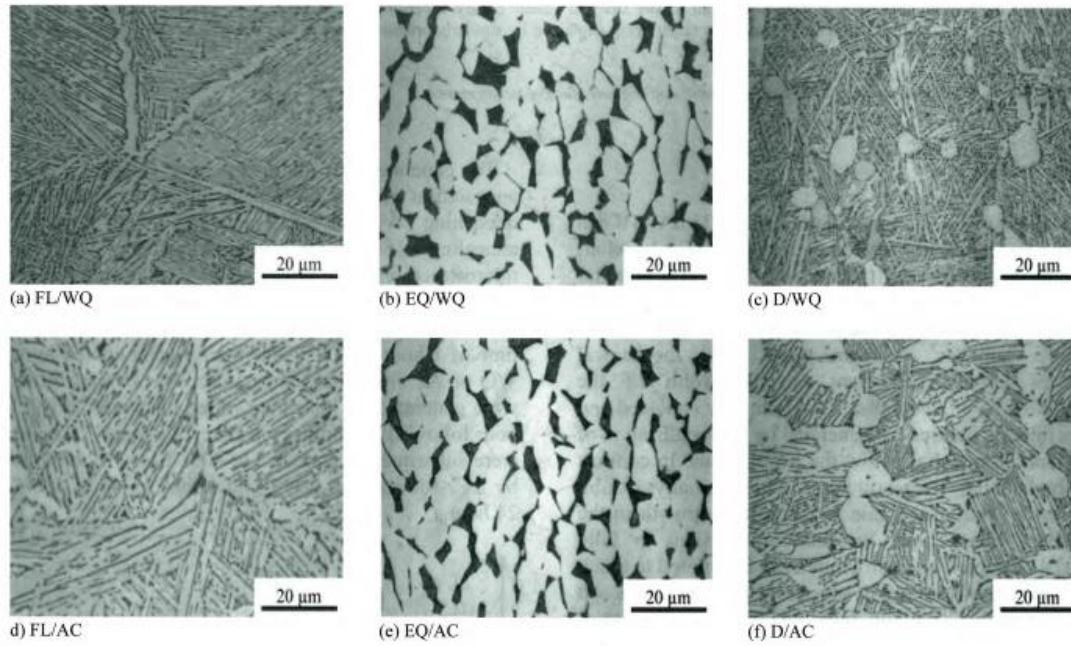
Figure 2. 39: Obtained microstructure after different heat treatment and cooling rate [158].

Several studies have been conducted and modelled on the effects of heat treatment temperature and cooling rate on resulting microstructures. Research conducted by Woo *et al*. [159] on cast Ti6Al4V, and studies conducted by Pinke *et al*. [160] on heat treatment of casted Ti6Al4V alloy are of similar nature. Figure 2. 40 shows the results of different types Ti6Al4v microstructures that were attained by Pinke *et al*. [160] through various heat treatment temperature.
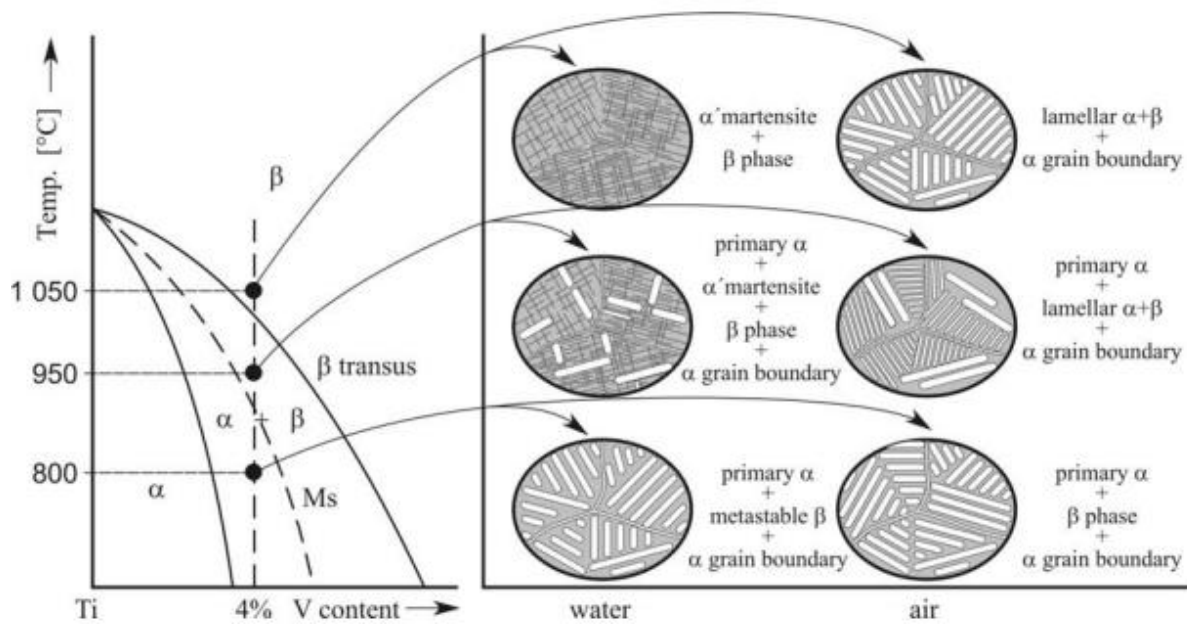
Figure 2. 40: Effects of heat treatment temperature and cooling rate on obtained microstructure [160].

These studies were conducted on effects of heat treatment (solution and ageing treatment) on cast Ti6Al4V for microstructural transformation and mechanical properties improvement. Woo *et al*. [159] studied the effects of heat treatment temperature (1000, 950, and 900°C) and cooling rate (water quenched and air cooling) on the microstructure of casted Ti6Al4V and correlated these result to change in volume fractions of α and β stabilizers as a result of temperature. Similarly, Pinke *et al*.[160] compared the effects of heat treatment temperature (1050, 950, and 800°C) and cooling rate (water quenching and air cooling) on microstructure . In both of these studies (conducted by Pinke *et al*. [160] after solution treatment samples were subjected to ageing treatment t 500°C followed by air-cooling.

When water quenching was used the attained results in Figure 2. 40 showed that [160]:

- ❖ When samples were heat treated above the β transus to a temperature of 1050°C followed by water quenching, the formed microstructure constituted of martensitic microstructure in β.

- ❖ When samples were heat treated at 950°C which is below the β transus followed by water quenching, the obtain microstructure was composed of martensite, primary α, presence of β phase and α grain boundary. The presence of α phase is due to the fact that the heat treatment was conducted in the α+β region, unlike the heat treatment conducted above the β transus (1050°C) where the difusionless transformation takes place and martensite is formed

- ❖ Samples heat treated and 800°C then water quenched resulted in microstructure containing primary α, metastable β, and α grain boundary. This solution treatment of cast Ti6Al4V was carried out in the α+β and at a temperature near the α phase, so even though the sample were water quenched the formed microstructure is a lamellar microstructure.

When air cooling was utilized as a cooling method after heat treatment the obtained result showed that:

- ❖ Sample heat treated above the β transus (1050°C) were air cooled, lamellar microstructure with α grain boundary was formed in Ti6Al4V, unlike in the case of water quenching where acicular martensite was formed for the same heat treatment temperature but different cooling method,

- ❖ Sample heat treated at 950°C were composed of primary α lamellar α+β and retained β and α grain boundary. While at this temperature when samples were water quenched there was martensite present in the sample microstructure.

- ❖ Samples heat treated at 800°C were air cooled, primary α, β phase and α grain boundary.

For the same heat treatment temperature, there are observed difference between microstructure obtained from water quenched and air-cooled method.

The observed results highlight the impact of heat treatment selected temperature, and cooling mode on final achieved microstructure.

Finally, to close the topic of effect of heat treatment and cooing rate on microstructure, study conducted by Janovic´ et al. [161] on the effect of heat treatment and cooling rate on microstructure of investment casting will be discussed. In this research, as-casted samples having the microstructure shown in Figure 2. 41 [161] were heat treated using different temperature.
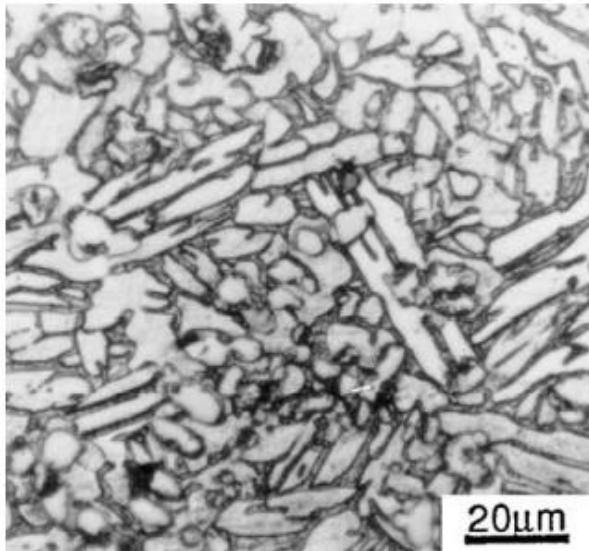
Figure 2. 41: As-cast Ti6Al4V [161].

Table 2. 7: Selected heat treatment temperature and ageing time [33],[161],[162].

Time (Hour)	Temperature °C				
1	800	850	900	1000	1050

The as-cast Ti6Al4V samples were annealed using temperature shown in Table 2. 7 for 1 hour in an argon atmosphere furnace. Samples were then cooled using furnace cooling, air cooling and water quenching.

1. Effect furnace cooling rate on microstructure:

The effects of furnace cooling can be observed in Figure 2. 42. It can be seen that for the same cooling rate, the higher solution treating temperature results in thicker or coarse microstructure [161]. So, increasing order, as the temperature increases from 800 to 1100°C, the thickness of α phase present increases as well. So, it can be seen that microstructure obtained from air cooling from 1100°C shown in Figure 2. 42 (a) has thicker microstructure then 950°CFigure 2. 42 (b), while 950°C has coarse microstructure or thicker lamellae in microstructure obtained through furnace cooling compared to 800°C Figure 2. 42.(c) [161],[162].
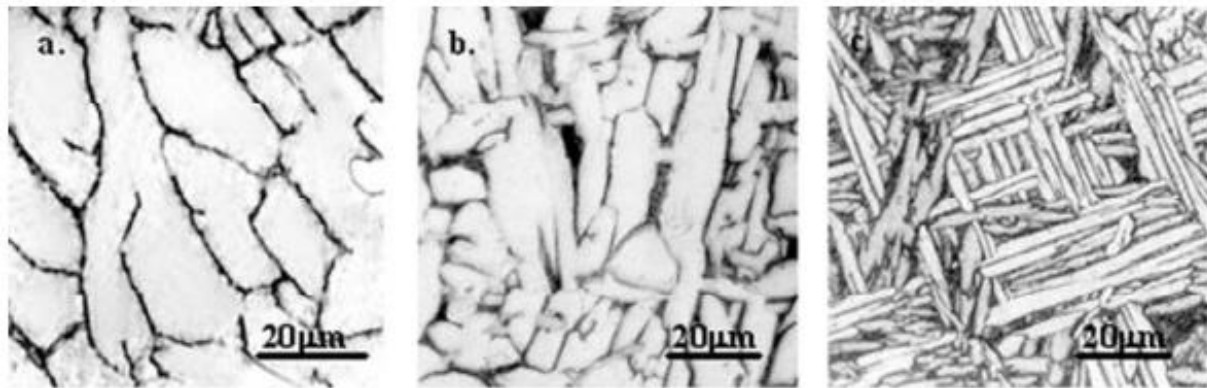
Figure 2. 42: Effect of furnace cooling from microstructure while cooling from different temperature (a) 1100 °C; (b) 950 °C; (c) 800 °C [161],[162].

2.   Effect of water quenching on microstructure:

Effect of water quenching as a cooling mode on the microstructure can be seen in Figure 2. 43. There is presence of martensite microstructure obtained from water quenching regardless of the annealing temperature [161],[162]. The microstructure obtained after annealing temperature of 1100°C followed by water quenching is characterized by completely by martensite, while the microstructure obtained after annealing temperature of 950°C followed by water cooling is characterized by a combination of α, and β phase and also the presence of martensite. Microstructure obtained after annealing temperature of 900°C followed by water quenching was of similar nature to the microstructure obtained at 950°C. Because it was characterized by higher volume of α phase, while having β phase present and martensite as well.

Figure 2. 43: Effect of water quenching on microstructure of Ti6Al4V heat treated at different temperature (a) 1100°C, (b) 950°C, (c) 900°C [161], [162].

3.   Effects of air cooling on microstructure:

Three different annealing temperature were utilised 1100, 1050 and 950°C, after which sample were air cooled after and the effects of air cooling on microstructure, can be seen in Figure 2. 44.
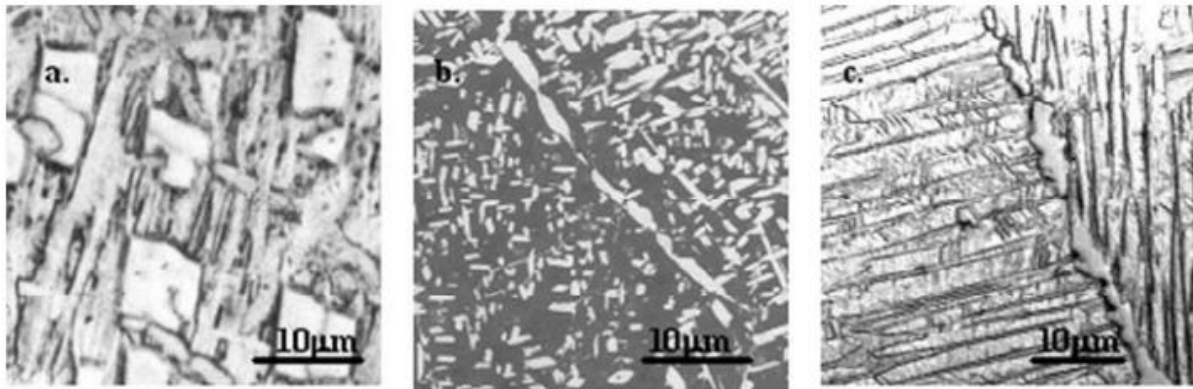
Figure 2. 44: Effects of air cooling rate on microstructure of Ti6Al4V heat treated (a) 1100, (b) 1050°C, (c) 950°C [161],[162].

Microstructure obtained after air cooling are different then microstructures obtained through water quenching. As, microstructure obtained after water quenching were characterized by martensitic microstructure. In the air-cooled samples at 1100°C Figure 2. 44 (a) there is presence of acicular α_{AC} in β matrix, and there is also presence of square or rectangular particle observed in the microstructure obtained after air cooling from 1100°C.[161],[162]. Obtained microstructure from air cooling from 1050°C is shown in Figure 2. 44 (b), this microstructure is characterized by β matrix illustrated by dark field, which has been transformed to α_{AC} and there is primary α phase at the edge of prior β grain. For samples air cooled from 950°C it was observed that there was elevated amount of α phase in the microstructure. There is an alternating morphology seen in the microstructure like the α and β plates were alternating [161],[162]. It can be maintained that microstructure wise, furnace cooling of Ti6Al4V leads to coarser microstructure than microstructure obtained from air cooling and air-cooled microstructure are coarser then microstructure attained through water quenching [161],[162].

Table 2. 8 shows effect of heat treatment temperature and cooling rate on phase volume fraction (%). obtained from different heat-treatment approaches.

Table 2. 8: Effect of heat treatment and cooling rate on phase volume fraction [161].

Temperature °C	Cooling mode						
	Water quenching			Air cooling		Furnace cooling	
	Phase volume fraction %			Phase volume fraction %		Phase volume fraction %	
	α'	α	B	α	β + α_{AC}	α	β
1100	98.7	-	1.3	14.7	85.3	95	5
1050	95	-	5	34.5	65.5	97	3
950	50	42.2	7.8	72.2	28.8	95	5
900	26.9	63.1	10	81.3	18.7	95	5
850	10	80	10	84.5	15.5	95	5

When looking at table Table 2. 8 for the same annealing temperature of 1100°C the observed phase composition and fraction for what quenching, air and furnace cooling is completely different. Water quenching is characterized by 98.7% martensite and a prior β volume fraction of 1.3%. For the same temperature (1100°C) when air cooled there is no presence of martensite, there is presence of α and

β + α$_{AC}$ which account for more than 80%. When furnace cooling is considered, at the temperature of 1100°C there is only α and β phase. The microstructure of furnace cooled is more α dominant with a volume fraction of 95% and the rest of the microstructure is 5% of retained β phase. While the phase volume fraction of furnace cooled samples seems to be approximately the same with change in temperature there is a very big variation in phase volume fraction as a function of temperature observed in the water quenched and air-cooled samples. Initially the water quenched samples were only composed of martensite 98.7% and prior β phase 1.3%, and as the annealing temperature decreases, there is a decrease in volume fraction of martensite, this is because the heat treatments was conducted in the α+β region and as the temperature decreased the heat treatment was conducted more and more near the α phase [161],[162]. As the annealing temperature is 850°C the α phase fraction that was not present at 1100°c is dominant in the microstructure at 850°C as the α phase volume fraction is 80% and the martensite and β phase are both only 10 % each. Unlike the water quenched samples the air-cooled samples were characterized with increasing volume fraction of α phase, while the β + α$_{AC}$ decreased considerably with decease in annealing temperatures.

Figure 2. 45 (a) shows the effect of cooling rate on α volume fraction.

Figure 2. 45: effect of cooling rate on volume fraction of α [163],[164].

It was observed that as the cooling rate increases the α volume fraction decreased this is because as the cooling rate increases a difusionless transformation takes place and instead of having α phase martensite is formed as a result of higher cooling rate [165]. Figure 2. 45 (b) shows evolution of volume fraction of primary α$_P$ as a function of solution heat treatment temperature [164]. It was observed that as the solution treatment temperature increases the volume fraction of primary α$_P$ decreases.
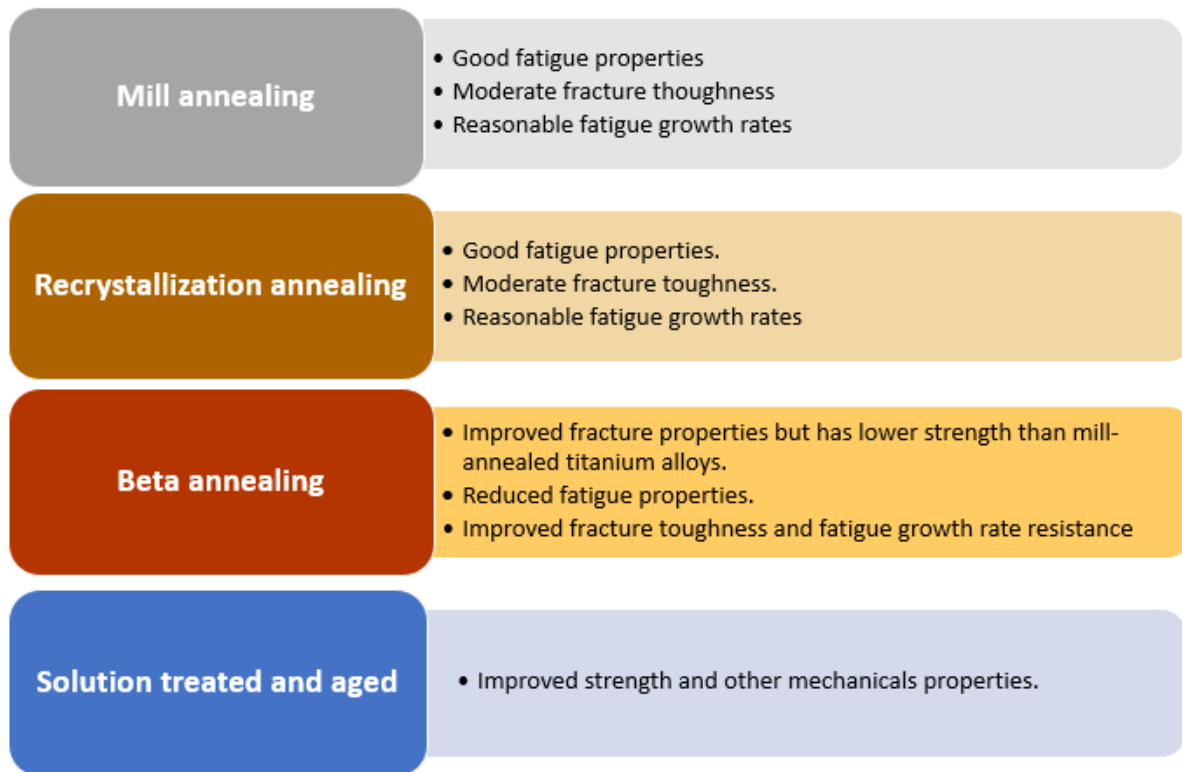
Figure 2. 46: Different heat treatment and their influence on Ti6Al4V [166].

So, the selected heat treatment and cooling rate plays a very critical role in microstructural features such as morphology, volume fraction and the microstructural plays important role in mechanical properties observed in metal and in our case in Ti6Al4v. Figure 2. 46 shows various heat treatment process that can be utilised and their benefit on mechanical properties.

2.6.2. Effects of microstructure on mechanical properties of Ti6Al4V

In titanium production and processing, several microstructure and desired mechanical properties can be achieved by thermos-mechanical processing [87]. This is because microstructure can be tailored to have certain characteristics by using temperature, cooling rate and mechanical force. Ti6Al4V microstructure can be transformed using thermo-mechanical process to achieve desired mechanical properties. While this literature has established the effect of heat treatment on microstructure, it is also important to establish connection between microstructure and mechanical properties [87] [134].

Several studies conducted on effects of heat treatment on microstructure and mechanical properties have shown that Ti6Al4V mechanical properties is dependent on microstructure and microstructure is dependent on thermal or thermomechanical processes used during and after its production. In a study conducted by Shian *et al.* [167] forger Ti6Al4 was heat treated to a solution treatment at 980°C for 1 hour the samples were either water quenched or 2 bar argon cooled. Followed by ageing at 550°C for 5 hours for 5 hours then again cooled in the same manners (water cooled and Ar-cooled).

The observed results are shown in Figure 2. 47 and Table 2. 9. The ar-cooled samples are having coarser microstructure when compared to microstructure observed in water quenched samples. It was also observed that the ar-cooled samples had higher percentage of volume fraction primary α_P 45% while water quenched samples had 23% volume fraction of primary α_P. it is also observed that the water quenched samples had lower elongation but having higher ultimate tensile strength while the ar-cooled samples were having higher elongation and lower ultimate tensile strength, the observed higher strength and lower elongation observed in water quenched sample was due to the presence of acicular martensite presence in water quenched samples, while the higher elongation and lower strength observed in ar-cooled samples is due to the fact that in the ar-cooled samples the is $\alpha+\beta$ microstructure [167]. **Fehler! Textmarke nicht definiert.**
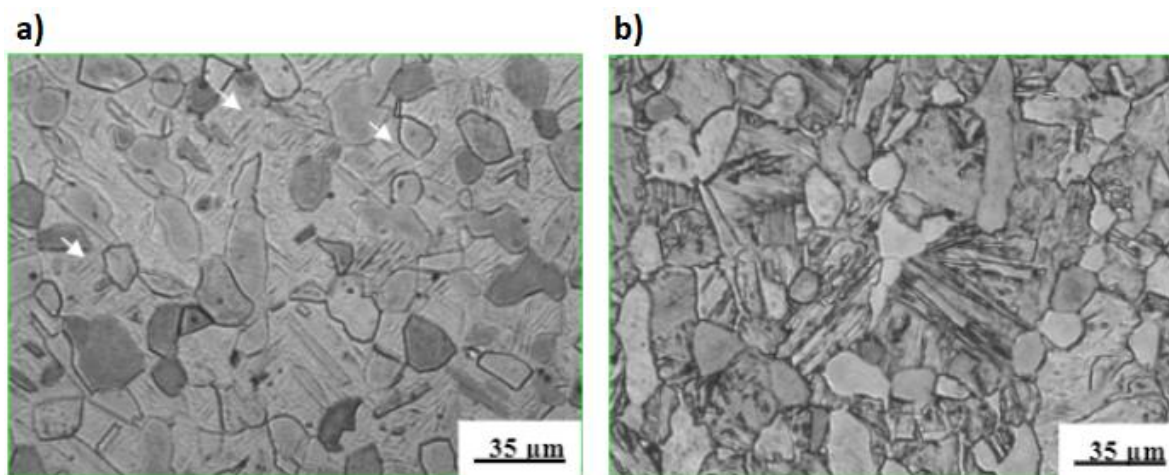
Figure 2. 47: Effect of different cooling rate on microstructure a) ar-cooling, b)water quenched [167].

Table 2. 9: Effect of cooling rate on microstructure and mechanical properties [167].

Samples cooling mode	UTS. (Kg/mm^2)	El (%)	Volume fraction α_P
Water quenched	114.88	7.8	23%
Water quenched	116.23	7.2	23
Ar-cooling	97.80	11.6	45
Ar-cooling	98.14	11.0	45

Woo et al. [168] conducted a study on the effects of heat treatment on mechanical properties of vacuum arc-remelting (VAR) Ti6Al4V. In this study, VAR produced Ti6Al4V was heat treated first at 950°C then water quenched and secondly aged for 1 to 24 hours using 450, 550, and 650°C as ageing temperature then air cooled. The initial microstructure observed in cast Ti6Al4V is shown in Figure 2. 48**Figure 2. 48: microstructure of as-cast Ti6Al4V (a) optical microstructure optical microscope (a), (b) SEM[168].**

. This microstructure was composed Widmanstätten consisting of alternating α and β phase present. Microstructure resulting from solution treatment at 950°C for 30 minutes followed by water quenching was composed of a mixture of αmartensite α' and retained β as shown in Figure 2. 49.
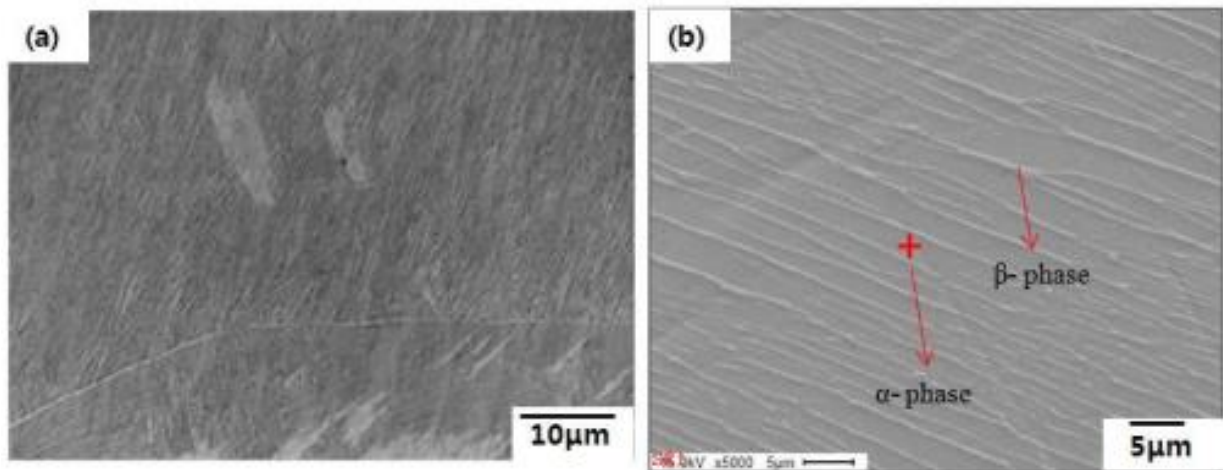
Figure 2. 48: microstructure of as-cast Ti6Al4V (a) optical microstructure optical microscope (a), (b) SEM[168].
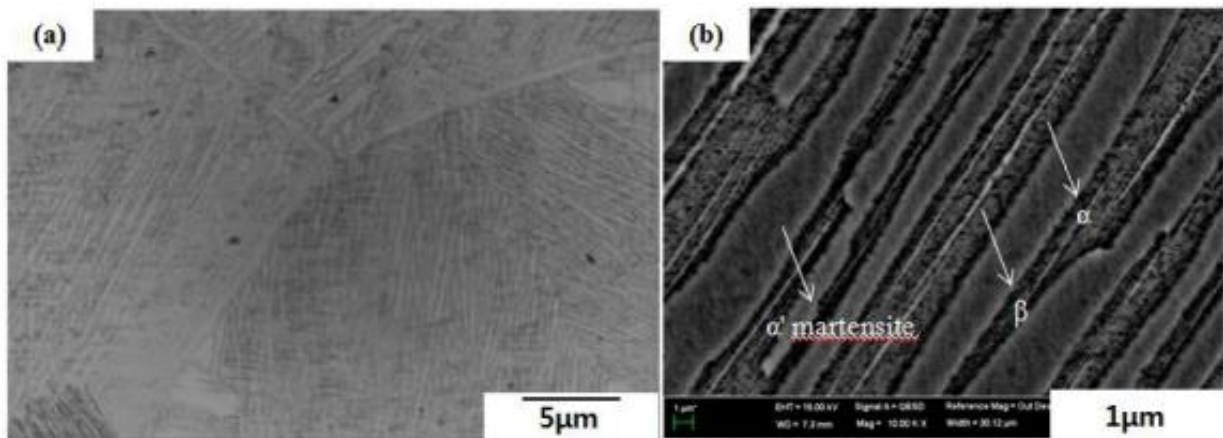
Figure 2. 49: Microstructure observed after solution treatment [168].

The observed martensite in microstructure obtained after solution treatment is due to higher cooling rate caused by water quenching.

The observed microstructures after ageing treatment are shown in Figure 2. 50. It was observed that these microstructures were composed of Widmanstätten microstructure consisting of precipitated α and β. There was no more presence of martensite in aged samples. Aged samples were having improved mechanical properties [168].
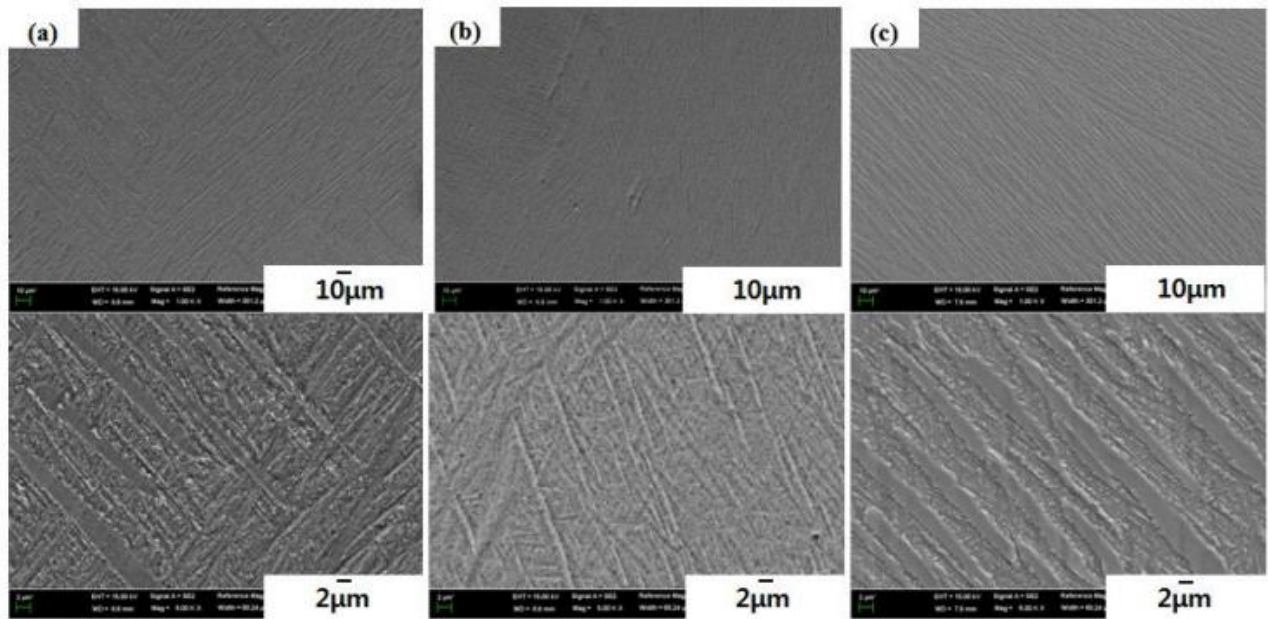
Figure 2. 50: Observed microstructure after different ageing temperature (a)450°C, (b) 550°C, (c) 650°C [168].

Table 2. 10**Table 2. *10*: Effect of ageing time on mechanical properties [168].** shows the effect of ageing on mechanical properties of Ti6Al4V. It was observed that as casted samples had lowest elongation, yield and tensile strength [168].

Table 2. 10: Effect of ageing time on mechanical properties [168].

Samples	Ageing time	Yield strength (MPa)	Tensile strength (MPa)	Elongation (%)
As-cast	24 h	475	524	9
Ageing at 450°C	24 h	655	723	11
Ageing at 550°C	24 h	757	833	11
Ageing at 650°C	24 h	659	728	13

The observed improved mechanical properties of in aged samples were attributed to ageing process which led to alloying element partitioning and a homogenizing effect for samples aged at 450°C and additionally to precipitant of α_2 as the solvus temperature for α_2 is between in Ti6Al4V is around 550°C-650°C while the improved mechanical [168].

So, the above studies and several other research conducted on this topic shows [169]–[172], have shown selected heat treatment temperature both solution treatment and ageing, ageing time, cooling rate, have a significant importance in the microstructure observed in Ti6Al4V and the microstructure in tis turn affect mechanical properties observed in Ti6Al4V. in sum, there is a correlation between heat treatment and microstructure obtained, there is link between microstructure and obtained mechanical properties observed in Ti6Al4V.

Interstitial element shown in Figure 2. 51 have been reported to affect mechanical properties of Ti6Al4V [105].
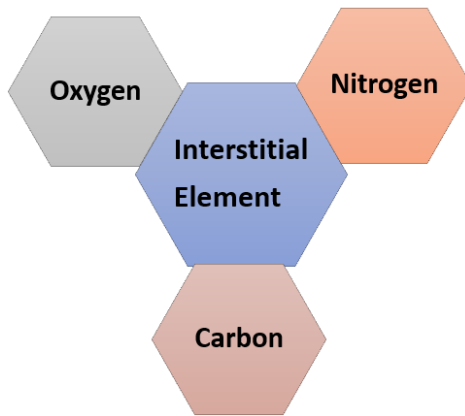
Figure 2. 51: Interstitial elements [105].

What happens is that during alloying of titanium for improvement of mechanical properties interstitial element can lead to solid solution strengthening, which is partly positive as it increases tensile strength and partly negative as it decreases alloys ductility when excessive amount is utilised. Figure 2. 52 shows the effects of interstitial elements on tensile strength and ductility of Ti6Al4V. It was observed that as the interstitial element percentage increases tensile strength increased however ductility decreased with their increase [96],[173],[174],[173]–[175]. One of the reasons why heat treating of Ti6Al4V is conducted using inert gas such as argon is because interstitial element such as oxygen leads to hard and brittle layer development in Ti6Al4V[40].
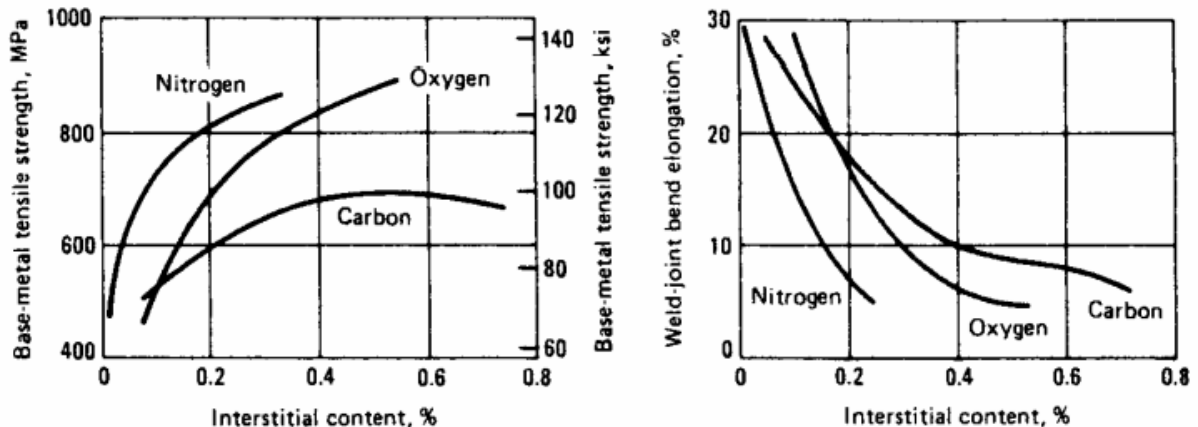
Figure 2. 52: Effects of interstitial elements on strength and ductility of titanium[105].

Figure 2. 53 shows parts result obtained in research conducted by Gil *et al.* [155] on the effects of cooling rate and grain size on morphology of Widmanstatten and on mechanical properties of Ti6Al4V. It was observed that can be seen that, as the cooling rate increases the ductility decreases. At a very low cooling rate below 0.5 °C/s the ductility is above 9% and the obtained microstructure is cauterized by α+β phase, while as the cooling rate increases there is a probability to obtain martensite in Ti6Al4V.
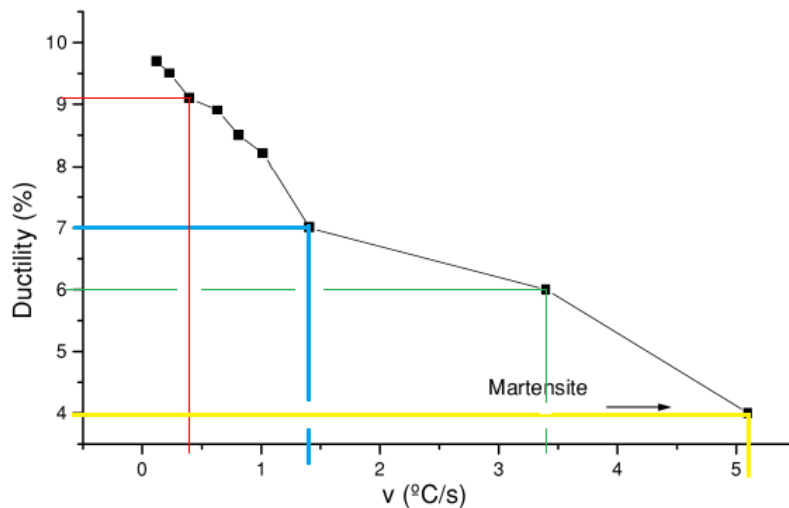
Figure 2. 53: Cooling rate effects on ductility of Ti6Al4V [155].

Similar to the ductility, tensile and yield strength are also affected by the cooling rate. Figure 2. 54 Shows the effect of cooling rate on tensile and yield strength. While it was observed in Figure 2. 53 that increase in cooling rate led to decrease in ductility of Ti6Al4, it is observed in Figure 2. 54 that increase in cooling rate leads to increase in increase in tensile and yield strength [155]. Martensitic microstructure has higher strength however lower ductility compared to samples having lamellar, bilamellar, equiaxed, and bi-modal microstructure.
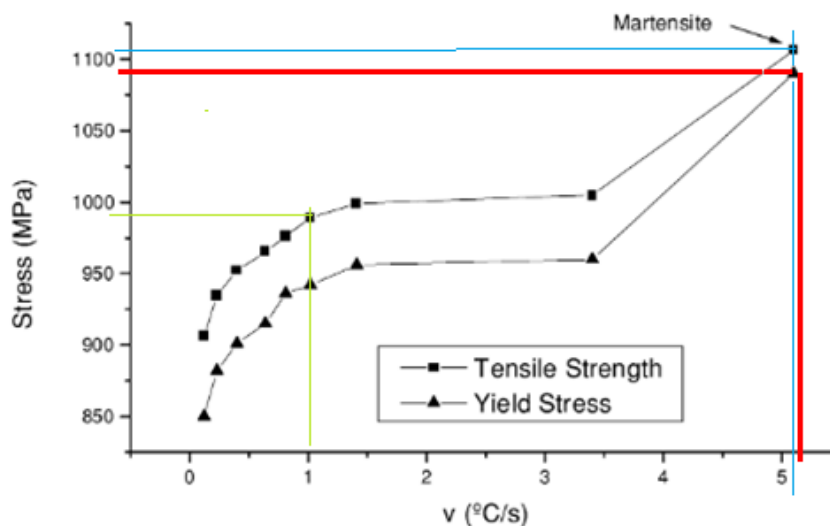
Figure 2. 54: Cooling rate effects on yield and tensile stress [155].

So, literature discussed in the above paragraph's correlates heat treatment (temperature, time, cooling mode) to microstructure and correlates microstructure to mechanical properties. It is indeed known that thermos-mechanical processing utilized in conventional production of Ti6Al4V is the precursor of all the observed microstructure and mechanical properties.

2.7. Additive manufacturing

Additive manufacturing (AM) or sometimes referred to as additive layer fabrication is an appellation given to 3D manufacturing process in which fully dense parts are manufactured using a 3D model through a layer-by-layer deposition of material powder and melting each layer of deposited powder using a laser beam and these layers are later fused together using heat. This process was initially considered production as a prototype manufacturing process in which new ideas were implemented [24]. However, in present day additive manufacturing process has evolved to industrial manufacturing process [18]–[20]. Figure 2. 56 and Figure 2. 57 show L-PBF process image and summary of process flow. This novel technology production process starts with a 3D generated model, the model is split in to 2D model that are splits based on heat flow, and then after the splitting process, powder is deposited layer by layer of powder are deposited on the substrate, each time a layer of powder is deposited the laser beam starts to melt the powder, and moves in a predefined pattern, the melted powder solidifies while the laser beam, is still meting other powder layers on it paths. The process recommences over and over till a fully dense part I produced [24]. As a process AM is opposite to conventional manufacturing processes in which parts of materials are subtracted during production. In AM layers of powders are added step by step. Various types of energy source are utilized in AM to melt the powder such as [12]–[17], [18]–[20]:

- electric welding arc
- high-power-density laser
- electron beam.

Figure 2. 56 shows different types of materials that can be manufacture using AM. [18]–[20].

When looking at Figure 2. 55 it can be seen that above AM are summarized into different groups based on the source of energy used to melt powder, methods utilized.

AM manufacturing processes are grouped into [12]–[17], [18]–[20]::

❖ Powder bed, sintering or binding

In which 3 different sub-groups are based on energy viz. laser, electron beam and binder which are further divided in different groups.

❖ Direct metal deposition which is referred to as fusion:

Metal powder deposition, and wire filament deposition.

❖ Ultrasonic:

Metal foil or sheet

❖ Liquid printing:

metal nanoparticles and nano metal jetting.

❖ Cold spray deposition: Metal powder.

All these different methods mentioned in the above paragraph can be found in Figure 2. 55 [8],[9],[10]. AM technologies existing thorough various processes are dived into groups shown in Table 2. 11.

Table 2. 11: Powder-fed and powder- bed categories [12]–[17], [18]–[20].

Powder-fed deposition	Powder-bed categories
a. Laser engineered net shaping methods, b. direct laser deposition (DLD).	a. selective laser sintering (SLS), b. selective laser melting (SLM), c. electron beam melting (EBM) technologies.
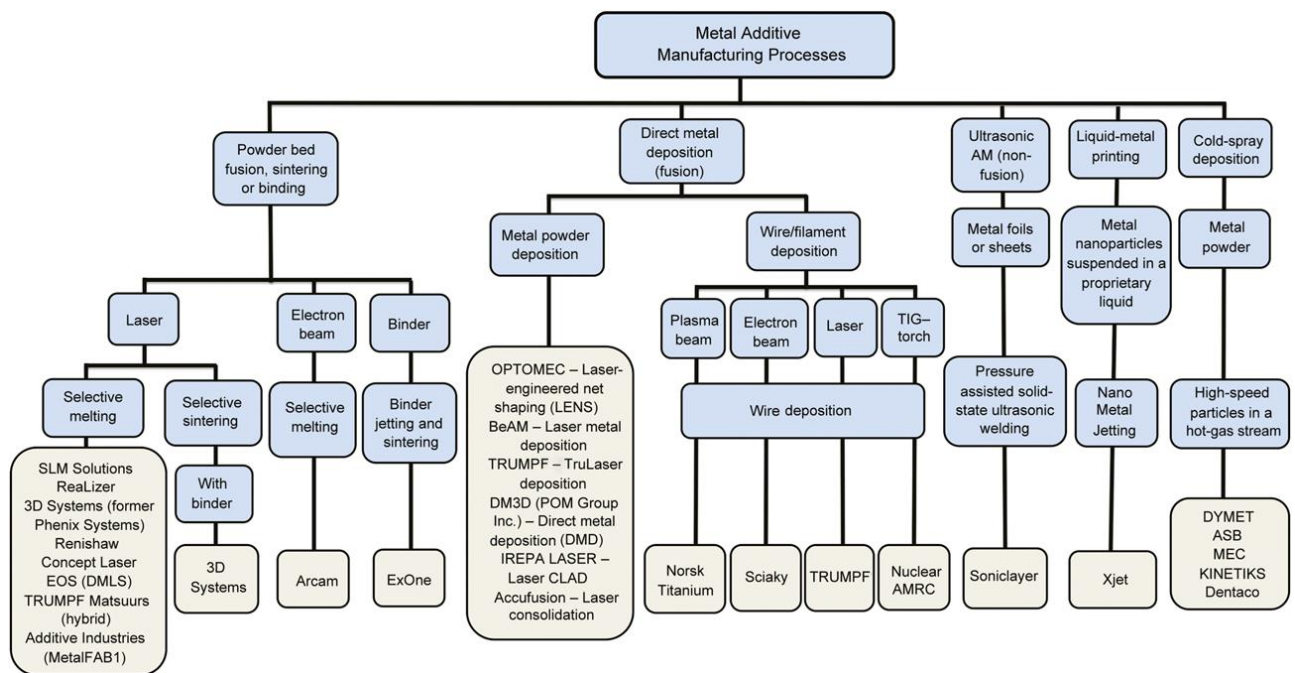
Figure 2. 55: Various Additive Manufacturing (AM) processes grouping [82].

2.8. Laser powder bed fusion (L-PBF)

A lot of interest has been given to L-PBF as a production process over the last few years, this is due to inherent advantages associated to it, for instance, the efficient material utilization linked to it, where not much material wastes are generated during parts production, there is also the rapid work cycle interval between start and end of a project and initiating another project, the possibility to produce a near net complex geometry shape, manufacturing fully dense part with up to 99%, etc.[24],[25].

Advantages that AM technologies offers in general and in particular the advantages that F-PBF offers have spark curiosity and fascination from both research communities, industrial sector, and invitation, medical and other sectors investors all over the word [176]–[180]. L-PBF is one of the most utilised or exploited AM method. Figure 2. 56 shows various materials and metals produced using L-PBF.
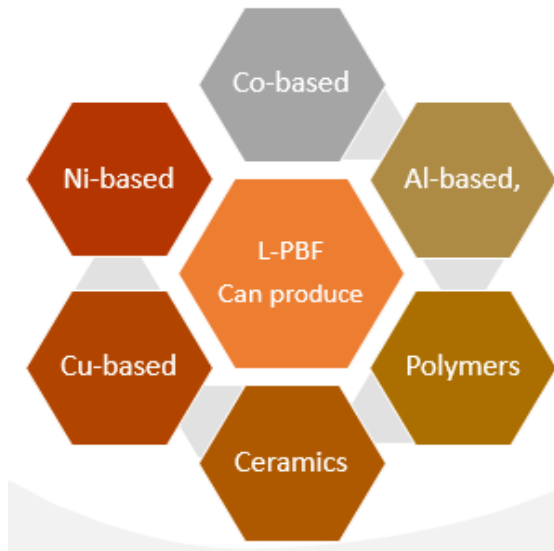
Figure 2. 56: diverse materials and metals produced by L-PBF [26]–[32], [77]–[81].

Figure 2. 57 and Figure 2. 58 shows a process flow summary of L-PBF steps and Summary of process steps for L-PBF production steps respectively [181].
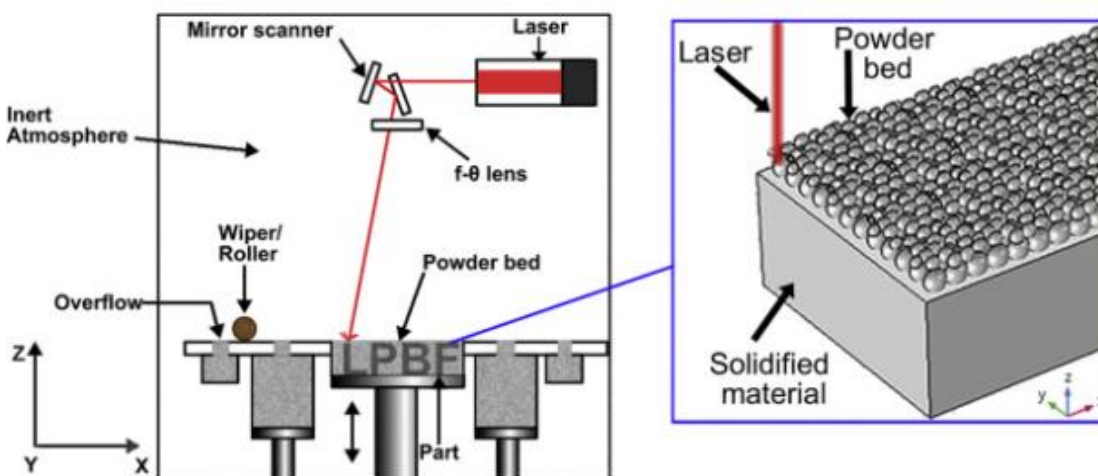
Figure 2. 57: Process flow summary of L-PBF steps [181],[182].
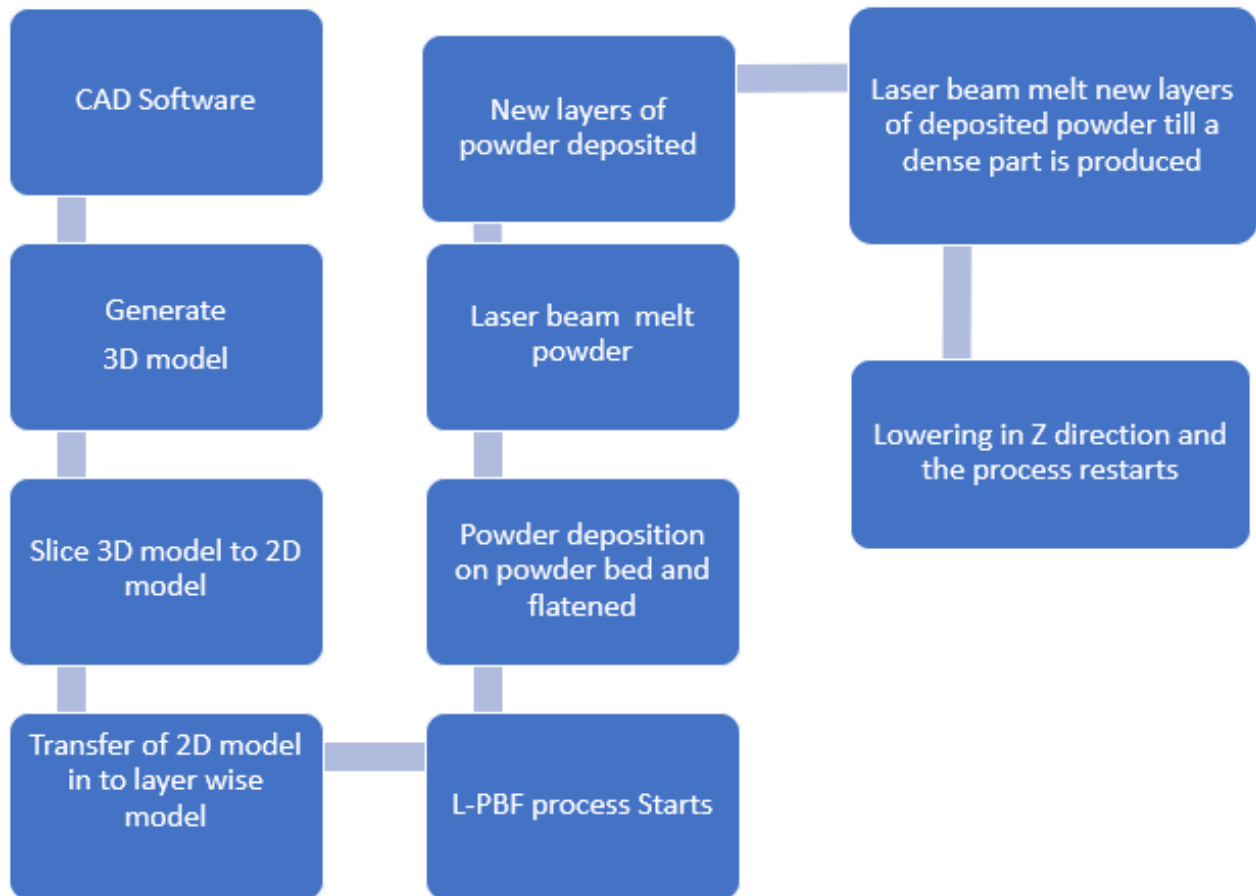
Figure 2. 58: Summary of process steps for L-PBF production [18]–[20], [179],[180],[183],[184].

During the L-PBF process shown in Figure 2. 57, and the process steps shown in Figure 2. 58 are followed. It is important to highlight those steps shown in Figure 2. 58 are not exhaustive list of steps and procedures followed during L-PBF production process.

So, in sum [18]–[20], [179],[180],[183],[184]:

1. Creating of 3D model using CAD software,
2. Slicing of the 3Dmodel into 2D model in layer wise model,
3. Deposition of powder-on-powder bed,
4. Flattening process of powder using a wiper,
5. Laser beams melt deposited powder,
6. A new layer of powder is again deposited,
7. Laser beam melts newly added powder the process continues until a fully dense part is formed.

Figure 2. 59 shows L-PBF production process.
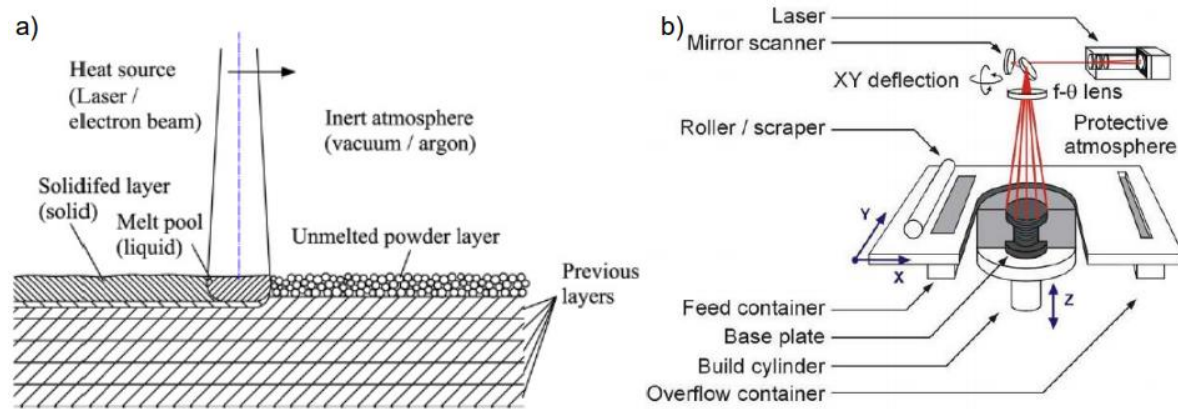
Figure 2. 59: b. Schematical representation of the L-PBF process [185].

2.8.1. L-PBF advantages and disadvantages

A combination of bother advantages and disadvantages associated to L-PBF process are shown in Table 2. 12. This table shows that while there exist positive attributes associated to L-PBF there are also some negative or disadvantages associated to this process.

One of the most important advantages associated with L-PBF process are efficient material usage, its ability to produce a fully dense part with density up to 99.9%, no need for sub assembly. Some of negative aspect associated with L-PBF are porosity, residual stress, it is a very expensive process, and the produced part need additional heat treatment to improve mechanical properties.

Table 2. 12: : Advantages and disadvantages of SLM process [186]–[188], [189]–[192].

Advantages	Disadvantages
Able to create fully dense components up to 99.9%	Very expensive
Higher flexibility in manufacturing very special geometries	Produced parts with low elongation
Very fast prototyping	Reduced mechanical properties
Production steps are reduced	Requires additional heat treatment steps
Reduced time to market	Presence of residual stress in produced parts
Less waste associated to production	Porosity, non-connected layers, residual powder
No time wasted in assembling	Need standardization
Higher material usage efficiency	There is no mixing during L-PBF
can be used t produce many material	There is less surface accuracy
Very encouraging research field due to several investment	Slower than injection moulding

2.8.2. Parameters affecting L-PBF

There are many parameters that affect quality of parts produced by L-PBF. Yadroitsev [193] maintained that there exist more than 130 parameters that affects L-PBF process. Several other studies conducted on L-PBF parameters concurred with Yadroitsev that there are several numbers of parameters that impacts quality and properties of components manufacture by L-PBF [194]–[196]. Thijs [83] conducted studies parameters influencing L-PBF production process and presented a comprehensive list of parameters that were grouped into [83]:

- Laser parameters,

- Scanning parameters,

- Material properties, and

- atmospheric parameters.

Through these researches it was established that parameters such as scanning speed have effects on relative density and relative density increased or decreased depending on scanning speed [194]–[196]. Further and more profound details on L-PBF Parameters and their effect on quality and properties of produced components can be obtained from Thijs scientific research [83].

While it is admittedly acknowledged that there are several parameters that affect quality and properties of L-PBF produced parts, it is important to highlight that only few of those parameters can be controlled, these parameters are shown in Table 2. 13 and

Table **2. *14***. These parameters can be utilized to determine the volumetric laser energy density E in the following equation (2.1):

$$E = \frac{P}{v \times h \times t},$$ (2.2)

where P (W) is the laser power, v (mm/s) is the laser scanning speed, h (mm) is the hatch spacing and powder layer thickness (t).

Table 2. 13: Parameters that can be controlled.

Laser power (P),
Scanning velocity (v)
Hatch space   (h)
Powder layer thickness (t)

Table 2. 14: Groups of main L-PBF parameters [181].

Laser parameters	Scanning parameters	Powder parameters	Temperature parameters
Laser power	Scan spacing	Particle size, distribution, and shape	Powder bed temperature
Spot size	Scan pattern	Powder bed density	Powder feed temperature
Pulse frequency	Scan spead	Layer thickness	Uniformity of temperature
Pulse duration		Material properties	

2.9. Ti6Al4V Produced by Laser Powder Bed Fusion (L-PBF)

As stated earlier various set of materials can be produced using LBF, aluminium, Titanium, Nickel and Iron alloys can be produced using this technology [77]–[81]. LBF is the most widely utilised AM process and one of the reasons for that is the fact that SLM can produce part that are dense up to 99.9%. LBF produced Ti6Al4V has different microstructure compared to the one produced by conventional Ti6Al4V. In conventional titanium alloys productions desired microstructure can be achieved due to

thermomechanical treatment involved during productions of these alloys, in the case of Ti6Al4V conventional production for instance, temperature control when cooling from β transus to the α+β region leads to various microstructure (lamellar, bi-modal, equiaxed, and bi-lamellar as well). In the case of LBF produced Ti6Al4V, due to the higher thermal gradient that occurs during LBF acicular martensite α' is obtained. The obtained acicular martensite α'resulting from higher cooling rate that happens in LBF has been reported to have tensile strength higher than conventional Ti6Al4V, however α' also have low ductility [9],[92],[93].

Knowing that Ti6Al4V is the most used titanium alloy as it accounts for more than 50% of titanium alloys utilised in many industries aerospace, automotive, chemical, medical, producing it with low ductility is not only a scientific shortcoming but also a threat to humans' life as using such product could lead to disastrous consequences. So, utilisation of LBF produced Ti6Al4V is dependent on enhancement of its mechanical properties.

As the laser interact with the powder and a melt pool is created at a very high temperature, and as the metal pool melt start to solidify, the cooling rate is very high sometimes cooling at a rate above 1000°C/s. This kind of cooling rate favors martensite formation in Ti6Al4V [137].

2.9.1. As-build microstructures and mechanical properties of LBF processed Ti6Al4V

While it is possible to produce variety of metal alloy using L-PBF, the allow studied in our case is Ti6Al4V. When produced by L-PBF, Ti6Al4V does not have the mechanical properties as the one produced using conventional manufacturing routs, in fact L-PBF produced Ti6Al4V is characterized by higher strength but lower elongation [9],[92],[93]. This because of the higher thermal gradient that exist in L-PBF process. As such, there is a difusionless transformation that leads to formation of acicular martensite. The observed microstructure is composed of acicular martensite in prior β [9],[92],[93]. Figure 2. 60 bellow shows martensite microstructure observed in L-PBF Ti6Al4V [118],[143].
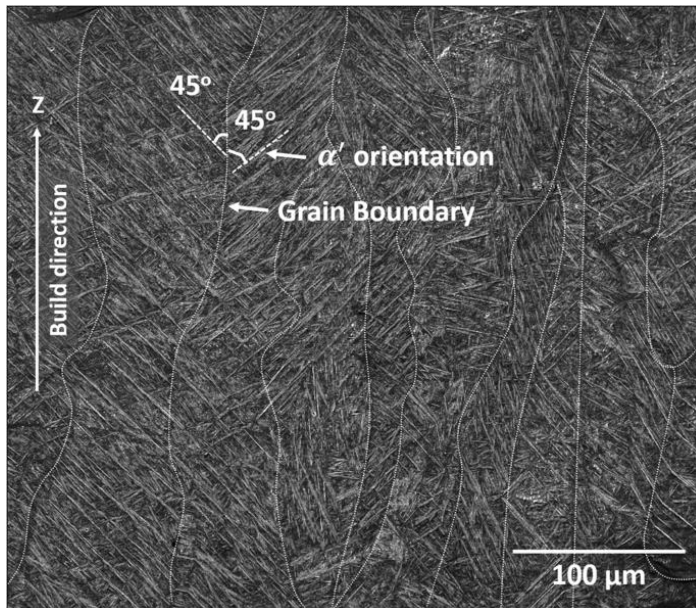
Figure 2. 60: Light microscope of as acicular martensite obtained after-PBF Ti6Al4V [197].

Table 2. 15, show mechanical properties of L-PBF produced Ti6Al4V. It was reported in each respective study that L-BF Ti6Al4V had higher yield and ultimate strength compared to conventional produced Ti6Al4V and very low elongation [38],[118],[143].

Table 2. 15: Mechanical properties of L-PBF as-build Ti6Al4V[178], [185].

No.	condition	UTS (MPa)	YS (Mpa)	Elongation (%)
1	As-build	1191±6	901±6	5.37±1.39
2	As-build	1220±60	1140±60	3.28±1.5
3	As-build	1267±5	1110±9	7.28±1.12

2.10. Heat Treatments

The principle of heat treatment existed in earlier society before its current utilization in industries for metal properties improvement. Some metallurgical history research trace casting usage of heat treatment of metal back to Yin dynasty 1600 to 1046 B.C [72],[198],[199]. Several archeological findings corroborate that metal work was an absolute crucial part of many medieval kingdom and empires in ancient Iran, Egypt, Carthage, Greek and Roman [72],[198],[199]. So, before the current industrialization of heat treatment in metal sector the concept was already utilized in several societies thousands of years ago. In today metal industrialization production process, heat treatment is utilized for microstructure transformation, tailoring, and improve of mechanical properties.

In this thesis, L-PBF Ti6Al4V have to be heat treated because it has higher tensile strength but lower elongation, in other words it does not have the same mechanical properties has conventional produced Ti6Al4V. The difference in mechanical properties between the same alloy produced by different methods (conventional methods and L-PBF) is because in conventional titanium fabrication a combination of thermos-mechanical treatment is employed to create preferred characteristics while in L-PBF the process has a higher thermal gradient that is prone to martensite formation.

Purpose of heat treatment in now day industries were discussed earlier as shown in Figure 2. 31 (Figure 2. 61) and it is re-illustrated for visual purpose in this part. In fabrication of titanium alloys heat treatment is applied for reducing residual stresses optimize combination of mechanical properties, in the case of L-PBF there is low ductility, also as heat treatment is applied, microstructure is transformed and ductility, fatigue, fracture toughness, and creep strength machinability are improved [200]–[202].
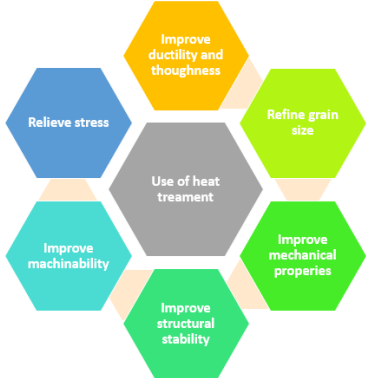
Figure 2. 61: Use of heat treatment in metal industry [152]–[154].

Figure 2. 62 shows groups of different heat treatment that can be applied to L-PBF Ti6Al4V.

Figure 2. 62: Four different categories [200],[202]–[204].

To improve mechanical properties of L-PBF used in this study, heat treatment has to be applied to modify the acicular martensite found in Ti6Al4V to produce bi-lamellar microstructure [200]–[202],[204].

Several studies have been performed with desire and hope to transform the acicular martensite obtained in LBF Ti6Al4V produced [185],[205]–[208] ,[209].

The observed results from these studies reported that modification of microstructure resulted from heat treatment, and through, microstructure modification mechanical properties optimization takes place [185],[205]–[208].

In this master thesis, L-PBF produced Ti6Al4V is subjected to two stage heat treatment with as purpose to:

- Transform the acicular martensite obtained in L-PBF Ti6Al4V,
- Achieve mechanical properties like the observed in conventionally produced Ti6Al4V
- Reduce internal stresses

According to Motyka [38], and other studies [139],[210] the reason why there is formation of martensitic microstructure in L-PBF production of Ti6Al4V is because there a very high temperature gradient that rise up to 10^6 K/m also there is a very fast solidification and cooling rate that rise to 10^8 K/s. Several studies have been conducted on decomposition of martensite phase found in L-PBF produced Ti6Al4V. In a study conducted by Brandl *et al* [211], L-PBF produced Ti6Al4BV was subjected to heat treatment at a temperature of 600°C for 4 hours followed by air cooling, it was observed that the acicular martensite in L-PBF produced Ti6Al4V was not modified as shown in Figure 2. 63.
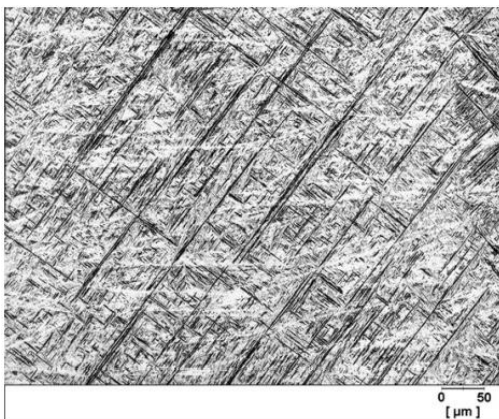
Figure 2. 63: Acicular martensite existing after heat-treatment at 600°C [211].

The observed results by Brandl *et al* [211] were due to the fact that this heat treatment was conducted using a temperature below the martensite transformation [185][211],[212].
 Some studies have suggested the martensite decomposition temperature in L-PBF Ti6Al4V at 650°C [139], [209], [210].

Common practice to ensure compete decomposition of martensite in L-PBF produced Ti6Al4V is to heat treat it above β transus and then slow cool the alloy [93], [139], [207], [210].

2.10.1. Effect of heat treatment on microstructure of L-PBF produced Ti6Al4V

2.10.1.1. Achieving lamellar microstructure in L-PBF production of Ti6Al4V

Several studies conducted on L-PBF produced TI6Al4V have address transformation of acicular martensite for improvement of its mechanical properties. Two approaches have been suggested [156],[203],[207],[213]–[216]:

1. During L-PBF production of Ti6AL4V, and

2. Post processing (heat treatment, HIP) of L-PBF produced Ti6Al4.

Recommended solutions for the first approach include controls of process parameters during L-PBF production, in-situ residual stress reduction, preheating of powder [214],[216]–[219]. However, since this thesis leans more towards the second approach which is post processing of L-PBF produced Ti6Al4V, will be discussed in the following paragraphs.

Microstructure found in L-PBF Ti6Al4V is acicular martensite [219]. To transform the martensite present in L-PBF produced Ti6Al4V, a temperature leading to martensite decomposition need to be applied. While decomposition temperature for martensite can be the answer, common practice recommends heat treating as-build Ti6Al4V above the β transus temperature to ensure complete transformation of martensite and slowly cool to achieve lamellar microstructure [215],[220].

Figure 2. 64 show microstructure obtained after heat treatment of L-PBF produced Ti6Al4V [185]. The β phase is characterised by lighter colour while the α phase is characterised by darker colour.
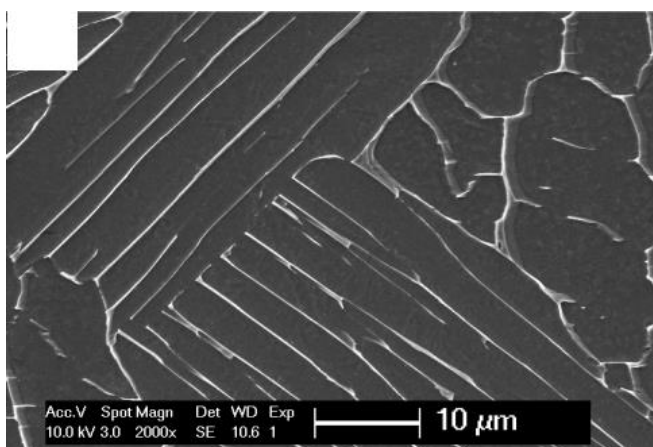
Figure 2. 64: Effect of heat treatment on transformation of acicular martensite in LPBF Ti6Al4V to lamellar microstructure [185].

Looking at Figure 2. 64 it is possible to achieve lamellar microstructure by heat treating L-PBF Ti6Al4V. Due to slow cooling involved in achieving lamellar microstructure in L-PBF Ti6Al4V. The obtained microstructure is characterized with coarse lamellae and have good strength and elongation [221]. The desire to further improved mechanical properties of L-PBF Ti6Al4 leads to conduct studies beyond the obtained lamellar microstructure because, lamellar microstructure as lower yield and ultimate strength when compared to bi-lamellar.

This explains the motivation behind the desire of achieving bi-lamellar microstructure in this study ti have an improved tensile and fatigue strength compared to the ones observed in lamellar microstructure [60],[222].

2.10.2.   Effect of heat treatment on mechanical property of L-PBF produced Ti6Al4V

It has been established through presented literature that the resultant microstructure from L-PBF production of Ti6Al4V due to higher thermal gradient existing in this process is acicular martensite. As such, in order to improve mechanical properties of L-PBF produced Ti6Al4V, microstructure need to be transformed to $\alpha+\beta$ microstructure though heat treatment. The following section will discuss the effects of heat treatment on mechanical properties.

2.10.2.1.   Effects of heat treatment on tensile properties of L-PBF produced Ti6Al4

Due to the presence of acicular martensitic microstructure formed in L-PBF produced Ti6Al4V, the as-build Ti6Al4V is characterized by higher strength and lower elongation. This creates challenges and renders usages of L-PBF produced Ti6Al4V undesirable, as these mechanical characteristics could lead to catastrophic failure when the as-build se parts Ti6Al4V are utilised in Aerospace and other industries in which Ti6Al4V is utilised. To surmount these mechanical limitations or surmount the lower elongations, fatigue resistance observed in Ti6Al4V the proposed and common practice used to improve Ti6Al4V mechanical properties is to thermo-mechanical (hot isostatic pressing) or thermally treat (heat treatment) as-build Ti6Al4V [185],[197],[203],[212],[223]. Over the years, several studies have provided insight on how to transform the martensite microstructure observed in as-build Ti6Al4V and improve its mechanical properties. This literature section will discuss some of those studies and their observed results to establish the effects of heat treatment on L-PBF Ti6Al4V.

Studies conducted by Zhang *et al*. [224] on the control of microstructure of L-PBF produced microstructure by heat treatment for improvement of ductility was conducted using 3 different heat treatment temperature viz 800, 850 and 900°C with ageing time of 6 hours for all the heat treatment temperature followed by air cooling. Effects of heat treatment on tensile and ultimate strength are shown in Figure 2. 65 This figure was modified adding black lines in order to point out where the

elongation of each sample is on the graph. The obtained results showed that the as-build Ti6Al4V showed higher tensile and ultimate strength when compared to heat treated samples this is due to the presence of martensite microstructure in as-build sample, however the as-build samples had lower elongation of approximately 6.4 this is very low when compared to heat treated samples. Heat treated samples showed lower yield and ultimate strength then the as-build samples while having higher elongation when compared to as-build samples. This is because the heat-treated samples after 6 hours of ageing they were air cooled. Air cooling leads to formation of lamellar α+β microstructure having alternated α and β plates. Unlike in the martensite microstructure where the microstructure was dominated by needle like microstructure in columnar β. The presence of α and β in achieved microstructure achieved through heat treatment and cooling makes the microstructure have higher elongation [224].
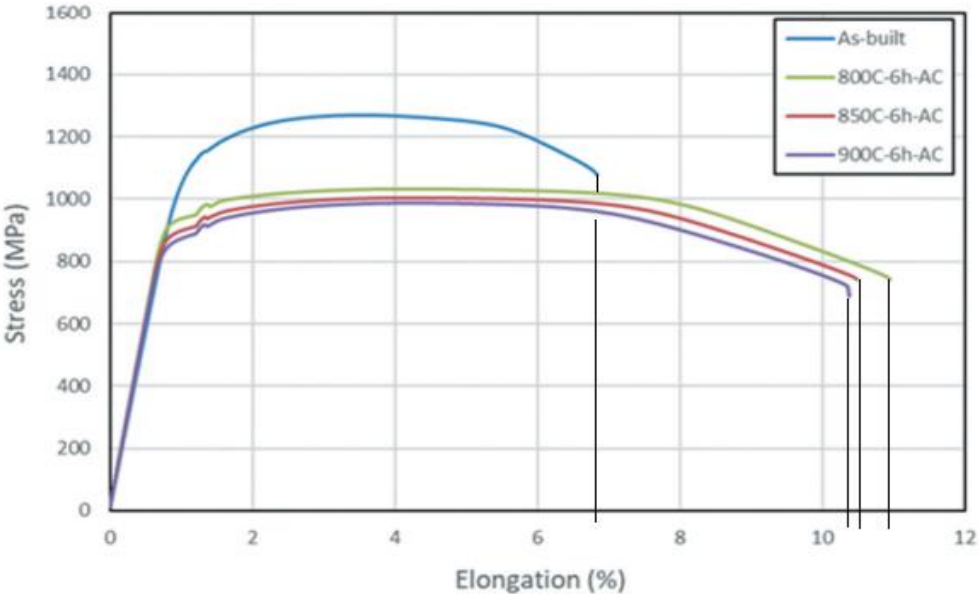
Figure 2. 65: Comparison between tensile strength of as-build Ti6Al4V and post process Ti6Al4V held at the same ageing time [224].

Table 2. 16 shows comparative results of mechanical properties between as-build sample and the eat-treated samples. Observed results agree with the stress vs elongation plots shown in Figure 2. 65. The observed in Table 2. 16 shows that for as-build sample the yield and Ultimate strength were 1112 and 1267 MPa. Which are higher than yield and ultimate strength of heat-treated samples [224].

Table 2. 16: Mechanical properties of as-build and heat treated samples [224].

T°C	Cooling mode	T(h)	Hardness (HV)	E(GPa)	YS(MPa)	UTS (MPa)	Elongation (%)
As-build	-		377 ± 3	107 ± 4	1112 ± 8	1267 ± 3	7 ± 1
800	AC	6	336 ± 5	121 ± 4	928 ± 6	1029 ± 3	9 ± 2
850	AC	6	329 ± 4	119 ± 3	889 ± 5	1002 ± 4	10 ± 2
950	AC	6	332 ± 7	110 ± 1	864 ± 3	986 ± 2	10 ± 1

Research conducted by Zhang *et al*. [224] on L-PBF produced Ti6Al4V shows the importance of heat treatment temperature. While post-processed samples were all aged using the same time (6 hours) and cooled using the cooling mode (Air cooling). The only varying parameter was different heat treatment temperature, and it was observed that these different temperatures led to different elongation, hardness, young's modulus, yield, and ultimate strength. So, selected temperature affects L-PBF final mechanical properties after heat treatment. Comparative studies on process parameters, defects and post process of L-PBF of TI6Al4V conducted Singla *et al.* [90] where L-PBF produced Ti6Al4V samples were subjected to different temperature and mechanical process. In this study samples were divided in to 5 groups [90]:

1. As-build Ti6Al4V samples,
2. Heat treated at 800°C,
3. Hot isostatic pressed at 920°C (HIP 920°C),
4. Heat treated at 1050°C,
5. Hot isostatic pressed at 1050°C (HIP 1050°C).

All these samples were cooled in the same manners. The observed results are shown in Figure 2. 66.
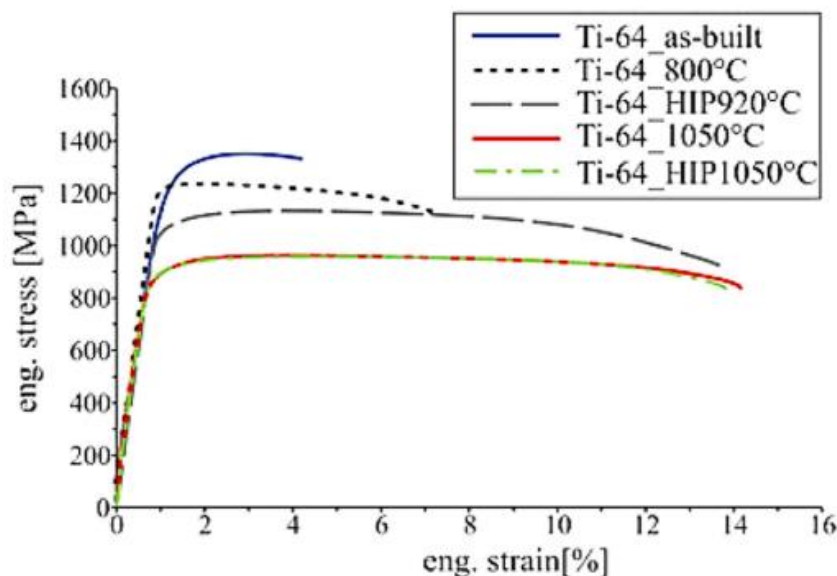
Figure 2. 66: Comparison of yield and ultimate strength of as-build and post processed SLM Ti6Al4V [90].

It was observed that as-build Ti6Al4V samples had the highest yield and ultimate strength however lower elongation at break as it was the case in the study conducted by Zhang *et al*. [224].

When looking at tensile test of the heat-treated in and Figure 2. 66 it was observed that samples heat treated at 800°C had higher elongation than as build samples but lowed yield and ultimate strength. Samples heat treated at HIP920°C, 1050°C, and HIP 1050°C seems to have close elongation at break, with the difference being HIP 920°C having higher yield strength compared to samples heat treated at

1050°C and HIP 1050°C. it can be maintained that as the temperature increases tensile and yield strength decreases.

Research performed by Vrancken *et al.* [185] compared mechanical properties of SLM Ti6Al4V with hot forged mill annealed equiaxed Ti6Al4V (Grade 5). Regarded as reference sample [185]. Results of Vrancken's study are shown Figure 2. 67.
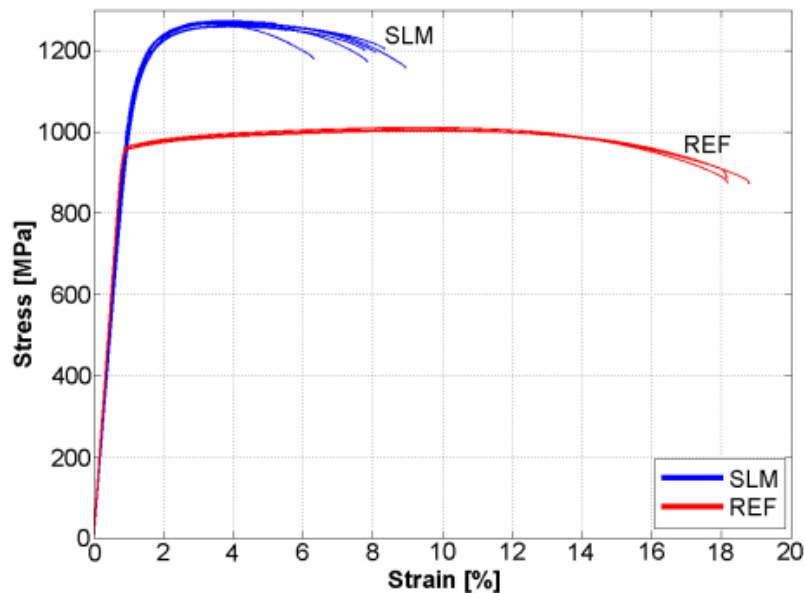
Figure 2. 67: Comparative tensile plot of AM as-build Ti6Al4V and
a reference sample produced through [185].

Obtained results by Vrancken on as-build Ti6Al4V are in agreement with observed behaviour of as-build Ti6Al4V observed by Zhang *et al*. [224], and Singla *et al.* [90], [50],[[178]. The as-build samples had higher yield and tensile strength than the reference sample [185]. However, the as-build samples had lower elongations like in other research presented and the reference samples had elongation percentage higher than the as-build. Vrancken compared mechanical properties of the as-buil Ti6Al4V and reference sample, the attained results are shown in Figure 2. 68. It can be seen that the as-build sample has higher tensile and ultimate strength viz. 1110, and 1267 MPa. While the reference sample has lower tensile strength compared to the reference sample what has the tensile and ultimate sample of 960, and 1006 MPa respectively [185]. Observed elongation of reference sample was 2.5 times higher than the as-build sample.

	E (Gpa)	σy (Mpa)	UTS (Mpa)	ε fracture (%)
SLM as-build	109±3.1	1110±9	1267±5	7.28±1.12
Reference sample	120±1.9	960±10	1006±10	18.37±0.88

Figure 2. 68: As-build and reference samples compared mechanical properties [185].

Lastly, Huang *et al.* [225] did research with as objective to enhance mechanical properties of L-PBF Ti6Al4V through heat treatment. In this study, heat treatment was conducted using the process flow shown in Figure 2. 69. L-PBF Ti6Al4V samples were divided in 5 groups based and heat treated and cooled according to temperature in these 5 groups (800, 950, 1050 and 1200°C air cooled and 1050°C water quenched) the mechanical properties obtained as results of different heat treatment were compared to as-build samples properties as shown inFigure 2. 70 and Figure 2. 71 [225].
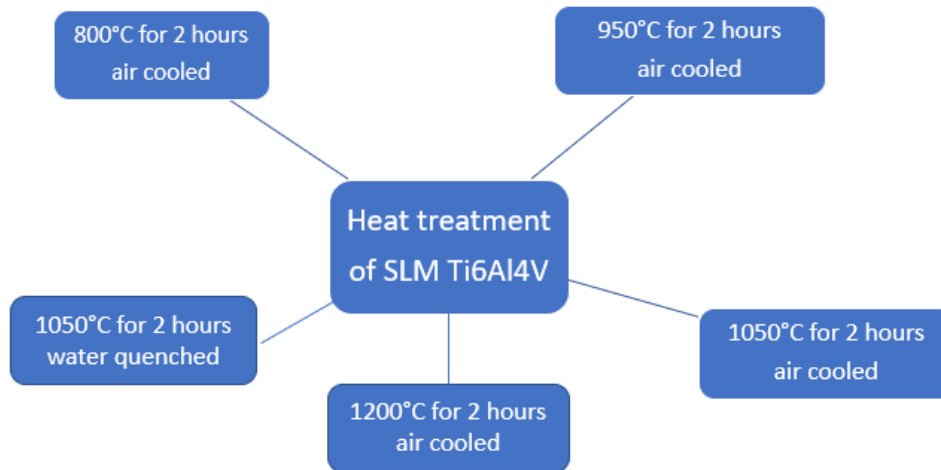
Figure 2. 69: Heat treatment approach for improvement of L-PBF Ti6Al4V [225].

The stress and strain plot results shown in Figure 2. 70 and comparison of mechanical properties between as-build and heat-treated samples shown in Figure 2. 71. It was observed that the as build sample like in previous studies discussed have higher ultimate tensile strength than all of heat treated samples however the heat treated samples have higher elongation than as build samples [225].

Water quenched samples have the lowest yield and ultimate strength. This is because in this heat treatment process water quench leads to formation of martensite when the second stage heat treatment is conducted is conducted just at the β transus at 990°C. Huang *et al.* [225] attributed lower mechanical properties observed in the two staged heat treatment (1050°C, water quenched and then 990°C air cooled) to partitioning effects as shown by electron probe microanalysis (EPMA) results prior α were enriched with O and Al which can impact elements strength and reduces strength of transformed β matrix. Samples heat treated at 800°C for 2 hours then air cooled were having the highest tensile, ultimate strength and elongation, these results were better than all the heat-treated samples. This was because in samples heat treated at 800°C, there was a combination of martensite, α and β. The α is thin, and the α colony is smaller. In titanium having lamellar microstructure mechanical properties are affected by the effective slip length and the effective slip lengths affected by the colony size. As the colony size increases effective slip length also increases and certain mechanical properties deteriorates while as the colony size decreases the effective slip length

decreases as well and certain mechanical properties are improved. Sample heat treated at 800°C had thinner α lamellae and smaller colony size, which led to the observed mechanical properties and also due to the presence of α'. Sample heat treated at 950°C shows lower mechanical properties then samples heat treated at 800°C because after 950°C there was complete decomposition of martensite and the α laths were coarse.
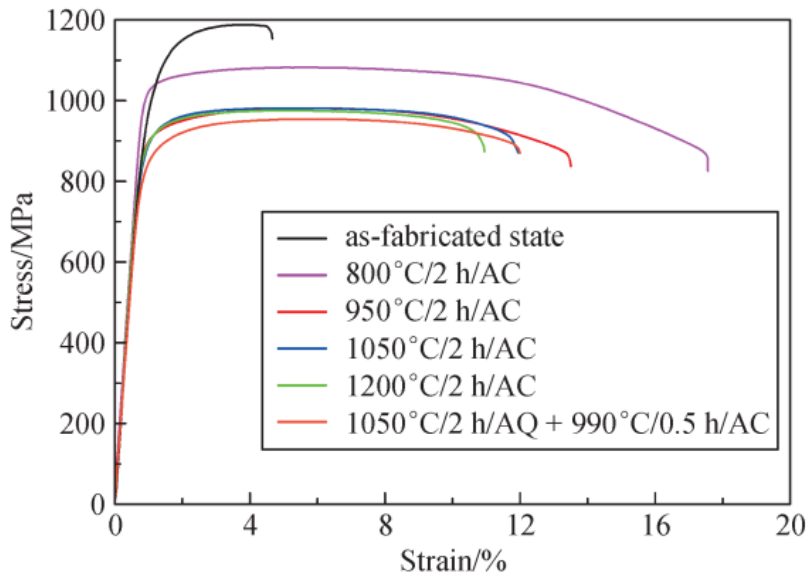
Figure 2. 70: Tensile of heat treated and as-build Ti6Al4V [225].

No.	condition	T (°C)	Time (hr)	Cooling mode	UTS (MPa)	YS (Mpa)	BE%
1	As-build				1191±6	901±6	5.37±1.39
2	Heat treated	800	2	AC (Air cooling)	1073±9	1010±6	17.05±1.14
3	Heat treated	950	2	AC (Air cooling)	984±5	893±3	14.15±1.49
4	Heat treated	1050	1	AC (Air cooling)	984±8	863±4	13.34±0.67
5	Heat treated	1200	1	AC (Air cooling)	988±8	878±7	11.25±1.25
6	Heat treated	1050	1	WQ (Water quenching)	962±12	838±6	11.96±0.07
		990 Followed by	0.5	AC (Air cooling)			

Figure 2. 71: Comparison between mechanical properties obtained after heat treatment and as-build sample[225].

2.10.2.2.   Effect of heat treatment on fatigue properties of L-PBF

Fatigue properties are affected by microstructures, and it is well established that microstructures are affected by cooling rate and selected solution and ageing temperature. However, there are much other several other aspects that impact fatigue properties as it has been stated by several research as shown in **Fehler! Verweisquelle konnte nicht gefunden werden.**.

Table 2. 17: Other factors influencing fatigue in Ti6Al4V [87],[226],[227].

Additional factors affecting fatigue properties
Degree of work hardening
Grain size (or phase dimension and morphology)
Age hardening condition
Crystallographic texture
Elastic constants

It is understood that in Ti6Al4V which is an α+ β titanium alloy, morphology and composition of the alloy (α, and β contained in microstructure) affects the mechanical properties of the alloy including fatigue properties [74],[226]–[228]. Studies conducted by Zuo *et al* [229] on the effect of microstructure on ultra-high fatigue showed that internal fatigue cracks began at the primary α_p grain boundary or inside the α_p in the case of bimodal microstructure whereas in basketweave microstructure it is introduced at the at the α-β interface or colony boundary, and it was highlighted that fatigue crack propagation or fatigue life dependent the size of the initial crack and where it was located [229]. It was furthermore noted during fatigue test conducted on these samples that even when the applied stress on studied samples was reduced the crack initiation transited from surface inside of the samples being studied, this highlighted the effect of cyclic fatigue failure on material that can occur even when the sample are operated below the initial stress that led to the crack to form.

Bridier *et al* [230] conducted research to study the relation between crystallographic texture and micromechanical fatigue behavior in Ti6Al4V on numerous scale using an EBSD method while analyzing plastic deformation of larger grains and observed that prismatic and basal slip had prevalent numbers of slip and there was higher presence of prismatic glides. Bridier *et al* [230] studies corroborated similar result to Zuo et al *al* [229] which maintained that fatigue crack formed inside primary α_P. The formed cracks were resulting from basal and prismatic slip planes. however, basal crack nucleated and propagated earlier than prismatic cracks. This is explained partly by the fact that fatigue crack favors [0 0 0 1]-texture development in macrozones hence the faster nucleation and propagation of crack in the basal plane, partly because it is believed that at the at the basal plane there is a specific deformation that takes place while there is also a general deformation that occurs globally at the macrozone. Finally, Bridier *et al* [230] recommended that Schmidt factor be utilized for basal and prismatic crystallographic domain.

 Numerous research on fatigue of L-PBF produced Ti6Al4V have shown that there is a number of factors that influences the fatigue behavior of L-PBF produced Ti6Al4V and these factors can be grouped in 3 categories as shown in Figure 2. 72 [231]–[233].
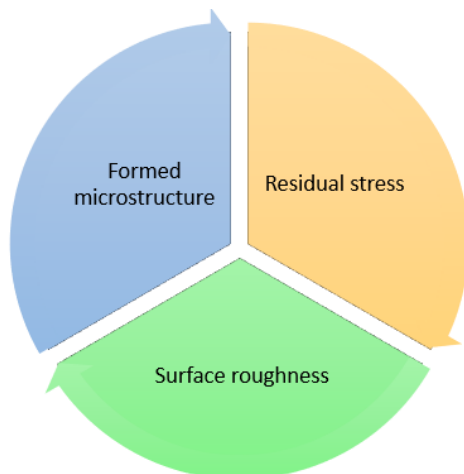
Figure 2. 72: Summary of factors affecting fatigue [231]–[233].

This thesis focuses on improvement of mechanical properties of L-PBF produced Ti6Al4V through series of heat treatment above and below the β transus to modify the acicular martensite found in as-build Ti6Al4V in to lamellar and bi-lamellar then conduct a comparative study on observed difference in mechanical properties of samples having as-build (acicular martensite), lamellar, bi-lamellar.

2.11. Fracture Mechanics Concepts

2.11.1. Introduction

Most structures fail due to the following two reasons [234]–[236]:

❖ Use of a new design or material, which produces an unpredicted and adverse result, and

❖ Negligence during design, construction, or operation of the structure.

'Fracture mechanics' is the name invented for the study that concerns itself with the mechanics of bodies (Solids) containing planes of displacement discontinuities (crack) and martial mechanical properties, it is used to do mechanical analysis of material [237]. It is used to conduct mechanical analysis of materials that contains one or more cracks in order to predict condition that may probably result in failure.

Fracture mechanics is an area of expertise used in the design of aircraft, aerospace, civil structures, large vehicle, and marine's applications. In past, several structures have collapsed or failed, for instance, while cruising at an altitude of 24 000ft, aloha airline aircraft lost one third of its roof as a result of stress fracture occurrence and failure of cathedral of Beauvais, golden gate bridge could have resulted due to hidden flaws, and stress concentrations. The aftermath of fracture occurrence can be negligible or they can be expensive result in loss of lives [238]–[240].

It is important to highlight that, fracture failure is a very challenging problem that every sector is confronted with, it not only a phenomenon that happen to aircraft, ships, and bridges. This explains the need to address it theoretically and practically [234]. In order to prevent fracture failure occurrence in manmade structures, and in designed products today, it is imperative to gain fundamental understanding of fracture mechanics, as it can be utilised for:

- Betterment of designs,

- prediction of fatigue and fracture strength of various materials

- guidance when selecting materials and developing alloys; and

- Understanding and ascertaining the implication of defects [234].

By definition, a fracture is the separation of a material into two or many parts as a result of stress being applied on this material. Two distinctive types of fracture exist: Ductile fracture, and brittle structure. When fracture happens abruptly with fracture perpendicular to the applied force, this is referred to as brittle fracture, and when there is occurrence of plastic deformation prior to fractures taking place, this is referred to as brittle fracture, unlike brittle fracture, the plastic deformation in ductile fracture allows the preventative measure to be taken [241].

2.11.2. Fracture Classification

2.11.2.1. Brittle Fracture

Brittle fracture is characterized by [242]:

- Lake of considerable plastic deformation,

- Which implies there is a very fast crack growth,

- The magnitude of stress at which crack takes place is unpredictable since happens fast,

- The crack propagation seems to be almost perpendicular to the applied stress,

- Crack growth is often by cleavage.

Figure 2. 73: Brittle fracture appearance [242].

Viewed as not stable, brittle crack grow very fast, there is formation of neck. Fractures occurs through grain. Figure 2. 73 shows brittle fracture.

2.11.2.2. Ductile Fracture

In ductile fracture, there is a substantial plastic deformation near the area where crack is developing [243]. The plastic deformation happens in the region where maximum stress is applied, as such there is a reduction of the cross section are of the material, and more there is more strain at the neck. During ductile fracture, there is large amount of energy absorbed (toughness) due to the large plastic deformation that occurs prior crack instability happens. Therefore, as a result of strain hardening at crack tip section, there is a slow crack growth occurs [236]. As a result of ductile fracture, the material resulting shape after fracture is referred to as cup and cone as shown in Figure 2. 74.
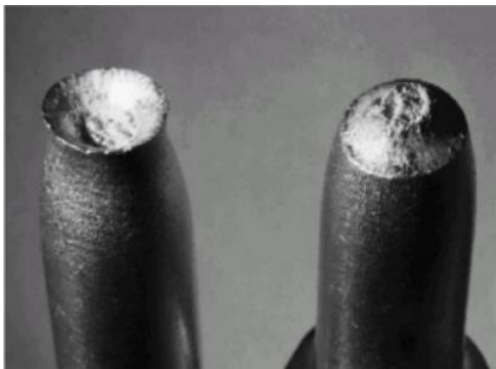
Figure 2. 74: Ductile cup and cone fracture in metal [243].

Stages of ductile fracture includes [235],[236],[244]:

- Necking

- Void nucleation

- Void growth

- Void coalescence to form a crack,

- Crack propagation

- Fracture.

2.11.3. Fracture analysis approaches

Tremendous effort and progress have been made in fracture mechanics field, from Wohler's experiment, Griffith theory, Irwin–Orowan modification of Griffith theory, and Paris and Elber contribution, fracture mechanics is today a well-established theory that can be used to describe, predict and to determine fatigue strength of materials, in order to prevent crack formation, identify areas susceptible to crack propagation during design, and so on. So, in sum fracture control [235],[236],[244].

In fracture mechanics, in order to analyse the stress field at the crack tip, two main fundamental approaches can be utilised namely Linear Elastic Fracture Mechanics (LEFM) and Elasto Plastic Fracture Mechanics (EPFM), the following section will cover these topics [235],[236],[244].

2.11.3.1. Mode of fracture

The stress systems around a crack tip can be split into 3 basic types, fracture analysis considers these 3 types of fracture modes. Mode I, Mode II and Mode III as shown in Figure 2. 75.
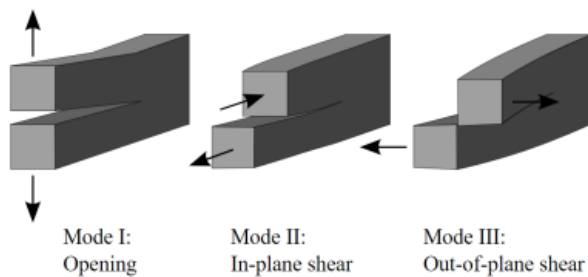
Figure 2. 75: Three modes of fracture [235], [245].

It is known that:

Mode I: Opening mode, the normal force is perpendicular to the fracture plane is perpendicular to the normal force.

Mode II: Shearing mode, the occurrence of fracture is caused by shear stress and grows in the direction of shear.

Mode III: Tearing mode, like in Mode II here as well the occurrence of fracture is caused shear however the fracture grows in the direction that is perpendicular to shear [235],[245].

2.11.3.2. Linear Elastic Fracture Mechanics (LEFM)

Linear elastic fracture mechanics is an approach used in fracture mechanics for determining fracture in brittle materials. It is utilised for calculating accurately fracture stress of brittle materials, with as assumption that the stress field around the crack tip is within the elastic limit (stress field at the crack tip is elastic), so it LEFM does not take in consideration the plastic flow at the crack tip that takes place in ductile materials [235] [246].

2.11.3.2.1. Fatigue

When a material is subjected to cyclic loads or stresses, failure of this material will occur at stresses lesser than it yield strength. This genre of material failure is referred to as fatigue. material failure This material will fail at a stress Materials and structures fatigue study emanated from 19th century, where various scientist attempted to address the observed mechanical failure that occurred to materials

after their exposure to cyclic load [247],[248]. Event such as the collapse of Montrose suspension bridge in 1830, the occurrence of failure in liberty ship in 1943 rose questions in scientific community and pushed scientists to pay more attention at the behavior of material when exposed to load in that era [249].

While lecturing in Metz at the military school, Poncelet referred and portrayed metals as being "tired"[247]. Later on, Wöhler conducted one of earliest investigations to identify fatigue phenomenon and used what referred to today as S-N curve Wöhler curves to express correlation between stress and cycle to failure [250].

2.11.3.2.2. Fatigue life (S-N) curves

Developed by a German scientist (August Wöhler) during his investigation on the Versailles railway accident of 8 May 1842 in France. The S-N curve is today used worldwide in material the design in order to determine the number of load cycles-to-failure in material or the material life span when exposed to load. Back in 1842, a catastrophic railway accident took place in Versailles and claimed several humans' lives and raised a lot of questions [249]. During his study of this event, Wöhler conducted experiments studies on various railways axels under repeated load and realized (found) that the number of cycles of time-variant stress was the culprit or the cause of premature failure witnessed in the railway's axels that was utilized. Wöhler also noted that axels in the railways failed as a result of low cyclic stress applied to it by trains in certain time interval (daily as the train passed on these railways axels) [249].

As part of S-N curve development, Wöhler further came up with the concept of endurance limit (Stress level that would be tolerated for a million of fully reversed cycles), meaning the stress at which material failure will not occur. So, if stress was applied to a material is bellow it endurance limit, failure will not occur, or material will have infinite life [249].
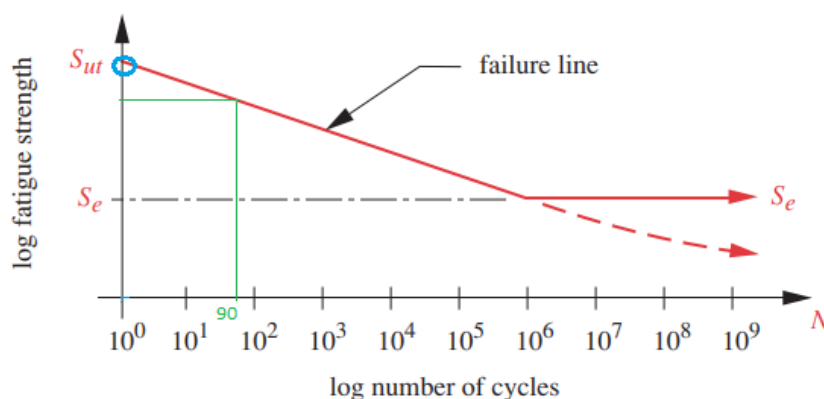
Figure 2. 76: S-N curve when log of stress vs log of number of cycles is utilized [251].

Figure 2. 76 above shows the S-N curve which is a plot of the alternating stress amplitude versus the number of cycles to failure for a given material. The log of stress amplitude on the y-axis and number of cycles on the x-axis. Sut is the ultimate tensile strength, and Se the endurance limit, and the red line represent the failure line or boundary. On a normal scale the S-N curve is not a straight line but on the log scale it appears to be a straight line as shown above [249], [251].

On the X-axis, 10^0 refers to 1 cycle (which is not time variant), and this is not really time variant stress. Material under static load will fail at ultimate strength, as it is the case for 10^0 cycle, where the material fails at Sut as shown by the blue circle on the graph. When the applied stress amplitude is reduces, the number of cycles to failure in material increases. So, for instance in the case of figure… when the stress amplitude is reduced bellow Sut as selected by the green line in figure… it can be seen that the material life cycle is no longer 10^0 or 1 which failed at Sut, but the material life cycle is 90. For the same stress load if the material is operated bellow 90 cycle the material will be fine however when operated above 90 cycles the material will fail. S, the applied stress and the number of cycles to failure plays an important role in fatigue failure [249], [251].

When looking at the Y-axis, at Se, the numbers of cycles to failure is approximately 10^6 or 1 million. As stated earlier, Se is the endurance limit or endurance strength of the material, for material such as steel and some titanium alloys when the stress that is applied to the material is bellow Se the material will not fail, and such behavior is referred to as having infinite life [249], [251]. Se is one of the most important material parameters or property. However, not all materials obey to the concept of endurance limit, or some materials do not show any endurance limit. For instance, in the case of aluminum alloys, when the stress amplitude is bellow Se failure can still occur, hence, for such material reduction in applied stress bellow Se increases the material life cycle but does not mean does not mean infinite life, and for such materials at Se, the curve will not be horizontal as it was in the case of material having endurance limit (steel material), but it will continue to go down, for these types of materials the reduction of stress amplitude means larger life but not infinite life as it is the case of steel materials [249], [251].

2.11.3.2.3. Stress Fluctuation with time

Variation of stress as a function of time. Cyclic loading refers to the loading and unloading in that is repeated after a time interval [249], [251]. When a mechanical part is subjected to fatigue or cyclic varying load, the induced stress is referred to as fluctuating stress. Fatigue stress can be classified in to 3 different types of namely repeated fatigue stress, reverse fatigue stress and fluctuating or altering fatigue stress.

(a) Fully Reversed fatigue stress

In fully reversed fatigue stress, the stress is completely reversible. The mechanical part (the material) is subjected to tensile and compressive stress of the same magnitude, the stress amplitude in tension is equal to the stress amplitude in compression, this means that the maximum stress is equal to the minimum stress, but they have opposite signs, one is positive (tension) and the other is negative (compression). So, σ_{max} = -σ_{min}. As a result of stress amplitude being equal in tension and compression phase, the mean stress is equal to zero (σ_m = 0) [249], [251].
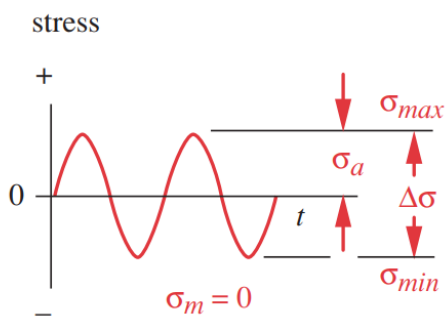
Figure 2. 77: Fully reversed stress [251].

Figure 2. 77 shows a stress versus time curve of fully reversed stress having the same magnitude in tension region (positive) and compression region (negative), with a mean stress value of zero [249], [251].

(b) Repeated fatigue stress

Unlike in the fully reverse fatigue stress where the stress cycle takes place in both tension and compression region with σ_{max} = -σ_{min}, in repeated fatigue stress, the stress applied on mechanical part takes place entirely in one region either in tension region as shown in figure... or compression region. However, the material is not exposed to both stress as it was the case of fully reversal stress. So, in for repeated stress, material experience or is exposed to either tensile or compressive stress but not both. It is understood that crack propagates when materials are tensed, so in the case of repeated load it is much more practical to consider the tension region. Hence, the σ_m is greater than zero. σ_m >0.
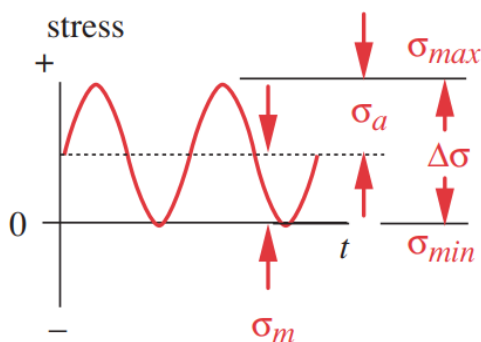
Figure 2. 78: Repeating stress [251].

Figure 2. 78 above shows a stress versus time curve of repeated stress in which the minimum stress is equal to zero,

(c) Fluctuating fatigue stress

In some situations where the applied load is not fully reversed but is changing and more complex, the load is referred to as fluctuating or alternating. In such system, the material can be exposed to both tensile and compressive stress, but the magnitude of these stresses will not be equal, because if they are equal, we will refer to them as fully reversed load and not fluctuating. So, the minimum stress is not zero, and it is not equal to maximum stress [249], [251].
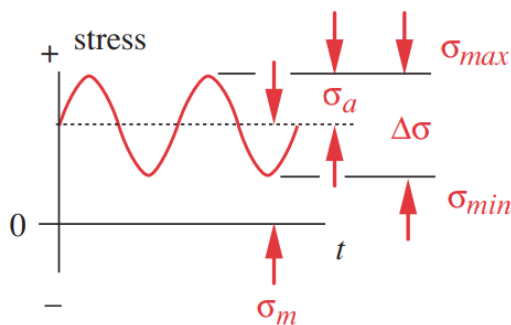
Figure 2. 79: Fluctuating stress [251].

Figure54 above shows a general stress versus time curve for fluctuating stress, it is general case because the stress can fluctuate between the tensile region and the compression region. In the fluctuating stress the minimum stress is not equal to zero, and it is not equal to maximum stress [249], [251].

In order to characterize the stress change versus time depicted in a, b and c the following equations (2.2- 2.8) can be used [249], [251]:

❖ The Alternating stress which is the magnitude of stress amplitude

$$\sigma_a = \frac{\sigma_{max} - \sigma_{min}}{2} \tag{1.3}$$

❖ The mean stress

$$\sigma_m = \frac{\sigma_{max} + \sigma_{min}}{2} \tag{2.4}$$

❖ Stress range

$$\Delta\sigma = \sigma_{max} - \sigma_{min} \tag{2.5}$$

❖ Stress ratio

$$R = \frac{\sigma_{min}}{\sigma_{max}} \tag{2.6}$$

❖ Amplitude ratio

$$A = \frac{\sigma_a}{\sigma_m} \tag{2.7}$$

❖ Upper stress

$$\sigma_{up} = \sigma_m + \sigma_a \qquad (2.8)$$

❖ Lower stress

$$\sigma_l = \sigma_m + \sigma_a \qquad (2.9)$$

2.11.3.2.4. Low cycle fatigue

Low cycle fatigue LCF and high cycle fatigue concept referred to the type of deformation that takes place (plastic, elastic) and the number of cycles to failure [252],[253].

In high pressure high temperature (HPHT), low cycle fatigue (LCT) is one of the most important considered factor [254]. Repeated plastic deformation characterizes LCF. In LCF fracture occurs when Lower stress $\sigma_l = R_m$ It is understood that the stress amplitude is generally given by:

$$\sigma_a = \frac{\sigma_{max} - \sigma_{min}}{2} \qquad (2.9)$$

Stress ratio $\quad R = \dfrac{\sigma_{min}}{\sigma_{max}} \qquad (3.10)$

However, the stress amplitude inducing fracture in LCF is determined by [252],[253]:

$$\sigma_{a,max} = R_m \frac{1-R}{2} \qquad (4.11)$$
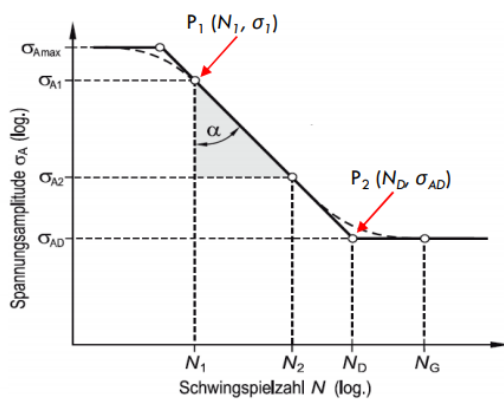
Figure 2. 80: Stress amplitude vs numbers of cycles [255].

LCF can be divided into [252],[253]:

❖ Very low life cycles where experiments are conducted with cycles to failure less than 100 cycles,

❖ Low cycle fatigue (LCF) where experiments are conducted with cycles to failure less than 10^4,

2.11.3.2.5. High cycle fatigue

Characterized by elastic deformation, High-cycle fatigue (HCF) is identified as one of the prime reasons behind failure of turbine-engines in military aircraft [256],[257].
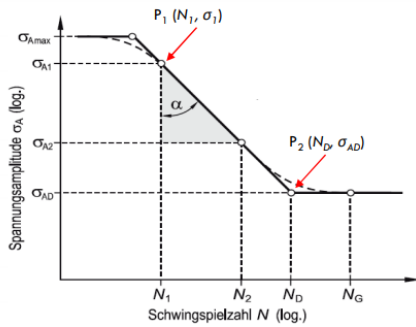
Figure 2. 81: Stress amplitude vs numbers of cycles [255].

In HC,F failure can take place unpredictably as result of fatigue crack initiation (Due to impact) and propagation in materials (turbine blades, disk) during load that are very high and capable of causing small cracks [256].

HCF can be broken down into [252],[253]:

* ❖ High cycle fatigue (HCF) which varies between 10^5 and 10^7

* ❖ Very High life cycle fatigue (VHCF) experiments that are conducted over 10^7 cycles to failure

Straight line equation is utilized to the S/N curve in order to find the slop of the curve.

One of the ways of calculating the slop is to find the tangent of the angle α formed by selecting two points on the number of cycles that are corresponding to two points on the stress amplitude as shown in figure57. The slop is given by tan α = K.

tan α = K. slope,

$$log\left(\frac{N_D}{N_1}\right) = K \, log\left(\frac{\sigma_{A1}}{\sigma_{AD}}\right) \tag{5.12}$$

$$N_1 = N_D \left(\frac{\sigma_{AD}}{\sigma_{A1}}\right)^K \tag{6.13}$$

2.11.3.2.6. Stress Intensity Factor K

The stress intensity factor (SIF) is utilised in determination of stress state, as such it plays a very important role in linear elastic fracture mechanics (LEFM) [251]. It is useful in the assessment of safety or reliability of a machine or structural component with a crack. It enables the calculation of crack growth rate through a component under fatigue loading, stress corrosion, [251].
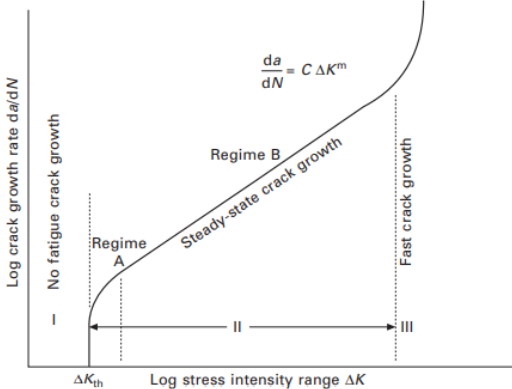
Figure 2. 82: Paris curve [251].

The K value from Paris curve can be obtained by using the following equation 2.14.

$$\log\left(\frac{N_D}{N_1}\right) = K \log\left(\frac{\sigma_{A1}}{\sigma_{AD}}\right) \tag{2.14}$$

This curve is used to determine crack initiation, crack propagation and failure due to fatigue load.

<div align="right">

CHAPTER 3

</div>

3. Experimental details and analytical procedures

3.1. Introduction

All of the experiments conducted for this thesis were performed using equipment's at KU Leuven laboratory in Belgium. The objective of this chapter is to provide description of the experimental procedures, and materials used (Chemicals, L-PBF-Ti64V, and equipment's) in this thesis. This chapter is divided in to 4 different sections or focus area, namely:

- Description of the utilised materials,

- Descriptions of the heat treatment program utilised including parameters and additional materials,

- Microstructure analysis and characterisation (Including metallography laboratory work, sample embedding, grinding, and polishing, etching, and processing of image), and

- Mechanical testing of tensile and fatigue samples.

3.2. Materials selected and studied in this work

The material studied in this thesis is the L-PBF produced Ti6Al4V that was manufactured at KU Leuven. While several studies [217],[258]–[260] have shown that build direction contributed to some degree to the observed difference in some mechanical properties. It is important to highlight that all the L-PBF produced Ti6Al4V parts used in this thesis were produced with the same build direction (vertically). Hence, difference observed in their mechanical properties cannot be attributed to difference in build orientation.

3.2.1. Samples Description

Three different batch or type of samples geometry wise were utilised in this experimental study:

1. Cylindrical samples that were used mainly for microstructure analysis. The cylindrical samples were heat treated using the heat treatment program then, embedded, grinded, etched and microstructure analysis.

2. Tensile samples were initially printed as rectangular bars that were later machined in desired dogbone shaped parts. These samples were heat treated using the heat treatment program

like the one utilised for cylindrical, then machined into desired shape, grinded and mechanically tested (tensile test). After the tensile samples were mechanically tested, they were etched and then analysed to observe the failure path.

3. Fatigue samples were initially printed as cuboidal blocks that were later machined, to desirable shape (CT specimen). These samples were heat treated using the heat treated in the same manners as cylindrical and tensile sample (using the same heat treatment program). Fatigue samples were then grinded to the thickness of 5.8 mm so as to remove the alpha casing layer after the heat treatment. They were then machined to have a notch, then mechanically tested (Fracture crack growth test). After the FCG test fatigue samples were etched and then analysed to observe the crack path.

3.2.2. Chemical composition

Fehler! Verweisquelle konnte nicht gefunden werden. below shows the chemical composition of L-PBF produced Ti6Al4V that are studied in this thesis.

Table 3. 1: Chemical composition of L-PBF Ti6Al4V.

Elements	Ti	Al	V	O	N	C	H	Fe	Y	Residual each	Residual total
Weight %	Balance	5.5 − 6.5	3.5 − 4.5	≤0.13	≤0.03	≤0.08	≤0.012	≤0.25	≤0.005	≤0.1	≤0.4

The density of L-PBF produced Ti6Al4V parts was the samples used in this thesis were measured using sartorius YDK03 in which Archimedes principle is used. Two sets of measurement were taken for each sample, the first in the air and the second using ethanol where the sample was subjected to buoyancy force which is equal to the weight of the ethanol displaced. So, the two obtained measurement of the sample weight in the air and in ethanol are represented by the letter A, and B as shown in the equation …below while the density of ethanol measured at room temperature is given by C (0. 795 g/cm^3) and the density reference Ti6Al4V sample depicted by the letter D (4.42 g/cm^3).

$$\rho_{Sample} = \frac{A}{A-B} * \frac{(C-0.0012)+(0.0012)}{D*100} \qquad\qquad (3.1)$$

Relative density measurement of L-PBF Ti6Al4V parts studied in this thesis showed that these parts were fully dense with an average density of more than 99% which is within the required specifications.

3.3.   Experimental design

In the second stage heat treatment, samples were separated in to 4 groups based on the 4 temperature groups 800, 840, 880 and 960°C. In each temperature group samples were heat treated to 4 different aging time viz. 2, 3, 4, and 5 hours. In all of these second stage heat treatment after the targeted temperature and ageing time were reached samples were air cooled, this is because

[33],[262],[268],[269]. In the first stage heat treatment all the samples were heat treated above the β transus to 1030°C then furnace cooled which is very slow in order to achieve lamellar microstructure. In the second stage heat treatment all the samples irrespective of what temperature and ageing time they were heat treated at the were air cooled in order to achieve bi-lamellar microstructure as achieved by chong [56].

Table 3. 2 below shows temperatures and ageing time to which different samples were subjected to during the second stage heat treatment. The letter in this tables distinctively highlights that each sample had only one second stage heat treatment with one ageing time.

Table 3. 2: Heat treatment program schedule temperature and ageing time.

Ageing time (Hours)	Temperature (°C)			
	800	840	880	960
2	A	A	A	A
3	B	B	B	B
4	C	C	C	C
5	D	D	D	D

As seen in the Table 3. 2 above samples were grouped based on the temperature they were heat treated. A comparative study of the microstructure features, properties, and mechanical properties (tensile and fatigue) was conducted between heat treated samples at different temperature. All of the heat-treated samples mechanical properties (lamellar, bi-lamellar) were compared to each other and then to mechanical properties of the as-build samples.

3.4. Heat treatment

3.4.1. Heat treatment strategies

Heat treatment conducted in this thesis was performed with as objective to transform the acicular martensite microstructure obtained from L-PBF produced Ti6Al4V to achieve bi-lamellar microstructure. This is motivated by the fact that in L-PBF production process there is a higher thermal gradient that leads to the formation of acicular martensite microstructure in Ti6Al4V, and as such the formed in martensite L-PBF Ti6Al4V present short coming like lower elongation percentage and brittleness [205]. The modification of the microstructure result in good strength, elongation and improves various other mechanical properties such as crack resistance properties, and good fatigue tolerance [185],[200],[225]. Even though lamellar microstructure have been achieved by studies conducted on transformation of acicular martensite microstructure observed in L-PBF produced ti6Al4V, it is understood that bi-lamellar microstructure is more resistance to crack propagation

compared to lamellar microstructure, this is because in bi-lamellar microstructure there is the presence of secondary α_S in transformed β which slows or alt crack propagation while lamellar microstructure is predominantly composed of α lamellae surrounded by thin retained β in such microstructure (lamellar) feature crack can easily propagate.

All 3 sets of samples (cylindrical, tensile, fatigue samples) used in this research studies went through two stage heat treatment shown Figure 3. 1.
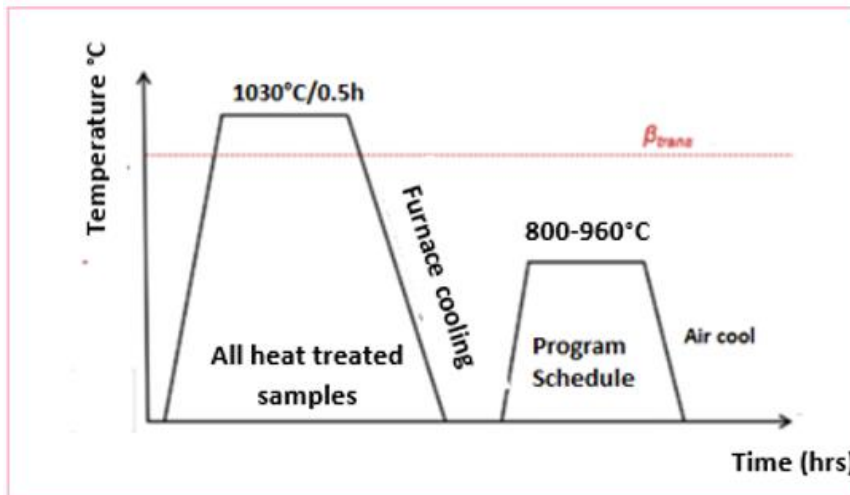
Figure 3. 1:Two stage heat treatment.

For all the samples the first stage heat treatment was the same. So, all the samples were heat treated (solution treating) to 1030°C for 30 minutes then furnace cooled. These samples are furnace cooled to allow a slow cooling rate and achieve lamellar microstructure. The second stage heat treatment was conducted below the β transus, in this stage samples were first grouped by temperature, in each temperature group samples were subdivided or sub-grouped based by the residence or ageing time samples were heat treated to as shown in Table 3. 2. In the second stage heat treatment samples were air cooled after the respective ageing temperature and time.

3.5. Microstructure characterization

3.5.1. Sample preparation process

In metallography, metals and metals alloy's structure are studied and analyzed by utilizing a metallurgical microscope to examine them. After observing these metals and metals alloy's structures, they can be recorder as a photo [270]. However, prior to using the metallographic microstructure, to observe, photograph and analyse the metals and metals alloys structures, the sample must go through several preparation steps. Those steps involve sample embedding, grinding, polishing, and etching. Sometimes, some samples cannot be embedded as they are very small, in such case such sample are

glued to a plate then grinded without being embedded or grinded manually using manual grinder and polisher.

During sample embedding process, a plastic mould as shown in Figure 3. 2a is used, the sample is placed in the plastic mould as shown in Figure 3. 2b, preferably in the middle of the plastic mould. A cold curing resin is prepared using technovit 4004 powder and technovit 4004 liquid by mixing two measures of technovit 4004 powder with one measure technovit 4004 liquids.

The result of the mixture of technovit 4004 powder and technovit 4004 liquid was a milky like suspension shown in figure Figure 3. 2e and f. The obtained milky suspension is then poured in the mould containing the sample that need to be embedded as shown in Figure 3. 2g and wait for the duration of approximately 30minutrs for the resin to cure. After the resin have cured, embedded sample in resin is removed from the mould as shown in Figure 3. 2h for grinding and polishing.
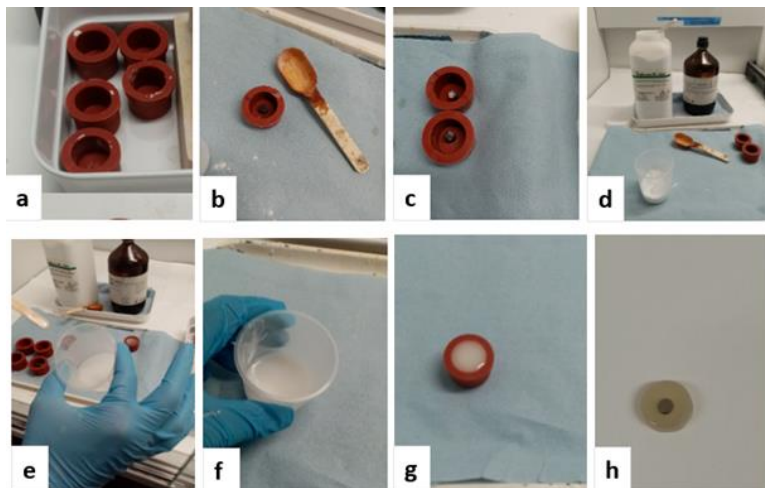
Figure 3. 2: Sample embedding process.

Sample grinding and polishing were done using two different methods. The first method was using METALPOL 260 dual-speed metallographic sample grinding and polishing machine as shown in Figure 3. 3 and the second one was done using LapForce-100 automatic grinding and polishing machine as shown in Figure 3. 5 .

During the first method grinding and polishing were done using silicon carbide papers with different grits size raging from P80 to P4000. With P80 being most abrasive and as the number increases the paper became less and less abrasive and smoother. The abrasive silicon carbide papers were used for griding while the smother ones were used for polishing.
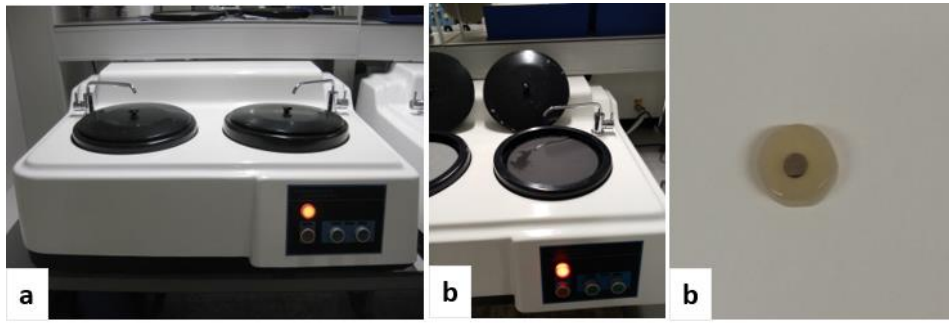
Figure 3. 3: METALPOL 260 dual-speed metallographic grinder and polisher used.

The embedded sample is held by hand against the rotating wheel during this process while rotating wheel or plate turns uniformly at a constant speed. The grinding and polishing are conducted with running water that cools and cleans the surface of the grinding paper.

Figure 3. 4 below shows an image of grinding and polishing papers utilised during manual grinding and polishing.
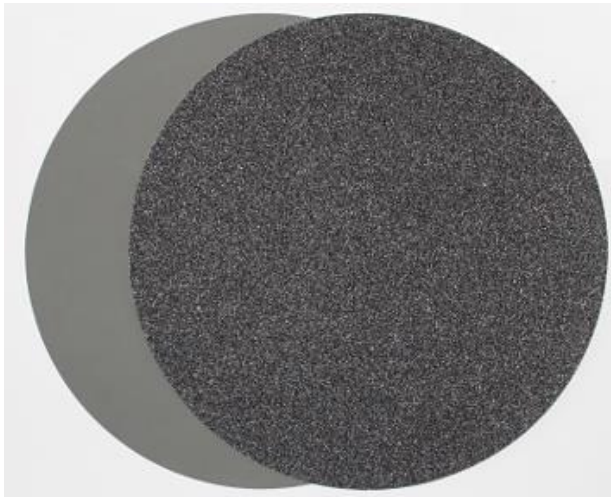
Figure 3. 4: Grinding and polishing paper used in grinding and polishing [271].

The second method for grinding and polishing of sample was an automatic method in which samples were grinded and polished using an LapForce-100 an automated grinding a polishing machine.
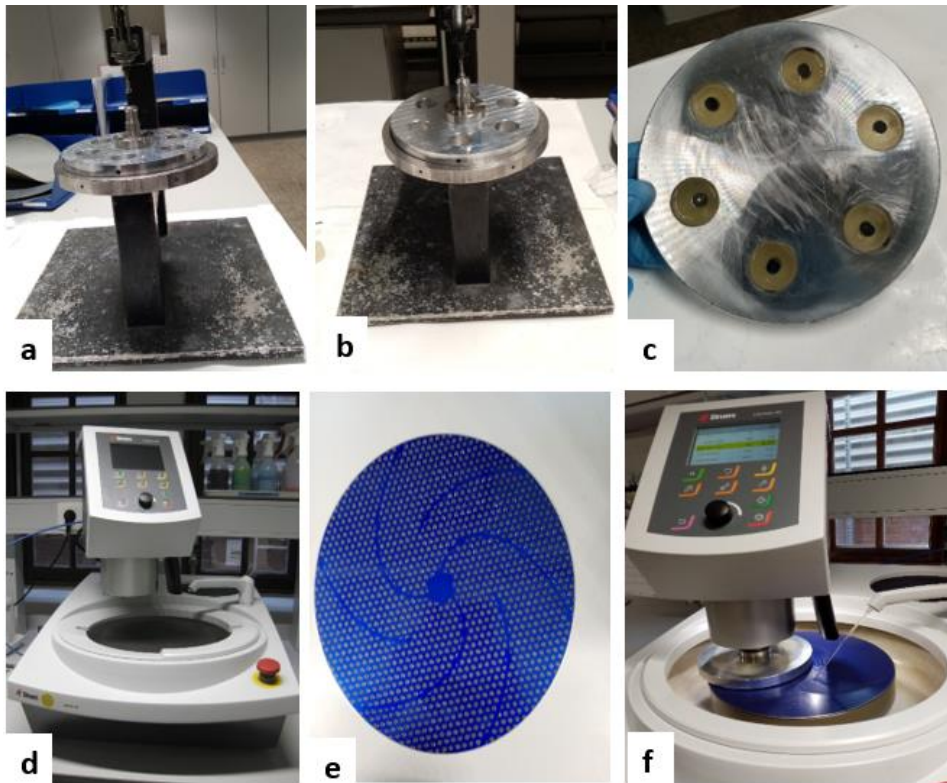
Figure 3. 5: Automated sample grinding and polishing process.

During this method, a metal sample holder is placed on the metal support as shown in Figure 3. 5 (a) and then sample holder is clamped to restrict it from moving and provide even height for samples that are placed in the sample holder. After the samples have been placed in the sample holder, they are tightened using an Allen key, since next to each sample is a screw that is used to restrict the sample from falling out of the holder. After tightening the samples using an Allen key, the sample are ready to be grinded and polished. Figure 3. 5 (c) above shows samples that have been tightened in the sample holder. The sample holder is then insert in the LapForce-100 machine in order to start with the grinding and polishing process. Various sets of magnetic plates are available and can be used for the process of grinding and polishing. The magnetic blue plat seen in Figure 3. 5(e) is used for grinding. So, once the magnetic plate is placed on the disk of the LabForce-100 the sample holder is lowered, and the grinding commenced as shown in Figure 3. 5 (f).

The force to be used is already predefined for each material that must be grinded. So, for Ti6Al4V the force to be utilised was 40-45 N for each sample so in case there is 6 samples the force to be used is 240N. The head and the bottom disk of the labfor-100 both engage in opposite motions one in clockwise and the other in counterclockwise motions to grind samples. The head part of LapForce-100 can be set to 300 N during grinding and 150N during polishing, while the bottom part turns at 150 N during grinding and polishing.
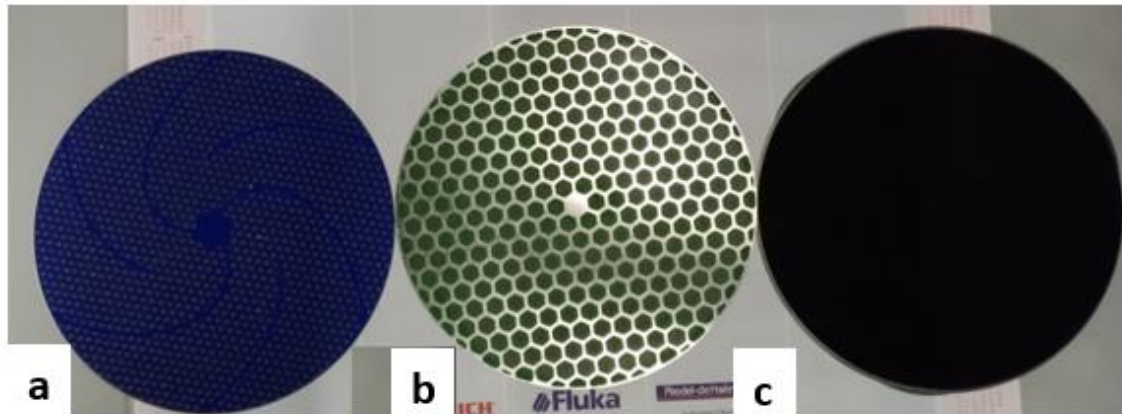
Figure 3. 6: Various plate used in grinding and polishing with LabForce-100 (a) grinding, (b)polishing (c) polishing.

During grinding with the blue plate shown in Figure 3. 6(a) only water is utilised, and during the polishing with the green plate shown in Figure 3. 6 (b) a diamond suspension is utilised, and when the black plate with velvet like surface as shown in Figure 3. 6 (C) is utilised an OPS solution is utilised for the polishing of Ti6Al4V samples. The OPS solution is made of OPS suspension and hydrogen peroxide. The OPS suspension and hydrogen peroxide are mixed in a container to a ratio of 70/30. The OPS was 70ml and the hydrogen peroxide 30ml.

After grinding and polishing, samples were etched to be able to examine the microstructure through the microscope (Optic and SEM). Sample etching was done using Keller's reagent. Keller's reagent having the following composition was utilised 3ml HF, 2ml HCL, 5ml HNO_3 and 190 ml H_2O. Samples were submersed in Keller's reagent for duration between 6 to 10 seconds after which these samples were then submersed in a diluted boric acid solution composed of 50% boric acid in water. This additional step is done for neutralization of HF on a laboratory scale. Due to the risk associated to HF utilization and safety, KU Leuven laboratory allowed etching to be done only by PhD researcher or laboratory technician. All the samples studied in this thesis were etched (Microstructure samples tensile, and fatigue,) to observe microstructures features, analyse them and correlate or associate crack initiation and propagation to the microstructure features.

3.5.2. Microstructure characterization

Samples characterization was done by using two types of microscopes at KU Leuven, the optical microscope and scanning electron microscopy (SEM Philips XL30 FEG). The SEM was paired with an EDS detector system from EDAX. Before samples were analysed by either of these microscopes, they (samples) were etched with the Keller's solution described in section 3.5.1.

3.6.   Mechanical testing

3.6.1. Hardness (VH) test

Vickers hardness measurement were conducted using FV700 Vickers hardness testing equipment as shown in Figure 3. 7.

Figure 3. 7: FV700 Vickers hardness testing.

3.6.2. Quasi-Static Mechanical Testing

The quasi-static mechanical behaviour of the obtained bi-lamellar microstructure was obtained by characterized by uniaxial tensile testing according to the ASTM E8 standard. The tensile test was performed on Instrom 4467 UTM machine equipped with a load cell of 30kN. The tensile test was performed at the crosshead speed of 0.5 mm/min to avoid any possible influence of strain rate on the mechanical properties. The strain during the tensile test was measured using an external extensometer with the gauge length of 12.5 mm.

3.6.3. Fatigue Crack Growth (FCG) test

The fatigue test conducted in this study is the fatigue crack growth (FCG) based based on the ASTM E647. The FCG test was conducted on several samples (as-build, lamellar, bi-lamellar) using Instron 3000 fatigue tester with as objective to measure and compare resistance to fatigue crack propagation properties of as-build and heat-treated samples (Lamellar and bi-lamellar). Additionally, to also verify if the newly developed microstructure (Bi-lamellar) has improved fatigue crack resistance compared to as-build and lamellar samples.

According to ASTM E647 standard used for FCG in this thesis, a compact sample having the design and dimension shown in Figure 3. 8 is cyclically loaded in tension mode until the sample fail. The sample

tested has an initial crack has an initial notch length of 4.8 mm, width (W) of 23 mm and the thickness(B) of 6 mm.
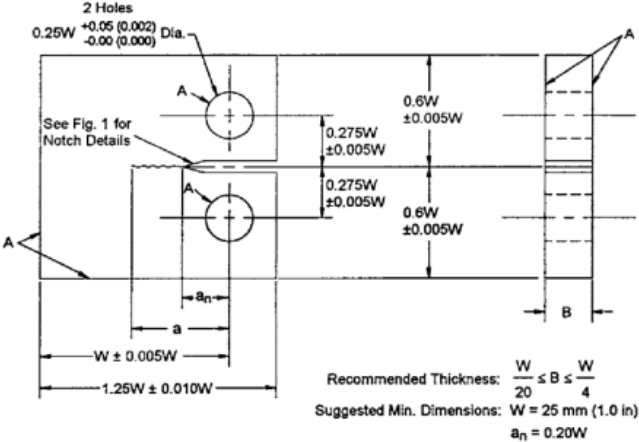
Figure 3. 8: ASTM E647 CT sample dimension.

The FCG test were conducted on as-build, lamellar and bi-lamellar (800, 880 and 960°C). 4 samples for each sample group were tested. During this test crack initiation was done by using a frequency (n) ranging from 20 Hz to 40 Hz, and an amplitude (ΔP) varying between 2000 to 2400N. Once the crack was introduced in the sample there was a cyclic load applied to the sample(R=0.1), with constant frequency and constant amplitude (ΔP).

The obtained FCG rate results from Instron E3000 were plotted in an X and Y plot (graph) with the crack growth rate (da/dN) as the Y-axis and the stress intensity range (ΔK) as the X-axis in log (da/dN) vs log (ΔK) in other words, log of crack growth rate (da/dN) vs log of stress intensity range (ΔK). The experimental results plotted could be studied using Paris equation where C and M are material constant.

$$\frac{da}{dN} = C(dK)^m \tag{3.2}$$

Paris equation in this form is an exponential equation and it can be made linear by plotting it on logarithmic axes or by converting the data by taking the natural log the slop of the obtained line will be m while and C the Y-intercept.

These material constants (m and C) can be calculated using software such as originlab and many others. These obtained valued and initially measured fatigue samples data's including visual measurement made using a 2 mm sticker placed on samples in order to calculate ΔK.

4.   Results and discussions

This chapter (Chapter 4) will present result obtained from the experimental work carried out during this thesis and is divided in to 3 different sections:

- The first part deals with the microstructural characterization and analysis of bi-lamellar microstructure obtained by heat treating L-PBF processed Ti6Al4V.

- The second part deals with quasi-static mechanical properties of bi-lamellar microstructure obtained after the two-stage heat treatment.

- The last part focuses on the crack propagation behavior of the bi-lamellar microstructure.

4.1. Microstructure analysis

This section discusses the microstructure in three different conditions:

- L-PBF observed in as-build samples (Acicular martensite),

- First heat treatment (lamellar), and

- Two-stage heat treatment (Bi-lamellar)

Additionally, in microstructures after second heat treatment shown in Section 4.2.3 figures are denoted with later a, b, c, and d which represent different aging time within the same temperature used for heat treatment. So, for instance 4 samples were heat treated to a second stage heat treatment temperature of 800°C, they were aged at different time, a means 1 hour, b means 2 hours, c means 3 hours and d means 4 hours aging time respectively.

4.2. Microstructure evaluation

4.2.1. Microstructure after L-PBF production of Ti-6Al-4V

The as-built martensitic microstructure is presented in Figure 4. 1 Martensite transformation occurs in Ti-6Al-4V when the cooling rate is above410 K/s. Such high cooling rates are observed due to the use of laser for melting the powder bed. [38],[272].

The epitaxial beta grains observed in the columnar prior β grain in both thesis results and literature is due to partial re-melting of the previous layers that takes place when laser melts the powder bed.[275]–[277].
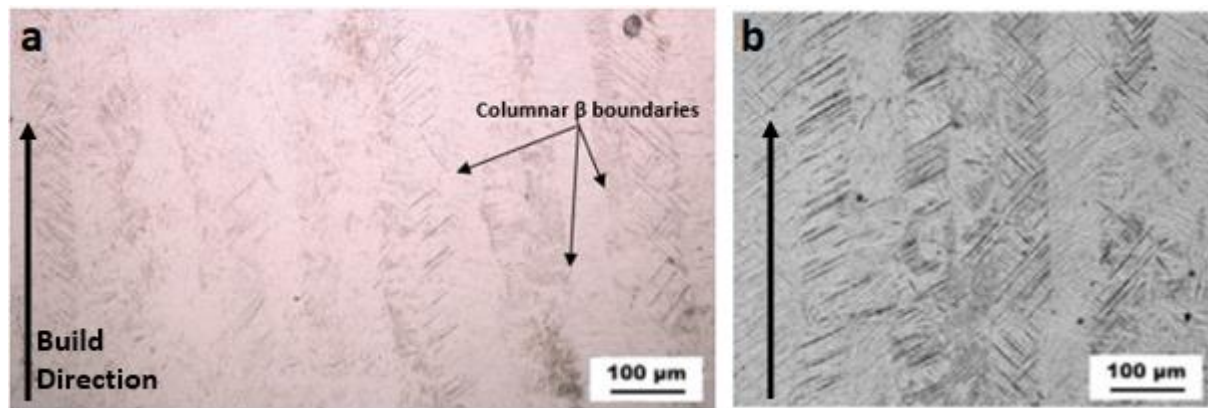
Figure 4. 1: Acicular martensite microstructure in columnar β a) experimental, b) literature [274].

4.2.2. Beta annealing

The as-built cylinders were heat treated at the temperature of 1030˚C (above beta transus) for 30 minutes followed by furnace cooling (3˚C/min). The resulting lamellar microstructure obtained after beta annealing is shown in Figure 4. 2 The formation of lamellar microstructure is composed of 4 different stages:

1. **Decomposition of martensite**: Martensite starts to decompose into the mixture of alpha and beta between the temperature range of 650-800˚C.

2. **Transformation of alpha into beta**: After the complete decomposition of martensite into alpha and beta, alpha starts to transform into the beta phase with increase in temperature.

3. **Complete transformation into beta**: At around 995-1000˚C, all the alpha is transformed into the beta phase. Above 1000˚C, Ti-6Al-4V behaves as a single-phase material.

4. **Transformation of beta into alpha phase**: After the temperature goes below 1000˚C during cooling, beta starts to transform into alpha phase.

    a. **Formation of grain boundary alpha**: Beta to alpha phase transformation always begins at the grain boundary of the prior beta grain boundary. Nucleation of alpha with different crystallographic orientation takes place at the grain boundary of prior beta grains (the grain boundary is delineated by the orange line in Figure 4. 2 and Figure 4. 3. The formation of grain boundary alpha always takes place upon slower cooling from single phase beta field in two phase Ti alloys.

    b. **Formation of lamellar alpha structure**: After complete decoration of the prior beta grain boundary with the alpha phase, the film of the alpha phase starts to grow inside the beta grain via interface instability mechanism. During the growth phase of GB alpha, protuberances are formed at the grain boundary alpha phase. If the protuberances are instable, they are dissolved back into the beta phase whereas, if the protuberances are stable, they start to grow inside the beta grain and thus

resulting in the formation of alpha colony structure (Sun). The alpha lamellae in one single colony have one crystallographic orientation. Similarly, alpha lamellae growing from different regions of the grain boundary will have different orientation. Different alpha colonies are highlighted by the red colour in Figure 4. 2 and Figure 4. 3. Thus, resulting in the formation of different colonies of alpha within one single beta grain.
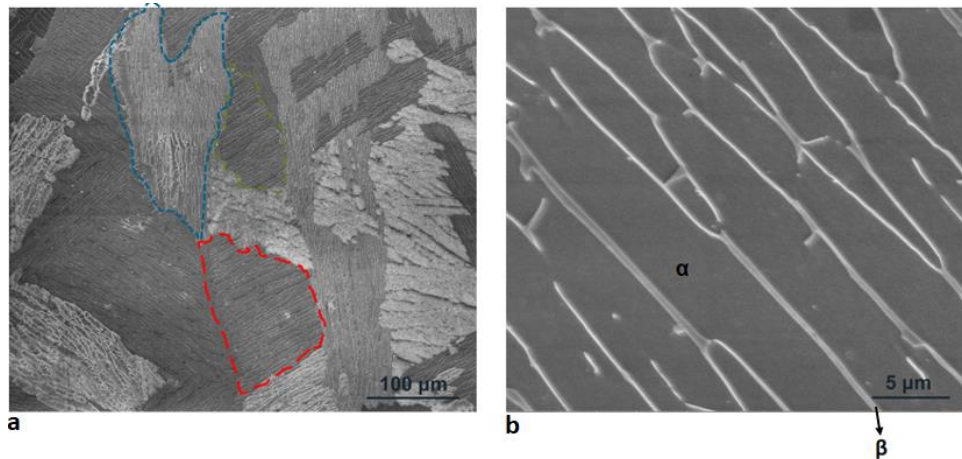
Figure 4. 2: Lamellar microstructure a) with colony, b) at higher magnification.
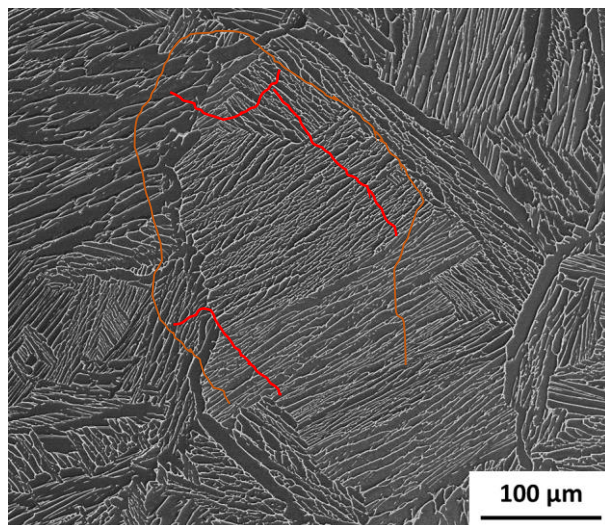
Figure 4. 3: Lamellar microstructure.

4.2.3. Microstructure after second heat treatment

Bi-lamellar microstructures presented in this section were obtained through the two two-stage heat treatment. The first step was kept same for all the samples that is heating the as-built sample to the temperature of 1030 ˚C and followed by furnace cooling, which results in the formation of lamellar microstructure.

For the second step of the heat treatment, time (1h, 2h, 3h and 4h) and temperature (800°C, 840°C, 880°C and 960°C were varied to investigate the effect of time and temperature on the resulting bi-lamellar microstructure.

4.2.3.1.   Microstructure at 800°C with different aging time

Figure 4. 4 shows bi-lamellar microstructures obtained after heat treatment at 800°C. The denotation a, b, c, and d present on the microstructure indicates the microstructure obtained after 1h, 2h ,3 h and 4h respectively. respectively.
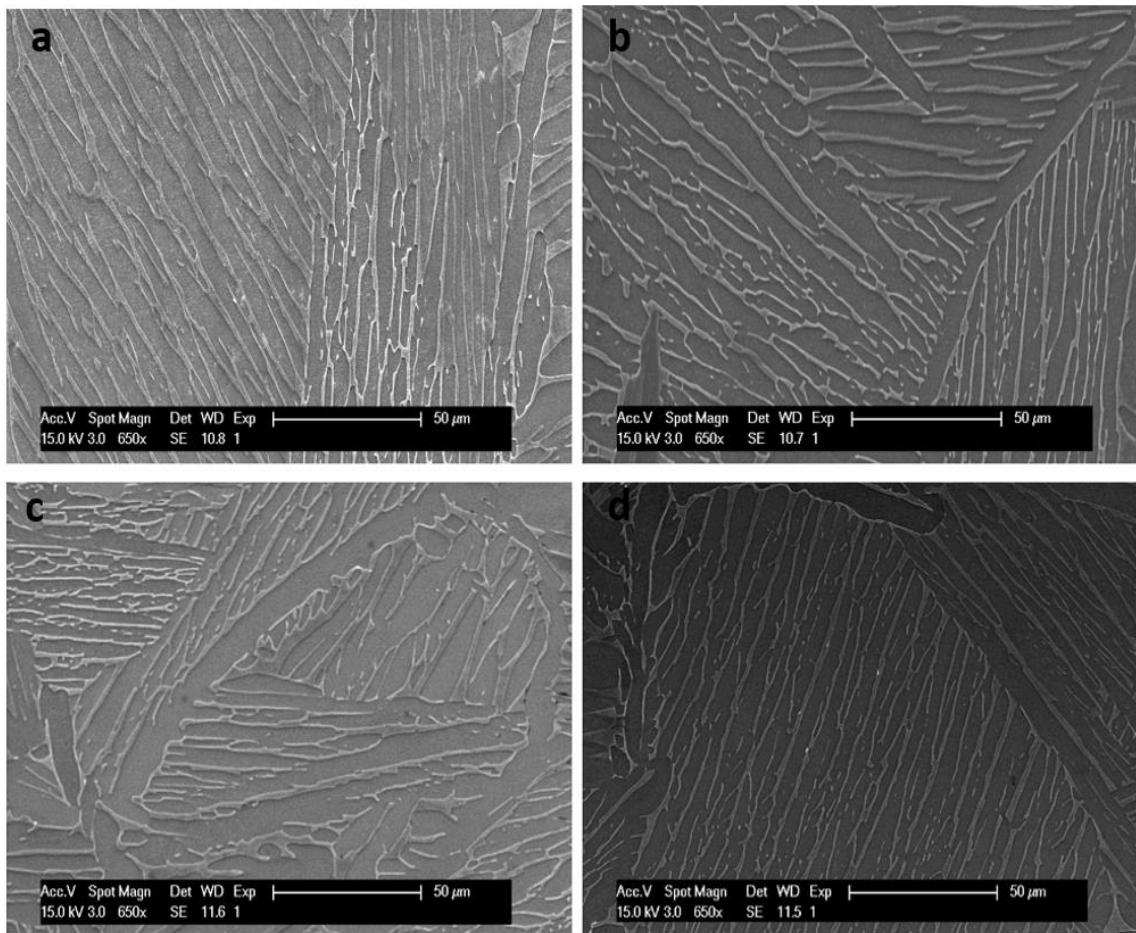
Figure 4. 4: Microstructure observed during heat treatment at 800°C with various aging time a is for 1 hr, b is 2 hrs, c is 3hrs and d is for 4hrs.

The following microstructural features can be identified in the image shown in Figure 4. 4:

- Primary α_p laths,
- Retained β phase,
- Grain boundary α noted GBα.

These features are shown in the expended image of sample heat treated at 800°C for 2 hours.
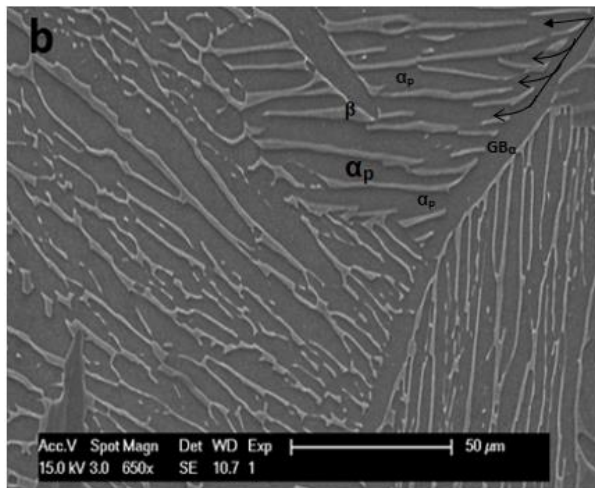
Figure 4. 5: Microstructural features observed at 800°C after 2 hours of aging time.

When looking at Figure 4. 5 and the rest of the microstructure shown in Figure 4. 4 it can be seen that some of the primary α_P lamellar are directly connected to grain boundary α without anything in between α_P and GBα.This indicates that the α_P (primary α) were growing from the grain boundary α. This trend is observed in some part of the microstructure in all the samples (a, b, c and d) and this trend shows how phase transformation occur in lamellar α+β. So, when looking at these microstructures it can be maintained that the first nucleation of alpha takes place along the prior beta grain boundary. Upon complete coverage of the prior beta grain boundary with alpha phase, alpha phase starts to grow inside the beta grain. When looking at the microstructure of samples presented in Figure 4. 4 it can also be observed that primary alpha growing in different directions, this indicates that these primary α_P originated from different regions of prior β grain boundary. This means grain boundary α has different orientations along the prior β grain boundary and as they start to grow inside the β there is different morphological orientations of primary α_P observed. It can also be observed that there are some colonies of the primary α that are not directly connected to the grain boundary α as there is a very fine β layer between the grain boundary α and the primary α_P, this might give the impression that these primary α_P did not grow from this grain boundary α, however this is not the case (Or that is not true) because the microstructure images shown in Figure 4. 4 shows microstructures on a certain plane, however a 3D view would show that this primary α_P also originates from this grain boundary α. So, for the α_P that do not look connected to the grain boundary α it is just because these primary α_P are on different plan than the primary α_P that are seen connected to the grain boundary α. Cao *et al*(Cao reference) studied the effect of the dwell time on lamellar thickness (one stage heat treatment) showed that the lamellae width increased with increasing ageing temperature and ageing time, Cao *et al* they later characterised the increase in lamellar width as monotonic. Studies have shown Ti6Al4V yield strength decreases with increase in lamellar thickness leads to lower yield strength but increase in plastic strain therefore increases ductility as thicker lamellar enable slips and

prevent pile up of dislocation in α phase. There seems to be not much observable morphological the microstructures from different aging time, and there seems to be not much change in α_P thickness within the same temperature even though there is change in aging time.

The first heat treatment step results in the formation of lamellar microstructure, that predominantly consists of the primary alpha phase and thin beta phase along the lamella boundary. During the second stage of the heat treatment, part of the initial alpha starts to transform in the beta phase, the amounts of the alpha and beta phase are governed by the temperature of the heat treatment. Upon air cooling (cooling rate lower than 410 K/s) from the high temperature (800˚C-960˚C), beta transforms to alpha by diffusion mechanism. This beta lamella together with alpha is termed as transformed beta phase. Figure 4. 6 presents the structure of the transformed beta phase. The secondary alpha has a needle shaped morphology (with length of 500-700 nm and width less than 100 nm). The transformation of the secondary alpha, inside the beta lamellae, also starts at the interface of the primary alpha and beta lamellae. However, due to extremely small size of the secondary alpha, it is not possible to visualize the origin of transformation from the micrograph depicted in Figure 4. 6. This phenomenon will be shown for the samples heat treated at 880˚C, where the size of the secondary alpha is comparatively larger.

Figure 4. 6: Secondary α_S after second stage heat treatment at 800°C.

4.2.3.2.   Microstructure at 840°C with different aging time

Figure 4. 7 below shows the obtained bi-lamellar microstructure after heat treating the as-build L-PBF in two-stage heat treatment, the first stage heat treatment is the same for all the samples in this these. The second stage heat treatment was 840°C while using different aging time and the samples were then air cooled. Similar to Figure 4. 4 the denotation a, b, c, and d represent different aging time.
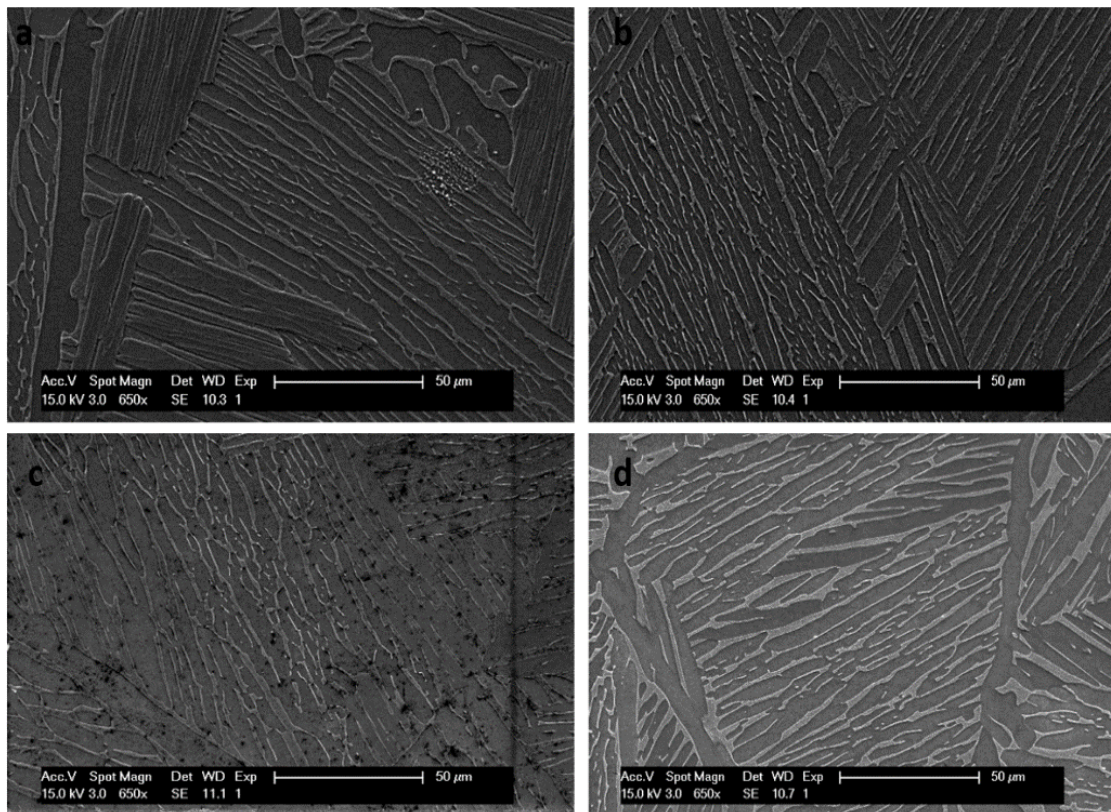
Figure 4. 7: Microstructure observed during heat treatment at 840°C with as aging time a)1 hr, b) 2 hrs, c) 3hrs and d) 4hrs.

Morphologically, bi-lamellar microstructure obtained at 840˚C is same as that of the one obtained at 800˚C but with lower fraction of the primary alpha. Similar features (viz. grain boundary alpha, primary alpha and transformed beta) can be observed in the microstructure. The secondary alpha in this bilamellar microstructure appears to be bit thicker compared to the one obtained at 800˚C.

Figure 4. 8: Secondary α_S after second stage heat treatment at 840°C.

4.2.3.3. Microstructure at 880°C with different aging time

Figure 4. 9 shows the bi-lamellar microstructure obtained after heat treatment performed at 880 ˚C for different periods of dwell time.

When looking at the morphology of the microstructures shown in Figure 4. 9 additional to morphological description of the bi-lamellar microstructures already given for samples heat treated at 800°C section it can be seen that the primary α_P phase starts to break this is due to the fact that when samples are heat treated as the temperature increases primary α_P will first transform to β at higher temperature or the β phase fraction will increase as it can be understood using lever rule for phase diagram. At 880°C in $\alpha+\beta$ phase there is more β volume fraction then during 800°C heat treatment. The place where α_P are broken or starts to break are point or places where phase transformation was happening, the places where β cuts through the α lamellae are the places where α dissolves in to β phase, it can be seen that at some of these places the retained β phase has completely cut the α phase and leads to smaller α lamellar.
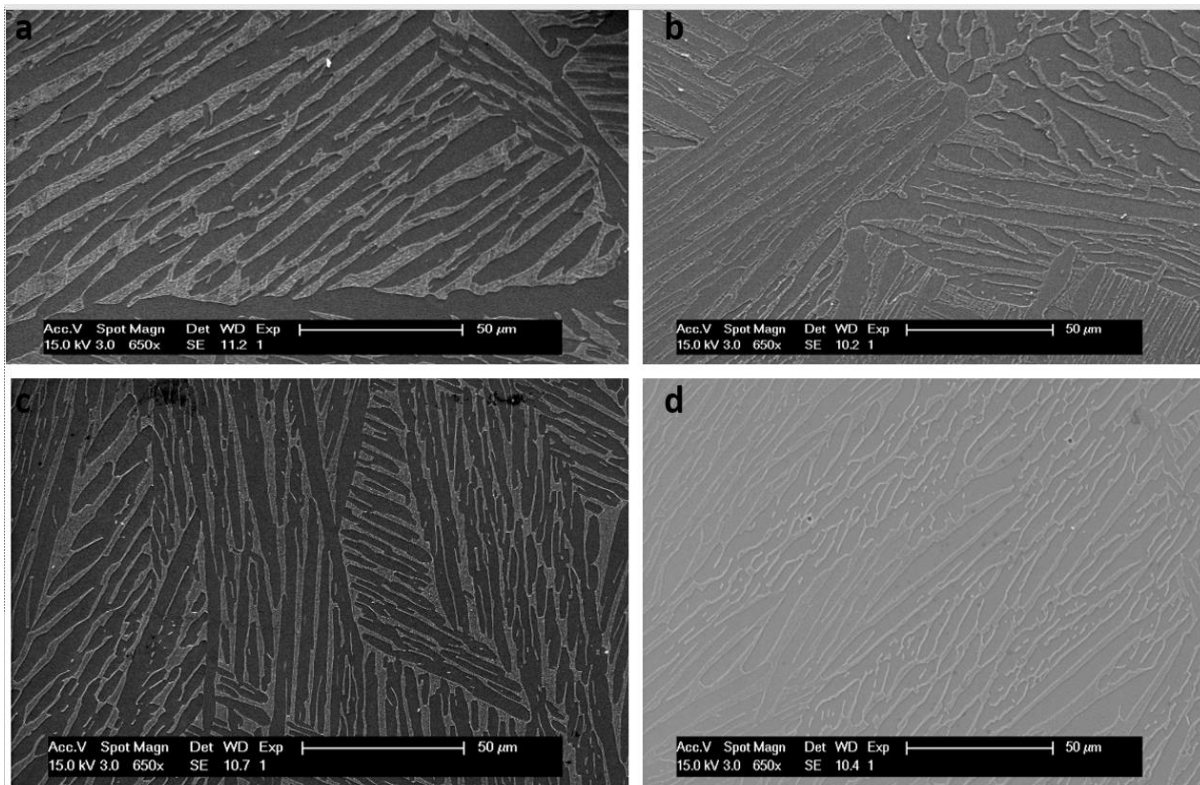
Figure 4. 9: Microstructure observed during heat treatment at 880°C with various aging time a) is for 1 hr, b) is 2 hrs, c) is 3hrs and d) is for 4hrs.

There is a grain boundary α nucleation taking place. It should also be mentioned that unlike in the case of 800 and 840°C where microstructural morphological difference seems not be well noticed, and there seems not be as well a noticeable morphological difference between the microstructure observed at 840 and 880°C. This could be because the temperature interval is not so much, between 800 to 840°C

and because 840 and 880 have the same temperature interval in which there not so much change, and because all these samples were air cooled, it is known that cooling rate plays a very important role in microstructural morphology, when samples have the same cooling rate, the important parameters are temperature and aging time. However, for the temperature interval seems not much to produce a difference in morphological features. There is however a noticeable morphological difference between 800 and 880°C, there is a visible difference between these microstructures (800 and 880°C) microstructure morphology, difference in thickness of primary α_P, grain boundary α, retained β thickness of secondary α_S were observed.

Additionally, the α volume phase fractions changed and decreases as the temperature increased. So, as the ageing treatment increases from 800 to 840, 880 and 960°C α volume fractions deceased with increasing temperature and ageing time, and the β volume fractions increases as the temperature increases. Figure 4. 10 below Shows secondary α_S observed after 880°C heat treatment.
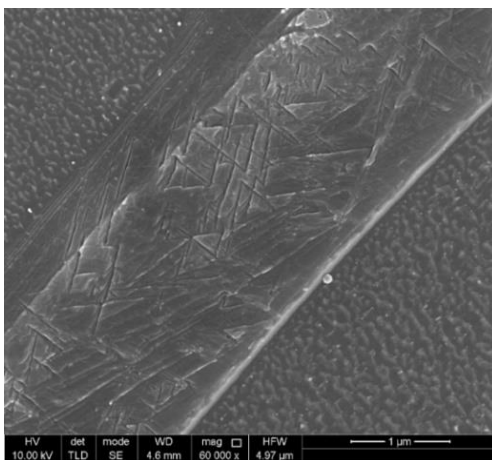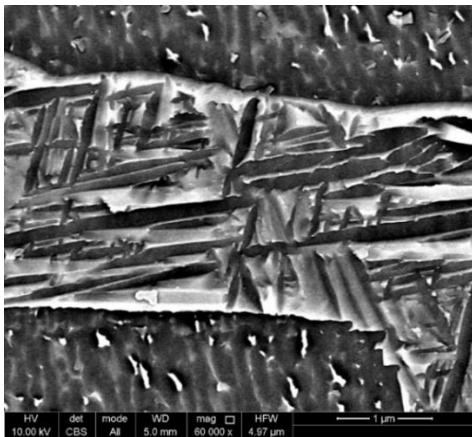

Figure 4. 10: Secondary α_S observed in second stage heat treatment at 880°C.
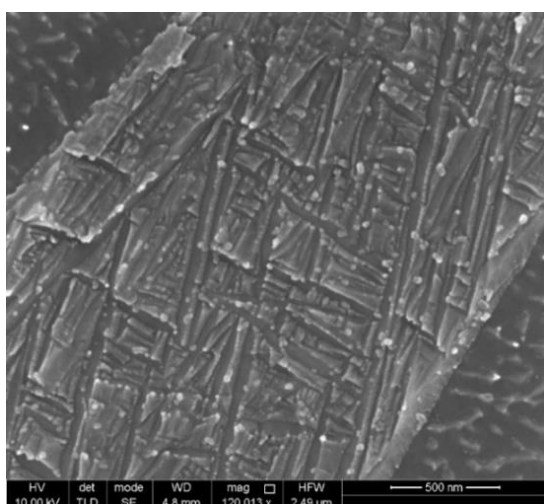
4.2.3.4.   Microstructure at 960°C with different aging time

Figure 4. 11 below shows the obtained microstructure after the second stage heat treatment conducted at 960°C and the different aging time are indicated by a, b, c, d for 1, 2, 3 and 4hrs.

The bi-lamellar microstructure obtained after heat treatment at 960˚C contains least amount of primary alpha compared to the bi-lamellar microstructure obtained at other lower temperatures as the amount of the primary alpha phase varies inversely with the temperature. The secondary alpha obtained at after heat treating at 960˚C is much coarser than the one obtained at lower temperature. This is due to the slower cooling rate achieved after air cooling from 960˚C as compared to ones obtained after air cooling from lower temperatures.
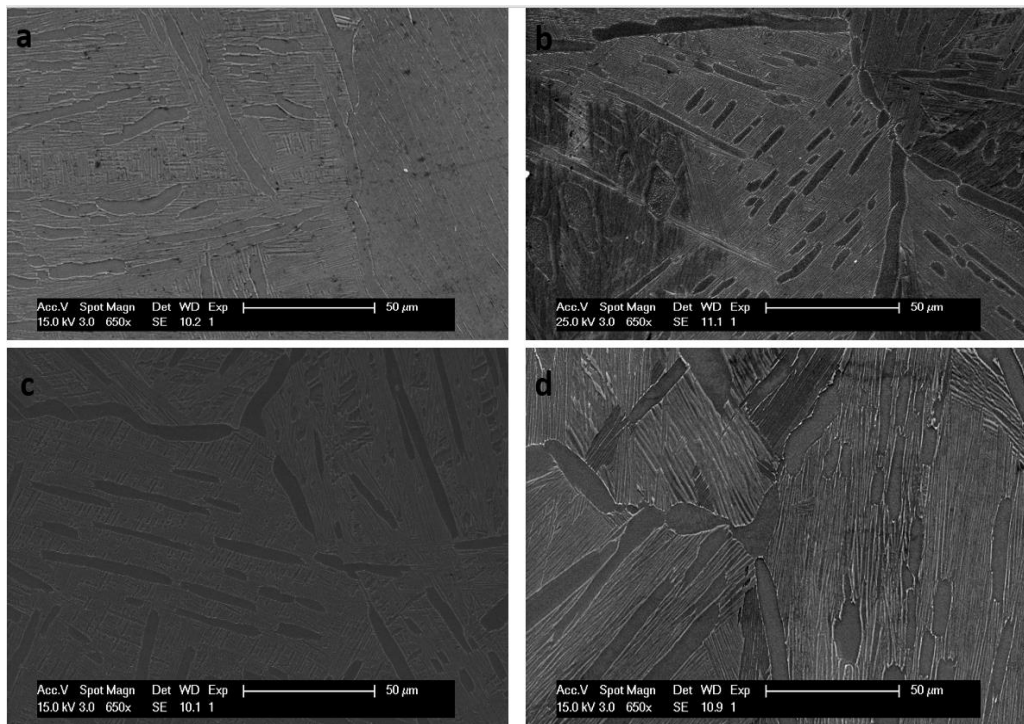
Figure 4. 11: Microstructure observed during heat treatment at 960°C with various aging time a is for 1 hr, b is 2 hrs, c is 3hrs and d is for 4hrs.

It is also evident from Figure 4. 12 that the secondary alpha grows the primary alpha lath (indicated by the red circle). This phenomenon could not be observed due to the very small size of the secondary alpha obtained at 800˚C, 840˚C or 880˚C. Since these secondary alpha lamellae grows from the primary alpha phase, these secondary alpha have similar crystallographic orientation as that of the primary alpha. Thus, the bi-lamellar microstructure at 960 ˚C is somewhat similar to that of the simple lamellar microstructure.
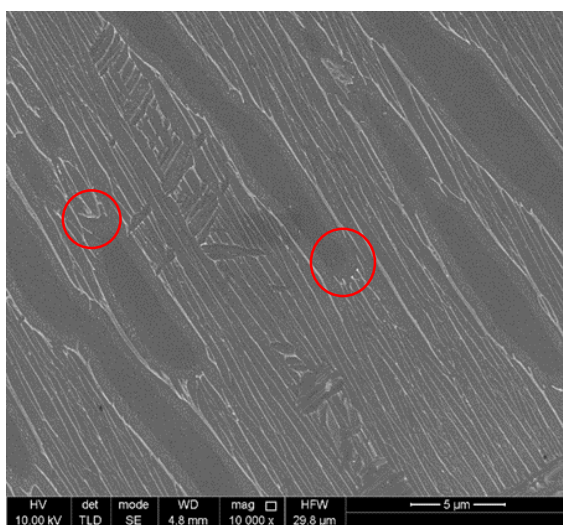
Figure 4. 12: Secondary α_S observed in second stage heat treatment at 960°C.

4.3. EDS analysis

This sub section deals with the chemical composition (concentration of Al and V and not Ti) of the primary alpha and the transformed beta phase in different bi-lamellar microstructures. Figure 4. 13, Figure 4. **14** and Figure 4. *15* displays the chemical composition of the primary alpha and the transformed beta phase for the bi-lamellar microstructure obtained at 800˚C, 880˚C and 960˚C respectively. It is evident that, for all the bi-lamellar microstructures, primary alpha phase contains a relatively higher concentration of Al compared to the transformed beta phase. Whereas, transformed beta phase is enriched in vanadium. This is in accordance with the Ti-6Al-4V phase diagram, where Al is an alpha stabilizer and V is the beta stabilizer. The chemical composition of the primary alpha phase doesn't change much with the temperature. There is slight increment of Al and decrement of V concentration with increase in the temperature of the second heat treatment step. Whereas, the chemical composition of the transformed beta phase changes drastically with temperature (Note that, the chemical composition of the transformed beta phase is the average of the chemical composition of the secondary alpha and the transformed beta phase As, the secondary alpha is very small in size compared to the interaction volume of the electrons inside SEM and thus it is almost impossible to determine the exact chemical composition of the secondary alpha and the beta phase.)

The vanadium concentration goes down from 11.3% at 800˚C to 4.34% at 960˚C This observation can be explained based on the stability of the beta phase depending upon the temperature. At lower temperature (800˚C), beta phase is relatively less stable and hence a higher concentration of vanadium is required to stabilize it. Upon, increasing the heat treatment temperature to 960˚C, beta phase become more stable and hence less amount of vanadium is required to stabilize it Similar observations on the trend of the variation of the chemical composition of the beta phase with temperature is also reported in the literature.
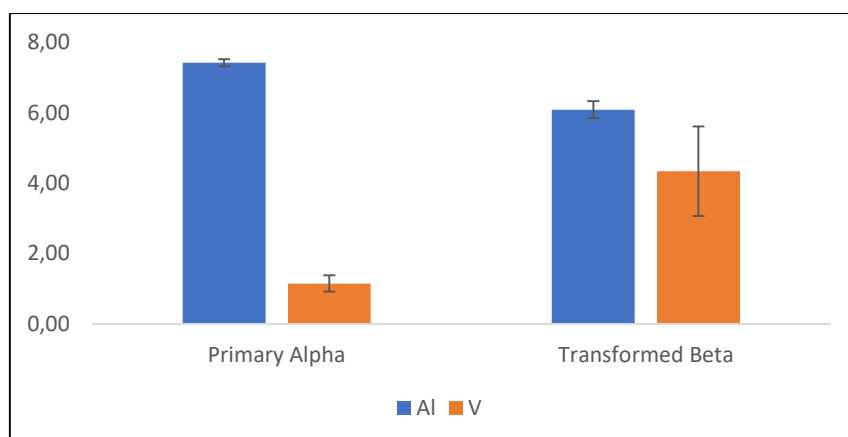
Figure 4. 13: EDS results for 800°C.
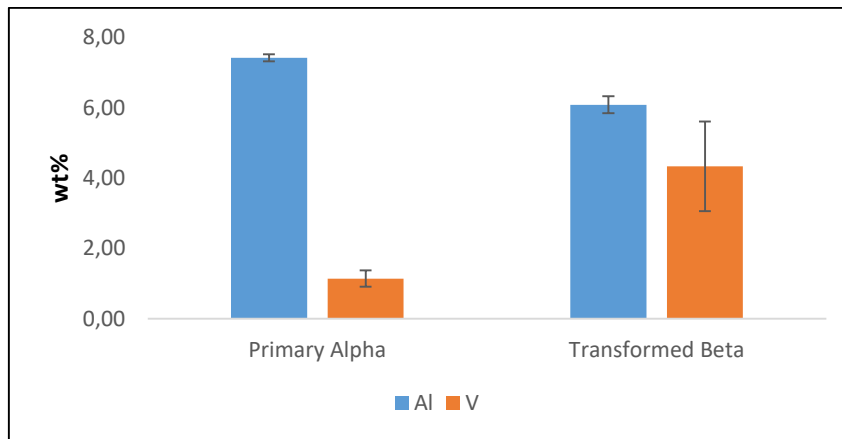
Figure 4. 14: EDS results for 880°C.
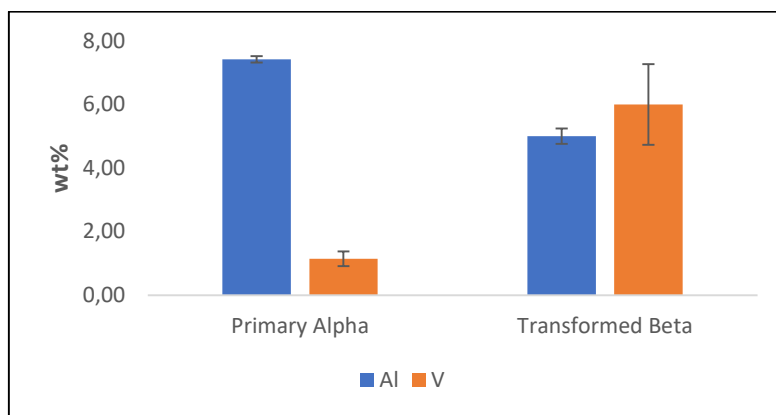
Figure 4. 15: EDS results for 960°C.

4.4.   Phase volume fraction

Phase volume fractions of primary alpha and transformed beta are shown in this section. These phase volume fractions were obtained using ImageJ software. The presented volume fractions were obtained using a contrast of color technic in ImageJ.

4.4.1. α phase volume fraction change

When looking at Figure 4. 16 it can be seen that the α phase fractions decreases with increasing temperature this because as the heat treatment temperature increases the α volume fraction deceases according to the Lever rule for phase composition calculation. It is important to mention that further on when discussing quasistatic mechanical properties, the effect of heat treatment on microstructures and their effect of microstructure features on mechanical properties c well observed.

This is because in the two phase α+β titanium as the ageing temperature increase the β coarsens and also increases in volume. It is crucial to achieve a good contrast between primary $α_P$, secondary $α_S$, and retained β as these features plays important role in mechanical properties of Ti6Al4V.
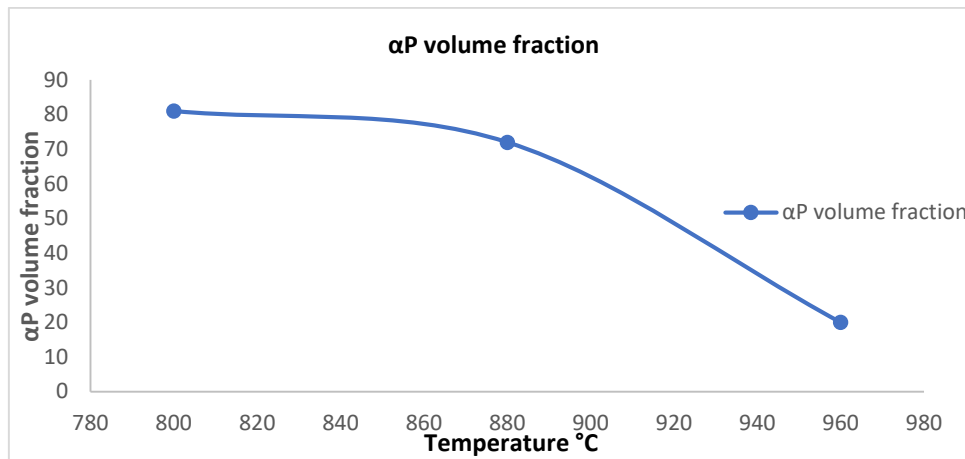
Figure 4. 16: Volume fraction of α as function of increasing temperature.

4.5.   Quasi-static mechanical behaviour

This sub-section presents the results of quasi-static uniaxial tensile test for the lamellar and the bi-lamellar microstructures. The bi-lamellar microstructures were achieved after performing second heat treatment step at 800˚C, 880˚C and 960˚C for 1 hour.

4.5.1.   Quasi-static tensile test

Figure 4. 17 shows the tensile curve of the specimen with lamellar microstructures. The yield strength of the lamellar is lower than the bi-lamellar microstructure obtained at 800˚C and 880˚C (shown later).
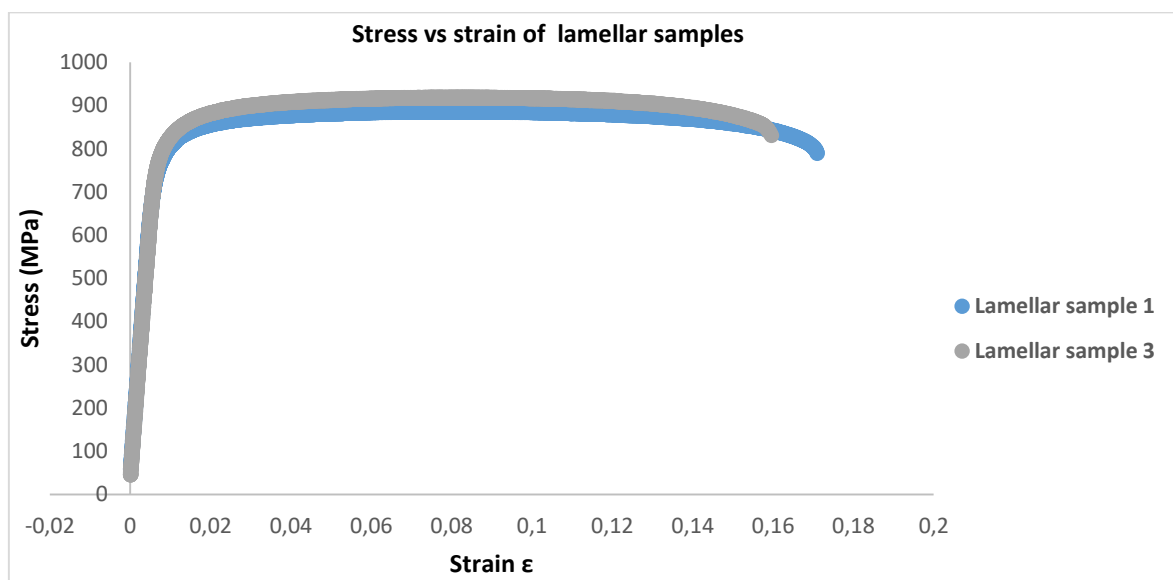
Figure 4. 17: comparison of tensile result of all lamellar samples.

Table 4. 1 shows the percentage elongation observed before failure of lamellar samples. The elongation obtained after the first stage heat treatment is higher than compared to the as-built Ti-6Al-4V (with acicular martensite). This is due to the decomposition of the martensite upon beta annealing

Table 4. 1: Percentage elongation at break for lamellar samples.

Lamellar Samples	Percentage elongation at break (%)
Sample 1	17. 095
Sample 2	15. 766
Sample 3	15.951

Figure 4. 18 shows the result of the uniaxial quasi-static tensile test for the bi-lamellar microstructure samples obtained at 800°C (second stage heat treatment temperature). It can be seen that the tensile elongation for these samples are lower than the lamellar microstructure, due to the strength ductility trade-off. The higher strength for bi-lamellar microstructure is observed due to the blocking of the dislocations at the interface of the primary alpha and transformed beta interface Whereas, the lamellar microstructure presents lower strength because the beta lamellae does not offer resistance against dislocation motion and the dislocation can easily traverse whole alpha colony. For lamellar microstructure, alpha colony size acts as a controlling factor. While for bi-lamellar microstructure, size of alpha lamella acts as a controlling factor.
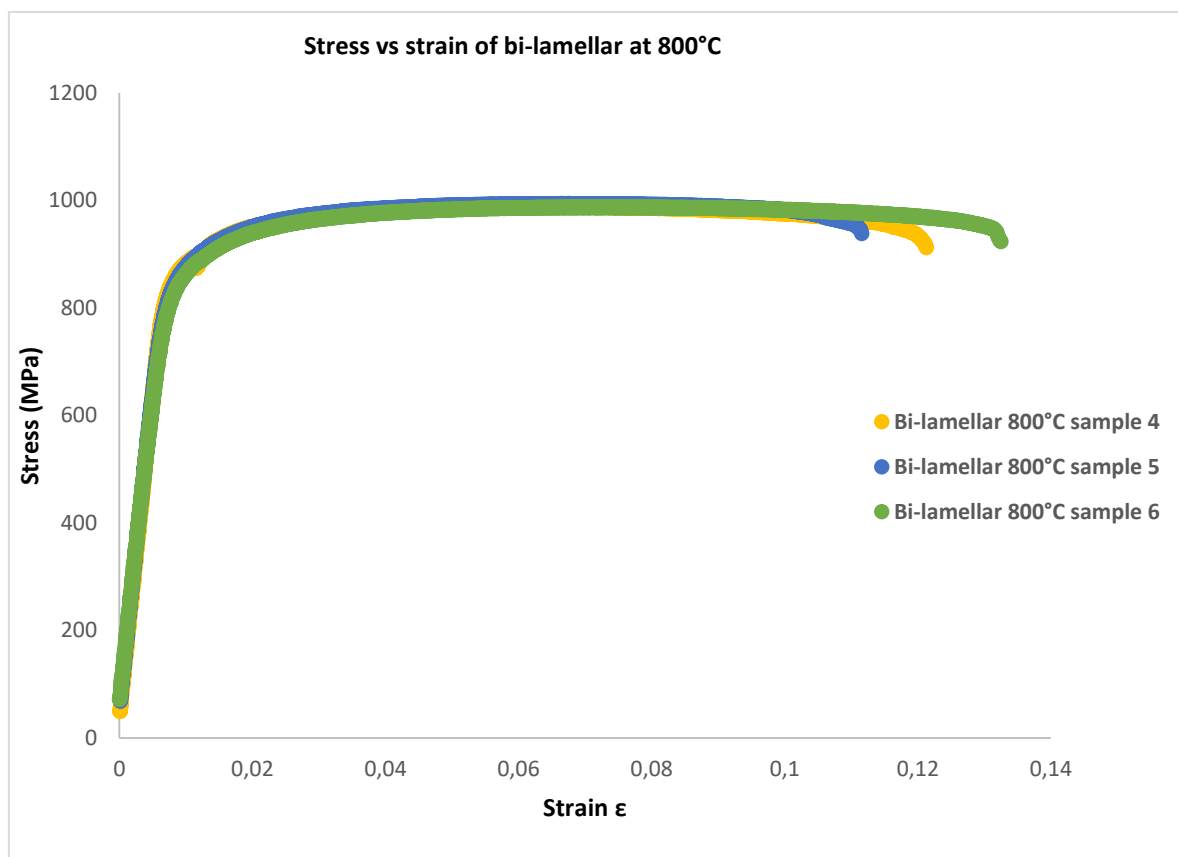
Figure 4. 18: Tensile result of all bi-lamellar samples result from 800°C heat treatment.

Table 4. 2 shows the percentage elongation observed before failure of bi-lamellar samples obtained at 800°C.

Table 4. 2: Percentage elongation at break for bi-lamellar samples obtained at 800°C.

Bi-lamellar 800°C	Percentage elongation at break (%)
Sample 4	12.1
Sample 4	11.2
Sample 6	13.2

Figure 4. 19 below shows results of tensile curvefor the bi-lamellar samples obtain at 880°C. It can be seen that the yield strength of the 880°C bi-lamellar microstructure is highest among all the 4 microstructures.
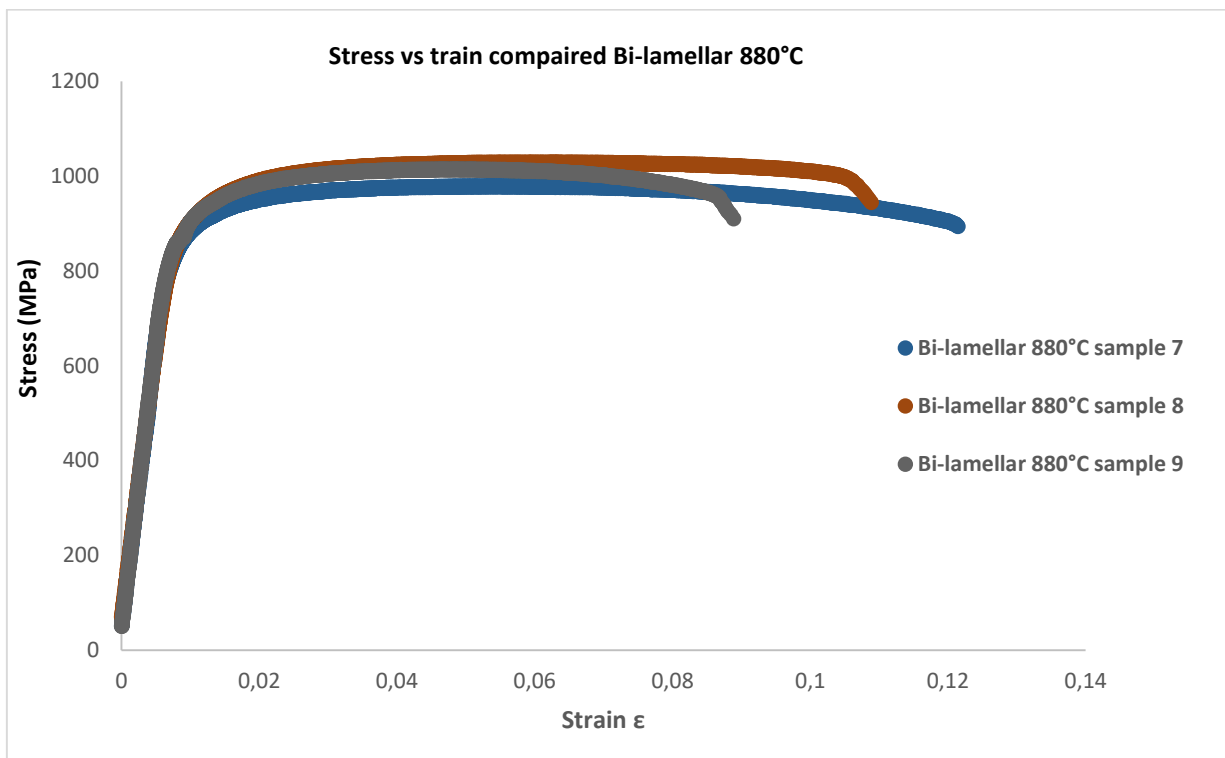
Figure 4. 19: Comparison of tensile result of all bi-lamellar samples result from 880°C heat treatment.

The observed tensile curve shows that the bi-lamellar samples achieved at 880°C yield and ultimate strength in this Table 4. 3 shows the percentage elongation observed before failure of bi-lamellar samples obtained at 880°C.

Table 4. 3: Percentage elongation at break for bi-lamellar samples obtained at 880°C.

Bi-lamellar Samples	Percentage elongation at break (%)
Sample 7	12.1
Sample 8	11.9
Sample 9	9

Figure 4. 20 below shows tensile test results of bi-lamellar samples obtain at 960°C. it can be seen samples heat treated at 960°C have the lowest yield strength among the bi-lamellar microstructures, lower than both previous bi-lamellar samples (800°C, 880°C). The observed poor mechanical properties are due to the fact that in bi-lamellar microstructures 960°C as explained during the microstructure's sections. At 960°C the secondary α_S have similar orientation as the primary α_P, and this morphological orientation contributes to lowering tensile mechanical properties. Thus, there is no hindrance to the slip dislocations compared to what was observed to the bi-lamellar microstructures obtained at 800˚C and 880˚C.
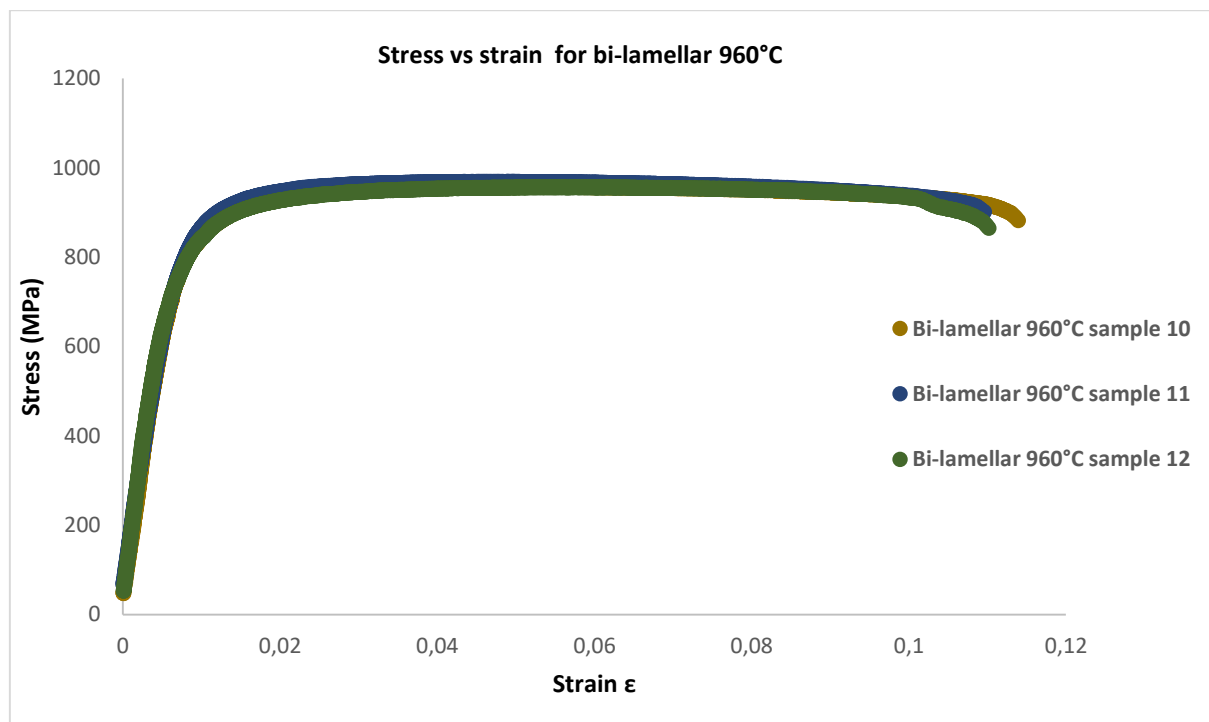
Figure 4. 20: Comparison of tensile result of all bi-lamellar samples result from 960°C heat treatment.

Table 4. 4 below shows the percentage elongation observed before failure of bi-lamellar samples obtained at 960 °C.

Table 4. 4: Percentage elongation at break for bi-lamellar samples obtained at 960°C.

Lamellar Samples	Percentage elongation at break (%)
Sample 10	11.4
Sample 11	11.0
Sample 12	11.0

It can be seen that the bi-lamellar microstructure obtained at 880˚C has the highest yield strength among the different microstructures.

4.5.2.   Compared tensile properties

Figure 4. 21 and Figure 4. 22Table 4. 5 shows comparisong of tensile properties observed from as build, lamellar and bilamellar microstructure (800, 880, 960°C).
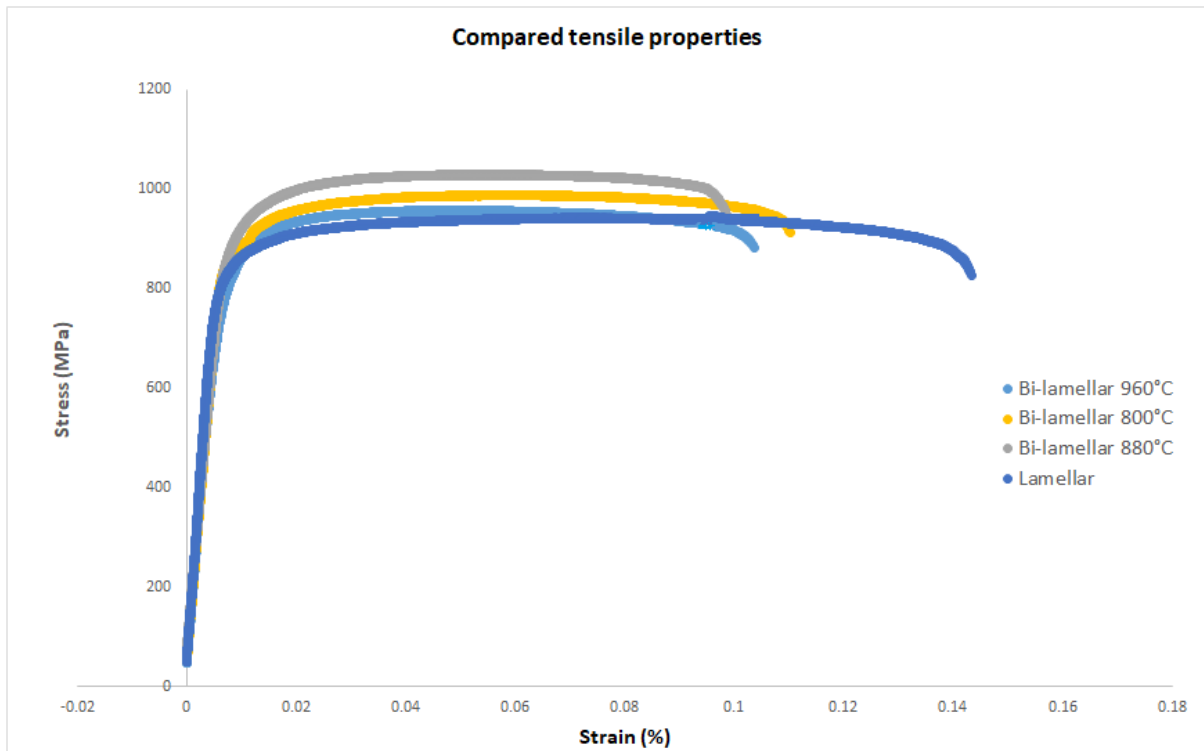
Figure 4. 21: Comparison of tensile result of all heat-treated samples (lamellar, bi-lamellar 800, 880, 960°C).
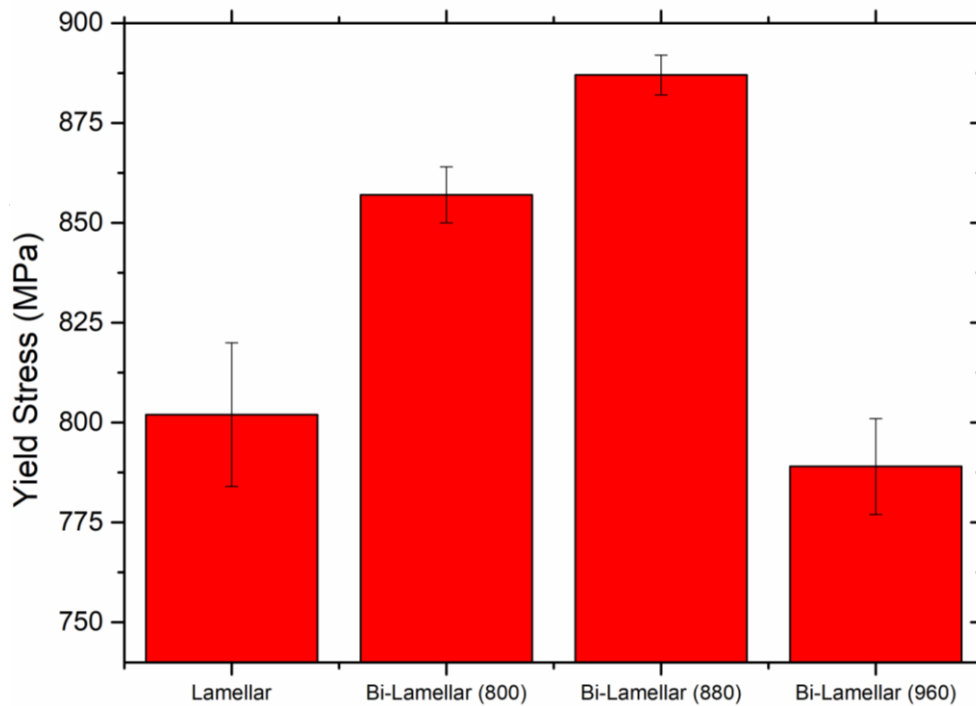
Figure 4. 22: Compared yield strength results of heat-treated samples.

Table 4. 5: Compared tensile properties of all samples.

Samples	Yield strength (MPa)	UTS (MPa)	Elongation (%)
As build*	1112	1267	4-6
Lamellar	805	940	16.27
Bi-lamellar 800°C	865	998.5	13.25
Bi-lamellar 880°C	886	1030	12.52
Bi-lamellar 960°C	790	929	11.11

4.5.3.   Post failure microsctructural analysis

This sub-section will discuss the microstructural characterization of the failed tensile bar.

Figure 4. 23 and Figure 4. 24 shows lamellar microstructure behavior after being failed under the uniaxial tensile load. It can be seen that the voids are present along the alpha beta interface (Figure 4. 23) At other instances (Figure 4. 24), trans-colony voids are observed. These trans colony voids could be due the propagation of the dislocations across the alpha-beta interface. As, (0001) plane of alpha phase is parallel to the (110) plane of the bcc phase. Thus, if a dislocation is travelling on the basal plane of alpha, it can easily penetrate into the beta phase without encountering much resistance. Hence, the lamellar microstructure has lower yield strength compared to the bi-lamellar microstructure.
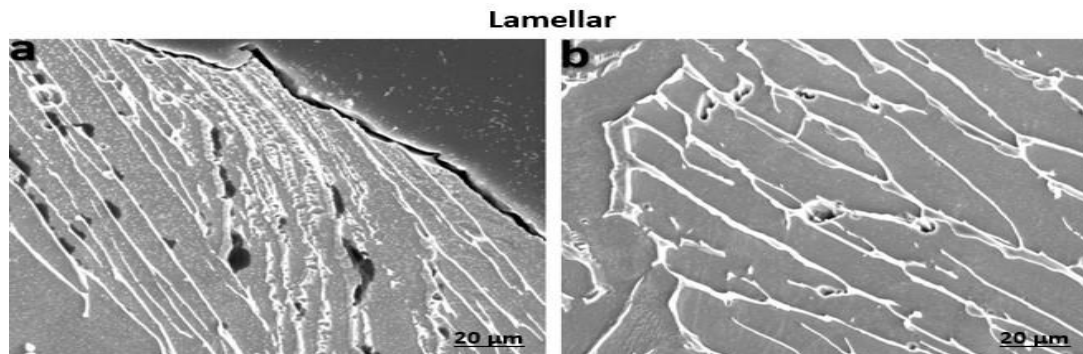
Figure 4. 23: Observed ensile failure in lamellar microstructure.
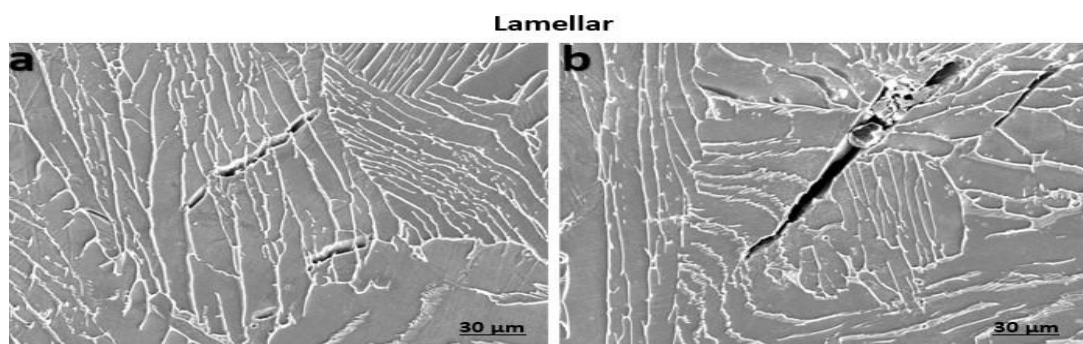
Figure 4. 24: Observed tensile failure in lamellar microstructure.

Fehler! Verweisquelle konnte nicht gefunden werden., Figure 4. *26* and Figure 4. *27* below shows tensile behavior observed in bi-lamellar microstructure obtained at 800°C. Preferential nucleation of voids at the interface between the primary alpha and the transformed beta phase is observed. It can be due to the fact that the dislocations originating from the primary alpha phase gets blocked at the interface. The transformed beta phase is populated with the randomly oriented secondary alpha needles. Due to the presence of the randomly oriented secondary alpha phase, dislocations cannot travel across the interface and hence get blocked. Upon further deformation, dislocation density gradually increases at the interface, that results in the formation of the stress concentration zone and that finally leads to the nucleation of the voids at the interface.
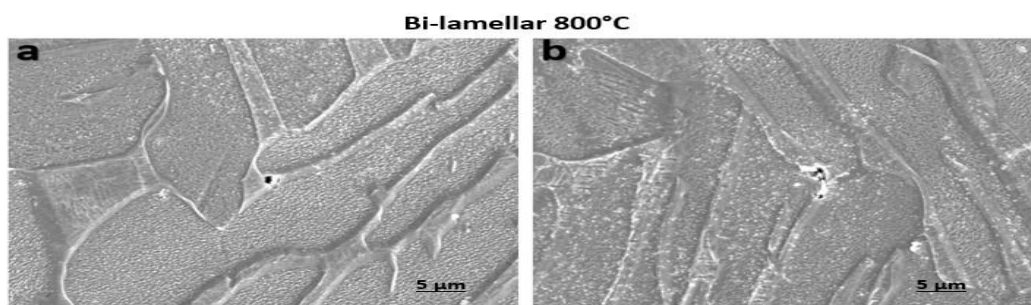
Figure 4. 25: Observed tensile failure in bi-lamellar microstructure obtained at 800°C.
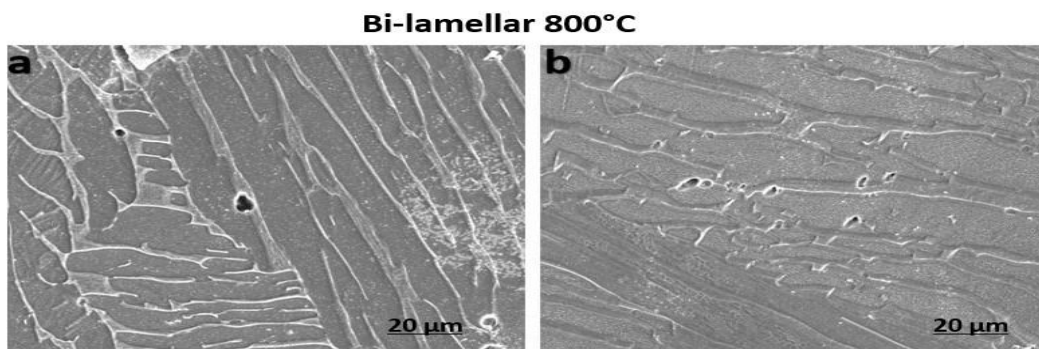
Figure 4. 26: Observed tensile failure in bi-lamellar microstructure obtained at 800°C.

When looking at Figure 4. 27 it can be seen that for dislocation to happen it has to starts as singular spot point on the α/β interface then later connect to each other for dislocation to take place.
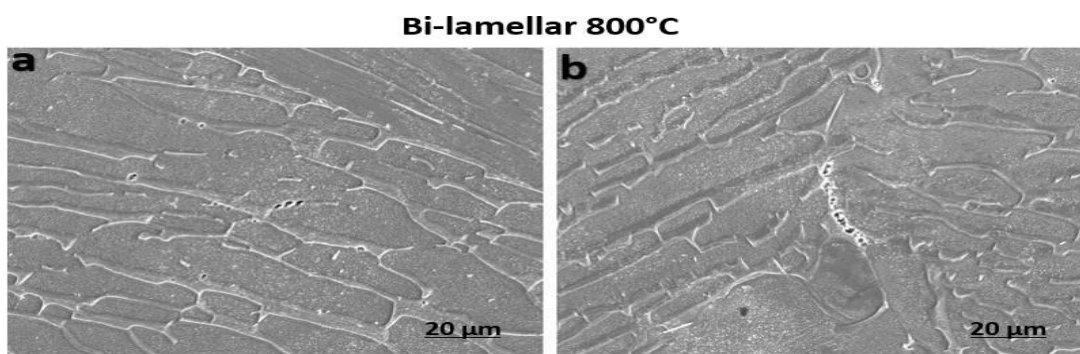
Figure 4. 27: Observed tensile failure in bi-lamellar microstructure obtained at 800°C.

Figure 4. 28 and Figure 4. *29* below tensile behavior observed in bi-lamellar microstructure at 880°C. Here also, voids are preferentially present at the interface, similar to the bi-lamellar microstructure obtained at 800°C. Similar reasoning can be extended to this bi-lamellar microstructure. The presence of the randomly oriented secondary alpha needles blocks the dislocation at the interface, which further gives rise to the void nucleation. However, 880°C bi-lamellar microstructure showed higher yield strength among all the bi-lamellar microstructure. This observation can be explained based on the difference in the phase fractions of primary alpha and transformed beta phase. For the bi-lamellar microstructure heat treated at 800°C, microstructure contains a higher fraction of the primary alpha phase and a very small amount of the transformed beta phase Whereas, for the bi-lamellar microstructure obtained at 880°C, relatively lower fraction of primary alpha and a higher fraction of transformed beta phase is achieved. Thus, for the bi-lamellar microstructure obtained 880°C has larger interfacial areas compared to the bi-lamellar microstructure obtained at 800°C. Thus, the higher amount of interface translates into more sites for blocking the dislocation motion. Hence, it can result in higher yield strength.
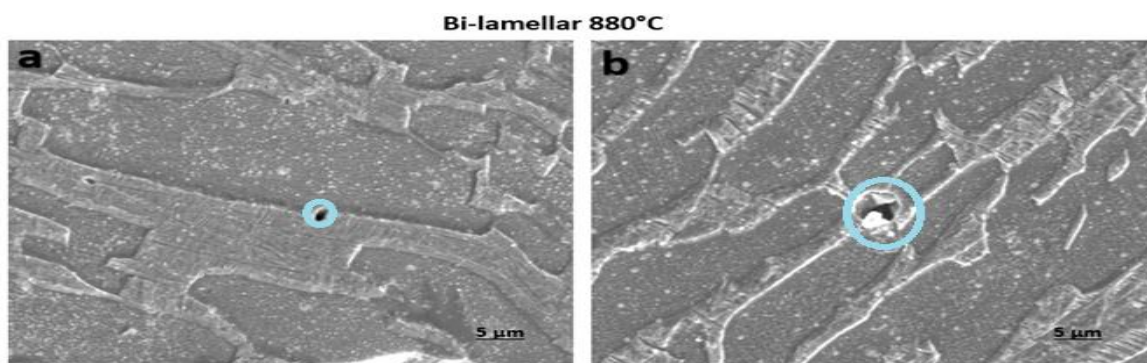
Figure 4. 28: Observed tensile failure in bi-lamellar microstructure obtained at 880°C.
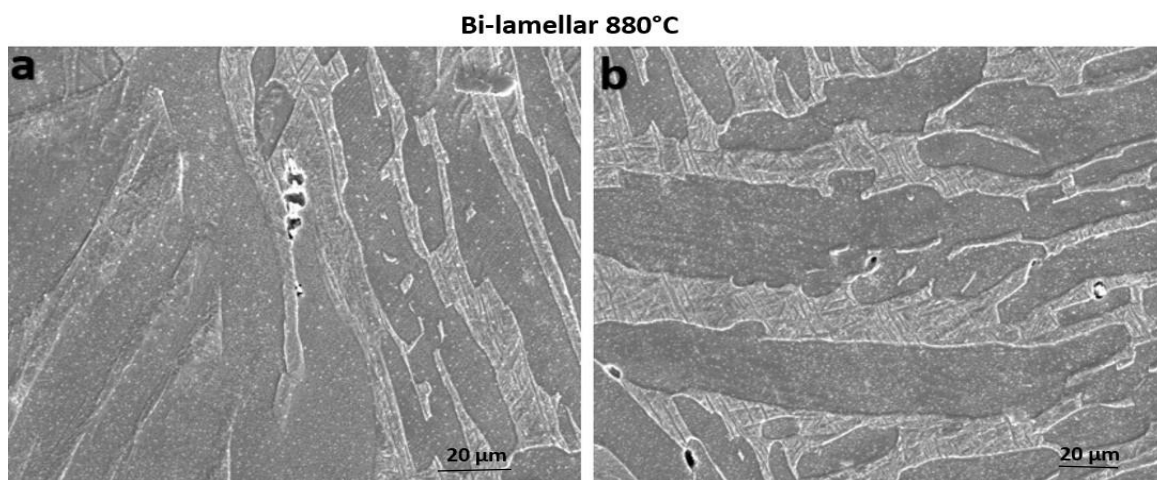
Figure 4. 29: Observed tensile failure in bi-lamellar microstructure obtained at 880°C.

Samples obtained at 880°C seems to have a very good tensile propertied as there are only few dislocations spots on the microstructure shown in Figure 4. 28 and Figure 4. 29 image above.

Figure 4. 30 and Figure 4. 31 below tensile behavior observed in bi-lamellar microstructure obtained at 960°C.
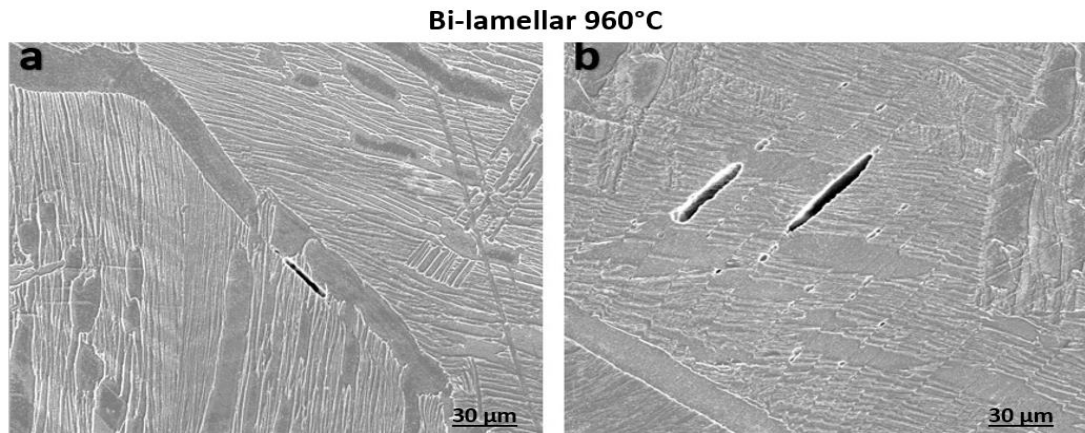
Figure 4. 30: Observed tensile failure in bi-lamellar microstructure obtained at 960°C.
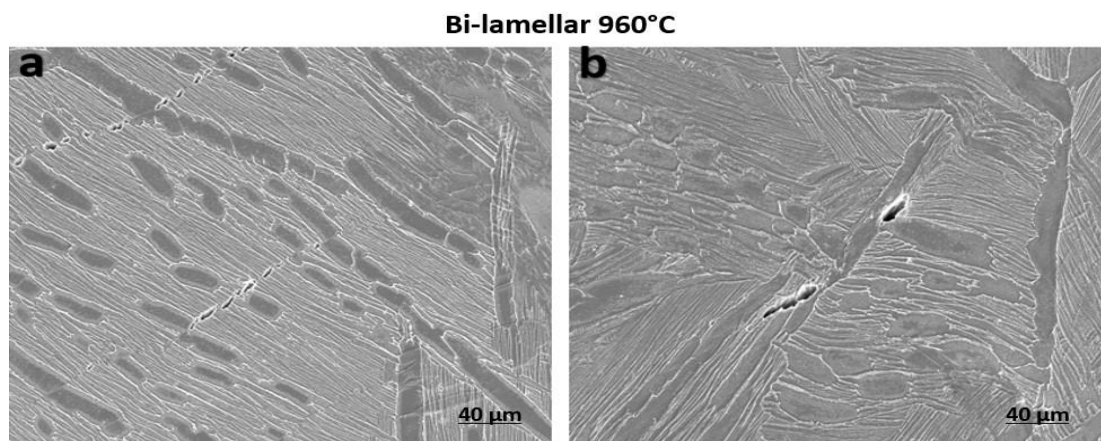
Figure 4. 31: Observed tensile failure in bi-lamellar microstructure obtained at 960°C.

For the bi-lamellar microstructure, obtained at 960°C, voids appear in a straight line and not preferentially nucleated at the interface, observed for the bi-lamellar microstructure at 800°C and 880°C It can be due to different microstructure of the transformed beta phase obtained at 960°C. For the samples heat treated at 800°C and 880°C, transformed beta phase contained randomly oriented alpha, whereas, at 960°C, the secondary alpha doesn't seem to be randomly oriented, rather they seem to have similar morphological orientation as that of the primary alpha laths. Because of the similar orientation of primary and secondary alpha, dislocations do not get blocked at the interface and can easily propagate through transformed beta phase. Thus, the bi-lamellar microstructure obtained at 960°C behaves similarly to that of the lamellar microstructure.

4.6. Fatigue crack growth tests

This sub section discusses the results of the fatigue crack growth tests performed on lamellar and 3 different bi-lamellar microstructures.

4.6.1.   Fatigue crack growth test

Figure 4. 32 below shows the curve between da/dN (crack growth rate) and ΔK (stress intensity factor) of samples having lamellar microstructure. Lamellar microstructure possesses better resistance against crack propagation. The fatigue plot observed in samples having lamellar microstructure is a bit steep and the slop and y-intercept value will be presented
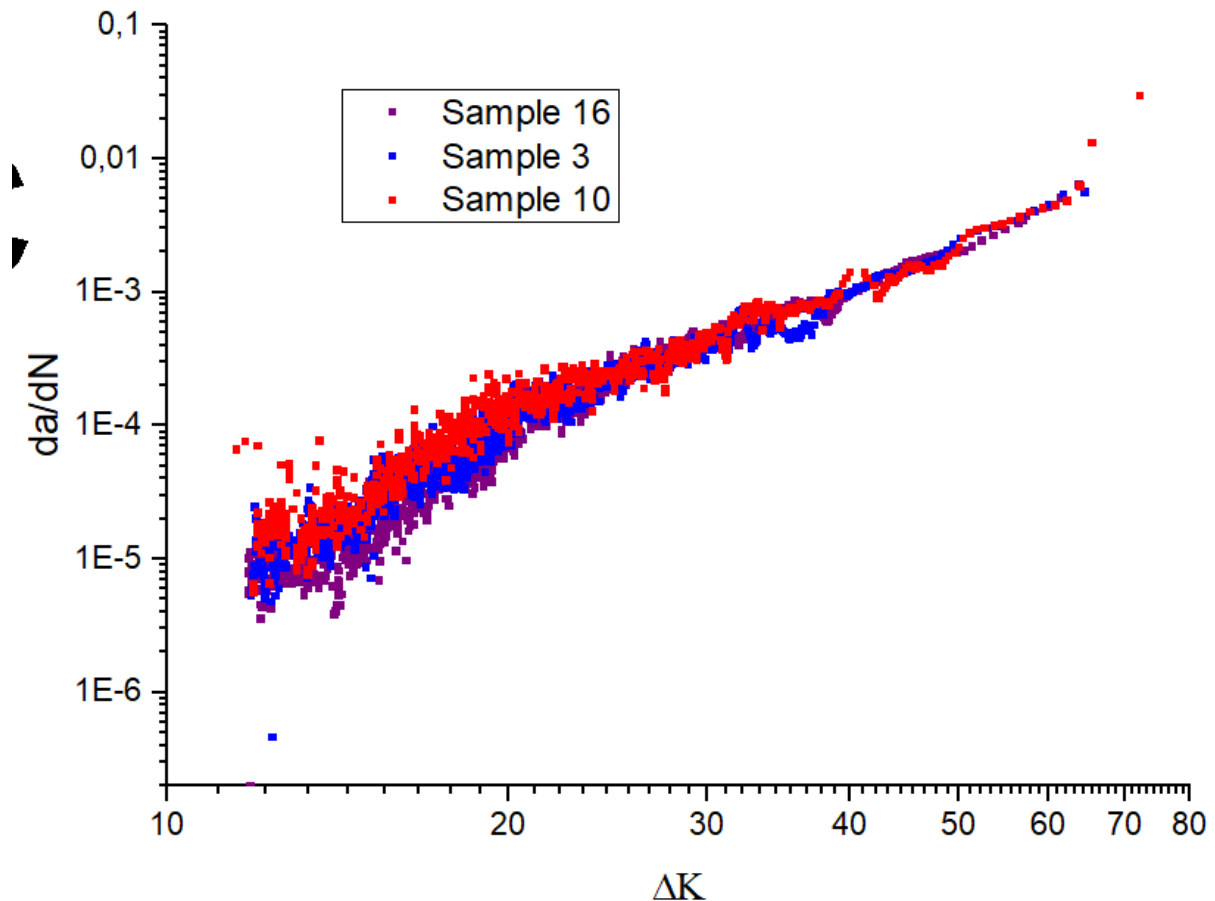
Figure 4. 32: comparison of crack growth behaviour of sample 3 and 10 having lamellar microstructure.

Figure 4. 33 below shows fatigue propagation behaviour of samples having bi-lamellar microstructure obtained after second stage heat treatment at 800°C. When looking at the crack growth rate plot of bi-lamellar microstructure obtained at 800°C the curves is not as steep as the curve of samples having lamellar microstructure. There is a slight improvement, steep curve implies higher gradient, and higher gradient value implies faster crack growth rate. So, the lamellar samples have steep slope.
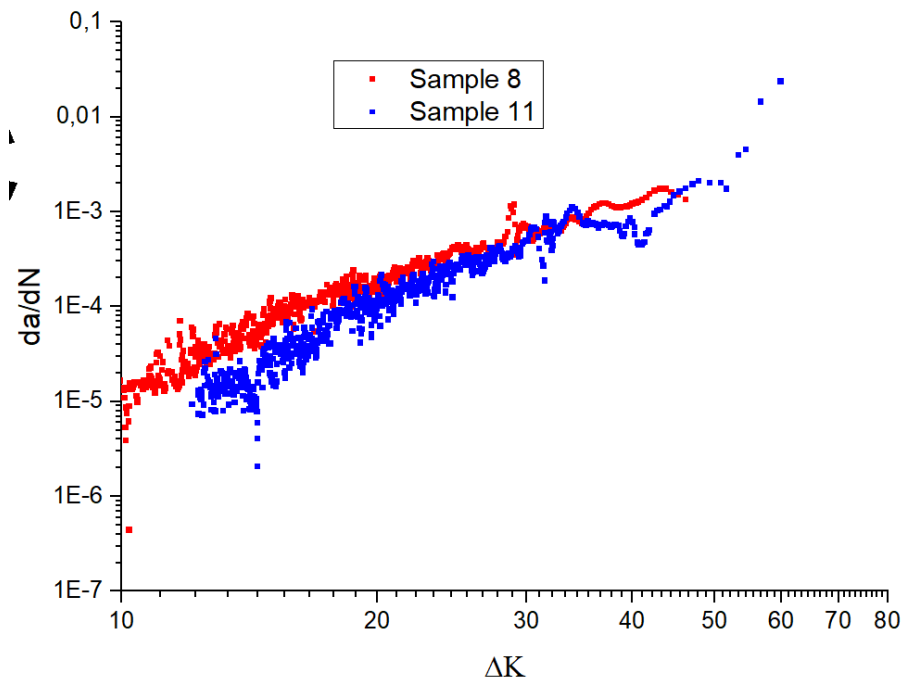
Figure 4. 33: crack growth behaviour in sample 8 and11 having bi-lamellar microstructure obtained at 800°C.

Figure 4. 34 below shows fatigue propagation behavior in bi-lamellar microstructure obtained after second stage heat treatment of 880°C. It can be seen that samples having bi-lamellar microstructure obtained at 880°C seem that have lower slope or is not as steep as plot of fatigue crack growth of samples having lamellar, and bi-lamellar microstructure obtained at 800°C.
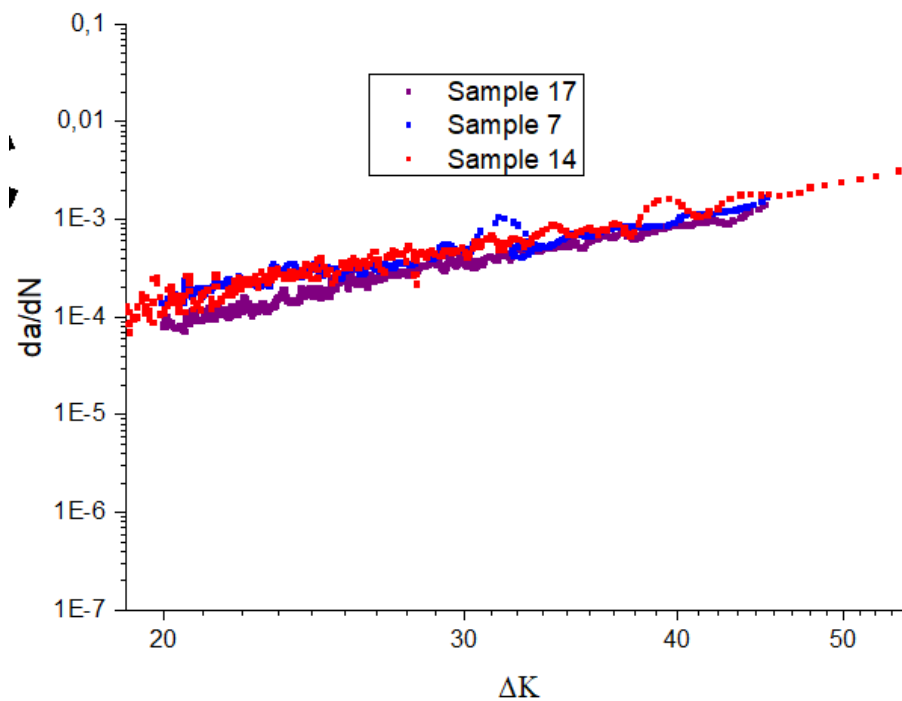
Figure 4. 34: Crack growth behaviour of sample 7 and 14 having bi-lamellar microstructure obtained at 880°C.

Figure 4. 35 below shows fatigue propagation behavior in bi-lamellar microstructure obtained after second stage heat treatment at 960°C.
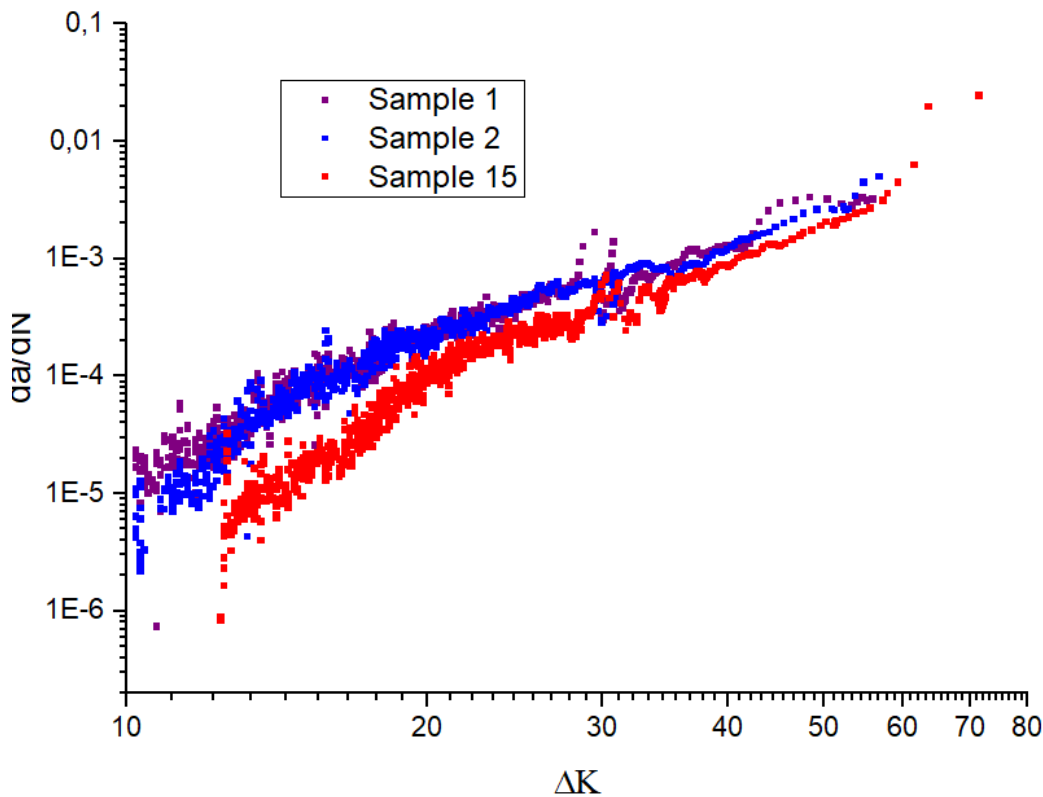
Figure 4. 35: Comparison of crack growth behaviour of sample 1, 2 and 15 having bi-lamellar microstructure obtained at 960°C.

4.6.2.   Slop and intercept

The obtained slope and intercept can be utilized in Paris equation shown below:

$$\frac{da}{dN} = C(\Delta K)^m \tag{4. 1}$$

Table 4. 6 below shows slope and intercept obtained from the crack growth plots. The exponent of the Paris law equation is an indicator of the crack propagation velocity of the crack. Table 4. 6 presents the Paris law equation for the lamellar microstructure and 3 different bi-lamellar microstructures. The m index for the bi-lamellar microstructures obtained at 800˚C and 880˚C are similar to that of the lamellar microstructures. Whereas the m-index for the bi-lamellar microstructure obtained at 960˚C is bit higher (3.8). In literature, m values for the as-built martensitic microstructure is reported to be around 4.76, significantly higher than the ones obtained for the heat-treated samples. Thus, it is clear that the two stage heat treatment clearly improves the resistance against the crack propagation. To further

understand the influence of the microstructure on the crack propagation, post-mortem microstructural characterization was performed.

Table 4. 6: Slop (m) and intercept (C) used in Paris equation.

Microstructure	Paris Law Equation
As-Built (literature)*	$\frac{da}{dN} = 2 * 10^{-12} * \Delta K^{4.76}$
Lamellar	$\frac{da}{dN} = 10^{-8} * \Delta K^{3.15}$
Bi-lamellar (800°C)	$\frac{da}{dN} = 10^{-8} * \Delta K^{3.1}$
Bi-Lamellar (880°C)	$\frac{da}{dN} = 2 * 10^{-8} * \Delta K^{2.97}$
Bi-lamellar (960°C)	$\frac{da}{dN} = 10^{-9} * \Delta K^{2.89}$

4.6.3. Microstructural Analysis of failed fatigue samples

This section deals with the microstructural characterization of the failed fatigue samples. Figure 4. 36 below shows the crack behaviour of the as build Ti6Al4V samples manufactured using L-PBF. The crack path observed in Figure 4. 36 relatively straight with almost no deviation in the crack path, this is because of the acicular martensitic microstructure found in as build part. The faster crack propagation in the as-built microstructure can also be seen from the higher m index of the as-built part.
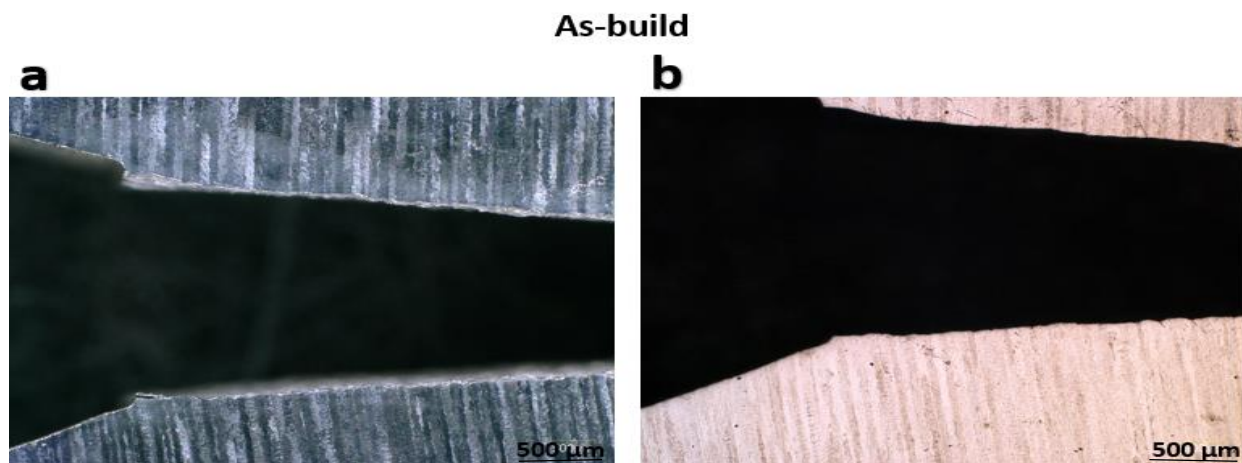
Figure 4. 36: Fatigue crack in as-build samples.

Figure 4. 36 shows the crack propagation profile for the as-built in the beginning phase. The initial phase of the crack is studied because at this stage the crack length is of the order of the microstructural feature. So, if we want to compare different behaviour of the crack through various samples by considering microstructures, we must look at the initial part of the crack. It is important to mention that there are several parameters that influence mechanical properties of L-PBF produced samples,

from printing parameters, material properties, post processing parameters. All these parameters require different competence and separated studies. This MSc. Thesis focus on the effect of post process heat treatment on improvement of mechanical properties of L-PBF produced Ti6Al4V.

Figure 4. 37 and Figure 4. 38 below the optical microstructure image, at different magnification, of the crack profile in the lamellar microstructure. The crack observed in Figure 4. 37 are fairly straight cracks at the lower magnification, there are however new kinds of features observed on the high magnification optical image of the lamellar crack samples that were not seen in as-build samples, these are small zigzag or small deviations observed on the lamellar crack surface. These small deviations represent the resistance to crack propagation during its propagation through lamellar microstructure samples. However, the degree of these deformations implies that lamellar microstructure has very low resistance to crack nucleation and propagation, this is because like tensile strength crack resistance behaviour in lamellar microstructures is influence by the slip length, and colony size. This explains the low resistance to crack observed in lamellar samples. Figure 4. 37 and Figure 4. 38.
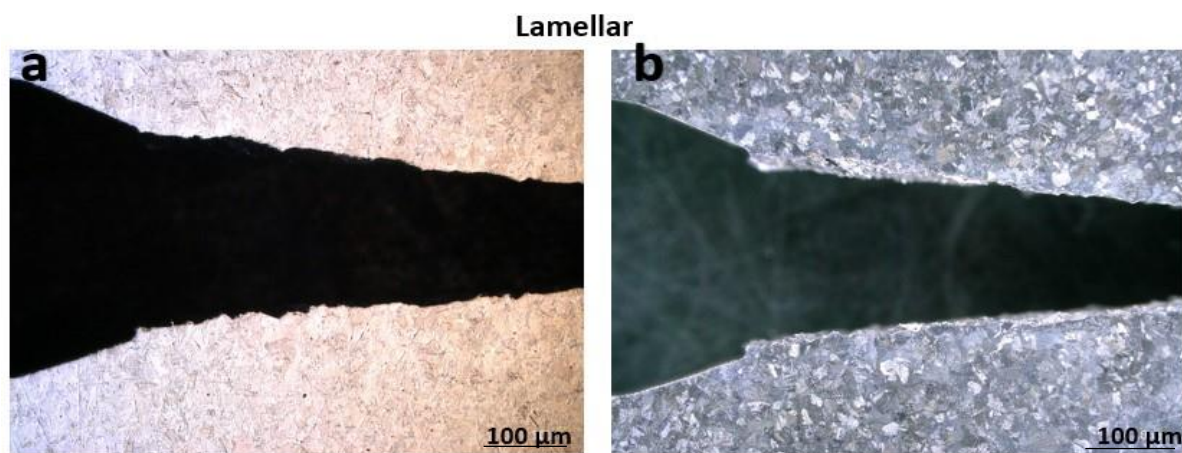
Figure 4. 37: Fatigue crack behaviour lamellar samples.
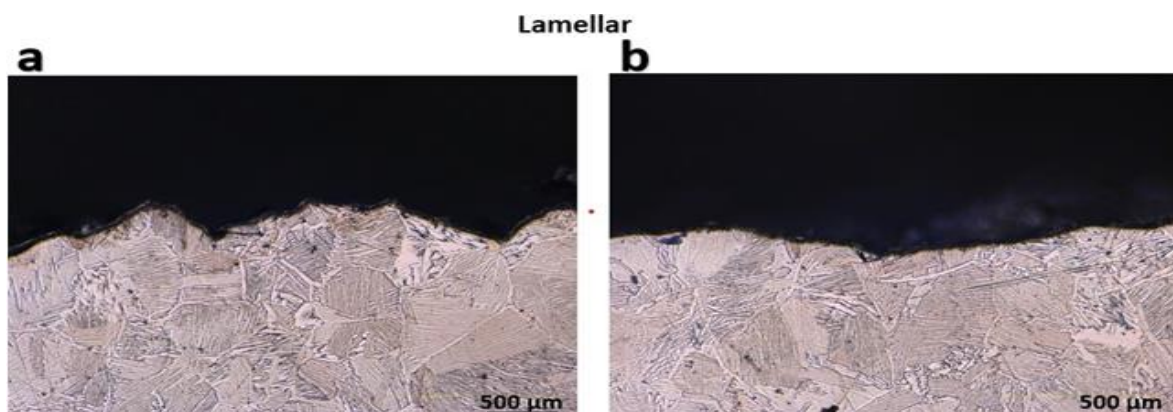
Figure 4. 38: Observed Fatigue crack behaviour lamellar samples.
The lamellar microstructure has better fatigue properties compared to the as-build samples. So, it can be maintained that post process heat treatment contributes to modification of microstructures and to improvement of mechanical properties.

Figure 4. 39, Figure 4. *40* and Figure 4. *41* shows the optical microstructure images, taken at different locations, of crack propagation path for the bi-lamellar microstructure, heat treated at 880˚C. Apart from the crack deflections, secondary cracks can also be seen along the crack path, that were not visible in the lamellar microstructure. Fig 4.40 nicely demonstrates the "zig-zag" crack deflection phenomenon happening in the bi-lamellar microstructure. For the initial part, the crack seems to travel along the interface between primary alpha and transformed beta and then cuts the primary alpha lath and again repeats the same pattern. The presence of crack deflections and the secondary crack increases the energy required for the crack propagation and hence a decrement in the crack propagation velocity is observed for the bi-lamellar microstructure compared to the as-built martensitic microstructure. Thus, bi-lamellar microstructure is advantageous compared to the as-built microstructure in terms of the crack propagation behavior.
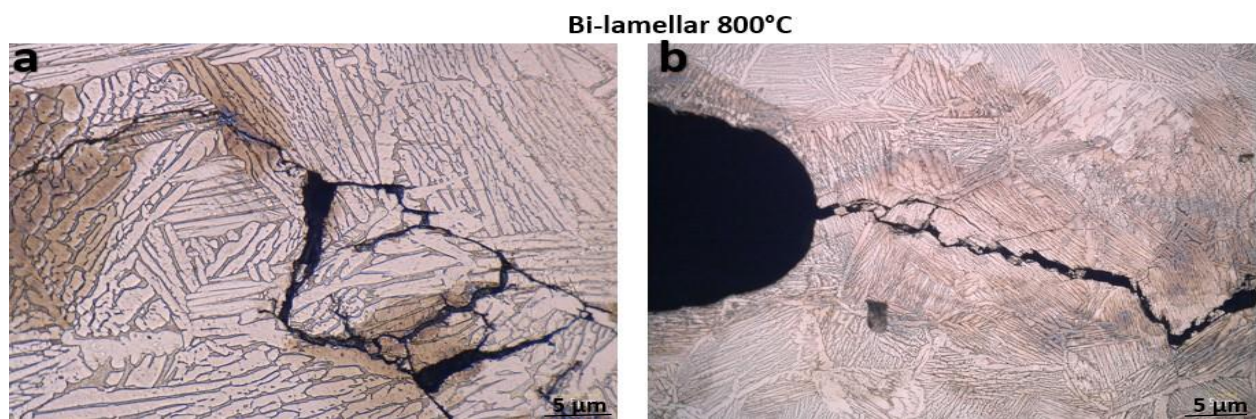
Figure 4. 39: Fatigue crack behaviour bi-lamellar microstructure at 800°C.
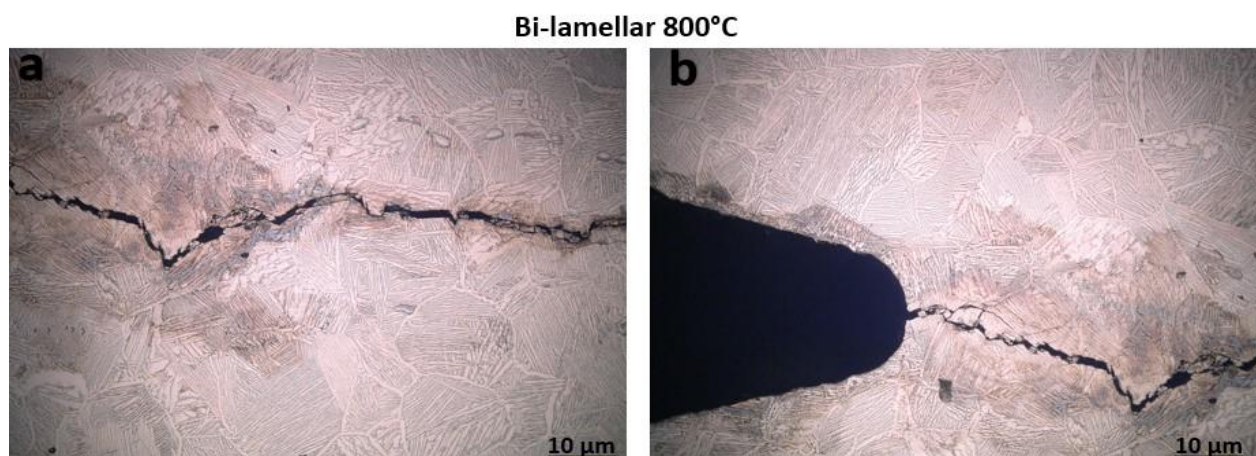
Figure 4. 40: Fatigue crack behaviour bi-lamellar microstructure at 800°C.
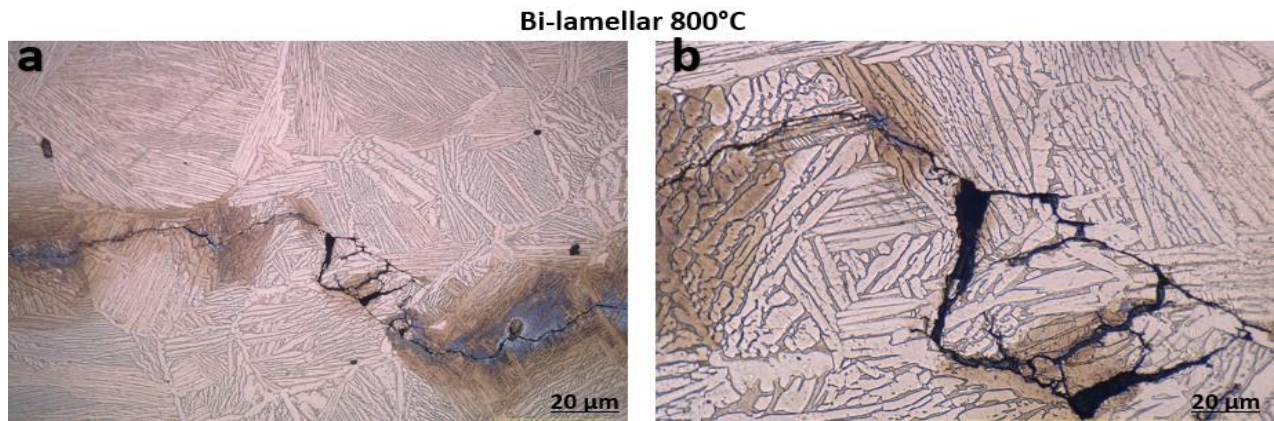
Figure 4. 41: Fatigue crack behaviour bi-lamellar microstructure at 800°C.

Figure 4. 42 and Figure 4. 43 below shows fatigue behavior of bi-lamellar samples obtained at 880°C. When looking at the microstructure image shown in theses figure (Figure 4. 42 and Figure 4. 43) it can be seen that when the crack turns through these deviations it takes more energy hence there is reductions of crack propagation, there are also secondary cracks that can be observed coming out of main crack path, and furthermore there are branching resulting from secondary cracks. So, crack curvature, deflection or resistance to crack, secondary cracks, branching cracks. This crack behavior is the advantage of bi-lamellar microstructures, as there is more energy needed for crack to propagate, so the bi-lamellar microstructure at 880°C show very good crack resistance properties, that were not observed in as-build and lamellar microstructure. This is due to microstructural morphology discussed earlier (primary α_P, secondary α_S, GBα, retained β and phase volume fractions).
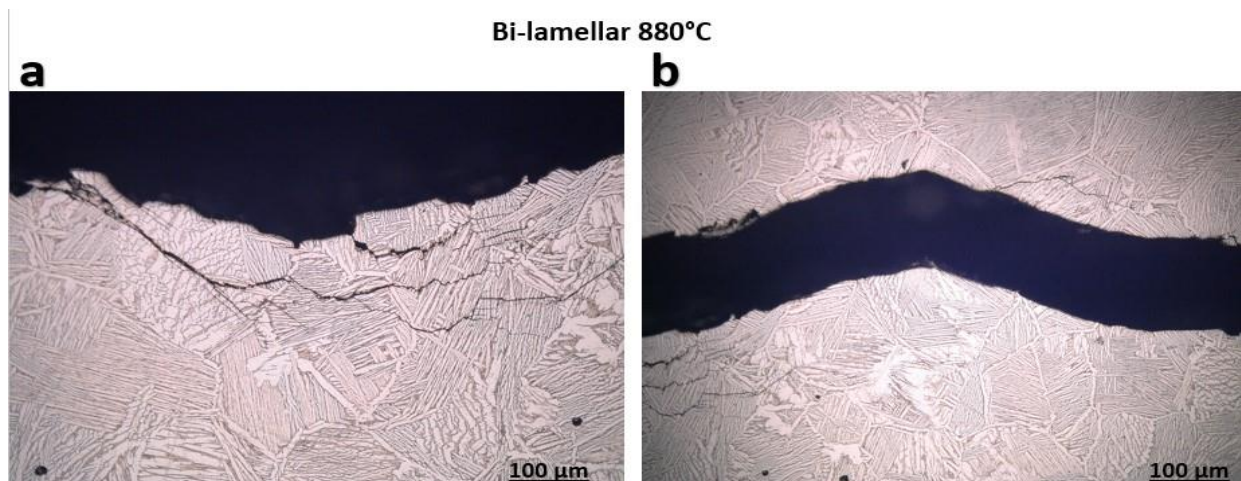
Figure 4. 42: Fatigue crack behaviour in bi-lamellar 880°C.

In bi-lamellar as shown in Figure 4. 42 where smaller secondary crack looks straight, the way crack grows through this is in the microstructure first cracks grow along the interface of primary α_P and transformed β, once it grows enough then it cuts through the transformed β phase and its again comes back to the interface, travels along the interface again and cut through the primary α_P and so on and

so forth, so it moves in the zigzag manners observed in the microstructure and leads to reduction of crack propagation energy. However, this only happens at the beginning of the crack or for smaller cracks. This effect and resistance to crack growth was not found in lamellar nor in as-build samples.
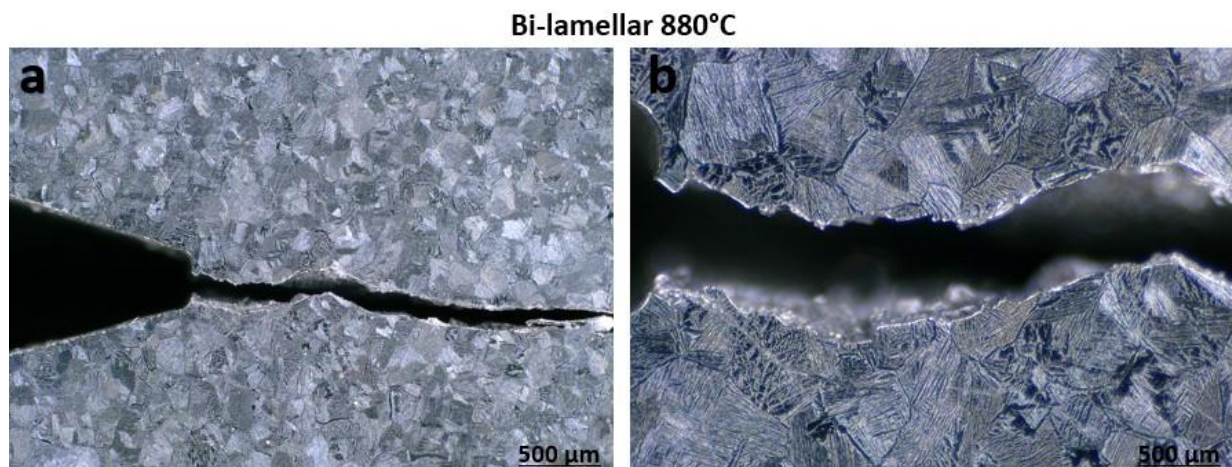
Figure 4. 43: Fatigue crack behaviour in bi-lamellar 880°C.

Figure 4. 44 below shows fatigue failure SEM image of samples having bi-lamellar microstructure obtained at 960°C. It can be seen that samples having bi-lamellar microstructure obtained after heat treatment 960°C is not have crack deflection observed in 800 and 880°C. crack propagates easily in it without crack growth resistance, hence the absence of zigzag behaviour or crack deflection.
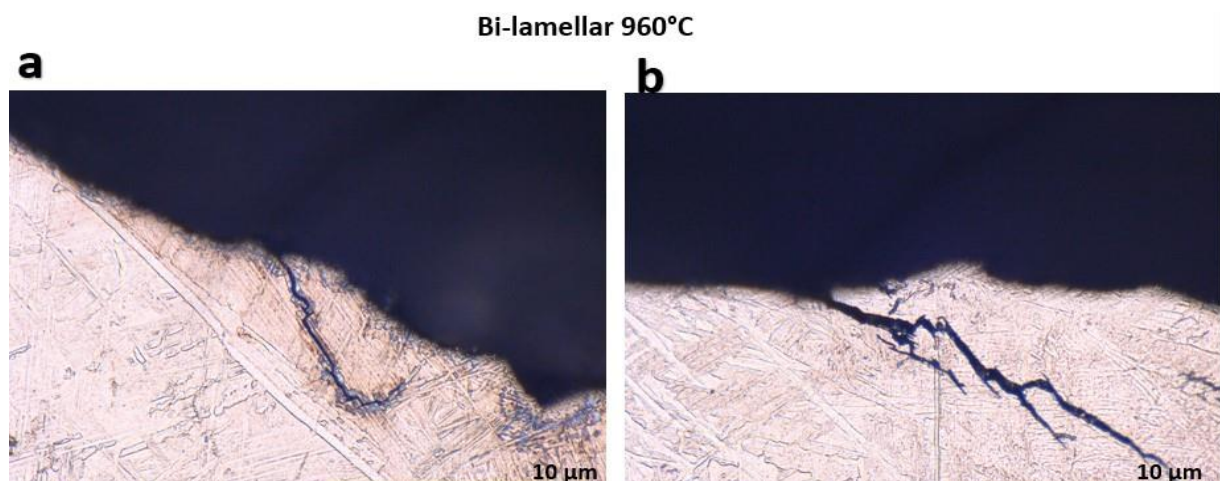
Figure 4. 44: Fatigue crack behaviour in bi-lamellar 960°C.

When looking at Figure 4. 45 it can be observed that there is not much crack resistance as the crack does not move in zigzag manners as it was the case of 800, and 880°C. This is due to the fact that the primary α_P and secondary α_S have the same morphological orientation, and also because there are thicker primary α_P present in the bi-lamellar microstructure obtained at 960°C. Even though there is existence of secondary cracks in samples having bi-lamellar microstructures obtained at 960°C, can

also be seen that there are limited numbers of secondary cracks in samples having bi-lamellar microstructure obtained at 960°C.

It can be maintained that within bi-lamellar microstructure samples heat treated at 960°C have lower resistance to crack propagation. When the crack behaviour observed in 960°C is compared to crack observed in lamellar microstructure, it can be seen that in unlike in the 960°C the lamellar microstructure has some zigzag while the 860°C have less zigzag observed. So, there is less deviation or deflection to crack in 960°C.
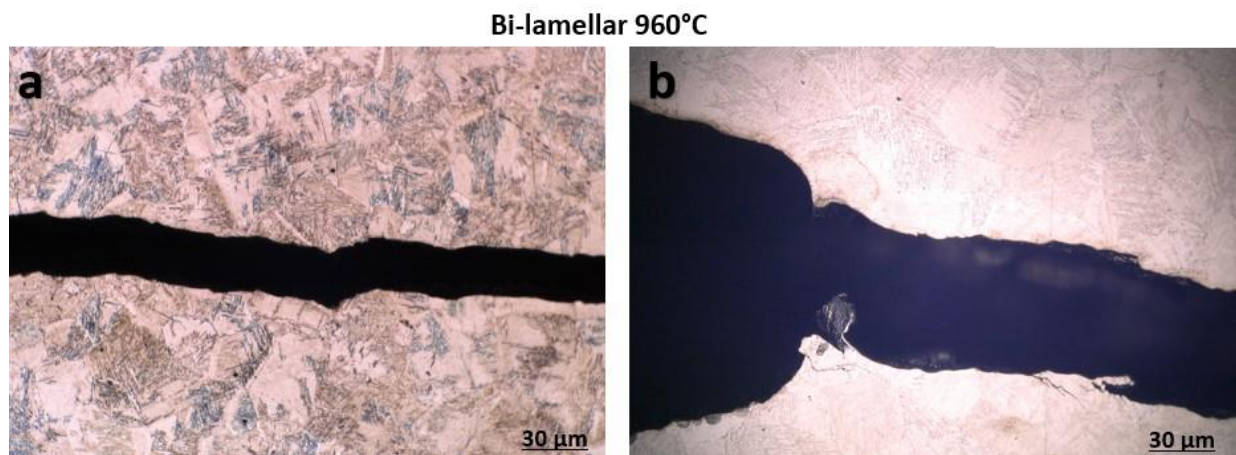
Figure 4. 45: Fatigue crack behaviour in bi-lamellar 960°C

5.   Conclusion

Post Heat Treatment:

1. A novel two-stage post heat treatment was designed to achieve bi-lamellar microstructure in the L-PBF processed Ti-6Al-4V. The second step of the heat treatment was performed at different temperatures and different fractions of primary alpha and transformed beta phase were obtained. It was found that the amount of the primary alpha and transformed beta phase varies indirectly and directly with the temperature respectively.

2. The size of the secondary alpha varies directly with the temperature of the heat treatment due to longer time available for growth while cooling from higher temperature.

3. The time for the second heat treatment step seems to have limited influence upon the resulting microstructure.

4. The chemical analysis revealed that the primary alpha has higher amount of Al and lower amount of V compared to that of the transformed beta phase.

Quasi-Static Mechanical Behaviour:

1. Quasi-static uniaxial mechanical test was performed on three different bi-lamellar microstructures obtained at different temperature (800˚C, 880˚C and 960 ˚C). The bi-lamellar microstructure heat treated at 880˚C showed highest strength among all the obtained bi-lamellar microstructure and also compared to the lamellar microstructure.

2. Microstructural analysis was performed on the failed tensile specimen to investigate the deformation mechanism. Voids were preferentially found at the interface boundary between the primary alpha and transformed beta phase.

Fatigue Crack propagation behaviour:

1. Fatigue crack growth (FCG) tests were performed to access the crack propagation behaviour under the dynamic loading condition. Little or no difference was found between the crack propagation behaviour of three different bi-lamellar and lamellar microstructure.

2. Crack branching and crack deflection were observed after microstructural characterization of the failed fatigue specimen.

6. References

[1] Hofmann, D.C., J. Kolodziejska, S. Roberts, R. Otis, R.P. Dillon, J.-O. Suh, Z.-K. Liu and J.-P. Borgonia, Compositionally graded metals: A new frontier of additive manufacturing, J. Mater. Res. 29 (2014), 17, pp. 1899–1910.

[2] Gibson, I., Additive manufacturing technologies, Springer, New York, London, 2010.

[3] Gong, H., Rafi, K., Gu, H., Janaki Ram, G., Starr, T. and Stucker, B., Influence of defects on mechanical properties of Ti–6Al–4V components produced by selective laser melting and electron beam melting. (2015).

[4] Neikter, M., Microstructure and texture of additive manufactured Ti-6Al-4V, Luleå University of Technology, Luleå, 2017.

[5] Zhai, Y., D.A. Lados and J.L. LaGoy, Additive Manufacturing: Making Imagination the Major Limitation, JOM 66 (2014), 5, pp. 808–816.

[6] Bourell, D.L., Perspectives on Additive Manufacturing, Annu. Rev. Mater. Res. 46 (2016), 1, pp. 1–18.

[7] Rosen, D.W., A review of synthesis methods for additive manufacturing, Virtual and Physical Prototyping 11 (2016), 4, pp. 305–317.

[8] Wu, X., Sharman, R., Mei, J., Voice, W., Microstructures of laser-deposited Ti6Al4V (2004).

[9] Vandenbroucke, B. and J.-P. Kruth, Selective laser melting of biocompatible metals for rapid manufacturing of medical parts, Rapid Prototyping (2007), Journal 13 (2007), 4, pp. 196–203.

[10] R. Wauthle, Industrialization of selective laser melting for the production of porous titanium and tantalum implants, PhD, Leuven, Belgium, 2014.

[11] Vaezi, M., H. Seitz and S. Yang, A review on 3D micro-additive manufacturing technologies, Int J Adv Manuf Technol 67 (2013), 5-8, pp. 1721–1754.

[12] Mallik, M.K., C.S. Rao and V.V.S.K. Rao, Effect of heat treatment on hardness and wear behavior of weld deposited Co-Cr-Mo alloy, Matéria (Rio J.) 20 (2015), 2, pp. 544–549.

[13] Fatoba, O.S., S.A. Akinlabi and E.T. Akinlabi, Laser Metal Deposition Influence on the Mechanical Properties of Steels and Stainless Steel Composites: A Review, Materials Today: Proceedings 5 (2018), 9, pp. 18603–18620.

[14] Hu, Y. and W. Cong, A review on laser deposition-additive manufacturing of ceramics and ceramic reinforced metal matrix composites, Ceramics International 44 (2018), 17, pp. 20599–20612.

[15] Shi, Y., Z. Lu, Y. Ren and G. Yang, Microstructure and tensile properties of laser engineered net shaped reduced activation ferritic/martensitic steel, Materials Characterization 144 (2018), pp. 554–562.

[16] Li, Y., Y. Hu, W. Cong, L. Zhi and Z. Guo, Additive manufacturing of alumina using laser engineered net shaping: Effects of deposition variables, Ceramics International 43 (2017), 10, pp. 7768–7775.

[17] Ziętala, M., T. Durejko, M. Polański, I. Kunce, T. Płociński, W. Zieliński, M. Łazińska, W. Stępniowski, T. Czujko, K.J. Kurzydłowski and Z. Bojar, The microstructure, mechanical properties and corrosion resistance of 316L stainless steel fabricated using laser engineered net shaping, Materials Science and Engineering: A 677 (2016), pp. 1–10.

[18] Murr, L.E., E. Martinez, K.N. Amato, S.M. Gaytan, J. Hernandez, D.A. Ramirez, P.W. Shindo, F. Medina and R.B. Wicker, Fabrication of Metal and Alloy Components by Additive Manufacturing: Examples of 3D Materials Science, Journal of Materials Research and Technology 1 (2012), 1, pp. 42–54.

[19] Körner, C., Additive manufacturing of metallic components by selective electron beam melting — a review, International Materials Reviews 61 (2016), 5, pp. 361–377.

[20] Galati, M. and L. Iuliano, A literature review of powder-based electron beam melting focusing on numerical simulations, Additive Manufacturing 19 (2018), pp. 1–20.

[21] Levy, G.N., The role and future of the Laser Technology in the Additive Manufacturing environment, Physics Procedia 5 (2010), pp. 65–80.

[22] Kruth, J.P., Material Incress Manufacturing by Rapid Prototyping Techniques, CIRP Annals 40 (1991), 2, pp. 603–614.

[23] Kruth, J.-P., G. Levy, F. Klocke and T.H.C. Childs, Consolidation phenomena in laser and powder-bed based layered manufacturing, CIRP Annals 56 (2007), 2, pp. 730–759.

[24] Xu, W., M. Brandt, S. Sun, J. Elambasseril, Q. Liu, K. Latham, K. Xia and M. Qian, Additive manufacturing of strong and ductile Ti–6Al–4V by selective laser melting via in situ martensite decomposition, Acta Materialia 85 (2015), pp. 74–84.

[25] Sun, J., Y. Yang and Di Wang, Parametric optimization of selective laser melting for forming Ti6Al4V samples by Taguchi method, Optics & Laser Technology 49 (2013), pp. 118–124.

[26] Tan, S, Li, D, Liu, H, Liao, X, Jiang and L, Microstructure and mechanical properties of 80Ni20Cr alloy manufactured by laser 3D printing technology. (2017).

[27] Azizi, H., H. Zurob, B. Bose, S. Reza Ghiaasiaan, X. Wang, S. Coulson, V. Duz and A.B. Phillion, Additive manufacturing of a novel Ti-Al-V-Fe alloy using selective laser melting, Additive Manufacturing 21 (2018), pp. 529–535.

[28] Beese, A.M. and B.E. Carroll, Review of Mechanical Properties of Ti-6Al-4V Made by Laser-Based Additive Manufacturing Using Powder Feedstock, JOM 68 (2016), 3, pp. 724–734.

[29] Demir, A.G. and B. Previtali, Additive manufacturing of cardiovascular CoCr stents by selective laser melting, Materials & Design 119 (2017), pp. 338–350.

[30] Herzog, D., V. Seyda, E. Wycisk and C. Emmelmann, Additive manufacturing of metals, Acta Materialia 117 (2016), pp. 371–392.

[31] Ikeshoji, T.-T., K. Nakamura, M. Yonehara, K. Imai and H. Kyogoku, Selective Laser Melting of Pure Copper, JOM 70 (2018), 3, pp. 396–400.

[32] Yadroitsev, I., L. Thivillon, P. Bertrand and I. Smurov, Strategy of manufacturing components with designed internal structure by selective laser melting of metallic powder, Applied Surface Science 254 (2007), 4, pp. 980–983.

[33] Losertová, M. and V. Kubeš, Microstructure and mechanical properties of selective laser melted Ti6Al4V alloy, IOP Conf. Ser.: Mater. Sci. Eng. 266 (2017), pp. 12009.

[34] 16. Jia, Q. & Gu, D. Selective laser melting additive manufacturing of Inconel 718 superalloy parts: Densification, microstructure and properties. J. Alloy.

[35] Dinda, G.P., A.K. Dasgupta and J. Mazumder, Texture control during laser deposition of nickel-based superalloy, Scripta Materialia 67 (2012), 5, pp. 503–506.

[36] Suzuki, M., R. Yamaguchi, K. Murakami and M. Nakada, Inclusion Particle Growth during Solidification of Stainless Steel, ISIJ International 41 (2001), 3, pp. 247–256.

[37] Kong, D., C. Dong, X. Ni, L. Zhang, C. Man, J. Yao, Y. Ji, Y. Ying, K. Xiao, X. Cheng and X. Li, High-throughput fabrication of nickel-based alloys with different Nb contents via a dual-feed additive manufacturing system: Effect of Nb content on microstructural and mechanical properties, Journal of Alloys and Compounds 785 (2019), pp. 826–837.

[38] Motyka, M., Martensite Formation and Decomposition during Traditional and AM Processing of Two-Phase Titanium Alloys—An Overview, Metals 11 (2021), 3, pp. 481.

[39] Marazani, T., D.M. Madyira and E.T. Akinlabi, Microhardness profiling of Ti-6Al-4V components repaired through multiple laser additive re-melt technique, Procedia Manufacturing 35 (2019), pp. 897–902.

[40] Lütjering, G., Influence of processing on microstructure and mechanical properties of (α+β) titanium alloys, Materials Science and Engineering: A 243 (1998), 1-2, pp. 32–45.

[41] Nalla, R.K., R.O. Ritchie, B.L. Boyce, J.P. Campbell and J.O. Peters, Influence of microstructure on high-cycle fatigue of Ti-6Al-4V: Bimodal vs. lamellar structures, Metall and Mat Trans A 33 (2002), 3, pp. 899–918.

[42] Guan, R.G., Y.T. Je, Z.Y. Zhao and C.S. Lee, Effect of microstructure on deformation behavior of Ti–6Al–4V alloy during compressing process, Materials & Design (1980-2015) 36 (2012), pp. 796–803.

[43] Ahmed, T. and H.J. Rack, Phase transformations during cooling in α+β titanium alloys, Materials Science and Engineering: A 243 (1998), 1-2, pp. 206–211.

[44] Ran, J., F. Jiang, X. Sun, Z. Chen, C. Tian and H. Zhao, Microstructure and Mechanical Properties of Ti-6Al-4V Fabricated by Electron Beam Melting, Crystals 10 (2020), 11, pp. 972.

[45] Cain, V., L. Thijs, J. van Humbeeck, B. van Hooreweder and R. Knutsen, Crack propagation and fracture toughness of Ti6Al4V alloy produced by selective laser melting, Additive Manufacturing 5 (2015), pp. 68–76.

[46] Zhang, J., B. Song, L. Yang, R. Liu, L. Zhang and Y. Shi, Microstructure evolution and mechanical properties of TiB/Ti6Al4V gradient-material lattice structure fabricated by laser powder bed fusion, Composites Part B: Engineering 202 (2020), pp. 108417.

[47] Haghdadi, N., M. Laleh, M. Moyle and S. Primig, Additive manufacturing of steels: a review of achievements and challenges, J Mater Sci 56 (2021), 1, pp. 64–107.

[48] Popov, V.V., M.L. Grilli, A. Koptyug, L. Jaworska, A. Katz-Demyanetz, D. Klobčar, S. Balos, B.O. Postolnyi and S. Goel, Powder Bed Fusion Additive Manufacturing Using Critical Raw Materials: A Review, Materials (Basel, Switzerland) 14 (2021), 4.

[49] TMS 2019 148th Annual Meeting & Exhibition Supplemental Proceedings, Springer International Publishing, Cham, 2019.

[50] Popovich, A., V. Sufiiarov, I. Polozov, E. Borisov and D. Masaylo, Producing hip implants of titanium alloys by additive manufacturing, Int. J. Bioprint. 2 (2016), 2.

[51] Cao, S., Q. Hu, A. Huang, Z. Chen, M. Sun, J. Zhang, C. Fu, Q. Jia, C.V.S. Lim, R.R. Boyer, Y. Yang and X. Wu, Static coarsening behaviour of lamellar microstructure in selective laser melted Ti–6Al–4V, Journal of Materials Science & Technology 35 (2019), 8, pp. 1578–1586.

[52] Liu, S. and Y.C. Shin, Additive manufacturing of Ti6Al4V alloy: A review, Materials & Design 164 (2019), pp. 107552.

[53] Ruth Bircha and Thomas Benjamin Britton, Effective structural unit analysis in hexagonal close packed alloys – reconstruction of parent beta microstructures & crystal orientation post processing analysis (2021).

[54] Titanium, Springer Berlin Heidelberg, Berlin, Heidelberg, 2007.

[55] Ahmadi, S.M., R.K. Ashok Kumar Jain, A.A. Zadpoor, C. Ayas and V.A. Popovich, Effects of heat treatment on microstructure and mechanical behaviour of additive manufactured porous Ti6Al4V, IOP Conf. Ser.: Mater. Sci. Eng. 293 (2017), pp. 12009.

[56] Chong, Y., T. Bhattacharjee, J. Yi, S. Zhao and N. Tsuji, Achieving bi-lamellar microstructure with both high tensile strength and large ductility in Ti–6Al–4V alloy by novel thermomechanical processing, Materialia 8 (2019), pp. 100479.

[57] Ter Haar, G.M. and T.H. Becker, Selective Laser Melting Produced Ti-6Al-4V: Post-Process Heat Treatments to Achieve Superior Tensile Properties, Materials (Basel, Switzerland) 11 (2018), 1.

[58] B. Oberwinkler, M. Riedler, W. Eichlseder, Importance of local microstructure for damage tolerant light weight design of Ti-6Al-4V forgings (2010).

[59] M. Stoschka, W. Tan, W. Eichlseder, M. Stockinger, Introduction to an approach based on the (α+β) microstructure of elements of alloy Ti-6Al-4V, (2009).

[60] Schroeder, G., J. Albrecht and G. Luetjering, Fatigue crack propagation in titanium alloys with lamellar and bi-lamellar microstructures, Materials Science and Engineering: A 319-321 (2001), pp. 602–606.

[61] Jamshidi, P., M. Aristizabal, W. Kong, V. Villapun, S.C. Cox, L.M. Grover and M.M. Attallah, Selective Laser Melting of Ti-6Al-4V: The Impact of Post-processing on the Tensile, Fatigue and Biological Properties for Medical Implant Applications, Materials (Basel, Switzerland) 13 (2020), 12.

[62] Qiu, C., N.J.E. Adkins and M.M. Attallah, Microstructure and tensile properties of selectively laser-melted and of HIPed laser-melted Ti–6Al–4V, Materials Science and Engineering: A 578 (2013), pp. 230–239.

[63] Rafi, H.K., T.L. Starr and B.E. Stucker, A comparison of the tensile, fatigue, and fracture behavior of Ti–6Al–4V and 15-5 PH stainless steel parts made by selective laser melting, Int J Adv Manuf Technol 69 (2013), 5-8, pp. 1299–1309.

[64] Motyka, M., W. Ziaja and J. Sieniawski, Introductory Chapter: Novel Aspects of Titanium Alloys' Applications, in: Titanium Alloys - Novel Aspects of Their Processing [Working Title], IntechOpen, 2018.

[65] R.H. Jones, R.E.R., Stress-Corrosion Cracking Materials Performance and Evaluation: CHAPTER 1. Mechanisms of Stress-Corrosion Cracking (1992).

[66] Trends in Oil and Gas Corrosion Research and Technologies, Elsevier, 2017.

[67] Wen, J.-b., C.-Y. Zhou, X. Li, X.-M. Pan, Le Chang, G.-D. Zhang, F. Xue and Y.-F. Zhao, Effect of temperature range on thermal-mechanical fatigue properties of P92 steel and fatigue life prediction with a new cyclic softening model, International Journal of Fatigue 129 (2019), pp. 105226.

[68] David, C., B. Menéndez and M. Darot, Influence of stress-induced and thermal cracking on physical properties and microstructure of La Peyratte granite, International Journal of Rock Mechanics and Mining Sciences 36 (1999), 4, pp. 433–448.

[69] Beavers, J. and T.A. Bubenik, Stress corrosion cracking, in: Trends in Oil and Gas Corrosion Research and Technologies, Elsevier, 2017, pp. 295–314.

[70] ASTM International:, ASTM F2792-12a, Standard Terminology for Additive Manufacturing Technologies. In. West Conshohocken, PA; 2012.

[71] Rolled alloys, Thermal Fatigue Cracking, https://www.rolledalloys.com/technical-resources/blog/thermal-fatigue-cracking, Abgerufen am: 01.07.2021.

[72] Omoniyi, P.O., E.T. Akinlabi and R.M. Mahamood, Heat Treatments of Ti6Al4V Alloys for Industrial Applications: An Overview, IOP Conf. Ser.: Mater. Sci. Eng. 1107 (2021), 1, pp. 12094.

[73] Di, L. and Y. Yang, Cost Modeling and Evaluation of Direct Metal Laser Sintering with Integrated Dynamic Process Planning, Sustainability 13 (2021), 1, pp. 319.

[74] Schiffauerova, A. and V. Thomson, A review of research on cost of quality models and best practices, Int J Qual & Reliability Mgmt 23 (2006), 6, pp. 647–669.

[75] www.strategy and pwc, Metals industry: Growth strategies to outlast commoditization, https://www.strategyand.pwc.com/de/en/industries/steel-metals/metals-industry.html, Abgerufen am: 01.07.2021.

[76] Mukherjee, P.M. and D. Roy, Global Competitiveness in the Steel Industry, Asia Pacific Business Review 6 (2010), 4, pp. 155–163.

[77] Attar, H., K.G. Prashanth, A.K. Chaubey, M. Calin, L.C. Zhang, S. Scudino and J. Eckert, Comparison of wearproperties of commercially pure titanium prepared by selective laser melting and casting processes. (2011).

[78] Yung, H.Y., S.J. Choi, K.G. Prashanth, M. Stoica, S. Scudino, S. Yi, U. Kühn, D.H. Kim, K.B. Kim and J. Eckert, Fabrication of Fe-based bulk metallic glass by selective laser melting: A parameter study. (2015).

[79] Song, C., M. Zhang, Y. Yang, D. Wang and Y. Jia-Kuo, Morphology and properties of CoCrMo parts fabricatedby selective laser melting. Mater. Sci. Eng. A 2018,713, 206–213.

[80] Wang, J., X.L. Zhou, J. Li, M. Brochu and Y.F. Zhao, Microstructures and properties of SLM manufacturedCu-15Ni-8Sn alloy. (2020).

[81] Zhang, Z.Zhang, Q., S. Hao, Y. Liu, Z. Xiong, W. Guo, Y. Yang, Y. Ren, L. Cui and L. Ren, The microstructureof a selective laser melting (SLM)-fabricated NiTi shape memory alloy with superior tensile property andshape memory recoverability (2020).

[82] Tofail, S.A.M., E.P. Koumoulos, A. Bandyopadhyay, S. Bose, L. O'Donoghue and C. Charitidis, Additive manufacturing: scientific and technological challenges, market uptake and opportunities, Materials Today 21 (2018), 1, pp. 22–37.

[83] L. Thijs., Microstructure and Texture of Metal Parts Produced by Selective Laser Melting. (2014).

[84] Alfaify, A.Y., J. Hughes and K. Ridgway, Critical evaluation of the pulsed selective laser melting process when fabricating Ti64 parts using a range of particle size distributions., Addit. Manuf. 19, 197–204 (2018,).

[85] Gong, H., K. Rafi, H. Gu, T. Starr and B. Stucker, Analysis of defect generation in Ti-6Al-4V parts made using powder bed fusion additive manufacturing processes., Addit. Manuf. 1, 87–98 (2014).

[86] Khorasani, A., I. Gibson, U.S. Awan and A. Ghaderi, The effect of SLM process parameters on density, hardness, tensile strength and surface quality of Ti-6Al-4V., Addit. Manuf. 25, 176–186. (2019,).

[87] Lütjering G, W.J., Titanium, Second ed.: Springer, 2007.

[88] Karolina Karolewska, Bogdan Ligaj (Ed.), Comparison analysis of titanium alloy Ti6Al4V produced by metallurgical and 3D printing method, Author(s), 2019.

[89] Karolewska, K. and B. Ligaj, Comparison analysis of titanium alloy Ti6Al4V produced by metallurgical and 3D printing method, Comparison analysis of titanium alloy Ti6Al4V produced by metallurgical and 3D printing method, Bydgoszcz, Poland, (2019), 20025.

[90] Singla, A.K., M. Banerjee, A. Sharma, J. Singh, A. Bansal, M.K. Gupta, N. Khanna, A.S. Shahi and D.K. Goyal, Selective laser melting of Ti6Al4V alloy: Process parameters, defects and post-treatments, Journal of Manufacturing Processes 64 (2021), pp. 161–187.

[91] Eshawish, N., S. Malinov, W. Sha and P. Walls, Microstructure and Mechanical Properties of Ti-6Al-4V Manufactured by Selective Laser Melting after Stress Relieving, Hot Isostatic Pressing Treatment, and Post-Heat Treatment, J. of Materi Eng and Perform (2021).

[92] Thijs, L., F. Verhaeghe, T. Craeghs, J. van Humbeeck and J.-P. Kruth, A study of the microstructural evolution during selective laser melting of Ti–6Al–4V, Acta Materialia 58 (2010), 9, pp. 3303–3312.

[93] T. Vilaro, C. Colin, and J. D. Bartout, "As-Fabricated and Heat-Treated Microstructures of the Ti-6Al-4V Alloy Processed by Selective Laser Melting," (2011).

[94] Boyer, R., E.W. Collings and G. Welsch, Materials properties handbook: Titanium alloys, 4. printing, ASM International, Materials Park, Ohio, 2007.

[95] M. Peters and C. Leyens, Titanium and Titanium Alloys., Wiley-VCH Verlag,, 2003.

[96] Donachie MJ., Titanium: a technical guide., Second ed.: ASM international 20009780871706867, 2000.

[97] V. André, R. Henriques, P. Paulo, D. Campos, C. Alberto, A. Cairo, and J. Carlos, "Production of Titanium Alloys for Advanced Aerospace Systems by Powder Metallurgy," (2005).

[98] Froes, F.H., M. Qian and M. Niinomi, Titanium for consumer applications: Real world use of titanium, Elsevier, Amsterdam, Netherlands, 2019.

[99] Titan metal fabricators, APPLICATIONS OF TITANIUM, https://www.titanmf.com/alloys/applications-of-titanium/, Abgerufen am: 05.09.2021.

[100] Froes, F.H., Friedrich, H., Kiese, J. and Bergoint, D., "Titanium in the family automobile: the cost challenge".

[101] Banerjee, D.a.W., "Perspectives on Titanium Science and Technology". (2013).

[102] Welsch, G., Boyer, R. and Collings, E.W., "Materials Properties Handbook: Titanium Alloys". (1994).

[103] Laszeray Technology, What Are Secondary Manufacturing Processes?, https://laszeray.com/blog/what-are-secondary-manufacturing-processes/, Abgerufen am: 29.12.2021.

[104] Murr, L., Gaytan, S., Medina, F., Martinez, E., Martinez, J., Hernandez, D., Lopez, B., Ramirez, "Microstructure and mechanical behaviour of Ti-6Al-4V produced by rapidlayer manufacturing"., Journal of the mechanical behavior of biomedical materials (2009), 2.1: 20-32.

[105] Donachie, M.J., Titanium: A technical guide, 2nd ed., digital print, ASM International, Materials Park, Ohio, 2010.

[106] Cui, C., B. Hu, L. Zhao and S. Liu, Titanium alloy production technology, market prospects and industry development, Materials & Design 32 (2011), 3, pp. 1684–1691.

[107] Aubert and Duval, Closed die forgings, https://www.aubertduval.com/products/forgings-aerospace-titanium-steel-aluminum-superalloy-closed-die-hammer-drop-forge/, Abgerufen am: 10.03.2021.

[108] Peter Schumacher, Castin microstructure and, Montanuniversität Leoben.

[109] H.V. Atkinson and S. Davies, "Fundamental Aspects of Hot Isostatic Pressing: An Overview," Metallurgical and Materials Transactions, 31A (12) (2000), p. 2981. (2000), Metallurgical and Materials Transactions, 31A (12) p2981.

[110] J. Klepeisz and S. Veeck, "The Production of Large Structural Titanium Castings," JOM, 49 (11) pp. 18–21. (1997).

[111] Titanium and Titanium Alloy Castings, in: S. Viswanathan, D. Apelian, R.J. Donahue, B. DasGupta, M. Gywn, J.L. Jorstad et al. (Eds.), Casting, ASM International, 2008, pp. 1128–1142.

[112] custompartnet, Investment Casting, https://www.custompartnet.com/wu/investment-casting, Abgerufen am: 15.03.2021.

[113] Ma, Q. and F.H. Froes, Titanium powder metallurgy, First edition, 2015.

[114] ittg, Powdermetallurgy, https://www.iitg.ac.in/engfac/ganu/public_html/Powdermetallurgy.pdf, Abgerufen am: 12.03.2021.

[115] Dunkley, J.J., Metal Powder Atomisation Methods for Modern Manufacturing, Johnson Matthey Technology Review 63 (2019), 3, pp. 226–232.

[116] Fukuda, Plasma Rotating Electrode Process, https://www.fukuda-kyoto.co.jp/en/technology/making/powder_chemical_plasma.html, Abgerufen am: 13.03.2021.

[117] Vander Voort George F., Metallography and Microstructures of Titanium and its Alloys. ASM Handbook, Volume 09 - Metallography and Microstructures: (2004).

[118] Lütjering, G. and J.C. Williams, Titanium, 2nd ed., Springer, Berlin, New York, 2007.

[119] Bhadeshia, H., Titanium & its Alloys. Materials Science & Metallurgy,, 2005: p. 1-12., Cambridge University,, 2005.

[120] Polmear, I.J., Light Alloys, From Traditional Alloys to Nanocrystals, Fourth Edition., United Kingdom: Elsevier Ltd., 2005.

[121] S. Gialanella, A. Malandruccolo (Eds.), Aerospace Alloys, Springer International Publishing, Cham, 2020.

[122] Farrah, A. and Z. Hussain, A Brief Review on the Properties of Titanium as a Metallic Biomaterials (2020).

[123] Tao, P, Shao, H, Ji, Z, Nan, Xu and Q., Numerical simulation for the investment casting process of a large-size; titanium alloy thin-wall casing. Prog. Nat. Sci; No last name! (2018), 28, 520–528.

[124] I. Inagaki, T. Takechi, Y. Shirai, N. Ariyasu, Application and features of titanium for the aerospace industry (2014), pp. 22–27.

[125] Boyer, R.R., An overview on the use of titanium in the aerospace industry, Materials Science and Engineering: A 213 (1996), 1-2, pp. 103–114.

[126] Singh, P., H. Pungotra and N.S. Kalsi, On the characteristics of titanium alloys for the aircraft applications, Materials Today: Proceedings 4 (2017), 8, pp. 8971–8982.

[127] Uhlmann, E., R. Kersting, T.B. Klein, M.F. Cruz and A.V. Borille, Additive Manufacturing of Titanium Alloy for Aircraft Components, Procedia CIRP 35 (2015), pp. 55–60.

[128]] L. Ciocca, M. Fantini, F. De Crescenzio, G. Corinaldesi, R. Scotti, Direct metal laser sintering (DMLS) of a customized titanium mesh for prosthetically guided bone regeneration of atrophic maxillary arches (2011), 1347–1352.

[129] Emmelmann, C., P. Scheinemann, M. Munsch and V. Seyda, Laser Additive Manufacturing of Modified Implant Surfaces with Osseointegrative Characteristics, Physics Procedia 12 (2011), pp. 375–384.

[130] Properties, Titanium Alloys - Ti6Al4V Grade 5., https://www.azom.com/properties.aspx?ArticleID=1547., Abgerufen am: 03.12.2020.

[131] Rajan, S., Analysis of Microstructure Evolution and Mechanical Properties of Linear Friction Welded Titanium Alloys, 2020.

[132] Zhong, C., J. Liu, T. Zhao, T. Schopphoven, J. Fu, A. Gasser and J.H. Schleifenbaum, Laser Metal Deposition of Ti6Al4V—A Brief Review, Applied Sciences 10 (2020), 3, pp. 764.

[133] Qazi JI, Senkov ON, Rahim J, Froes FS., Kinetics of martensite decomposition in Ti– 6Al–4V–xH alloys. (2003).

[134] Gerd Lutjering, James C. Williams, Titanium, Springer, 2003.

[135] Tarzimoghadam, Z., S. Sandlöbes, K.G. Pradeep and D. Raabe, Microstructure design and mechanical properties in a near-α Ti–4Mo alloy, Acta Materialia 97 (2015), pp. 291–304.

[136] M. Geetha, A. K. Singh, R. Asokamani, and A. K. Gogia, "Ti based biomaterials, the ultimate choice for orthopaedic implants – A review," (2009).

[137] G. Kasperovich and J. Hausmann, "Improvement of fatigue resistance and ductility of TiAl6V4 processed by selective laser melting," Journal of Materials Processing Technology (2015).

[138] J. S. Tiley, "Modeling of Microstructure Property Relationship in Ti-6Al-4V," PhD Thesis, ., 2002.

[139] M. Thöne, S. Leuders, A. Riemer, T. Tröster, and H. Richard, "Influence of heat-treatment on Selective Laser Melting products–eg Ti6Al4V," (2012).

[140] T. Ahmed and H. J. Rack, Phase transformations during cooling in α+β titanium alloys. (1998).

[141] Seo, S., H. Choi, G. Lee, K.-A. Lee, J. Han and M. Jung, Effect of Cooling Rate on Microstructure and Hardness during Solution Treatment and Aging Process of Ti-6Al-4V Alloy for Aerospace Components, J. of Materi Eng and Perform 30 (2021), 5, pp. 3406–3415.

[142] H. J. Rack and J. I. Qazi, "Titanium alloys for biomedical applications," (2006).

[143] Marco Simonelli, Microstructure evolution and mechanical properties of selective laser melted Ti-6Al-4V, 2014.

[144] BENEDETTI, M. and V. FONTANARI, The effect of bi-modal and lamellar microstructures of Ti-6Al-4V on the behaviour of fatigue cracks emanating from edge-notches, Fatigue & Fracture of Engineering Materials & Structures 27 (2004), 11, pp. 1073–1089.

[145] Zheng, C., F. Wang, X. Cheng, K. Fu, J. Liu, Y. Wang, T. Liu and Z. Zhu, Effect of microstructures on ballistic impact property of Ti–6Al–4V targets, Materials Science and Engineering: A 608 (2014), pp. 53–62.

[146] Lütjering, G., "Influence of processing on microstructure and mechanical properties of α+ β Titanium Alloys". (1998).

[147] B. Gaspar, Microstructural Characterization of Ti-6Al-4V and its Relationship to Sample Geometry," U.G Thesis, Deptartment of Material Engineering., California, 2012.

[148] Burgers WG., The process of transition of the cubic body centered modification into the hexagonal close packed modification of zirconium. (1993).

[149] M. Benedetti and V. Fontanari, "THE ROLE OF BI-MODAL AND LAMELLAR MICROSTRUCTURES OF Ti-6Al-4V ON THE BEHAVIOR OF FATIGUE CRACKS EMANATING FROM EDGE-NOTCHES,"

[150] Ricardo, B., W. Desirée, K. Alfred, L. Michael and P. Maria Cecilia, Phase transformation sequence of Ti-6Al-4V as a function of the cooling rate, MATEC Web Conf. 321 (2020), pp. 12038.

[151] Peters M., L.C., Titan und Titanlegierungen, Wiley-VCH, Weinheim, Germany, 2002.

[152] Lee, K.-H., S.-Y. Yang and J.-G. Yang, Optimization of heat-treatment parameters in hardening of titanium alloy Ti-6Al-4V by using the Taguchi method, Int J Adv Manuf Technol 90 (2017), 1-4, pp. 753–761.

[153] S. Banerjee P. Mukhopadhyay, Phase Transformations, Volume 12: Examples from Titanium and Zirconium Alloys (4th 2007).

[154] K. P. A.RAJAGOPAL, A. M. JOSE, A. SOMAN, C. J. DCRUZ, N. SANKA,S. SYAMRAJ,P. VIMALKUMAR, INVESTIGATION OF PHYSICAL AND MECHANICAL PROPERTIES OF Ti ALLOY (Ti-6Al-4V) UNDER PRECISELY CONTROLLED HEAT TREATMENT PROCESSES, International Journal of Mechanical Engineering and Technology(IJMET) (Vol.6, No. 2) (2015).

[155] F. J. Gil, M. P. Ginebra, J. M. Manero and J. A. Planell., Formation of a- Widmanstätten structure: effect of grain size and cooling rate on the Widmansthtten morphologies and on the mechanical properties in Ti6A14V alloy. (2001), 329: 142-52.

[156] Seong-Ji Seo, Gi-hoon kwon,Gee-Young Lee, Min-su Jung, Effects of Mill Annealing Temperature on the Microstructure and Hardness of Ti-6Al-4V Alloys, J. of the Korean Society for Heat Treatment, 2019.

[157] Shaikh, A., S. Kumar, A. Dawari, S. Kirwai, A. Patil and R. Singh, Effect of Temperature and Cooling Rates on the α+β Morphology of Ti-6Al-4V Alloy, Procedia Structural Integrity 14 (2019), pp. 782–789.

[158] J. Mueller, H.J. Rack, L. Wagner, Effects of Supra- and Subtransus Heat Treatments on Fatigue Performance of Ti6A1-4V (2007).

[159] Seong-Tak Oh, Kee-Do Woo, Jae-Hwang Kim, Seung-Mi Kwak, The Effect of Al and V on Microstructure and Transformation of β Phase during Solution Treatments of Cast Ti-6Al-4V Alloy, Korean J. Met. Mater. 55 (2017), 3.

[160] Pinke, L. eaplovid and T. Kovics., The influence of heat treatment on the microstructure of the casted Ti6A14V Titanium alloy. (2007).

[161] M. T. Jovanovic, S. Tadi6, S. Zec, Z. Miskovie and I. Bobid., The effect of annealing temperatures and cooling rates on microstructure and mechanical properties of investment cast Ti-6A1-4V alloy. (2006).

[162] M. T. Jovanović, I. Bobić, Z. Mišković, S. Zec, PRECISION CAST Ti-BASED ALLOYS – MICROSTRUCTURE AND MECHANICAL PROPERTIES (2009).

[163] Villa, M., J.W. Brooks, R.P. Turner, H. Wang, F. Boitout and R.M. Ward, Microstructural Modeling of the α + β Phase in Ti-6Al-4V: A Diffusion-Based Approach, Metall Mater Trans B 50 (2019), 6, pp. 2898–2911.

[164] Wang, Q., X. Lei, M. Hu, X. Xu, R. Yang and L. Dong, Effect of Heat Treatment on Microstructure and Tensile Property of Ti-6Al-6V-2Sn Alloy, Metals 11 (2021), 4, pp. 556.

[165] Villa, M., J. W. Brooks, R. P. Turner and M. Ward, Microstructural Modeling of Thermally-Driven β Grain Growth, Lamellae & Martensite in Ti-6Al-4V, MNSMS 10 (2020), 03, pp. 55–73.

[166] Leyens, C. and Peters, M., "Titanium and Titanium Alloys" (2003).

[167] Shiang-Cheng Jeng, H.-S.C., Effects of Cooling Rate on the Microstructure and Mechanical Propertiesof Ti-6Al-4V Alloy (2013), pplied Mechanics and Materials Vols. 284-287 (2013) pp 103-107.

[168] Seong-Tak Oh, Kee-Do Woo, Tack Lee, Hae-Cheol Lee, Effects of Heat Treatment on Mechanical Properties of VARCast Ti-6Al-4V Alloy Proceedings of the World Congress on Mechanical, Chemical, and Material Engineering (MCM 2015) (2015).

[169] Wei, Z.J., L. Cao, H.W. Wang and C.M. Zou, Microstructure and mechanical properties of TiC/Ti–6Al–4V composites processed by in situ casting route, Materials Science and Technology 27 (2011), 8, pp. 1321–1327.

[170] Peng, X., H. Guo, T. Wang and Z. Yao, Effects of β treatments on microstructures and mechanical properties of TC4-DT titanium alloy, Materials Science and Engineering: A 533 (2012), pp. 55–63.

[171] Sieniawski, J., W. Ziaja, K. Kubiak and M. Motyk, Microstructure and Mechanical Properties of High Strength Two-Phase Titanium Alloys, in: J. Sieniawski (Ed.), Titanium Alloys - Advances in Properties Control, InTech, 2013.

[172] Vigraman, T., D. Ravindran and R. Narayanasamy, Effect of phase transformation and intermetallic compounds on the microstructure and tensile strength properties of diffusion-bonded joints between Ti–6Al–4V and AISI 304L, Materials & Design (1980-2015) 36 (2012), pp. 714–727.

[173] H. R. Ogden and R. I. Jaffe, The effects of carbon, oxygen and nitrogen on the mechanical properties of titanium and titanium alloys, (1955).

[174] W. L. Finlay and J. A. Snyder, Effects of three interstitial solutes (Nitrogen, Oxygenand Carbon) on the mechanical properties of high–purity alpha titanium, (1950).

[175] I. Jaffee, et al., "Alloys of Titanium with Carbon, Oxygen and Nitrogen", Transactions of the American Institute of Mining and Metallurgical Engineers, (1950).

[176] Gebhardt, A., et al., Additive manufacturing by selective laser melting the realizer desktop machine and its application for the dental industry (2010).

[177] Osakada, K. and M. Shiomi, Flexible manufacturing of metallic products by selective laser melting of powder. (2006).

[178] Yasa, E., J.P. Kruth, and J. Deckers, Manufacturing by combining selective laser melting and selective laser erosion/laser re-melting (2011).

[179] Yadroitsev, I., et al., Manufacturing of fine-structured 3D porous filter elements by selective laser melting. (2009.).

[180] Yadroitsev, I., et al., Strategy of manufacturing components with designed internal structure by selective laser melting of metallic powder. (2007).

[181] Zhang, L.-C., J. Wang, Y. Liu, Z. Jia and S.-X. Liang, Additive Manufacturing of Titanium Alloys, in: Reference Module in Materials Science and Materials Engineering, Elsevier, 2020.

[182] Sidambe, A.T., D.S. Judson, S.J. Colosimo and P. Fox, Laser powder bed fusion of a pure tungsten ultra-fine single pinhole collimator for use in gamma ray detector characterisation, International Journal of Refractory Metals and Hard Materials 84 (2019), pp. 104998.

[183] Qian, M., W. Xu, M. Brandt and H.P. Tang, Additive manufacturing and postprocessing of Ti-6Al-4V for superior mechanical properties, MRS Bull. 41 (2016), 10, pp. 775–784.

[184] K. Ek, "Additive Manufactured Metals", Master of Science thesis, 2014.

[185] Vrancken, B., L. Thijs, J.-P. Kruth and J. van Humbeeck, Heat treatment of Ti6Al4V produced by Selective Laser Melting: Microstructure and mechanical properties, Journal of Alloys and Compounds 541 (2012), pp. 177–185.

[186] Kruth, J. P., Badrossamay, M., Yasa, E., Deckers, J., Thijs, L., & Van Humbeeck, J., Part and material properties in selective laser melting of metals. (2010).

[187] Attar, E., Simulation of selective electron beam melting processes., Ph. D. Thesis, 2011.

[188] Thijs, L., F. Verhaeghe, T. Craeghs, J. van Humbeeck and J.-P. Kruth, A study of the microstructural evolution during selective laser melting of Ti–6Al–4V, (2010).

[189] Edwards, P. and Ramulu, M., Fatigue performance evaluation of selective laser melted Ti–6Al–4V. (2014).

[190] Leyens, C. and Peters, M., Titanium and Titanium Alloys, Hoboken: Wiley, 2006.

[191] Shunmugavel, M., Polishetty, A. and Littlefair, G., Microstructure and Mechanical Properties of Wrought and Additive Manufactured Ti-6Al-4V Cylindrical Bars (2015).

[192] Leuders, S., Lieneke, T., Lammers, S., Tröster, T. and Niendorf, T., On the fatigue properties of metals manufactured by selective laser melting – The role of ductility (2014).

[193] I. Yadroitsev, Selective laser melting: Direct manufacturing of 3D-objects by selective laser melting of metal powders, 1st Editio. LAP LAMBERT Academic Publishing (2009).

[194] Maamoun, A.H., Y.F. Xue, M.A. Elbestawi and S.C. Veldhuis, Effect of Selective Laser Melting Process Parameters on the Quality of Al Alloy Parts: Powder Characterization, Density, Surface Roughness, and Dimensional Accuracy, Materials (Basel, Switzerland) 11 (2018), 12.

[195] Xiong, W., L. Hao, Y. Li, D. Tang, Q. Cui, Z. Feng and C. Yan, Effect of selective laser melting parameters on morphology, microstructure, densification and mechanical properties of supersaturated silver alloy, Materials & Design 170 (2019), pp. 107697.

[196] Brandt, M., Laser additive manufacturing, Elsevier, Woodhead, Amsterdam, 2017.

[197] Rafi, H.K., N.V. Karthik, H. Gong, T.L. Starr and B.E. Stucker, Microstructures and Mechanical Properties of Ti6Al4V Parts Fabricated by Selective Laser Melting and Electron Beam Melting, J. of Materi Eng and Perform 22 (2013), 12, pp. 3872–3883.

[198] JF Heat treating, Heat Treating and the History Behind It, https://jfheattreatinginc.com/2019/02/heat-treating-and-the-history-behind-it/.

[199] Jueming, H., Metallurgy in China, in: H. Selin (Ed.), Encyclopaedia of the History of Science, Technology, and Medicine in Non-Western Cultures, Springer Netherlands, Dordrecht, 2008, pp. 1622–1624.

[200] Heat Treating of Titanium and Titanium Alloys, in: G.E. Totten (Ed.), Heat Treating of Nonferrous Alloys, ASM International, 2016, pp. 511–534.

[201] Boyer, R.R., Titanium and Its Alloys: Metallurgy, Heat Treatment and Alloy Characteristics, in: R. Blockley, W. Shyy (Eds.), Encyclopedia of Aerospace Engineering, John Wiley & Sons, Ltd, Chichester, UK, 2010.

[202] Dr. Khuram Shahzad, Heat treatment of ti6Al4V parts produced by selective, https://www.slideshare.net/khshehzad/heat-treatment-of-ti6al4v-parts-produced-by-selective?from_action=save, Abgerufen am: 25.03.2021.

[203] Frkan, M., R. Konecna, G. Nicoletto and L. Kunz, Microstructure and fatigue performance of SLM-fabricated Ti6Al4V alloy after different stress-relief heat treatments, Transportation Research Procedia 40 (2019), pp. 24–29.

[204] G.E. Totten (Ed.), Heat Treating of Nonferrous Alloys, ASM International, 2016.

[205] Li, F., B. Qi, Y. Zhang, W. Guo, P. Peng, H. Zhang, G. He, D. Zhu and J. Yan, Effects of Heat Treatments on Microstructures and Mechanical Properties of Ti6Al4V Alloy Produced by Laser Solid Forming, Metals 11 (2021), 2, pp. 346.

[206] Teixeira, Ó., F.J.G. Silva, L.P. Ferreira and E. Atzeni, A Review of Heat Treatments on Improving the Quality and Residual Stresses of the Ti–6Al–4V Parts Produced by Additive Manufacturing, Metals 10 (2020), 8, pp. 1006.

[207] Li, H., D. Jia, Z. Yang, X. Liao, H. Jin, D. Cai and Y. Zhou, Effect of heat treatment on microstructure evolution and mechanical properties of selective laser melted Ti–6Al–4V and TiB/Ti–6Al–4V composite: A comparative study, Materials Science and Engineering: A 801 (2021), pp. 140415.

[208] Kiel-Jamrozik, M., W. Jamrozik and I. Witkowska, The heat treatment influence on the structure and mechanical properties of Ti6Al4V alloy manufactured by SLM technology, in: M. Gzik, E. Tkacz, Z. Paszenda, E. Piętka (Eds.), Innovations in Biomedical Engineering, Springer International Publishing, Cham, 2018, pp. 319–327.

[209] Wissenbach K., Müller-Lohmeier K., Brandl E., Skrynecki N., Buchbinder D., Meiners W., Rapid manufacturing of aluminium parts for serial production via selective laser melting (slm). (2009).

[210] T. Vilaro, C. Colin, and J. D. Bartout, "As-Fabricated and Heat-Treated Microstructures of the Ti-6Al-4V Alloy Processed by Selective Laser Melting," (2011).

[211] Brandl, E., F. Palm, V. Michailov, B. Viehweger and C. Leyens, Mechanical properties of additive manufactured titanium (Ti–6Al–4V) blocks deposited by a solid-state laser and wire, Materials & Design 32 (2011), 10, pp. 4665–4675.

[212] Yan, M. and P. Yu, An Overview of Densification, Microstructure and Mechanical Property of Additively Manufactured Ti-6Al-4V — Comparison among Selective Laser Melting, Electron Beam Melting, Laser Metal Deposition and Selective Laser Sintering, and with Conventional Powder, in: A. Lakshmanan (Ed.), Sintering Techniques of Materials, InTech, 2015.

[213] Tsai, M.-T., Y.-W. Chen, C.-Y. Chao, J.S.C. Jang, C.-C. Tsai, Y.-L. Su and C.-N. Kuo, Heat-treatment effects on mechanical properties and microstructure evolution of Ti-6Al-4V alloy fabricated by laser powder bed fusion, Journal of Alloys and Compounds 816 (2020), pp. 152615.

[214] Ali, H., Le Ma, H. Ghadbeigi and K. Mumtaz, In-situ residual stress reduction, martensitic decomposition and mechanical properties enhancement through high temperature powder bed pre-heating of Selective Laser Melted Ti6Al4V, Materials Science and Engineering: A 695 (2017), pp. 211–220.

[215] Lui, E.W., W. Xu, A. Pateras, M. Qian and M. Brandt, New Development in Selective Laser Melting of Ti–6Al–4V: A Wider Processing Window for the Achievement of Fully Lamellar α + β Microstructures, JOM 69 (2017), 12, pp. 2679–2683.

[216] Xu, W., E.W. Lui, A. Pateras, M. Qian and M. Brandt, In situ tailoring microstructure in additively manufactured Ti-6Al-4V for superior mechanical performance, Acta Materialia 125 (2017), pp. 390–400.

[217] Simonelli, M., Y.Y. Tse and C. Tuck, Effect of the build orientation on the mechanical properties and fracture modes of SLM Ti–6Al–4V, Materials Science and Engineering: A 616 (2014), pp. 1–11.

[218] Simonelli, M., Y.Y. Tse and C. Tuck, The formation of α + β microstructure in as-fabricated selective laser melting of Ti–6Al–4V, J. Mater. Res. 29 (2014), 17, pp. 2028–2035.

[219] Xu, W., S. Sun, J. Elambasseril, Q. Liu, M. Brandt and M. Qian, Ti-6Al-4V Additively Manufactured by Selective Laser Melting with Superior Mechanical Properties, JOM 67 (2015), 3, pp. 668–673.

[220] Maciej Motyka, Martensite Formation and Decomposition during Traditional and AM Processing of Two-Phase Titanium Alloys—An Overview (2021).

[221] Liu, Y., Li, X., Zhang, L. and Sercombe, T., Processing and properties of topologically optimised biomedical Ti–24Nb–4Zr–8Sn scaffolds manufactured by selective laser melting. (2015).

[222] Chong, Y., T. Bhattacharjee and N. Tsuji, Bi-lamellar microstructure in Ti–6Al–4V: Microstructure evolution and mechanical properties, Materials Science and Engineering: A 762 (2019), pp. 138077.

[223] Gao, J.B., X.L. Zhao, J.K. Yue, M.C. Qi and D.L. Zhang, Microstructure and Mechanical Properties of Ti-6Al-4V Alloy Samples Fabricated by Selective Laser Melting, KEM 770 (2018), pp. 179–186.

[224] Zhang, K., W.H. Kan, Y. Liu, X. Gao, Y. Zhu, S.C.V. Lim, H. Peng and A. Huang, Microstructure control by heat treatment for better ductility and toughness of Ti-6Al-4V produced by laser powder bed fusion, Australian Journal of Mechanical Engineering 19 (2021), 5, pp. 680–691.

[225] Huang, Q., X. Liu, X. Yang, R. Zhang, Z. Shen and Q. Feng, Specific heat treatment of selective laser melted Ti–6Al–4V for biomedical applications, Front. Mater. Sci. 9 (2015), 4, pp. 373–381.

[226] F.H. Froes (Ed.), Titanium, ASM International, 2015.

[227] Leyens, C. and M. Peters, Titanium and Titanium Alloys, Wiley, 2003.

[228] Jadhav, S., A. Powar, S. Patil, A. Supare, B. Farane and R. Singh, Effect of volume fraction of alpha and transformed beta on the high cycle fatigue properties of bimodal Ti6Al4V alloy, IOP Conf. Ser.: Mater. Sci. Eng. 201 (2017), pp. 12035.

[229] H. Zuoa, Z.G. Wang E.H. Han, Effect of microstructure on ultra-high cycle fatigue behavior of Ti–6Al–4V (PDF) Effect of volume fraction of alpha and transformed beta on the high cycle fatigue properties of bimodal Ti6Al4V alloy. Available from: https://www.researchgate.net/publication/317307329_Effect_of_volume_fraction_of_alpha_and_transformed_beta_on_the_high_cycle_fatigue_properties_of_bimodal_Ti6Al4V_alloy [accessed Aug 04 2021]., Materials Science and Engineering A473(2008) 147–152. (2008).

[230] Bridier, F., P. Villechaise and J. Mendez, Slip and fatigue crack formation processes in an α/β titanium alloy in relation to crystallographic texture on different scales, Acta Materialia 56 (2008), 15, pp. 3951–3962.

[231] Borrego LP, Ferreira JAM, Costa JDM, Capela C, de Jesus J, A study of fatigue notch sensibility on titanium alloy Ti6Al4V parts manufactured by selective laser melting. Procedia Struct Integr 13:1000–1005 (2018).

[232] Wycisk E, Solbach A, Siddique S, Herzog D, Walther F, Effects of defects in laser additive manufactured Ti-6Al-4V on fatigue properties. Phys Procedia 56:371–378 (2014).

[233] Edwards P, R.M., Fatigue performance evaluation of selective laser melted Ti-6Al-4V.

[234] Total Materia, Application of Fracture Mechanics, https://www.totalmateria.com/page.aspx?ID=CheckArticle&site=kts&NM=353.

[235] Anderson, T.L., Fracture mechanics: Fundamentals and applications, Third edition, CRC Press, Boca Raton, FL, 2005.

[236] Perez, N., Fracture Mechanics, Springer US, Boston, MA, 2004.

[237] C.H Wang, Introductiono to fracture mechnics (1996).

[238] Zehnder, A.T., Fracture mechanics, Springer Science+Business Media, London, New York, 2012.

[239] Time magasine, "The Plane Was Disintegrating", http://content.time.com/time/magazine/article/0,9171,149181,00.html, Abgerufen am: 22.03.2021.

[240] Britanica, Golden Gate Bridge, https://www.britannica.com/topic/Golden-Gate-Bridge, Abgerufen am: 20.03.2021.

[241] nuclear-power, Fracture of Material – Fracture Mechanics, https://www.nuclear-power.net/nuclear-engineering/materials-science/material-properties/toughness/fracture-of-material-fracture-mechanics/.

[242] Itas, Brittle and Ductile Materials, http://www.ltas-cm3.ulg.ac.be/FractureMechanics/overview_P3.html, Abgerufen am: 21.03.2021.

[243] R. Wanhill and S.Barter, Fatigue of beta processes and beta heat treeated titanium alloys (2012).

[244] Broek, D., The Practical Use of Fracture Mechanics, Springer Netherlands, Dordrecht, 1989.

[245] M. Janssen, J. Zuidema and R.J.H. Wanhill, Fracture Mechanics,, Second edition,, Delft,, 2002.

[246] Adrian Mouritz, Fracture processes of aerospace materials, in: Introduction to Aerospace Materials, Elsevier, 2012, pp. 428–453.

[247] Westmoreland mechanical testing and research, The History of Fatigue Testing, https://www.wmtr.co.uk/history_of_fatigue_testing.html#:~:text=In%201829%20Wilhelm%20August%20Julius,recorded%20account%20of%20metal%20fatigue., Abgerufen am: 20.03.2021.

[248] Schijve, J., Fatigue of structures and materials in the 20th century and the state of the art, International Journal of Fatigue 25 (2003), 8, pp. 679–702.

[249] Siemens, History of fatigue, https://community.sw.siemens.com/s/article/history-of-fatigue, Abgerufen am: 01 Junuary 2021.

[250] Wöhler, A., "Über die Festigkeitsversuche mit Eisen und Stahl",, Zeitschrift für Bauwesen, 20: 73–106. (1870).

[251] Norton, R.L., Machine design: An integrated approach, 4th ed., Prentice Hall, Boston, Mexico City, 2011.

[252] Zimmermann, M., Very High Cycle Fatigue, in: S. Schmauder, C.-S. Chen, K.K. Chawla, N. Chawla, W. Chen, Y. Kagawa (Eds.), Handbook of Mechanics of Materials, Springer Singapore, Singapore, 2018, pp. 1–38.

[253] Berger C, K.B., Results of very high cycle fatigue tests on helical compression springs,, International Journal Fatigue 28(2006): pp.1658–63 (2006).

[254] Shuaeib, F.M., K.Y. Benyounis and M.S.J. Hashmi, Material Behavior and Performance in Environments of Extreme Pressure and Temperatures, in: Reference Module in Materials Science and Materials Engineering, Elsevier, 2017.

[255] Aboulkhair, N.T., N.M. Everitt, I. Ashcroft and C. Tuck, Reducing porosity in AlSi10Mg parts processed by selective laser melting, Additive Manufacturing 1-4 (2014), pp. 77–86.

[256] Ritchie, Davidson, Boyce, Campbell and Roder, High-cycle fatigue of Ti-6Al-4V, Fatigue & Fracture of Engineering Materials & Structures 22 (1999), 7, pp. 621–631.

[257] Fatec engieering, What is the Difference between Low & High Cycle Fatigue?, https://www.fatec-engineering.com/2018/08/23/what-is-the-difference-between-low-high-cycle-fatigue/, Abgerufen am: 10.07.2021.

[258] Agius, D., K. Kourousis and C. Wallbrink, A Review of the As-Built SLM Ti-6Al-4V Mechanical Properties towards Achieving Fatigue Resistant Designs, Metals 8 (2018), 1, pp. 75.

[259] Pasang, T., B. Tavlovich, O. Yannay, B. Jackson, M. Fry, Y. Tao, C. Turangi, J.-C. Wang, C.-P. Jiang, Y. Sato, M. Tsukamoto and W.Z. Misiolek, Directionally-Dependent Mechanical Properties of Ti6Al4V Manufactured by Electron Beam Melting (EBM) and Selective Laser Melting (SLM), Materials (Basel, Switzerland) 14 (2021), 13.

[260] Dareh Baghi, A., S. Nafisi, R. Hashemi, H. Ebendorff-Heidepriem and R. Ghomashchi, Experimental realisation of build orientation effects on the mechanical properties of truly as-built Ti-6Al-4V SLM parts, Journal of Manufacturing Processes 64 (2021), pp. 140–152.

[261] Carrozza, A., A. Aversa, P. Fino and M. Lombardi, A study on the microstructure and mechanical properties of the Ti-6Al-2Sn-4Zr-6Mo alloy produced via Laser Powder Bed Fusion, Journal of Alloys and Compounds 870 (2021), pp. 159329.

[262] Eshawish, N., S. Malinov and W. Sha, Effect of Solution Treatment and Cooling Rate on the Microstructure and Hardness of Ti-6Al-4V Alloy Manufactured by Selective Laser Melting Before and After Hot Isostatic Pressing Treatment, J. of Materi Eng and Perform (2022).

[263] Shuangyin Zhang, 张., 林. Xin Lin, 陈. Jing Chen and 黄. Weidong Huang, Effect of solution temperature and cooling rate on microstructure and mechanical properties of laser solid forming Ti-6Al-4V alloy, Chin. Opt. Lett. 7 (2009), 6, pp. 498–501.

[264] Seifi, M., A. Salem, D. Satko, J. Shaffer and J.J. Lewandowski, Defect distribution and microstructure heterogeneity effects on fracture resistance and fatigue behavior of EBM Ti–6Al–4V, International Journal of Fatigue 94 (2017), pp. 263–287.

[265] Baufeld, B., E. Brandl and O. van der Biest, Wire based additive layer manufacturing: Comparison of microstructure and mechanical properties of Ti–6Al–4V components fabricated by laser-beam deposition and shaped metal deposition, Journal of Materials Processing Technology 211 (2011), 6, pp. 1146–1158.

[266] Zhai Y, Lados D A, Brown E J and Vigilante G N, Fatigue crack growth behavior and microstructural mechanisms in Ti-6Al-4V manufactured by laser engineered net shaping (2016).

[267] Neikter, M., P. Åkerfeldt, R. Pederson and M.-L. Antti, Microstructure characterisation of Ti-6Al-4V from different additive manufacturing processes, IOP Conf. Ser.: Mater. Sci. Eng. 258 (2017), pp. 12007.

[268] Lekoadi, P., M. Tlotleng, K. Annan, N. Maledi and B. Masina, Evaluation of Heat Treatment Parameters on Microstructure and Hardness Properties of High-Speed Selective Laser Melted Ti6Al4V, Metals 11 (2021), 2, pp. 255.

[269] Jaber, H., J. Kónya, K. Kulcsár and T. Kovács, Effects of Annealing and Solution Treatments on the Microstructure and Mechanical Properties of Ti6Al4V Manufactured by Selective Laser Melting, Materials (Basel, Switzerland) 15 (2022), 5.

[270] MIT, THE METALLOGRAPHIC EXAMINATION OF ARCHAEOLOGICAL ARTIFACTS: Laboratory Manual (2003).

[271] Schimtz metallographie Gmbh, SiC abrasive paper, https://metallographie.shop/SiC-abrasive-paper-R250-mm-grit-size-P800, Abgerufen am: 10.07.2021.

[272] Yang, J., H. Yu, J. Yin, M. Gao, Z. Wang and X. Zeng, Formation and control of martensite in Ti-6Al-4V alloy produced by selective laser melting, Materials & Design 108 (2016), pp. 308–318.

[273] Hrabe, N., R. White and E. Lucon, Effects of internal porosity and crystallographic texture on Charpy absorbed energy of electron beam melting titanium alloy (Ti-6Al-4V), Materials Science and Engineering: A 742 (2019), pp. 269–277.

[274] Bourell, D., J.P. Kruth, M. Leu, G. Levy, D. Rosen, A.M. Beese and A. Clare, Materials for additive manufacturing, CIRP Annals 66 (2017), 2, pp. 659–681.

[275] Sangid, M.D., A. Nicolas, K. Kapoor, E. Fodran and J. Madsen, Modeling the Role of Epitaxial Grain Structure of the Prior β Phase and Associated Fiber Texture on the Strength Characteristics of Ti-6Al-4V Produced via Additive Manufacturing, Materials (Basel, Switzerland) 13 (2020), 10.

[276] Wang, L., C. Ma, J. Huang, H.Y. Ding and M.Q. Chu, Microstructure and tensile properties of Ti-6Al-4V alloys manufactured by selective laser melting with optimized processing parameters, IOP Conf. Ser.: Mater. Sci. Eng. 265 (2017), pp. 12015.

[277] Zhang, X., C.J. Yocom, B. Mao and Y. Liao, Microstructure evolution during selective laser melting of metallic materials: A review, Journal of Laser Applications 31 (2019), 3, pp. 31201.

[278] Sallica-Leva, E., R. Caram, A.L. Jardini and J.B. Fogagnolo, Ductility improvement due to martensite α' decomposition in porous Ti-6Al-4V parts produced by selective laser melting for orthopedic implants, Journal of the mechanical behavior of biomedical materials 54 (2016), pp. 149–158.

[279] Sercombe T, Jones N, Day R, Kop A., Heat treatment of Ti-6Al-7Nb components produced by selective laser melting. (2008).

[280] Thijs L, Verhaeghe F, Craeghs T, Humbeeck JV, Kruth JP., A study of the microstructural evolution during selective laser melting of Ti-6Al-4V.

[281] M. Simonelli, Y. Tse, C. Tuck, Microstructure and Mechanical Properties of Ti-6A1-4V Fabricated by Selective Laser Melting (2012).

[282] Portier, R. and D. Gratias, SYMMETRY AND PHASE TRANSFORMATION, J. Phys. Colloques 43 (1982), C4, C4-17-C4-34.

[283] Qian, M., W. Xu, M. Brandt and H.P. Tang, Additive manufacturing and postprocessing of Ti-6Al-4V for superior mechanical properties, MRS Bull. 41 (2016), 10, pp. 775–784.

[284] Hung, W., Post-Processing of Additively Manufactured Metal Parts, in: D.L. Bourell, W. Frazier, H. Kuhn, M. Seifi (Eds.), Additive Manufacturing Processes, ASM International, 2020, pp. 298–315.

[285] Brandl, E. and D. Greitemeier, Microstructure of additive layer manufactured Ti–6Al–4V after exceptional post heat treatments, Materials Letters 81 (2012), pp. 84–87.

[286] Zhao, Z.-Y., L. Li, P.-K. Bai, Y. Jin, L.-Y. Wu, J. Li, R.-G. Guan and H.-Q. Qu, The Heat Treatment Influence on the Microstructure and Hardness of TC4 Titanium Alloy Manufactured via Selective Laser Melting, Materials (Basel, Switzerland) 11 (2018), 8.

[287] Zhao, Z., J. Chen, X. Lu, H. Tan, X. Lin and W. Huang, Formation mechanism of the α variant and its influence on the tensile properties of laser solid formed Ti-6Al-4V titanium alloy, Materials Science and Engineering: A 691 (2017), pp. 16–24.

[288] Cecchel, S., D. Ferrario, G. Cornacchia and M. Gelfi, Development of Heat Treatments for Selective Laser Melting Ti6Al4V Alloy: Effect on Microstructure, Mechanical Properties, and Corrosion Resistance, Adv. Eng. Mater. 22 (2020), 8, pp. 2000359.

[289] Etesami, S.A., B. Fotovvati and E. Asadi, Heat treatment of Ti-6Al-4V alloy manufactured by laser-based powder-bed fusion: Process, microstructures, and mechanical properties correlations, Journal of Alloys and Compounds 895 (2022), pp. 162618.

[290] James C M Li, Microstructure And Properties Of Materials, Vol 2 (2000).

[291] Bartsch, K., D. Herzog, B. Bossen and C. Emmelmann, Material modeling of Ti–6Al–4V alloy processed by laser powder bed fusion for application in macro-scale process simulation, Materials Science and Engineering: A 814 (2021), pp. 141237.

[292] Masoomi, M., S.M. Thompson and N. Shamsaei, Laser powder bed fusion of Ti-6Al-4V parts: Thermal modeling and mechanical implications, International Journal of Machine Tools and Manufacture 118-119 (2017), pp. 73–90.

[293] Harkin, R., H. Wu, S. Nikam, J. Quinn and S. McFadden, Reuse of Grade 23 Ti6Al4V Powder during the Laser-Based Powder Bed Fusion Process, Metals 10 (2020), 12, pp. 1700.

[294] Wei, C., Z. Zhang, D. Cheng, Z. Sun, M. Zhu and L. Li, An overview of laser-based multiple metallic material additive manufacturing: from macro- to micro-scales, Int. J. Extrem. Manuf. 3 (2021), 1, pp. 12003.

[295] Cutolo, A., C. Elangeswaran, C. de Formanoir, G.K. Muralidharan and B. van Hooreweder, Effect of Heat Treatments on Fatigue Properties of Ti–6Al–4V and 316L Produced by Laser Powder Bed Fusion in As-Built Surface Condition, in: TMS 2019 148th Annual Meeting & Exhibition Supplemental Proceedings, Springer International Publishing, Cham, 2019, pp. 395–405.

[296] Chen, Z., X. Wu and C.H.J. Davies, Process variation in Laser Powder Bed Fusion of Ti-6Al-4V, Additive Manufacturing 41 (2021), pp. 101987.

[297] Vilaro, T., C. Colin and J.D. Bartout, As-Fabricated and Heat-Treated Microstructures of the Ti-6Al-4V Alloy Processed by Selective Laser Melting, Metall and Mat Trans A 42 (2011), 10, pp. 3190–3199.